

CHRISTIAN-ALBRECHTS-UNIVERSITÄT ZU KIEL  
MATHEMATISCH-NATURWISSENSCHAFTLICHE FAKULTÄT  
SEKTION GEOGRAPHIE  
INSTITUT FÜR ÖKOSYSTEMFORSCHUNG

---

Palaeolimnological evidence for environmental  
transformation in southern Greece

---

**Kumulative Dissertation**

zur Erlangung des Doktorgrades der Naturwissenschaften

(Dr. rer. nat.)

der Mathematisch-Naturwissenschaftlichen Fakultät

der Christian-Albrechts-Universität zu Kiel

vorgelegt von

Joana Seguin, M.Sc.

Kiel, 2020



Vorsitzender der Prüfungskommission: Prof. Dr. Florian Dünckmann

Erstgutachter: Prof. Dr. Ingmar Unkel

Zweitgutachter: Prof. Dr. Hans-Rudolf Bork

Tag der mündlichen Prüfung: 20. März 2020

## Acknowledgement

I owe a debt of gratitude to all those involved in making this study possible.

My first and biggest thanks goes to my first supervisor, Ingmar Unkel, without whom this project would not have come alive. Thank you for the best supervision and support, I could have wished for. Whenever possible, you gave me the freedom to develop and pursue my own research ideas, and whenever needed, you pushed me into the right direction. I strongly appreciate the fact that we always communicated openly, honestly, and at eyelevel. Thank you Hans-Rudolf Bork, for being my second supervisor and for guiding me with your wealth of experience. I will miss your exciting stories and the joint fieldwork. Another thanks goes to Henny Piezonka – it was a comforting feeling to know that I have you as a mentor at my side if needed. My further committee members are also thanked for their time and effort to read and assess my dissertation. I owe gratitude to everyone who invested time to read my drafts and to provide valuable feedback. I am particularly thankful to all the co-authors, who worked with me on the manuscripts and gave constructive feedback and suggestions.

I am grateful to all my colleagues, I had the chance to meet during my time at Kiel University, notably in the CRC 1266 and in the Institute of Ecosystem Research. Thank you everyone for the fruitful interdisciplinary discussions, sometimes raising and solving conceptual misunderstandings at the same time.

The composition of a cumulative dissertation is not the merit of a single person, but it is also a teamwork and I would like to thank everyone, who had his share in this process. Namely, I would like to further express my gratitude to Sophia Dazert, for your advice in the lab and our joint R practices, Georg Hörmann, for profound R support and the opportunity to give a course in China, Britta Witt, for patiently explaining me how to find my way through the jungle of university bureaucracy, Hartwig Bünning, for support with statistical issues and proofreading, Kay Adam, for rescuing me whenever I struggled with my computer, Clemens von Scheffer, for being a great office mate and supplying me with physically healthy garden fruits and mentally healthy chocolate, Svetlana Khamnueva-Wendt, for advice and exchange on scientific issues, Walter Dörfler, for your coring expertise and support of the fieldwork as well as for sharing the apartment during the IPA-IAL in Stockholm, Doris Kramer, for the realisation of my sketchy pictures of landscape transformation, and Piet Grootes, for shedding light on the complexity of radiocarbon dating and modelling.

Work life at the institute was always structured by the fixed lunch hours at Mensa 2 followed by a cosy and informative gathering around the coffee machine to chat, socialize and discuss urgent questions of life – I am grateful for this and to everyone, who was part of it. A special thanks goes to my secret meeting crew Erica, Clara, and Sonja, for the great mixture of scientific and private discussions, always making me feel more motivated again afterwards.



I would also like to extend thanks to our colleagues at Patras University, first and foremost to Pavlos Avramidis, Alexandros Emmanouilidis and Eleni Zagana. I very much appreciated the valuable collaboration and joint field campaigns. Besides, I am grateful that I got the opportunity to participate in the RISE DAAD programme during my doctoral phase, and I enjoyed working with McKenzie Elliott – thank you for coming all the way to Germany to support my lab work.

I would also like to acknowledge the financial support I received from the CRC1266 and indirectly the DFG, which allowed me to join two summer schools and to participate at numerous conferences to present my work and get in contact with kind and cooperative colleagues from all over the world. I extend a special thanks to the IODP Expedition 381 team. It was an intense but great onshore science party in Bremen in 2018. Special thanks to the co-chiefs Lisa McNeill and Donna Shillington for making me become a member of the science team and to the geochemistry team (Luzie Schnieders, Simone Sauer, Carol Mahoney, and Clint Miller) for effective, instructive, and entertaining lab work.

On a personal level, I am highly indebted to my family and friends. I want to express my thanks to my dancing partners and UniTanzKiel – dancing was the best medicine to relax my brain and body after a tough working day. Thanks to all of my friends, who encouraged or diverted me, depending on what I needed at the time. I would like to take this opportunity to express my endless gratitude to my parents and my sister. My academic education, culminating in this thesis, would not have been possible without your unconditional love, trust, and support. Last but not least, I would like to thank my wonderful husband Jascha for being at my side for so many years now and especially for your patience and encouragement during the roller coaster ride of my doctoral phase.

I will always remember this memorable chapter of my life and extend my thanks to everyone who accompanied me during this phase and who contributed in any way to the successful outcome of my work.

## Abstract

The richness of archaeological sites in Greece reflects the long history of human activity in the area and thus makes it an attractive region for studying human-environmental interaction. Palaeoclimatic and palaeoenvironmental archives in the area, however, are still relatively sparse or discontinuous.

The main aims of this thesis are to reconstruct palaeoenvironmental conditions and hydrological dynamics in southern Greece for the past approximately 5,000 years and to infer climatic variations on different spatial and temporal scales. For this purpose, lake sediments present meaningful geoarchives, because they can provide continuous, high-resolution proxy records of palaeoenvironmental changes.

The study area around the Gulf of Corinth is located in a limestone rich environment and in a climatic transition zone between the temperate high latitudes and the dry subtropics that is highly sensitive to changes in both climatic zones. Four lake and palaeolake sites (Stymphalia, Kaisari, Pheneos, and Trichonida) have been investigated using a multi-proxy approach, mainly concentrating on the geochemical composition of the sediments. The  $\log(\text{Rb}/\text{Sr})$  ratio, obtained from X-ray fluorescence (XRF) core scanning, was identified as the most valuable proxy and allowed to reconstruct palaeohydrological, palaeoenvironmental and palaeoclimatic changes for the area. The results are discussed in six manuscripts.

A interdisciplinary consilience allowed the reconstruction of palaeoenvironmental changes at Lake Stymphalia for the last 2,500 years. The construction of the Hadrianic Aqueduct (ca. 130 AD) was identified as the main trigger for unbalancing the lake ecosystem, increasing its vulnerability over the following centuries. The proxies record complex interactions of climatic variations, such as the Late Antique Little Ice Age (LALIA), coupled with anthropogenic landscape changes that induce erosion, such as medieval deforestation, and result in a more balanced and deeper understanding of landscape transformation.

Furthermore, a multi-archive approach was performed by applying the same set of sedimentological, geochemical, and statistical analyses to four lacustrine archives on the Peloponnese. This allowed studying proxy variation on different spatial scales and differentiate supra-regional fluctuations in the climate system from local signals for the last 5,000 years. Site-specific differences occurred e.g. due to differences in sedimentation rates, temporary desiccation of the palaeolakes, or varying human impact in the catchment areas. On a meso-scale level, the archives indicated drier conditions during the Bronze Age / Iron Age transition (ca. 3,200 – 2,800 cal BP).

The sediment sequence from Lake Trichonida suggested that the climatic variation during the last 2,600 years was considerably influenced by changes in the North Atlantic Oscillation pattern.

Besides, a methodological refinement of a master core compilation from parallel sediment cores based on continuous colour parameters was developed and contributes to enhancing transparent, reproducible research in palaeoenvironmental sciences.

Additionally, a spatial modelling approach was developed by an interdisciplinary collaboration and implemented for the NE Peloponnese. It investigates how much cultivable land was required to supply a society with its basic needs and what the consequences were, when environmental conditions aggravated. The results indicated that potential societal crisis were less a factor of changing climatic conditions or a shortage of arable land but primarily caused by socio-economic factors.

As the author was a member of the Science Party of the International Ocean Discovery Programme (IODP) Expedition 381, the first joint results on climate-driven environmental and sedimentary changes in the Corinth Rift during the Pleistocene were also included in this thesis. Research on the Gulf of Corinth is covered by the spatial scale of the PhD project and expands the temporal scale to the last ca. 2 million years.

This thesis contributes to increased knowledge on climate variability and environmental transformations in southern Greece on multiple temporal and spatial scales, notably during the Late Holocene.

## Zusammenfassung

Die Reichhaltigkeit archäologischer Stätten in Griechenland spiegelt dessen lange Geschichte menschlicher Aktivität wider und macht es so zu einer attraktiven Region für Studien zu Mensch-Umwelt-Beziehungen. Paläoklima- und Paläoumweltarchive in der Gegend sind jedoch vergleichsweise selten oder weisen diskontinuierliche Datensätze auf.

Die Hauptziele dieser Dissertation sind die Rekonstruktion der Umweltbedingungen und hydrologischen Schwankungen in Südgriechenland während der letzten ca. 5000 Jahre und, daraus abgeleitet, klimatische Schwankungen auf unterschiedlichen räumlichen und zeitlichen Skalen. Zu diesem Zweck wurden Seesedimente als bedeutsame Geoarchive untersucht, da sie zumeist kontinuierliche, hoch aufgelöste Proxy Datensätze liefern, aus denen sich Paläoumweltveränderungen ablesen lassen.

Das Untersuchungsgebiet rund um den Golf von Korinth liegt in einer kalksteinreichen Umgebung sowie in einer klimatischen Übergangszone zwischen den gemäßigten Breiten und den trockenen Subtropen und ist somit sehr sensibel gegenüber Veränderungen in beiden Klimazonen. Vier Seen und Paläoseen (Stymphalia, Kaisari, Pheneos und Trichonida) wurden mittels eines Multi-Proxy-Ansatzes analysiert, wobei die geochemische Zusammensetzung der Sedimente im Fokus stand. Das mittels Röntgenfluoreszenz (XRF) Kernscanning gemessene  $\log(\text{Rb}/\text{Sr})$  Verhältnis wurde als aussagekräftigster Proxy identifiziert und ermöglichte die Rekonstruktion paläohydrologischer, paläoumwelt- und paläoklimatischer Schwankungen an den entsprechenden Standorten. Die Ergebnisse der Arbeit sind in sechs Manuskripten festgehalten.

Eine interdisziplinäre Verknüpfung natur- und geisteswissenschaftlicher Forschungsergebnisse ermöglichte die Rekonstruktion von Paläoumweltschwankungen am See Stymphalia während der letzten 2500 Jahre. Der Bau des Hadrianischen Aquädukts (ca. 130 n. Chr.) wurde als Hauptauslöser identifiziert, der das Seeökosystem aus seinem Gleichgewicht brachte und dessen Vulnerabilität über die folgenden Jahrhunderte erhöhte. Die Proxies zeigen komplexe Interaktionen zwischen klimatischen Schwankungen, wie beispielsweise der spätantiken kleinen Eiszeit (LALIA), und anthropogen verursachten Landschaftsveränderungen, wie beispielsweise mittelalterlicher Rodung, welche für stärkere Erosion sorgte. Die Analyse ermöglichte ein tieferes und ausgewogeneres Verständnis von Landschaftstransformationen.

Des Weiteren wurde ein multi-Archiv-Ansatz verfolgt, bei dem die gleichen sedimentologischen, geochemischen und statistischen Analysen an vier verschiedenen lakustrinen Archiven auf der Peloponnes durchgeführt wurden. So wurden Proxyschwankungen auf

unterschiedlichen räumlichen Skalen untersucht und zwischen überregionalen Schwankungen im Klimasystem und lokalen Einflussignalen während der letzten 5000 Jahre differenziert. Standortsspezifische Unterschiede entstanden u.a. aufgrund von unterschiedlichen Sedimentationsraten, zeitweiser Austrocknung der Paläoseen oder variierendem menschlichen Einfluss in den Einzugsgebieten. Ein Vergleich der mesoskaligen Variabilität lieferte Hinweise für trockenere Bedingungen während der Übergangsphase von der Bronze- zur Eisenzeit (ca. 3200 – 2800 cal BP) in allen untersuchten Archiven.

Der Sedimentkern vom See Trichonida zeigte, dass die beobachteten klimatischen Schwankungen während der letzten 2600 Jahre eindeutig durch Veränderungen im Nordatlantischen Oszillationsmuster beeinflusst wurden.

Darüber hinaus wurde eine methodische Weiterentwicklung der Zusammenstellung eines Masterkerns aus parallelen Sedimentkernen konzipiert, die auf kontinuierlichen Farbparametern basiert. Dieser Ansatz trägt dazu bei, nachvollziehbare, reproduzierbare Forschung in den Paläoumweltwissenschaften verstärkt anzuwenden und weiterzuentwickeln.

Außerdem wurde im Rahmen einer interdisziplinären Zusammenarbeit ein räumlicher Modellierungsansatz entwickelt und beispielhaft auf die Nordostpeloponnes angewandt. Dieser untersucht, wieviel Anbaufläche vergangene Gesellschaften zur Deckung ihrer Grundbedürfnisse benötigten und welche Konsequenzen daraus resultierten, wenn sich die Umwelt- und somit die Anbaubedingungen verschlechterten. Die Modellierung legt nahe, dass gesellschaftliche Krisen in der Region weniger durch Umweltveränderungen oder Knappheit an Anbaufläche, sondern primär durch sozioökonomische Faktoren ausgelöst wurden.

Da die Verfasserin dieser Arbeit zudem Mitglied des Forschungsteams der IODP Expedition 381 war, wurden die ersten Ergebnisse zu von Klima- und Umweltveränderungen ausgelösten Sedimentschwankungen im Corinth Rift ebenfalls als Teil dieser Doktorarbeit integriert. Die Lage des Golfs von Corinth im Zentrum des Untersuchungsgebietes verändert die räumliche Ausdehnung des Dissertationsprojektes nicht, wohingegen die zeitliche Dimension durch diesen Beitrag auf ca. 2 Millionen Jahre erweitert wird.

Die vorliegende Doktorarbeit trägt zu einem verbesserten Verständnis von Klimaschwankungen und Umwelttransformationen in Südgriechenland auf diversen räumlichen und zeitlichen Skalen, insbesondere im Spätholozän, bei.

## Paper contributions

This doctoral thesis consists of the present summary framework and six manuscripts listed below as Appendices I-VI. They are published (Appendix I, V, VI), submitted (Appendix II, III) or intended to be submitted (Appendix IV) to peer-reviewed journals. All manuscripts are referred to by their Appendix numbers in the text.

### Appendix I:

**Seguin, J.**, Bintliff, J.L., Grootes, P.M., Bauersachs, T., Dörfler, W., Heymann, C., Manning, S.W., Müller, S., Nadeau, M.J., Nelle, O., Steier, P., Weber, J., Wild, E.M., Zagana, E., Unkel, I., 2019. 2500 years of anthropogenic and climatic landscape transformation in the Stymphalia polje, Greece. *Quaternary Science Reviews* 213, 133–154. doi:10.1016/j.quascirev.2019.04.028.

[own contribution: 70 %]

### Appendix II:

**Seguin, J.**, Avramidis, P., Haug, A., Kessler, T., Schimmelmann, A., Unkel, I., 2019. Inter-comparison of palaeoenvironmental records from four lacustrine archives on the Peloponnese (Greece) over the last 5,000 years. *E&G Quaternary Science Journal*.

[Manuscript submitted in 09/2019, in review].

[own contribution: 85 %]

### Appendix III:

**Seguin, J.**, Avramidis, P., Emmanouilidis, A., Dörfler, W., Unkel, I., 2019. A 2,600 years high-resolution climate record from Lake Trichonida (SW Greece). *E&G Quaternary Science Journal*.

[Manuscript submitted in 01/2020].

[own contribution: 90 %]

### Appendix IV:

**Seguin, J.**, Unkel, I. Mastering a master sediment core compilation from parallel drill cores using RGB values.

[Manuscript intended for publication as an Express Report in EGQSJ]

[own contribution: 90 %]

Appendix V:

Knitter, D., Hamer, W., Günther, G., **Seguin, J.**, Unkel, I., Kessler, T., Weiberg, E., Duttmann, R., Nakoinz, O., 2019. Land use patterns and climate change - a modeled scenario of Late Bronze Age in Southern Greece. *Environmental Research Letters* 14. 125003. doi: 10.1088/1748-9326/ab5126.

[own contribution: 10 %]

Appendix VI:

McNeill, L.C., Shillington, D.J., Carter, G.D.O., Everest, J.D., Gawthorpe, R.L., Miller, C., Phillips, M.P., Collier, R.E.L., Cvetkoska, A., De Gelder, G., Diz, P., Doan, M.-L., Ford, M., Geraga, M., Gillespie, J., Hemelsdaël, R., Herrero-Bervera, E., Ismaiel, M., Janikian, L., Kouli, K., Le Ber, E., Li, S., Maffione, M., Mahoney, C., Machlus, M.L., Michas, G., Nixon, C.W., Oflaz, S.A., Omale, A.P., Panagiotopoulos, K., Pechlivanidou, S., Sauer, S., **Seguin, J.**, Sergiou, S., Zakharova, N. V., Green, S., 2019. High-resolution record reveals climate-driven environmental and sedimentary changes in an active rift. *Sci. Rep.* 9, 3116. doi: 10.1038/s41598-019-40022-w.

[own contribution: 5 %]





**Table of contents**

<b>Acknowledgement</b>	<b>II</b>
<b>Abstract</b>	<b>IV</b>
<b>Zusammenfassung</b>	<b>VI</b>
<b>Paper contributions</b>	<b>VIII</b>
<b>Table of contents</b>	<b>VII</b>
<b>List of figures</b>	<b>X</b>
<b>List of tables</b>	<b>XI</b>
<b>List of abbreviations</b>	<b>XII</b>
<b>1 Introduction</b>	<b>1</b>
1.1 Motivation and research gaps .....	1
1.2 Research aims and objectives .....	2
1.3 Project frame.....	3
1.4 Outline of the thesis.....	4
<b>2 Lacustrine sediments as palaeoenvironmental archives</b>	<b>6</b>
2.1 Lakes as geoarchives .....	6
2.2 Proxies for palaeoenvironmental reconstruction .....	7
2.3 The use of XRF scanning in palaeoenvironmental research.....	7
2.4 Chronology and dating .....	8
2.5 Geoarchives recording Holocene climate variability in Greece .....	10
<b>3 Study area</b>	<b>12</b>
3.1 Geographical setting .....	12
3.2 Geological setting .....	14
3.3 Climatic setting.....	15
3.4 Vegetation and soils .....	16
3.5 Site descriptions.....	18
3.5.1 Lake Stymphalia .....	19
3.5.2 Palaeolake Kaisari.....	20
3.5.3 Palaeolake Pheneos .....	20

---

3.5.4	Lake Trichonida.....	20
<b>4</b>	<b>Material and methods</b>	<b>22</b>
4.1	Fieldwork .....	22
4.2	Laboratory work.....	25
4.2.1	Sampling.....	25
4.2.2	Composite core construction .....	25
4.2.3	Lithological description.....	26
4.2.4	X-ray fluorescence scanning .....	26
4.2.5	Grain size distribution .....	27
4.2.6	Carbon/nitrogen ratio .....	27
4.2.7	Loss on ignition .....	28
4.3	Chronology.....	28
4.3.1	Chronological notation .....	28
4.3.2	Radiocarbon dating.....	29
4.3.3	Age-depth modelling.....	29
4.4	Statistical analysis .....	29
<b>5</b>	<b>Summary of papers</b>	<b>31</b>
5.1	Appendix I.....	31
5.2	Appendix II .....	32
5.3	Appendix III.....	33
5.4	Appendix IV.....	34
5.5	Appendix V .....	35
5.6	Appendix VI.....	36
<b>6</b>	<b>Additional results</b>	<b>38</b>
6.1	Graphical visualisation of landscape development at Lake Stymphalia .....	38
6.2	Grain size distribution analysis .....	39
6.2.1	Automated grain size distribution in R.....	39
6.2.2	Reflection on grain size measurement via laser diffraction.....	40

---

<b>7 Synthesis</b>	<b>43</b>
7.1 Evaluation of the suitability of the investigated karstic lakes as palaeoenvironmental archives.....	43
7.2 Radiocarbon dating in a limestone rich environment.....	45
7.3 The application of PCA as a suitable tool in palaeolimnology.....	46
7.4 Exploring and identifying the causes of landscape transformation in sediment cores ...	48
7.5 Scales of transformation – synthesis in the scope of the CRC1266 .....	49
7.5.1 Investigated scales of transformation.....	49
7.5.2 Reflection on interdisciplinary collaboration.....	50
<b>8 Prospects for further research</b>	<b>54</b>
<b>9 Conclusion</b>	<b>57</b>
<b>References</b>	<b>XVII</b>
<b>Appendices</b>	<b>XXVIII</b>

**List of figures**

Figure 1: The location of the study area in southern Greece. ....	12
Figure 2: Topography of the study area of the CRC1266 E1 subproject. ....	13
Figure 3: Impressions of the four lake sites. ....	21
Figure 4: Coring campaigns. ....	23
Figure 5: Landscape model for climatic variation, landscape development and human impact in the Stymphalia polje over the last 2,500 years. ....	39
Figure 6: Results of replicate measurements with different obscurations. ....	41
Figure 7: Results of replicate measurements with and without the removal of carbonates. ....	42
Figure 8: Sediment cores from the three polje sites on the NE Peloponnese. ....	44

**List of tables**

Table 1: Mean values for the main morphometric features of the modern investigated lakes. ...	19
Table 2: Summary of contributors to field and laboratory works for each study site.....	22
Table 3: Sediment cores retrieved, used, or discussed within the scope of this PhD project. ....	24
Table 4: Measurement settings for XRF core scanning.....	26

**List of abbreviations**

AMS	accelerated mass spectrometry
BP	before present (relative to the reference year 1950 AD)
cal	calibrated
CRC	Collaborative Research Centre
cps	counts per second
DFG	Deutsche Forschungsgemeinschaft (=German Research Foundation)
GSD	grain size distribution
IODP	International Ocean Discovery Programme
ITCZ	inter-tropical convergence zone
ka	one thousand years
KES	Kaisari
L*a*b*	CIELAB colour space (L* for the lightness from black (0) to white (100), a* from green (-) to red (+), and b* from blue (-) to yellow (+))
LALIA	Late Antique Little Ice Age
LOI	loss on ignition
m a.s.l.	meters above sea level
MCMC	Markov chain Monte Carlo
NAO	North Atlantic Oscillation
PCA	Principal Component Analysis
PHE	Pheneos
RGB	red, green, blue (colour channels)
SFB	Sonderforschungsbereich
STY	Stymphalia
TC	total carbon
TIC	total inorganic carbon
TN	total nitrogen
TOC	total organic carbon
TRI	Trichonida
XRD	X-ray diffraction
XRF	X-ray fluorescence

# 1 Introduction

## 1.1 Motivation and research gaps

The physical and biogeochemical cycles in lake ecosystems are tightly linked to environmental conditions, and thus they respond sensitively to natural or anthropogenic changes. Understanding the palaeoenvironmental history of the ecosystems provides insights into the impact of different forcing factors, which is also important in the light of future developments of freshwater systems. The assessment of the natural and anthropogenic drivers of climate change is one of the major challenges in climate research (IPCC, 2013) and a look into the past may enable us to disentangle natural variability from anthropogenic impact.

The Holocene has been a period of dynamic climatic fluctuations coinciding with an increasing human influence on the environment (Berglund, 2003; Mayewski et al., 2004). The direct and continuous measurement of climate parameters, however, covers only approximately the last 200 years. Geoarchives – such as ice cores, tree-ring records, speleothems, marine or lacustrine sediments – allow to extract palaeoclimatic information, which is indirectly preserved in proxy data, and extend climate information further back in time. Geoarchives are globally distributed, nevertheless they are highly heterogeneous in spatial and temporal coverage and in temporal resolution.

Greece is a country with a long history of cultural development, which had a considerable impact on the surrounding landscape and environment. More than a century of detailed archaeological excavations at ancient Greek sites have contributed to the fact that there are numerous archaeologically well investigated areas and well dated, detailed historical records on human activities from this region (Finné and Weiberg, 2018). This high data density calls for the investigation of human-environmental interaction. Palaeoclimatic reconstructions however, especially showing a high temporal resolution that could be compared to archaeological data, are still sparse and show significant gaps notably for southern Greece (Finné et al., 2011; Weiberg et al., 2016). One reason is that potential geoarchives are scarce in this area or do not provide a high temporal resolution. Thus, very little is known about palaeoenvironmental conditions and about the extent to which human activity affected the landscape and induced changes to the vegetation. Recent technological advances in mass spectrometry and X-ray fluorescence measurement have allowed for more precise measurements with higher resolution, widening the range of suitable geoarchives.

A general interplay between climate patterns, environmental change, and cultural development has been reported across the eastern Mediterranean (Finné and Weiberg, 2018; Hughes et al., 2018;

Izdebski et al., 2016; Roberts et al., 2017; Staubwasser and Weiss, 2006; Weiberg et al., 2019; Weiss, 1982; Weninger et al., 2009). However, the investigated geoarchives exhibit several constraints, which sometimes even affect their credibility: the temporal resolution of the applied geoarchive is too low to be compared to human activity (e.g. Drake, 2012; Kaniewski et al., 2015), the geoarchive has significant gaps in the proxy record for the relevant time slices (e.g. Finné et al., 2017, 2014), or there is a relatively large spatial distance between the geoarchive and the archaeological sites that they are compared to (e.g. Gogou et al., 2016; Weninger et al., 2009). The high local variability of climatic parameters, due to the heterogeneous Greek morphology, additionally complicates the correlation of hydrological and societal transformations (Finné and Weiberg, 2018; Roberts et al., 2011; Xoplaki et al., 2018) and it is thus desirable for interdisciplinary studies to have human and environmental archives in close proximity as well as a high spatio-temporal coverage of archives.

## 1.2 Research aims and objectives

This thesis aims to improve the understanding of palaeoenvironmental changes in southern Greece during the Mid to Late Holocene by geochemical and sedimentological investigations of lacustrine archives concentrating on sediment cores from the (palaeo)lakes Stymphalia, Kaisari, Pheneos, and Trichonida.

The four main research objectives are:

- (1) to analyse the natural environmental conditions in the region around the Gulf of Corinth;
- (2) to reconstruct changes in relative temperature variability and hydrological dynamics in this region during the past approximately 5,000 years;
- (3) to infer reactions of regional climate to climate perturbations on different spatial and temporal scales;
- (4) to differentiate natural forcing factors from effects of human influence.

Based on the research gaps outlined in chapter 1.1, the main motivation behind this thesis is to provide new, continuous, high resolution palaeoenvironmental records for southern Greece. They should originate from geoarchives in close vicinity to archaeologically important sites like Mycenae, Tiryns, or Delphi to allow for interdisciplinary research on human-environmental interaction. Thereby, the primary focus is less on quantitative changes in climate parameters, but more on a reconstruction of lake ecosystem processes and to decipher the interaction of different forcing factors – natural and anthropogenic. Based on these records, the thesis aims at contributing to the debate on human-environmental interaction and on climate as one potential influential



factor on human decisions and land use activities. This proceeding may add new insights to broader research questions such as: When did human influence on their surrounding environment start? How did humans form their surrounding landscape? To which extent did climate variability influence societal developments?

The following research questions were predominantly addressed within the scope of this project:

- How did humans and their environment interact on the NE Peloponnese? How are changes in land-use and land cover reflected in the sedimentological records, and how did these changes influence sedimentation and erosion processes? (cf. Appendix I, V)
- When can we detect changes in water availability within the geochemical and sedimentological record and how do these periods correlate with climatic changes or the archaeological record and land use practices? (cf. Appendix I, II, III)
- Can we use the same geochemical ratios for each site as palaeoenvironmental proxies to increase our understanding of past climate conditions in the regions and can we further quantify the scale of climatic changes in magnitude, timing, and/or spatial distribution and variability within the study area? (cf. Appendix II)

Methodologically, a strong focus was set on creating a transparent working environment in R (R Core Team, 2019) with specific attention given to reproducibility in order to contribute to further understanding, improving and developing the methodological proceeding.

### **1.3 Project frame**

This doctoral thesis was carried out within the framework of the Collaborative Research Centre (CRC) 1266 „Scales of Transformation: Human-Environmental Interaction in Prehistoric and Archaic Societies”, funded by the German Research Foundation (DFG). The CRC1266 investigates processes of transformation in a wide array of societal formations and environmental settings on different spatial and temporal scales within the last 15,000 years (Müller and Kirleis, 2019). Within this framework, transformations are defined as „condensed processes leading to a substantial and enduring reorganisation of socioenvironmental interaction patterns“ (Müller and Kirleis, 2019). An interdisciplinary combination of archaeological and palaeoenvironmental tools is used to detect different socio-environmental dimensions of transformations.

The present study was conducted within the scope of subproject E1 „Transformations in early Greek societies and landscapes“ that concentrates on the region around the Gulf of Corinth, notably the NE Peloponnese, Aetolia-Arcania, and Boetia. The main methodological aim of

this interdisciplinary subproject was to close the gap between physical geography, geology, geochemistry, geoarchaeology, and classical archaeology by working with the same research hypotheses and integrating methods of all disciplines to reconstruct changes in the palaeoenvironment and to detect human impact. Temporally, subproject E1 focusses on the transition phase from Late Bronze Age to Early Iron Age in Greece (12<sup>th</sup> to 8<sup>th</sup> century BC), when the Mycenaean palace culture disappeared and small polis states emerged. The reasons for this cultural transformation are still intensively debated (Drake, 2012; Finné et al., 2017; Kaniewski et al., 2019, 2015, 2013; Knapp and Manning, 2016; Middleton, 2010; Weiss, 1982).

For the PhD thesis presented here, Lake Stymphalia, the last remaining natural lake on the Peloponnese, and the adjacent palaeolakes Kaisari and Pheneos were selected for investigation because of their close proximity to important archaeological sites such as Mycenaean, Tiryns or Nemea. These (palaeo)lakes are located in poljes, karst valleys, that don't have a natural surface outflow and they only drain water through katavothres (sinkholes). Thus, they act as terminal sinks for sediment deposition. Hiati in the sediment sequence due to erosion are less likely and a high degree of depositional continuity can be expected (Cohen, 2003). The three poljes form a transect at the southern foot of Mt. Killini/Zyria. Lake Trichonida, in Aetolia-Acarnania, was selected as ultimate study site for this project. It is situated within the subproject's study area and allows to extend the E-W transect of investigated geoarchives to the northern shore of the Gulf of Corinth.

#### **1.4 Outline of the thesis**

This thesis is organised in nine chapters. The introduction chapter 1 summarises the motivation and research aims for the project itself and its embedding in the CRC 1266. Chapter 0 presents an overview of the state of the art in studying lacustrine sediments as palaeoenvironmental archives and of available Holocene geoarchives in southern Greece. Chapter 3 provides a description of the study area. All methods applied within the scope of this research are shortly presented in chapter 4. Further details are given in the material and methods sections of the respective manuscripts.

This doctoral thesis is based on three first author publications (Appendix I – III), focussing on palaeoenvironmental reconstruction within the different investigated lake catchments, as well as on three additional publications (Appendix IV – VI), that include further works that resulted from the first or slightly extended the framework. Each manuscript is provided as an appendix and the main findings are summarised in chapter 5. Appendix I deals with human-environmental

---

interaction at Lake Stymphalia during the last 2,500 years. Appendix II compiles geochemical data from four different lake catchments from the Peloponnese into a multi-archive study. Appendix III describes climatic variation during the last 2,600 years at Lake Trichonida. Appendix IV is a technical manuscript that deals with a methodological procedure to compile a master sediment core. Appendix V presents a spatial model that investigates how much land was required to supply a society with basic necessities and what happened when environmental conditions changed. Appendix VI is the first publication from the International Ocean Discovery Programme (IODP) Expedition 381, where I was a member of the science team, and depicts palaeoenvironmental fluctuations at the Gulf of Corinth during glacial and interglacial cycles. Additional results, that were obtained within the scope of this PhD research project but that were not used for any of the manuscripts, are provided in chapter 6. Chapter 7 contains a synthesis of the conducted research and chapter 8 provides an outlook on potential follow-up research. A final conclusion of the conducted investigations is given in chapter 9.

## 2 Lacustrine sediments as palaeoenvironmental archives

### 2.1 Lakes as geoarchives

Lake deposits are accumulated sediments from their surrounding environment and provide geoarchives that allow to study a continuous ecosystem history over a long duration and highly resolved in time (Bradley, 2015; Cohen, 2003). Every lake is unique and has its own variety of external and internal forcing variables that influence its history, such as climate, geological bedrock composition, vegetation cover, tectonic activity, aquatic biota, or human activities (Cohen, 2003). Naturally, the selection of the lake, the length of the obtained sediment core, and the accumulation rate define the possible scope of research with respect to the time period covered and the temporal resolution (Cohen, 2003). The aim of the palaeolimnologist is to study, decipher, and understand the sedimentary archive to be able to reconstruct its history. In order to do so, he analyses specific „content archives“ (Cohen, 2003) to obtain proxies that represent changes in specific forcing variables over time. A variety of geochemical and palaeoenvironmental indicators is preserved in lake sediments and can be used to investigate specific processes and conditions in the lake itself and in its catchment. Thereby, it is essential to disentangle the natural underlying factors from anthropogenic influence (Bradley, 2015).

The lake sediments consist of allochthonous and autochthonous material. Allochthonous material enters the lake from outside and is transported by erosional, fluvial, or aeolian processes, while autochthonous material is produced within the lake through inorganic precipitation or from biogenic origin (Bradley, 2015).

When studying questions related to human-environmental interaction, lake sediments are generally more suitable than marine archives, because lakes are smaller and respond more quickly to changes in forcing variables. They are generally more proximal to archaeological sites, they receive the material from a smaller catchment, and they deposit it with a higher accumulation rate (Cohen, 2003). Thus, the signal is generally higher resolved and less smoothed compared to marine deposits. At the same time, a lag may occur if the proxy, so the climate-dependent phenomenon, lags behind the climate perturbation or records abrupt changes as gradual transitions (Bradley, 2015). Furthermore, local, small scale interferences in the catchment of a small lake will be more visible and may overlay potential overregional, meso- to macro-scale climatic signals. Depending on the research questions, this may be an advantage or disadvantage and it is important to carefully choose an appropriate lake and subsequently consider suitable proxies with an appropriate resolution (Cohen, 2003).

## 2.2 Proxies for palaeoenvironmental reconstruction

Lacustrine sediments preserve a wide range of information in the form of the geochemical composition, microfossil assemblages, isotopic composition, organic matter content, or other components that need to be interpreted and allow the reconstruction of palaeoclimatic and palaeoenvironmental history (Blaauw et al., 2019). Each proxy has its individual position in an ecosystem and may be used to reconstruct different facets (Birks and Birks, 2006). Proxy variations over time may be interpreted as a result of climatic changes, but the signal may also be affected by other factors, such as human influence, and thus the different forcing factors need to be identified and separated in order to reconstruct changes in the palaeoenvironmental conditions and ideally quantify the climate-related component (Izdebski et al., 2016).

The geochemical composition of sediments depends on their geological origin, on the environmental conditions during which they weathered, eroded, and deposited, and potentially on diagenetic modifications (Cohen, 2003). The varying amount of clastic material in the sediment, for example, may explain shifts in erosional processes within the catchment area. Changes in the grain size distribution may be used among others as a proxy for transport energy of allochthonous material into the lake. The relation of organic matter to nitrogen content provides evidence of the varying amount of biota that have lived in the lake and its catchment (Meyers, 2003; Meyers and Ishiwatari, 1993). Changes in the sediment colour spectrum may also be investigated as an indicator for changes in the sedimentary conditions. Organic rich sediment, e.g. indicating more anoxic conditions at the sediment-water-interface, is usually darker than organic-poor or carbonate rich sediment, which generally has a brighter colour, while reddish colours usually hint towards the presence of iron oxides (Lucke et al., 2015).

## 2.3 The use of XRF scanning in palaeoenvironmental research

Since the late 1990s, X-ray fluorescence (XRF) core scanning is an increasingly applied method for the analysis of the chemical composition of sediment cores (Croudace et al., 2019a; Croudace and Rothwell, 2015; Jenkins, 1999; Ramsey et al., 1995). It is a fast, non-destructive technology to obtain high resolution, multi-element profiles from numerous core sections from marine and lacustrine environments (Boyle, 2000; Croudace et al., 2019a, 2019b, Löwemark et al., 2019, 2011). As the discipline is still rather young, new areas of application constantly develop (Croudace et al., 2019b). Two main communities exist that work with different commercially available XRF core scanners: Itrax and Avaatech (Croudace et al., 2019a, 2006; Richter et al.,

2006). In the scope of this thesis, an Avaatech core scanner was used; technical details are provided by Richter et al. (2006).

X-rays, produced by a radioactive source irradiate atoms in the sample. Electrons within the atoms get excited and are ejected from the inner shell. This creates an initial vacancy that is quickly filled up by electrons from outer shells, meanwhile emitting their excessive energy. By measuring this surplus energy, emitted as fluorescence energy, one can detect which elements are present in the sediment, as the collection of emitted wavelengths is specific for every element. The system is mounted in a vacuum chamber flushed with helium gas that allows the analysis of light elements, whose low-energy radiation would otherwise be absorbed by the air. The theoretical basis of XRF analysis is presented in more detail for example by Jenkins (1999) and Jenkins and De Vries (1970).

XRF core scanning yields semi-quantitative results, in the form of element intensities measured in counts per second (cps), due to the inhomogeneity and varying matrix effects of the scanned material and the non-constant measurement geometry (Bloemsma, 2015; Bloemsma et al., 2012; Tjallingii et al., 2007). It is thus mainly applied as a qualitative tool, although there are different calibration and quantification approaches (Barrett et al., 2017; Weltje et al., 2015; Weltje and Tjallingii, 2008). By normalizing elements against the total number of element counts or against a conservative element – Ti is often used in this context – or by applying a log-ratio transformation on elemental ratios, one can reduce or even circumvent these challenges as well as closed-sum effects and the results become comparable to conventional geochemical analysis (Löwemark et al., 2011; Weltje and Tjallingii, 2008). Down-core patterns of elemental ratios are unaffected by variations in the concentrations of other elements and are thus a useful tool to detect palaeoenvironmental changes and answer a wide range of environmental research questions (Löwemark et al., 2011).

## 2.4 Chronology and dating

The reconstruction of palaeoclimatic and palaeoenvironmental changes along lake sediment cores becomes more relevant when the information can be converted from a depth scale into a time scale. Although the true calendar ages of a core's dated depths will never be known, one can receive a robust and reliable approximation of the unknown true accumulation history of the site, depending on the type of age-depth curve applied (Blaauw, 2010). The accurate dating of the sediment sequence is thus an essential requirement to obtain a valuable, high-resolution palaeoenvironmental archive (Birks and Birks, 2006; Bradley, 2015).

The fundamental assumption of age-depth relation in sediment deposits assumes that in an undeformed sequence, sediments continuously become younger from bottom to top. Relative age information can already be useful or even very precise, as is the case of annually laminated sediments (Bronk Ramsey, 2008a; Zolitschka et al., 2015). Areas with higher sedimentation rates generally provide a higher resolution (Bradley, 2015).

Different dating methods exist that provide numerical or relative ages (Bradley, 2015). Sediments containing organic carbon deposited during the last approximately 40,000 years are mostly dated using the radiocarbon method (Bradley, 2015). Radiocarbon dating is based on the fact that radioactive  $^{14}\text{C}$  decays and if the storage is not replenished, e.g. because the organism died, the isotope concentration diminishes with a half-life of approximately  $5730 \pm 30$  years (Bradley, 2015). Measuring the concentration of the remaining  $^{14}\text{C}$  gives a numerical age. The principles of this method were developed by Libby et al. (1949).

There are variations in the atmospheric production of  $^{14}\text{C}$  over time and radiocarbon and calendar years have a non-linear relationship; hence, the measured radiocarbon ages need to be calibrated with an appropriate calibration curve to indicate calendar ages (indicated in cal BP). For terrestrial material from the northern hemisphere, this is currently done based on the IntCal13 calibration dataset (Reimer et al., 2013). In some cases, further corrections need to be applied. For example, when a considerable amount of „old“, reworked inorganic carbon is present, the radiocarbon date needs to be corrected for its reservoir age or it would indicate too old ages. This is often the case in marine environments or in limestone rich environments (Grootes et al., 2004; Keaveney and Reimer, 2012; Siani et al., 2000). Notably due to the limestone rich environment, „adequate“, “high-resolution” chronological control in the eastern Mediterranean region is extremely challenging (Finné et al., 2011; Finné and Weiberg, 2018; Knapp and Manning, 2016).

Classical age-depth models have long been using linear interpolation or linear/polynomial regression (Blaauw, 2010). For a little more than a decade now, more elaborated methods based on Bayesian statistics and iterative sampling are more commonly applied (Bronk Ramsey, 2008a). They combine expertise on the sedimentary processes and the dating context with statistical likelihood. This method does not only fit a curve through the dated points, but includes underlying processes such as the accumulation rate or lithological unit boundaries and is thus environmentally more realistic (Blaauw and Christen, 2011). Different tools exist that build chronologies based on Markov chain Monte Carlo (MCMC) algorithms such as Oxcal, Calib, Clam, or Bacon (Blaauw, 2010; Blaauw et al., 2019; Blaauw and Christen, 2011; Bronk Ramsey, 2008b; Stuiver and Reimer, 1993). The latest development in this area was the *rbacon* package

(Blaauw and Christen, 2011). Blaauw and Christen (2011) point out that the methodology produces reasonable interpolations in low-density dated cores. Similar to the P<sub>2</sub> sequence in Oxcal (Bronk Ramsey, 2008a), the core is divided into equally spaced slices (K), but the number of iterations in *rbacon* is determined by a self-adjusting MCMC algorithm. In this model, outliers are automatically excluded from the modelling process. Lithological changes and potential hiatus or turbidites can also be considered. Additionally, it is possible in *rbacon* to compile independent age information such as historical dates, or volcanic eruptions, preserved as tephra layers in the core.

## 2.5 Geoarchives recording Holocene climate variability in Greece

The Holocene time period is considered as one of stable climate conditions compared to longer geological time scales and temperature changes are smaller and more subtle than during the Pleistocene (Birks and Birks, 2006).

Finné et al. (2011) showed that, at the time of the investigation, only very few geoarchives existed in southern Greece with a sufficient resolution for the Late Holocene and these archives exhibited considerable gaps or heterogeneous results, which is inadequate when palaeoenvironmental changes shall be compared to human development. Since the publication of this study, a handful of palaeoclimatic and –environmental studies on geoarchives from Greece have been added to the record, contributing to improving the picture. Climate reconstructions for different periods during the Holocene based on speleothems exist from the Skala Marion Cave on Thassos island (Psomiadis et al., 2018), Kapsia Cave (Finné et al., 2014), Alepotrypa Cave (Boyd, 2015), and Mavri Trypa Cave (Finné et al., 2017) on the Peloponnese. Palaeoenvironmental dynamics have been identified in lagoonal sediments from Gialova (Katrantsiotis et al., 2018), Aliko (Avramidis et al., 2013; Emmanouilidis et al., 2019), and Etoliko (Haenssler et al., 2013). The marine M2 record was combined with socio-environmental investigations (Gogou et al., 2016). And a few limnic sediment cores have been studied for Late Holocene changes from Lake Lerna (Katrantsiotis et al., 2019), the Asea valley (Unkel et al., 2014), and the Agios Floros fen (Katrantsiotis et al., 2015; Norström et al., 2017).

Recently, Finné et al. (2019) published a synthetic reconstruction of hydro-climatic variability in the Mediterranean for the period 10,000 BP to present based on 44 published geoarchives. Only two of the above mentioned studies (Mavri Trypa and Agios Floros) have been included. For the Balkan region, including Greece, their climate reconstruction carefully depicts the following trends for the last 5,000 years. A drying trend reaches its peak around 4,900 BP but continues until



2,500 BP. A short wetter period (4,500 – 4,100 BP) interrupts this general trend. The period from 2,500 to 1,900 BP is also characterised by slightly wetter conditions. It is finally replaced by a clear trend toward drier conditions until present times. However, Finné et al. (2019) admit that the identification of regional climate patterns for this study area remains challenging and shows high uncertainties and very heterogeneous patterns. For example, for the time around 4,900 BP, the Peloponnesian archives clearly indicate wetter conditions contrary to the remaining Balkan region (Finné et al., 2019). Additional high-resolution geoarchives are thus needed to evince the spatio-temporal variability in the climate patterns.

### 3 Study area

#### 3.1 Geographical setting

This chapter provides an overview on the topographic setting in southern Greece and introduces the studied lakes. For more detailed information on the respective lake sites, the reader is referred to the publications Appendix I – III (Figure 1).

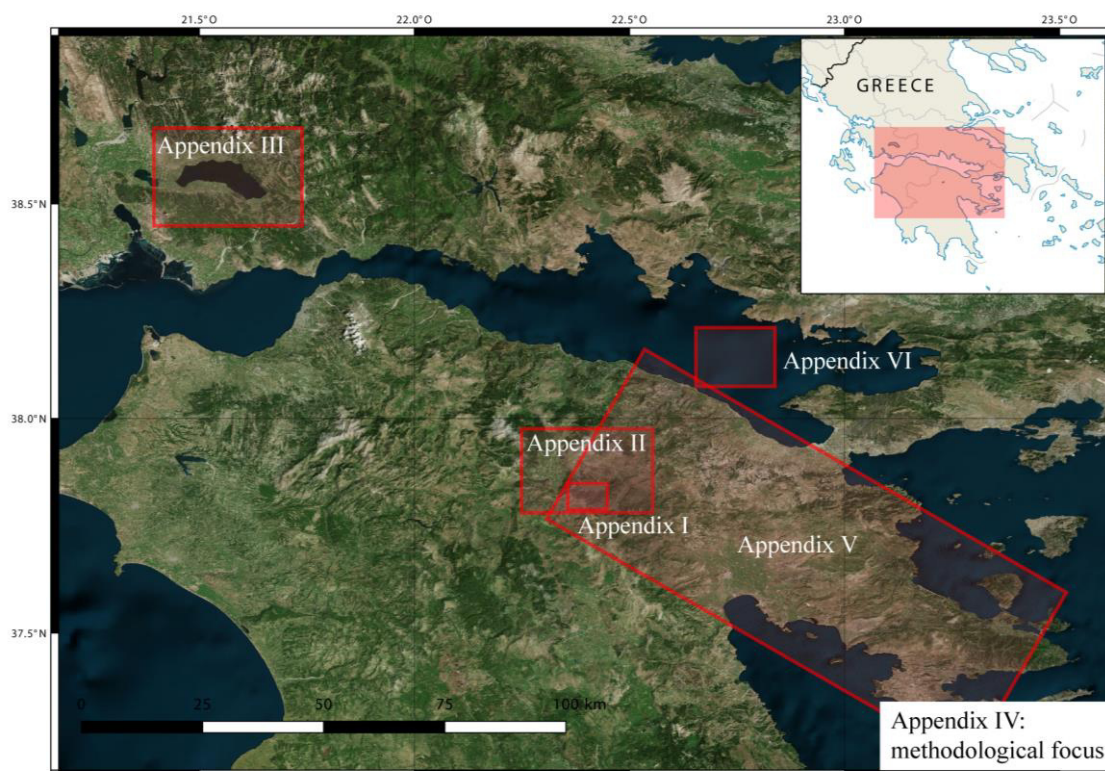


*Figure 1: The location of the study area in southern Greece. The red rectangles show the focus areas covered in the respective manuscript. The map was created using QGIS 3.6.3. (QGIS Development Team, 2019, map data: Esri).*

The surface area of Greece can be divided into northern mainland Greece, the southern Peloponnese peninsula and the numerous islands. The Peloponnese is separated from the mainland by the Gulf of Corinth, an active rift basin (Bell et al., 2009; Lisa C. McNeill et al., 2019; Moretti et al., 2003). Two thirds of the territory are mountainous, making Greece one of the most mountainous countries in Europe. The Pindos mountain range, cutting the country from north to south, is a considerable morphological barrier and also orographically affects the regional climatic conditions (Xoplaki et al., 2000). Archaeological remains are abundant in southern Greece, which mirrors the long history of human activity in the area extending back to the Palaeolithic (Bintliff, 2012).

The study area is located in southern Greece with the Gulf of Corinth in its centre and encompasses four lake basins (Figure 1,2). Three of the four investigated lake basins are situated in the north-eastern part of the Peloponnese peninsula. They surround the southern slopes of Mt. Ziria/Kyllini (2,360 m a.s.l.). The fourth, Lake Trichonida, is located on the north-western shore of the Gulf of Corinth.

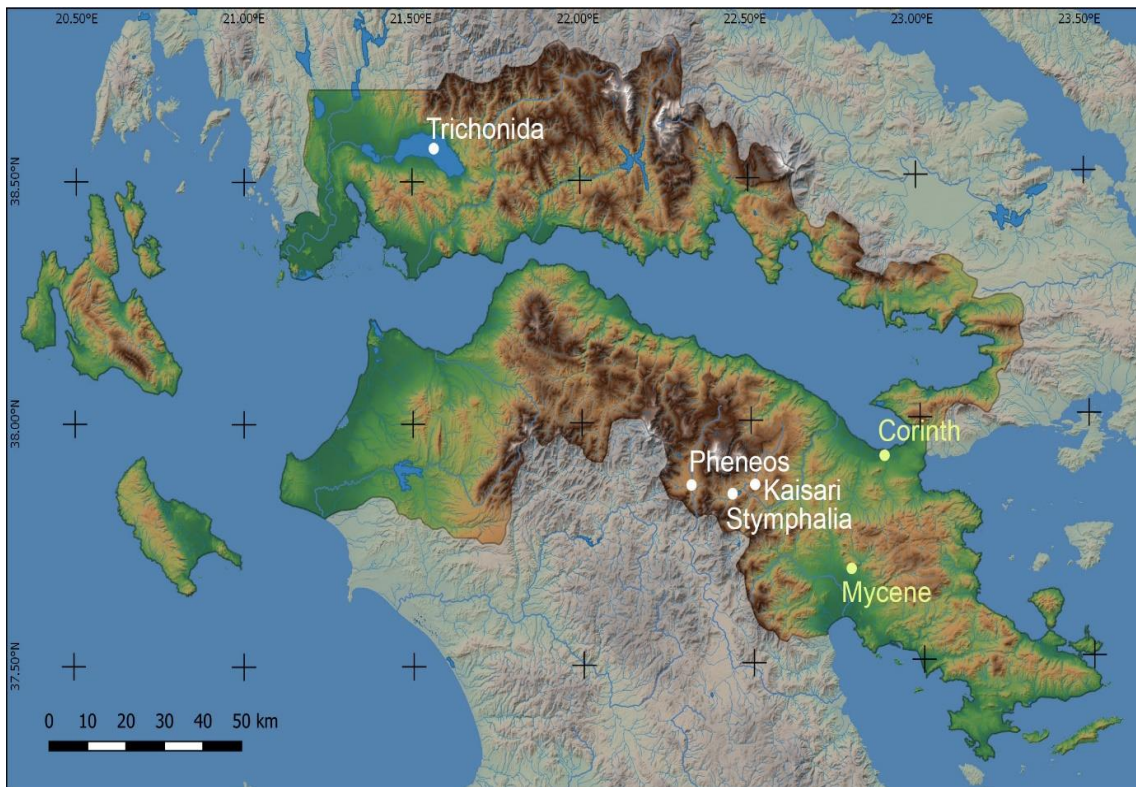


**Figure 2: Topography of the study area of the CRC1266 E1 subproject. The four lake sites investigated in this PhD project are indicated in white. For orientation, archaeologically important sites in the area are indicated in light yellow (map: T. Kessler).**

### 3.2 Geological setting

Greece is characterised by high seismo-tectonic activity and a highly complex geological structure shaped by complex interactions of different tectonic plates (Morfis and Zojer, 1986; Taymaz et al., 2007; Voudouris et al., 2007 and references therein). Major fault systems in the study area are strongly linked to relative movements between the African and the Eurasian plates as well as between the Aegean and Adriatic microplates. Notably the counter-clockwise rotation of the African plate and its subduction below the Eurasian plate, and more specifically below the small Aegean Plate, caused considerable tectonic deformation in the east Mediterranean-Alpine region (Kokinou et al., 2005). For Greece, the subduction zone at the Hellenic Arc is of main importance (Taymaz et al., 2007). Temporally, the Alpine orogenesis had the most formative influence on the modern setting. The mountain ranges shaping the present morphology of the Greek territory are remains of different basins of the Tethys Ocean that were incorporated into the Hellenide fold-and-thrust belt and uplifted (Kokinou et al., 2005; Morfis and Zojer, 1986). Major faults striking E-W cut through the active rift system of the Gulf of Corinth and cause the basin to expand (Gawthorpe et al., 2018; Taymaz et al., 2007). Active and inactive major and minor faults are present all along the northern and southern margins of the basin. The tectonic and stratigraphic development of this young, active rift and its evolution are studied within the scope of the IODP Expedition 381 (McNeill et al., 2019; Appendix VI, Chapter 6.4).

A detailed presentation of the Greek geotectonic zones and geological formations is given for example by Morfis and Zojer (1986). For the study area, the most relevant formations are the Gavrovo-Tripolis and the Olonos-Pindos Zone (Morfis and Zojer, 1986; Unkel et al., 2011), as they form the mountainous catchments, which provide sedimentary input to the studied lakes (figure 2). Due to its morphogenesis, the bedrock in the study area is strongly dominated by limestone. The Olonos-Pindos unit is mainly composed of sediments of pelagic facies, limestones, radiolarites, and marls, while the Gavrovo-Tripolis zone consists of sediments of neritic facies, phyllites, limestones and flysch (Morfis and Zojer, 1986; Unkel et al., 2011). Weathering of the carbonaceous bedrock produces a karstic landscape including poljes, dolines, katavotres, and caves (Vött et al., 2009). The high seismo-tectonic activity in the area causes frequent earthquakes of different intensities (Taymaz et al., 2007), which may be an influential factor to keep in mind when reconstructing palaeoenvironmental development from lakes in the area, because they may cause mixing or rapid displacement of the sediment such mass movement events.

### 3.3 Climatic setting

Greece is situated in a transitional climate zone between the westerly winds in the north and the arid subtropical high pressure system in the south (Psomiadis et al., 2018; Xoplaki et al., 2003a, 2003b). Due to the heterogeneous topography, the climate can be differentiated into three different types: temperate, mediterranean, and alpine climate. According to the Köppen-Geiger climate classification system (Geiger, 1954; Köppen, 1936), the largest part of Greece belongs to the Csa climate classification, which is described as hot summer mediterranean climate with a strong seasonality of mild, wet winters and warm, dry summers (Köppen, 1936). The alpine climate prevails in the mountainous areas and includes snowfall during winter. Because of the mountainous topography, the mean climate parameters, notably the amount of precipitation, vary strongly depending on the location, topography and altitude (Zacharias et al., 2002). In Agrinio close to Lake Trichonida, the annual temperature averages at 17.0 °C, ranging from 8.6 °C in January to 25.9 °C in July, while in Corinth on the NE Peloponnese, it averages at 17.8 °C (en.climate-data.org, 2019). Precipitation in Greece follows a clear decreasing gradient from west to east and north to south (Xoplaki et al., 2000; Zacharias et al., 2002). Maximum values occur in the western part of the country, mainly due to moist air advection from the west and orographic uplift at the Pindos and Peloponnese mountains. Minima are found in the leeward rain shadow, on the eastern Greek islands, and in the Ionian Sea (Xoplaki et al., 2000). Annual precipitation varies between >1000 mm in the NW of the country and 400 mm in Athens (Skoulikidis et al., 1998; Zacharias et al., 2002). In Agrinio, annual precipitation averages at 917 mm (en.climate-data.org, 2019). In the Stymphalia polje, mean annual precipitation varies around 850 mm and ranges from 719 to 1656 mm for the time period 1975 – 2015, which indicates a high inter-annual variability (Nanou and Zagana, 2018). Seasonal differences are also evident; the largest amount of precipitation occurs in the wet winter period (October to May), with only sparse storm events during the summer months (Finné et al., 2011; Xoplaki et al., 2003a, 2000). The seasonality in Greek climate is influenced by shifts of the inter-tropical convergence zone (ITCZ). In winter, the ITCZ as well as the westerlies shift further southward allowing depressions from the Atlantic to move eastward into the region transporting humidity. In summer, the relocation of the ITCZ to the north causes ascending air over the landmasses in the south and low precipitation or even periods of drought (Xoplaki et al., 2003a).

In addition to latitudinal, altitudinal, orographic and land-sea interactions (Xoplaki et al., 2000), the Greek climate is particularly influenced by large-scale atmospheric circulation patterns, notably the North Atlantic Oscillation (NAO) and the East Atlantic/Western Russian (EA/WR)

pattern (Barnston and Livezey, 1987; Gogou et al., 2016; Krichak and Alpert, 2005). While the influence of the NAO in the eastern Mediterranean has recently been investigated more intensively (Benito et al., 2015; Katrantsiotis et al., 2019; Longman et al., 2017; Perçoiu et al., 2017; Roberts et al., 2012; Warken et al., 2018), studies on the influence of the EA/WR pattern remain rather sparse (Krichak and Alpert, 2005; Lim, 2015). The NAO influences the climate variability pattern on a decadal scale mainly during winter (Katrantsiotis et al., 2019; Nieto-Moreno et al., 2011). Opposite to the conditions in central Europe, the positive phase of the NAO is associated with dry and cold winters in Greece, while during negative phases of the NAO wetter and warmer conditions prevail (Katrantsiotis et al., 2019; Nieto-Moreno et al., 2011; Xoplaki et al., 2000). The EA/WR teleconnection is likewise more active in winter (Krichak and Alpert, 2005). Negative EA/WR phases are connected with higher precipitation in the eastern Mediterranean. Winter months with positive EA/WR are associated with drier conditions due to the advection of air masses from central Europe (Barnston and Livezey, 1987; Krichak and Alpert, 2005; Lim, 2015). These interconnections are subject of the discussion in Appendix III. As southern Greece is affected by changes in more than one atmospheric circulation pattern, it is assumed that even slight changes in one of these teleconnections have implications on the study sites and thus make them a potentially suitable and valuable climate archive recording extensive climatic variations. As precipitation is one of the key parameters of the regional climate, because it plays a crucial role in agriculture, the management of water resources, and the ecosystems (Xoplaki et al., 2000), the reconstruction of palaeohydrological fluctuations is of particularly high asset for the region.

### **3.4 Vegetation and soils**

Vegetation is strongly affected by climate, topography, soils, and land use. The floral biodiversity in Greece is high, rich in endemics, and as heterogeneous as the landscape (for an introduction see Griffiths et al., 2013; Thompson, 2005). Furthermore, the succession of natural vegetation zones has strongly been modified by human impact since the Mid Holocene, for example by deforestation, crop cultivation, or managed grazing activities (Bintliff, 2012). All investigated lake catchments have in common, that nowadays agricultural ecosystems are dominating the areas. The lowlands and flat areas, e.g. the *polje* floors, are almost entirely used for agricultural fields. The former lakes Kaisari and Pheneos were purposely drained and transformed into fertile agricultural land around the turn of the 19/20<sup>th</sup> century. Most of the slopes show signs of terrace agriculture or abandoned terraces, some of which were in use until the mid

20<sup>th</sup> century. This suggests strong deforestation and anthropogenic landscape transformation at one point in the past to enable the use of this area (this issue is addressed in Appendix I). Some slopes have naturally or antropogenically been reforested in the last century (Bintliff, 2012). Most of the upper slopes, that are more difficult to access, are covered by Mediterranean evergreen or coniferous woodland or maquis vegetation.

The catchment area of Lake Trichonida is situated in a transitional zone between Mediterranean and deciduous forest; it is covered by pine, fir, oak, and Greek maquis shrubland, dominated by prickly oak bushes, and the lowland is used for agriculture (Bottema, 1982; Koussouris and Diapoulis, 1982). A pollen study by Bottema (1982) indicates some modern and past species composition.

An analysis of modern land cover in the Stymphalia polje was conducted by Papastergiadou et al. (2007) and yields more detailed information on species prevalence. Lake Stymphalia itself has an increasing reed coverage of *Phragmites australis* and only few remaining areas of open water (Papastergiadou et al., 2007). The surrounding polje floor is intensively covered by agricultural land. Tree species that can be found in the wetter areas are *Salix alba* and *Populus alba* (Papastergiadou et al., 2007). Land use on the slopes can mainly be classified as „Garrigues“ or maquis, dominated by scrub species of *Quercus coccifera*, *Pistacia lentiscus* und *Cistus spp.*, and the arboreal areas in the catchment are dominated by the endemic species *Abies cephalonica* (Papastergiadou et al., 2007). During modern climate conditions, the Stymphalia polje is too cold for growing wine, olives, or citrus fruits. In the neighbouring Nemea region however, viticulture is an important economic sector, and also in the proximal Phlious polje, vine and olive trees grow (Fuchs et al., 2004). This shows that marginal climatic changes would be sufficient to enable the cultivation of these plants in the Stymphalia polje and it would be interesting to investigate if palynological studies indicated the growth of these species already in the past, which would allow to draw conclusions on the palaeoclimatic conditions. However, palynological screenings of sediment samples from Lake Stymphalia core STY1, conducted by Oliver Nelle and Katerina Kouli in 2011 and 2018 respectively, revealed that pollen preservation was extremely bad due to the predominately hot, dry, and alkaline environmental conditions in the catchment (Nelle, Kouli, personal communications). Pollen counts in the screening often remained below the minimum of 300 grains/sample. Hence, no palynological study on Lake Stymphalia could be completed up to now.

Nowadays, some populations of endemic or endangered fauna species are negatively affected by the strong human impact on the natural environment. This holds particularly true for Lake

Stymphalia, although the polje is protected under the Natura 2000 regulations (Papastergiadou et al., 2007). The area surrounding Lake Trichonida is likewise part of the Natura 2000 Environmental protection network (Dimitriou and Zacharias, 2006). The vegetation density in the catchment area is an important influential factor, when studying lake sediments, because it acts as a protective cover and reduces allochthonous sediment input (this issue is taken up in Appendix I).

Very little information exists on soils in the study area. The semi-arid climate usually prevents the soils from developing elaborate profiles of great depth. Additionally, they strongly depend on the underlying parent rock and thus one would expect the presence of calcareous soils such as rendzina. For the lake catchments on the NE Peloponnese, Nanou and Zagana (2018) identify leptosol as the dominant soil type. For many slopes in the area, soils are very thin or completely absent, indicating strong (human induced) soil erosion (Fuchs et al., 2004; Vött et al., 2009). At erosion-protected sites, remnants of former red and brown Mediterranean soils can be found (Fuchs et al., 2004). More research on this topic is needed and is currently undertaken for the Stymphalia polje in the scope of a thesis by Thomas Birndorfer.

### 3.5 Site descriptions

Greek lakes originate from a combination of tectonic activity and the dissolving activity of water infiltrating into carbonate rocks. Hence, most of the natural lakes are situated in the karstified calcareous zone (Skoulikidis et al., 1998; Zacharias et al., 2002). Due to the hard and eutrophicated karstic waters, Zacharias et al. (2002) assume that a considerable amount of phosphate is absorbed to the calcite minerals and stored in the sediments, explaining the low amount of phosphate in the water column. The withdrawal of water and the run-off from agricultural activities both have an increasing effect on the water quality (Zacharias et al., 2002) and in the case of Lake Stymphalia even threaten its existence. Only very few Greek lakes have depths greater than 50 m and many shallow lakes only exist periodically (Zacharias et al., 2002). The three Peloponnesean lakes are located in karst poljes, which are defined as „an intra-mountainous tectono-karstic depression[s] in a limestone region which [are] cut off from the superficial drainage network“ and thus represent a suitable sink for sediments (Vött et al., 2009). An overview on Greek lakes is given by Zacharias et al. (2002).



*Table 1: Mean or approximated values for the main morphometric features of the modern investigated lakes (modified after Zacharias et al., 2002).*

lake	lake level [m a.s.l.]	lake area [km <sup>2</sup> ]	catchment [km <sup>2</sup> ]	volume [10 <sup>6</sup> m <sup>3</sup> ]	mean depth [m]	maximum depth [m]	retention time [years]
Stymphalia	600	3.8	219	5	1.3	2.3	-
Trichonida	18	96.5	421	2927	30.3	58	9.4

### 3.5.1 Lake Stymphalia

Lake Stymphalia (Λίμνη Στυμφαλία), in the NE Peloponnese, is the largest and last remaining natural lake on the peninsula. It covers an area of approximately 4 km<sup>2</sup> with an average water depth of only 1.3 m, which makes it comparatively easily accessible. The size of the lake area may vary considerably over the year. As the lake is very shallow, the water column is well oxygenised throughout the whole year and it may freeze in winter. Periodically, the lake may even dry out completely. The lake has no surface outflow; instead, water drains through katavothres, evaporates, drains through the Hadrianic Aqueduct, or is pumped away for agricultural use (Papastergiadou et al., 2007). It is susceptible to eutrophication and has high biological activity (Papastergiadou et al., 2007). Lake Stymphalia is an important refuge site for migratory birds and it is home of the endemic fish species *Pseudophoxinus s. stymphalicus* and the sub-species *Leuciscus cephalus peloponnensis* (Papastergiadou et al., 2007). Although the area is protected by the NATURA 2000 Network, it shows increasing environmental degradation (Papastergiadou et al., 2007) and its continued existence is at risk.

Lake Stymphalia is already known from Greek mythology, where Herakles exterminated the Stymphalian birds (Unkel, 2019). Human settlement in the region is proven at least since Antiquity – remainings of old Stymphalos date back to the 4<sup>th</sup> century BC – but there are indications that anthropogenic influence in the area might have begun much earlier (Walsh et al., 2017). The study site is extensively described in Appendix I.

### 3.5.2 Palaeolake Kaisari

Palaeolake Kaisari is situated in the Kaisari polje east of the Stymphalia polje. A lake is described for the southern end of the polje (Lolos, 2011), but it was purposely drained at the beginning of the 20<sup>th</sup> century to obtain land for agricultural use. References in the literature referring to this lake are sparse and don't even use a common name. Morfis and Zojer (1986) call it „valley of Klimenti“ and address it as part of the Stymphalia polje, as the two poljes are nowadays connected by an artificial tunnel (figure 3). For this research project, it was agreed to term it „Kaisari“ according to the largest village in the polje (Καισάριο). No archaeological sites are known from the polje. A more detailed description of the study site can be found in Appendix II.

### 3.5.3 Palaeolake Pheneos

Palaeolake Pheneos is situated in the western neighbouring polje of Lake Stymphalia. With 215 km<sup>2</sup>, it is the largest of the three studied poljes and can be divided into an eastern and a western bay (Morfis and Zojer, 1986). Similar to the Kaisari polje, the lake, which was located in the south of the polje, was drained in the 20<sup>th</sup> century for agricultural purposes. Palaeo-shorelines at the southeastern end of the polje (figure 3) may indicate high lake level stands in the past (Appendix II). Human activity in the area was studied by archaeologists of the University of Graz, Austria. An early settlement was found at the archaeological site of Archaia Pheneos, dating to the Middle Helladic Period (2100 – 1700 BC / 4050 – 3650 BP)(Erath, 1999; Tausend, 1999). To date, palaeolake Pheneos has not been investigated as geoarchive, although the polje received quite some attention, especially when Knauss (1990) set up vague theories about hydraulic engineering projects that potentially could have been realised during Mycenaean times. The study site is presented more extensively in Appendix II.

### 3.5.4 Lake Trichonida

Lake Trichonida (Λίμνη Τριχωνίδα) is the largest natural lake in Greece. We follow the new Greek terminology and call it Lake Trichonida, while other studies often refer to it under the old Greek name Trichonis, in various spelling variations, or even Lake Vrakhori (Albrecht et al., 2009). The lake covers approximately 97 km<sup>2</sup> and is up to 19 km long and 6 km wide, stretching in W-E direction. It has a mean depth of 30.3 m and a maximum depth of 58 m (Zacharias et al., 2002). Lake Trichonida lies within a tectonic graben and mainly evolved due to tectonic activity (Albrecht et al., 2009; Zacharias et al., 2002). It can be classified as a warm monomictic, karstic

lake (Zacharias et al., 2002). Due to its extent and depth, it never freezes, and it exhibits a pronounced thermal stratification throughout most of the year. In summer, oxygen depletion may occur at the sediment-water interface (Zacharias et al., 2002). The lake level may fluctuate by approximately 1 m over the year (Albrecht et al., 2009). Due to the karst aquifers dominating the hydrological environment, the lake shows very low conductivity values (ca. 40  $\mu\text{S}/\text{cm}$ ) and high water residence times (ca. 9.4 years)(Zacharias et al., 2002). The water is slightly alkaline with pH values averaging at 8.1 (Zacharias et al., 2002). Annual Secchi disc values are very high, ranging from 8.5 m to maximum 15.8 m and chlorophyll-a content is quite low (2.3  $\text{mg}/\text{m}^3$ ) (Zacharias et al., 2002), which hints towards oligotrophic conditions in the lake. While other larger Greek lakes deal with eutrophication in summer, this phenomenon does not occur in Lake Trichonida (Zacharias et al., 2002). Appendix III elaborates further on Lake Trichonida.

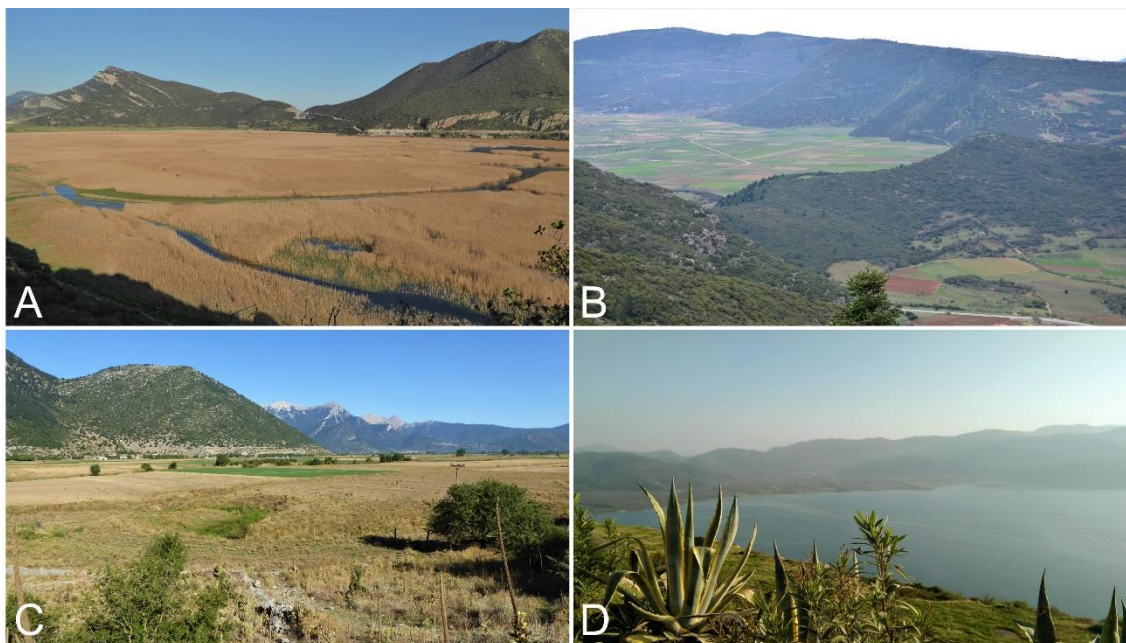


**Figure 3: Impressions of the four lake sites. (a) Lake Stymphalia with its intensive reed vegetation. View from acropolis hill to NE (photo: J. Seguin, April 2017) (b) Hill chain between the Kaisari polje (upper left) and the northernmost part of the Stymphalia polje. The outflow of the artificial tunnel connecting both poljes is visible in the bottom right corner. View to the NE (photo: I. Unkel, April 2017). (c) The southeastern bay of the Pheneos polje. Palaeo-shorelines visible on the slope in the back. A canal, in the centre, leads towards the Heracles katavothre to the right. View to the NW (photo: J. Seguin, August 2019). (d) The eastern edge of Lake Trichonida. View from Petrochori to S (photo: J. Seguin, April 2018).**

## 4 Material and methods

Within the frame of the thesis, a number of destructive and non-destructive methods was applied. To facilitate the comparability between the different lake sites, the sampling, sample preparation and methodological proceeding remained the same for every sediment core, if not stated otherwise. However, not every analysis was applied for every sediment core (cf. table 2) and the applied methods are itemised and described in more detail for each study site individually in Appendix I – III. As the methodological focus of this work lies on XRF core scanning, this method is discussed in higher detail (cf. chapter 4.2.4).

*Table 2: Summary of contributors to field and laboratory works for each study site.*

	<b>Stymphalia</b>	<b>Kaisari</b>	<b>Pheneos</b>	<b>Trichonida</b>
<b>Fieldwork</b>	C. Heymann, I. Unkel	J. Seguin, I. Unkel, P. Avramidis, A. Emmanouilidis	J. Seguin, I. Unkel, P. Avramidis, A. Emmanouilidis	J. Seguin, I. Unkel, W. Dörfler, P. Avramidis, A. Emmanouilidis
<b>Core Correlation</b>	C. Heymann, I. Unkel, J. Seguin	J. Seguin, I. Unkel	J. Seguin, I. Unkel	J. Seguin
<b>Lithological description</b>	C. Heymann, I. Unkel	J. Seguin, I. Unkel	J. Seguin	J. Seguin
<b>C<sup>14</sup> Sampling</b>	C. Heymann, I. Unkel	J. Seguin	J. Seguin	J. Seguin, C. von Scheffer
<b>age-depth modelling</b>	I. Unkel, P. Grootes, J. Seguin	J. Seguin	J. Seguin, I. Unkel	J. Seguin
<b>XRF Scanning</b>	C. Heymann	J. Seguin	J. Seguin	J. Seguin
<b>GSD</b>	C. Heymann	J. Seguin	J. Seguin	J. Seguin
<b>C/N preparation</b>	C. Heymann	J. Seguin	J. Seguin	J. Seguin
<b>LOI</b>	C. Heymann	-	-	J. Seguin
<b>XRD</b>	A. Emmanouilidis	-	-	A. Emmanouilidis

### 4.1 Fieldwork

Within the scope of this project, two field campaigns were conducted in March/April 2017 and in April 2018 to obtain sediment cores from the different sites.



**Figure 4: Coring campaigns. (a) March 2017, coring palaeolake Pheneos with a piston corer (photo: I. Unkel). (b) April 2018, installation of the coring platform at Lake Trichonida (photo: J. Seguin).**

In 2017, sediment cores from the palaeolakes at Pheneos and Kaisari were recovered using a Stitz piston corer system (figure 4a). As both lake sites are drained and covered by agricultural fields and pastures, the coring spots were easily accessible, but due to ploughing the uppermost approximately 50 cm of material were disturbed.

In Pheneos (N 37.85114°, E 22.33510°), two overlapping parallel cores PHE1b (3.90 m) and PHE1c (3.73 m) were retrieved. In the Kaisari polje, two different coring locations were selected: KES1 with a composite length of 4.90 m (N 37.9455861°, E 22.5764139°) and KES2 (N 37.9348667°, E 22.5537028°) with a composite length of 3.50 m. While coring we reached the ground water level already at a depth of only 1 m. At site KES2, we had to stop coring when we reached a layer of very firm, dry clay that we were not able to penetrate with our system. For all overlapping parallel cores, we aimed at a vertical displacement of about 50 cm. The coring system allows for accurate sampling with respect to depth. Horizontal displacement of the parallel cores was kept below 1 m. All cores obtained at these sites were 5.5 cm in diameter. In the scope of this thesis, in Kaisari only core KES2 was analysed in detail, as it was assumed that this coring spot was located in closer vicinity to the depocentre of the former lake and thus was more suitable for palaeoenvironmental reconstruction.

In 2018, a modified Usinger piston corer system was used from a 4 x 4 m floating platform to core Lake Trichonida (figure 4b). The characteristics and the functionality of the coring system are described in detail by Mingram et al. (2007). The advantage of the Usinger system is the possible recovery of a long sediment sequence (up to 120 m), a good depth control and thanks to

the latest improvements an applicability in deep lakes (Mingram et al., 2007). The modification allowed to drill in deeper water depths without casings, as the device works with a pulley system and a funnel that is lowered to the lake floor and allows to thread the coring system always in the same bore hole. Using this system, we retrieved two overlapping parallel sediment cores, TRI1A and TRI1B, with a composite length of 6.50 m, from a water depth of 57 m (N 38.55017°, E 21.5891°). The upper 4.5 m sediment cores have a diameter of 8 cm, while the lowest section was cored with a diameter of 5.5 cm. Two-meter segments were recovered at a time; these sediment cores were directly opened in the field and cut into 1 m long segments for transportation and storage reasons. Due to stormy conditions and technical difficulties, we were unable to core deeper than 6.50 m during this field campaign, although the fine grained sediment would allow for deeper coring and further studies.

Additionally, the 15.5 m long archived sediment sequence of Lake Stymphalia, which was retrieved in 2010 and 2011, was used and provided the starting point of the PhD project. The Stymphalia cores were also retrieved with an Usinger system. Some palaeoclimatic results from the late Pleistocene and early Holocene were published by Heymann et al. (2013). For the project presented here, the uppermost 5 m of STY1 were used. Due to new, additional age data, I re-compiled the upper 5 m of the master sequence STY1 and re-calculated the age-depth model for the upper 3.24 m (chapter 4.3.3, Appendix I). The sedimentological results for the upper 2.08 m are presented in detail in Appendix I.

*Table 3: Sediment cores retrieved, used, or discussed within the scope of this PhD project.*

<b>ID</b>	<b>location</b>	<b>core acronym</b>	<b>coordinates</b>	<b>approx. altitude [m a.s.l.]</b>	<b>year of coring</b>	<b>used/total cored length</b>
1	Stymphalia	STY1	37.84944° N, 22.46056° E	610	2010/2011	324 cm/ 1550 cm
2	Kaisari	KES1	37.94559° N, 22.57641° E	740	2017	None/ 390 cm
3	Kaisari	KES2	37.94558° N, 22.57641° E	730	2017	350 cm/ 350 cm
4	Pheneos	PHE1	37.85114° N, 22.33510° E	710	2017	390 cm/ 390 cm
5	Asea	Asea-1	37.37603° N, 22.26592° E	630	2010	500 cm/ 800 cm
6	Trichonida	TRI1	38.55017° N, 21,58910° E	10	2018	438 cm/ 650 cm

## 4.2 Laboratory work

### 4.2.1 Sampling

While sediment cores from Lake Trichonida were already split open in the field, sediment cores from Pheneos and Kaisari were only opened in the laboratory using a vibration saw and a wire. The archive half was left intact and was only scraped clean and used for non-destructive, high resolution imagery as well as XRF-scanning, while the working half was sampled for discrete measurements. The proceeding was similar for all study sites. All sediment cores are stored at +4°C in a cooling container at Kiel University, Germany.

Priority in sampling was given to suitable material for radiocarbon dating (chapter 4.3.2). Hence, the working halves were initially examined for organic macro-remains and secondly for charcoal particles or blackish coloured layers, that have a higher probability of containing a larger amount of organic carbon. Organic macro-remains were cleaned from sediment before sending off for dating. When none of this was available, bulk sediment samples (approximately 6 – 8 g wet mass) were taken dispersed over the core length.

For regularly spaced proxy samples, extraction of discrete samples concentrated on the main constitute of the composite core sequence (chapter 4.2.2) in the first instance and afterwards replenished with the respective parallel section if necessary. Prior to sampling, the uppermost surface of the sediment half at the respective depth was cleaned and sediment in direct contact to the plastic liner was left untouched or cleared away to avoid or remove possible contamination.

For grain size distribution (GSD) analysis, sampling was conducted systematically at 30 cm depth intervals and if necessary at higher resolution to ensure that every identified lithological unit was sampled at least once. Samples consisted of 0.3 – 1.0 g of wet material. Samples for CN analysis ( $1 \pm 0.1$  g wet mass), were taken in close proximity to the GS samples.

For XRD measurements, conducted for STY1 and TRI1, a minimum of 5 g of wet material were sampled at selected locations. For loss on ignition, only conducted for TRI1, 14 samples of  $14.5 \pm 0.5$  g wet mass were taken at visually chosen spots close to lithological unit boundaries.

### 4.2.2 Composite core construction

In order to obtain a continuous proxy record for each study site, the construction of a composite core profile based on the two overlapping parallel cores is necessary. In the field, directly prior to coring, a preliminary depth was attributed to each recovered core section. A first correlation between the two parallel cores was done visually during the core description in the laboratory. After high resolution imagery of all core segments (chapter 4.2.3), line plots of RGB values of

overlapping sections were used to refine the preliminary correlations. Tie points were identified in both parallel cores, where the master sequence alternates from one core to the parallel one to build the composite profile (Appendix IV).

### 4.2.3 Lithological description

Core description was undertaken on fresh, moist sediment soon after core splitting to avoid post-hoc reactions that may alter the appearance. Sediment structure, Munsell colour (Munsell, 2000), and texture were determined on split and cleaned sediment surfaces. Lithostratigraphic units are numbered consequently from bottom to top. The boundaries between the units were described as gradual, planar/sharp, or erosional.

RGB colour imagery was acquired prior to XRF scanning using a line scan camera attached to the Avaatech core scanner. The RGB colour images as well as the RGB line diagrams support the lithostratigraphy and help to more accurately identify unit boundaries.

### 4.2.4 X-ray fluorescence scanning

The inorganic geochemistry was analysed using an Avaatech X-ray fluorescence (XRF) core-scanner at the department of Geosciences at Kiel University. The split-core surfaces were smoothed and they were covered with Ultralene foil to avoid contamination. All cores were scanned with a rhodium tube in different resolutions (Table 4). Lighter elements (Al, Si, K, Ca, Ti, Mn, Fe) were scanned with 10 kV and for heavier elements (Sr, Rb, Zr) 30 kV and a Pd-thick filter were used.

*Table 4: Measurement settings for XRF core scanning applied within the scope of this project.*

core-ID	coring site	tube settings 10 kV	tube settings 30 kV	resolution
STY1	Lake Stymphalia	1000 $\mu$ A for 10 s	2000 $\mu$ A for 15 s	1 mm
PHE1	Palaeolake Pheneos	750 $\mu$ A for 10 s	2000 $\mu$ A for 20 s	5 mm
KES2	Palaeolake Kaisari	750 $\mu$ A for 10 s	2000 $\mu$ A for 20 s	5 mm
TRI1	Lake Trichonida	250 $\mu$ A for 10 s	1000 $\mu$ A for 10 s	1 mm



#### 4.2.5 Grain size distribution

Grain size distribution (GSD) analysis by laser diffraction was applied for all samples presented here.

Sample pre-treatment processing followed the protocol provided in the digital supplementary material and is shortly outlined in the following. Depending on the composition of the material, 0.3 – 1.0 g of sediment were weighed into a centrifuge tube. Successively, the samples were treated with three times 10 ml of hydrogen peroxide ( $\text{H}_2\text{O}_2$ ) until the organic matter was removed. Cleaning was done using distilled water and centrifugation.

As the study area is strongly dominated by limestone, removal of the carbonates was not applied, because preliminary works showed that hardly any material remained for GSD analysis after carbonate destruction. Furthermore, it was assumed that a large share of the present carbonates were of allochthonous origin and their size would thus likewise be of interest. For comparison, some sample were treated with and without 0.5 M sodium acetate buffer solution for carbonate destruction (chapter 6.2.2).

As a last preparation step, distilled water and sodium pyrophosphate ( $\text{Na}_4\text{P}_2\text{O}_7$ ) were added to the samples, which were then left in a shaker for at least 16 h, to ensure disaggregation of particles.

At the Institute of Geography (Kiel University), a Malvern Mastersizer 2000 Particle Size Analyzer in combination with a Hydro 2000 for fluids was used to determine the grain size distribution of the sediment in a measurement range from 0.02  $\mu\text{m}$  to 2000  $\mu\text{m}$ . Each sample was run 10 times with a measuring time of 60 sec. The laser obscuration was envisaged to be in the range of 10 – 20 %. Chapter 6.2.2 investigates a comparison of measurements with different obscuration levels.

At the used device, the GSD resulted in a classification into 70 classes of particle sizes. The measured particle size groups were condensed to the seven common grain size fractions according to the ad-hoc Arbeitsgruppe Boden (2005). Therefore, semi-automated R script was developed (chapter 6.2) and further data processing and evaluation was likewise done in R.

#### 4.2.6 Carbon/nitrogen ratio

Carbon and nitrogen analyses were applied to differentiate between organic and inorganic carbon and to determine the source of organic matter in the sediment.

In preparation, dried samples were manually ground to a powder using mortar and pestle and the homogenised material was weighed into tin capsules. The amount of total inorganic carbon

(TIC), total organic carbon (TOC), and total nitrogen (TN) was measured at the Institute for Ecosystem Research (Kiel University) using a Euro EA, Elemental Analyser.

Two aliquots of the same sample were measured, first for TC and TN and second for TIC only. TOC was obtained as  $TC - TIC$ . The C/N ratio ( $=TOC/TN$ ) is used as an indicator of the relative abundance of terrestrial versus aquatic organic matter (Meyers and Ishiwatari, 1993). Aquatic organic matter has low C/N values of 4 to 10, whereas terrestrial organic matter shows values of 20 and higher (Meyers, 2003; Meyers and Ishiwatari, 1993).

#### **4.2.7 Loss on ignition**

Loss on ignition (LOI) is a straightforward method to estimate the organic and inorganic matter content (Birks and Birks, 2006; Heiri et al., 2001). Samples of approximately 2 g wet mass were weighed into porcelain crucibles and were dried over night at 105 °C. Subsequently, they were combusted in a muffle furnace at 550 °C for 2 hours. The loss of weight between the heating procedures at 105 °C and the combustion at 550 °C is the loss on ignition (LOI<sub>550</sub>), estimating the organic content in sediments indicated in weight percentage. In a second step, the samples were combusted for another 2 hours at 950 °C to estimate the inorganic carbon content (LOI<sub>950</sub>).

In the scope of this thesis, LOI was measured only for Lake Trichonida prior to sampling bulk sediment for radiocarbon dating to get a broad idea about the organic carbon and inorganic carbon content in the sediment and its variation along the core.

### **4.3 Chronology**

#### **4.3.1 Chronological notation**

In archaeological and historical context, dates are mostly indicated in BC and AD notation. Additionally, it is common to refer to the cultural periods, which are specific for each cultural area. For southern Greece, this study refers to the cultural chronology as defined by Weiberg et al. (2016).

On longer geological time scales, the notation BP (before present) is most commonly used as long as ages were obtained by radiocarbon dating, when present generally refers to the year 1950 AD. Some more recent studies also use the year 2000 AD (b2k) as reference base. In this study, conversions between BP and BC/AD ages always take 1950 AD as reference year. Conventional radiocarbon ages were converted into calibrated calendar years (cal BP) by using the IntCal13 calibration dataset (Reimer et al., 2013). Calibrated radiocarbon ages are presented as cal BP according to Mook and van der Plicht (1999).

### 4.3.2 Radiocarbon dating

Radiocarbon dating was carried out via accelerator mass spectrometry (AMS) at the Radiocarbon Laboratory in Poznan, Poland, as described by (Goslar et al., 2004; Goslar and Czernik, 2000).

For Stymphalia, dating of bulk sediment samples was performed on extracted alkali residues and for some samples additionally on humic acids. For sediments with extremely low carbon content, dating humic acids has proven to yield more reliable results than alkali residue ages, which seemed to have been up to several thousands of years too old due to the incorporation of old, reworked carbon (Grootes et al., 2004). The dating approach is presented and discussed in detail in Appendix I.

For Kaisari and Pheneos, due to the absence of organic macro-remains, the analysis was generally applied on extracted alkali residues from bulk sediment. The age-depth modelling is presented in Appendix II.

For Trichonida, organic macro-remains as well as bulk sediment have been sampled and dated. The bulk sediment samples revealed ages up to several thousands of years too old and were excluded from the age-depth model (cf. Appendix III).

### 4.3.3 Age-depth modelling

For this study, age-depth modelling was done in R using the *rbacon* package, which is based on a gamma autoregressive process and a self-adjusting Markov chain Monte Carlo (MCMC) algorithm (Blaauw and Christen, 2011, chapter 2.4). Radiocarbon dates, lithological and independent age information, such as historical dates, were included in the modelling process. The information was stored in and accessed from a csv-file. The modelling is described in detail in Appendix I – III. The *rbacon* codes of all final age-depth models for each sediment sequence used are provided as supplementary material on the data disc attached to this thesis.

## 4.4 Statistical analysis

The complete workflow of the numerical data analysis of this thesis was implemented using the open source software R.

Multivariate statistics were applied to reduce a high dimensional multi-proxy dataset, e.g. containing all measured XRF elements, to a limited amount of meaningful, uncorrelated variables that still contain most of the information (Birks and Birks, 2006; Filzmoser et al., 2009). Principal component analysis was performed using the *prcomp* command from the stats package. Plotting

the sample scores against depth or age highlights the major variation patterns in the dataset, which may in turn be interpreted as indicating palaeoenvironmental transformations (cf. Appendix I – III). For log-ratio transformation of geochemical elements, the natural logarithm was used (default setting in R).

A hierarchical cluster analysis was performed for Lake Trichonida to split the sediment sequence into different zones with similar proxy characteristics that may indicate similar environmental conditions during sediment deposition (cf. Appendix III).

## 5 Summary of papers

### 5.1 Appendix I

*Seguin, J., Bintliff, J.L., Grootes, P.M., Bauersachs, T., Dörfler, W., Heymann, C., Manning, S.W., Müller, S., Nadeau, M.J., Nelle, O., Steier, P., Weber, J., Wild, E.M., Zagana, E., Unkel, I., 2019. 2500 years of anthropogenic and climatic landscape transformation in the Stymphalia polje, Greece. Quaternary Science Reviews 213, 133–154. doi:10.1016/j.quascirev.2019.04.028*

For this paper, sedimentological and geochemical analyses were carried out on sediment core STY1 from Lake Stymphalia. Preliminary works of C. Heymann were revised, modified, and extended. Sedimentological and XRF analyses were linked with biomarker analyses, conducted by co-authors T. Bauersachs and J. Weber, and with archaeological data contributed by co-author J.L. Bintliff. The close connection of natural and cultural scientific results was possible due to intensive age-depth modelling supervised by co-author P.M. Grootes.

The Stymphalia record gives insights into the vulnerability of a shallow lake ecosystem and shows how a mixture of palaeoclimatic and anthropogenic forcing factors influenced the sedimentation processes for the last 2,500 years. These changes are visible in the XRF proxies, notably in the log(Rb/Sr) ratio, supported by a principal component analysis. While the existence of the highly populated ancient city of Stymphalos at the lake shore (ca. 4<sup>th</sup> century BC) doesn't seem to have caused a significant impact on the lake ecosystem, the building of the Hadriatic Aqueduct (ca. 130 AD) caused an incisive and persistent change in the sediment record strongly increasing the vulnerability of the system over several centuries. The Late Antique Little Ice Age (7<sup>th</sup> – 8<sup>th</sup> century AD), proclaimed by Büntgen et al. (2016), was identified in the sediment sequence as a phase of high climatic instability combined with considerable lake level changes. The sedimentation rate increased strongly during the Middle Byzantine Period (9<sup>th</sup> – 12<sup>th</sup> century AD), which was potentially caused by long-term effects of vulnerability due to the aqueduct construction, warm and wet climatic conditions during the Medieval Warm Period, as well as modest but careless land use and deforestation. The latter becomes more incisive during the Late Byzantine Period (13<sup>th</sup> – 14<sup>th</sup> century AD). Phases of complete desiccation of the lake could be identified for the modern period (18<sup>th</sup> – 19<sup>th</sup> century AD).

This study is in agreement with recent modelling of environmental change, which is critical of mono-causation and rather focusses on complex interactions of human and natural factors impacting on landscape transformation.

## 5.2 Appendix II

*Seguin, J., Avramidis, P., Haug, A., Kessler, T., Schimmelmann, A., Unkel, I., 2019. Inter-comparison of palaeoenvironmental records from four lacustrine archives on the Peloponnese (Greece) over the last 5,000 years. E&G Quaternary Science Journal [in review]*

This paper compares multi-proxy investigations on four (palaeo)lake sediment sequences (Stymphalia, Kaisari, Pheneos, and Asea). The sediment record from Asea valley has already been published by Unkel et al. (2014). The results on Lake Stymphalia were presented in Appendix I and by Heymann et al. (2013). The same geochemical proxies were investigated for each individual archive and analysed with a focus on hydrological fluctuations and environmental changes for the last 5,000 years.

Lake Stymphalia is the only lake of the four still existing today; the other three dried up or were purposely drained in the past. All the lakes can be classified as being predominantly shallow lakes and it was assumed that small changes in the hydrological regime may have already led to large impacts on the lake ecosystems.

The transformations observed in the sediment sequences were analysed in respect to different spatial scales in order to estimate the validity range of the proxy signals. The macro-scale level included globally or overregionally occurring phenomena. The meso-scale level concentrated on changes occurring within an approximate 50 km radius on the Peloponnese. The micro-scale level included local, site-specific variation that could not be observed in the comparative records.

On a meso-scale level, a high conformance and generally similar trends were evident in the proxies across all sites. An overall drying trend was detected for the transition phase from the Late Bronze age to the Early Iron age (ca. 3,200 – 2,800 cal BP), although the signal varied considerably in timing and duration. On the micro-scale level, notable differences were observed that may be explained by site-specific responses of the individual ecosystem various forcing factors. It can be concluded that due to the regional heterogeneity, it may be an oversimplification to link palaeoenvironmental changes in a single geoarchive with contemporaneous societal transformations across the whole Peloponnese.

### 5.3 Appendix III

**Seguin, J., Avramidis, P., Dörfler, W., Emmanouilidis, A., Unkel, I., 2020. A 2,600 years high-resolution climate record from Lake Trichonida (SW Greece). *E&G Quaternary Science Journal* [submitted]**

This paper aims at reconstructing the palaeoclimatic changes during the last 2,600 years in southern Greece based on a proxy record from Lake Trichonida. For the first time, we provide a solid age-depth-model and continuous geochemical data for the largest and deepest lake in Greece. We use XRF geochemical data supported by discrete measurements of XRD, grain size distribution, and organic matter content to investigate changes in the ecosystem and identify the major forcing mechanisms. A principal component analysis identifies the variation between carbonate rich and terrigenous material as the dominating process and we interpret it as depicting fluctuations in the hydrological conditions. The first principal component (PC1) shows a very strong correlation with  $\log(\text{Rb}/\text{Sr})$ . When comparing the PC1 summary proxy to independent proxies from the Balkan region, we find generally concurring patterns on a multi-decadal to centennial scale. We show that phases with wetter conditions at Lake Trichonida coincide with a more negative North Atlantic Oscillation (NAO) index, suggesting that the precipitation variability in southern Greece is linked to changes in the NAO atmospheric pattern, as one major driving force. A cluster analysis highlights the similarities in the sediment characteristics deposited during wetter phases, notably during 1850 – 1750 cal BP, 1500 – 1400 cal BP, ca. 1100 cal BP, and ca. 100 cal BP.

As human impact on the lake seems to be constantly present but marginal, the 2,600-year long sedimentary record of Lake Trichonida contributes to our understanding of late Holocene palaeohydrological changes in an important climatic transitional zone in the Eastern Mediterranean.

#### 5.4 Appendix IV

*Seguin, J., Unkel, I., 2019. Mastering a master sediment core compilation from parallel drill cores using RGB values. Unpublished manuscript of an Express Report intended for publication in E&G Quaternary Science Journal.*

The manuscript focusses on a methodological aspect in palaeolimnology: the master core compilation based on different drill core sections. Sediment cores from marine or lacustrine environments, serving as geo-archives, are often not drilled en bloc but section by section. Additionally, parallel drillings are frequently performed with an offset to ensure that the transitional parts are also covered undisturbedly. Many studies work with a final, continuous master core sequence without clarifying how the compilation was obtained. This study provides a transparent and reproducible approach, using the R environment, on how to compile this master sediment core based on several core sections from two parallel drill cores. We use continuous high-resolution RGB values as recorded by line-scan camera imagery. Tie points in the parallel cores are set, where both cores are connected. Proxy measurements from both cores are merged computationally to obtain one continuous master core sequence that serves for palaeoenvironmental reconstruction. This approach leads to more accurate results compared to the visual compilation and is particularly useful for research on human-environmental interaction, where highly resolved datasets are needed i.a. to study cause and effect mechanisms.



## 5.5 Appendix V

Knitter, D., Hamer, W., Günther, G., **Seguin, J.**, Unkel, I., Kessler, T., Weiberg, E., Duttmann, R., Nakoinz, O., 2019. *Land use patterns and climate change - a modeled scenario of Late Bronze Age in Southern Greece. Environmental Research Letters 14. 125003. doi: 10.1088/1748-9326/ab5126*

This paper presents a modelling approach that investigates how much cultivable land was required to supply a society with everyday commodities, mainly food, and whether societies were in need when environmental conditions deteriorated. D. Knitter, W. Hamer, G. Günther, R. Duttmann, and O. Nakoinz developed a reproducible procedure using the R environment to portray the diet of the people and an assessment of the areal demand to cultivate different products. The assumptions were turned into spatial information using a fuzzy rule-based model, to identify areas that are most suitable for the different land-use activities. T. Kessler and E. Weiberg provided archaeological information, while J. Seguin and I. Unkel supplied expertise on geographical, climatological and environmental conditions of the study area.

The spatial modelling is exemplarily implemented for the north-eastern Peloponnese and is based upon the location of Late Helladic IIIB (1,300 – 1,200 BC) archaeological sites, an assessment of their sizes, and a proposed diet of the people. Based on this data basis, the areal requirement of each site is calculated and mapped. This approach may give additional answers to questions investigating vulnerability and to which degree societies were impacted by climatic change. Furthermore, it improves the understanding of the interaction between humans and their environment.

The results show that large settlement sites do not have sufficient space in their surroundings in order to supply themselves with the required food resources and thus they depended on supplies from the hinterland. Drier climatic conditions further aggravated the situation. This supports the hypothesis that settlement sites were less vulnerable, if they were strongly interconnected. This indicates that potential societal crises were less a factor of changing environmental conditions or a shortage of arable land but primarily caused by socioeconomic factors.

## 5.6 Appendix VI

McNeill, L.C., Shillington, D.J., Carter, G.D.O., Everest, J.D., Gawthorpe, R.L., Miller, C., Phillips, M.P., Collier, R.E.L., Cvetkoska, A., De Gelder, G., Diz, P., Doan, M.-L., Ford, M., Geraga, M., Gillespie, J., Hemelsdaël, R., Herrero-Bervera, E., Ismaiel, M., Janikian, L., Kouli, K., Le Ber, E., Li, S., Maffione, M., Mahoney, C., Machlus, M.L., Michas, G., Nixon, C.W., Oflaz, S.A., Omale, A.P., Panagiotopoulos, K., Pechlivanidou, S., Sauer, S., **Seguin, J.**, Sergiou, S., Zakharova, N. V., Green, S., 2019. High-resolution record reveals climate-driven environmental and sedimentary changes in an active rift. *Sci. Rep.* 9, 3116. doi: 10.1038/s41598-019-40022-w

This paper presents the first results of the IODP Expedition 381 “Corinth Active Rift Development”. The central research aim of the expedition was to gain information on the development of the Corinth Rift, as it a young, active rift basin with rapid extension (10 – 15 mm/yr) and high seismic activity. Young rifts are shaped by combined tectonic, climatic and surface processes. However, only few records exist to evaluate the interplay of these processes over an extended period of early rift-basin development.

As the investigation area of the expedition was covered by the spatial extent of my PhD project, I applied to become a member of the science team with the intention to include the research on the sediment cores from the Gulf of Corinth into the spatial transect of my PhD project and to extend the temporal scale of my palaeoenvironmental research in southern Greece to the Pleistocene and beyond. As a member of the geochemistry team, I conducted pore water analyses and geochemical analysis of bulk sediment (McNeill et al., 2019; Shillington et al., 2019). One of the main results was that we observed cyclic variations in the basin palaeoenvironment in the sediment stratigraphy as well as in the geochemistry of the pore water.

This paper presents the longest and highest resolution record of sediment flux and palaeoenvironmental changes when a young rift connects to the global oceans. It concentrates on the last ~750 kyr at coring site M0079 in the central Corinth basin. The results show 10s – 100s of thousand years cyclic variations in basin palaeoenvironment as eustatic sea level fluctuated with respect to sills bounding this semi-isolated basin and reveal substantial corresponding changes in the volume and character of sediment delivered into the rift.

During interglacials, when the basin was marine, sedimentation rates were lower, and bioturbation and organic carbon concentration higher. The Holocene represents an exception, where higher sediment fluxes reached the coring site, which may be explained by human activity in the region. During glacials, the basin was isolated from the ocean, and sedimentation rates were

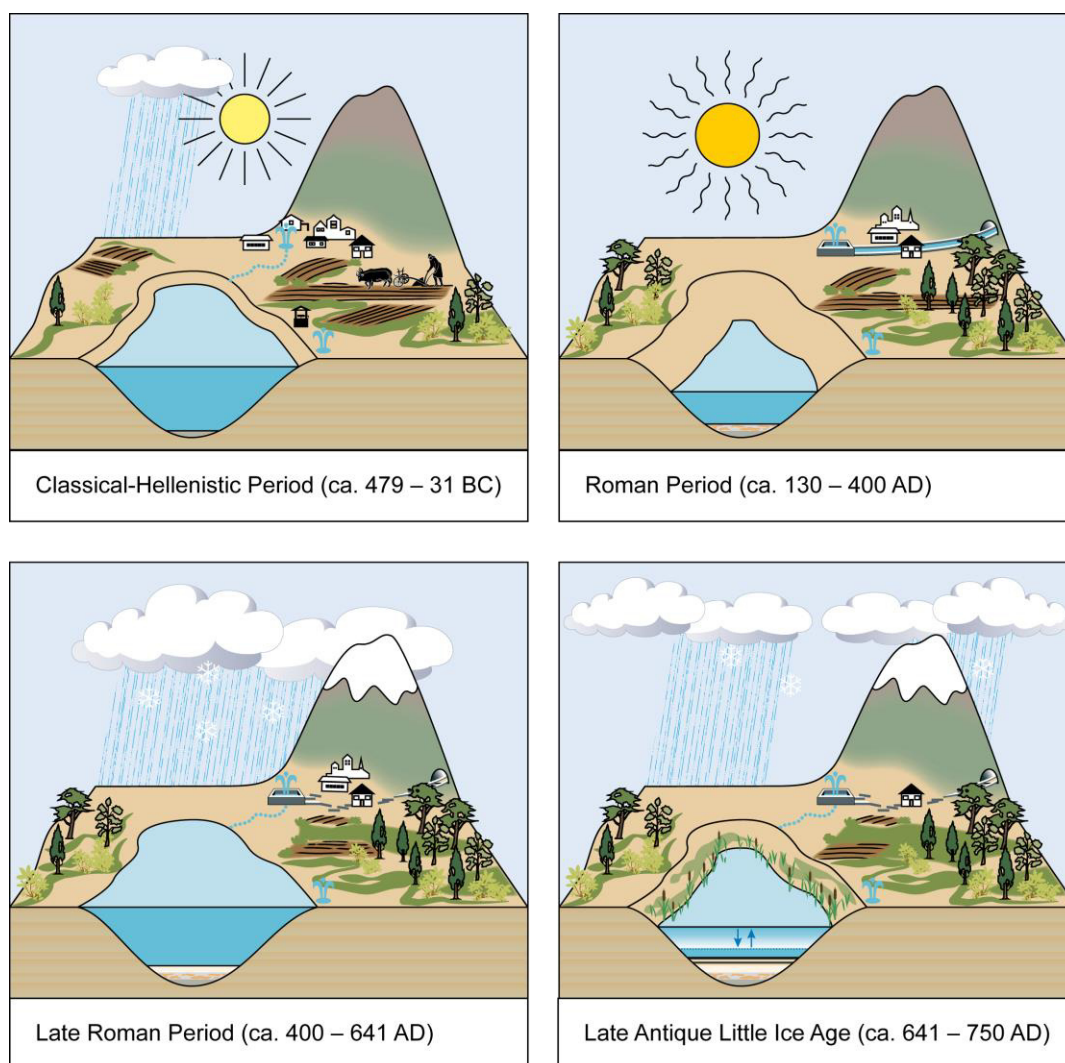
---

higher (ca. 2 – 7 times those in interglacials). We infer that reduced vegetation cover during glacials drove higher sediment flux from the rift flanks. These orbital-timescale changes in rate and type of basin infill will likely influence early rift sedimentary and faulting processes, potentially including syn-rift stratigraphy, sediment burial rates, and organic carbon flux and preservation on deep continental margins worldwide.

## 6 Additional results

### 6.1 Graphical visualisation of landscape development at Lake Stymphalia

In follow-up to Appendix I, a graphical model of landscape transformation at Lake Stymphalia was developed. Together with graphical designer Doris Kramer, we constructed a sequence of eight simplified images of the lake and its catchment, which illustrate the palaeoenvironmental changes during the last 2,500 years, as visible from our proxies. The images visualise changes in climate, vegetation, lake level fluctuation, erosion, and human impact in the area (figure 5). Especially in the interdisciplinary context, this graphical visualisation has proven to be a useful assistance to the traditional climate and proxy curves, as it paves the way for a common ground of interdisciplinary communication as demanded by Izdebski et al. (2016) (chapter 7.5.2). It stimulates the interdisciplinary discussion and sheds light on the interrelationship of different driving mechanisms that are more complicated to grasp from curves and diagrams only.



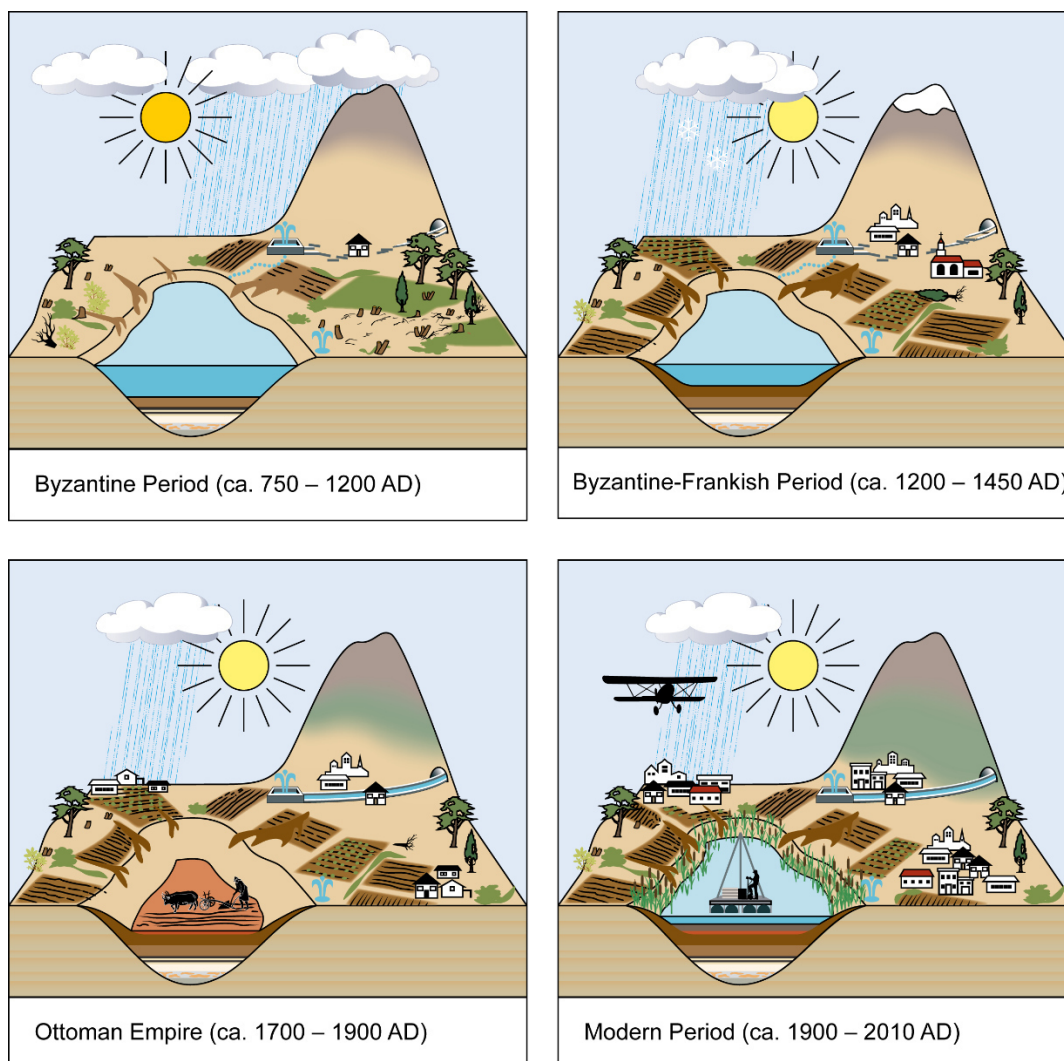


*Figure 5: Landscape model for climatic variation, landscape development and human impact in the Stymphalia polje over the last 2,500 years, divided into 8 time slices (2 pages).*

## 6.2 Grain size distribution analysis

### 6.2.1 Automated grain size distribution in R

For this study, the granulometry of discrete sediment samples was measured by laser diffraction using a Malvern Mastersizer 2000 particle size analyser (chapter 4.2.5; Malvern Instruments, 2007). The standard particle size range is 0.02 to 2000  $\mu\text{m}$  (Malvern Instruments, 2007). The results were classified into 70 automatically generated size bands. For the sediment analysis, these classes needed to be summarised into the commonly used grain size fractions as defined by the ad-hoc Arbeitsgruppe Boden (2005). Hence, I developed an automated R script that transforms the raw output txt-file from the Mastersizer into a uncluttered table format differentiating seven grain size fractions, adding the corresponding soil type abbreviation, and

optionally plotting a grain size ternary diagram or a bar chart (figure 6). The script is presented in the digital supplementary material to this thesis.

### **6.2.2 Reflection on grain size measurement via laser diffraction**

The grain size distribution is one of the most important characteristics of a sediment or soil and influences its properties (Ryzak and Bieganowski, 2010). Variation in the granulometry along the sediment core may indicate among others changes in the transport energy and transport mechanisms, which may be traced back to changes in the environmental conditions.

The main reason for applying the laser diffraction method in this study, instead of the conventional sieving approach (Konert and Vandenberghe, 1997), is that the amount of sample material available from a sediment core is limited and that laser diffraction can be performed on small (<1.0 g) samples (Storti and Balsamo, 2010).

This chapter reflects on two methodological aspects that were modified during the analysis: the laser obscuration and the carbonate content.

#### Obscuration

Sample preparation was done according the protocol presented in the digital supplementary material and remained unchanged for all samples. When using the Mastersizer 2000, the protocol suggests to measure samples with a laser obscuration in the range of 10 – 20 % to achieve the best results (Malvern Instruments, 2007). The obscuration is an indicator of how much sample material is present in the laser beam at the same time. If the obscuration is too low, an insufficient signal will be detected, causing a high level of measurement uncertainty. Too high obscuration may lead to multiple scattering of the laser beam, which introduces measurement errors (Konert and Vandenberghe, 1997; Malvern Instruments, 2007).

For Lake Trichonida, samples have been measured with extremely high (>55 %) and normal obscuration (6 – 16 %). This is due to the fact that different amounts of material were weighed in for each replicate. For high obscuration, 0.6 g of dry material was used and completely added to the Hydro 2000G. For the replication, the material was added into the Hydro 2000G via a pipette and thus it could be dosed more accurately until the ideal obscuration was reached. The instrument settings, e.g. the speed of the stirrer etc., as well as the measurement procedure were kept identical for all measurements.

A comparison of the results obtained with the different runs for all samples converted into the seven standard grain size fractions is presented in figure 6. The sample size used for comparison

is too small to yield statistically significant results, but it indicates some trends: Typical for all samples measured in this study is that they only consist of fine, clay and silt size, particles, with hardly any sand size fraction present. The coarse sand fraction was completely absent in all replicate measurements (figure 6b). This is not a typical GSD and the results presented here cannot be regarded as generally valid.

The highest differences can clearly be observed in the amount of clay (figure 6a). The high obscuration shows a clear overestimation of the clay fraction and an underestimation of the silt size fractions compared to the other run. Comparison studies for different GSD measurements exist, but no study has been found that investigated the effects of differences in the obscuration rates. Konert and Vandenberghe (1997) conclude that the clay size fraction shows the largest deviations between different methods due to the non-spherical form of the particles. A laser diffraction spectrophotometer regards particles as two-dimensional objects and thus the particle shape is most important (Konert and Vandenberghe, 1997). This may be another explanation for the alteration in the distribution curve: If many non-spherical, platy clay particles are oriented along their longer axis, their real size may be overestimated and it will lead to coarser results (Konert and Vandenberghe, 1997).

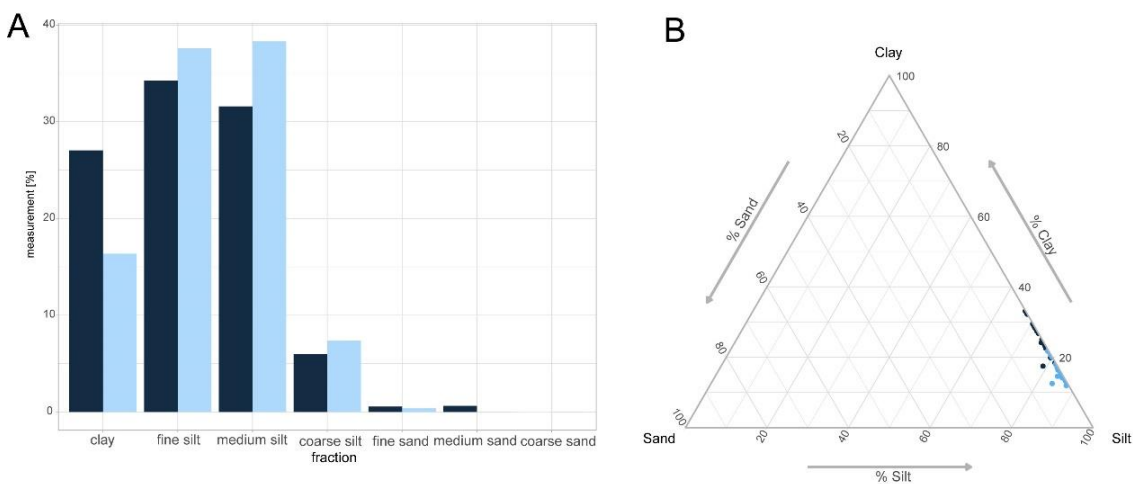


**Figure 6: Results of replicate measurements with different obscurations. (a) Bar chart showing differences between measurements with high obscuration (dark blue) and normal obscuration (light blue) according to the grain size fraction. (b) Ternary diagram shows that measurements with high obscuration (dark blue) compared to normal obscuration (light blue) are shifted on the clay axis.**

### Carbonate removal

In the standard procedure, the analysis is done on humus-free and carbonate-free sediments to avoid aggregation or flocculation of the material. For the present study in the limestone rich environment, the carbonates have generally not been removed prior to analysis, because earlier own analyses showed that after this preparation step, hardly any material was left for laser diffraction analysis. However, it is known for long time and still not fully overcome that laser particle size analysis of carbonate-rich sediments are highly problematic and potentially not representative, especially if the predominate allochthonous material is carbonate rich (Murray, 2002). As we suppose that most of the carbonates are of allogenic origin, we decided not to exclude them here, even though that may lead to a slight overestimation of larger particle sizes due to carbonate aggregates (figure 7).

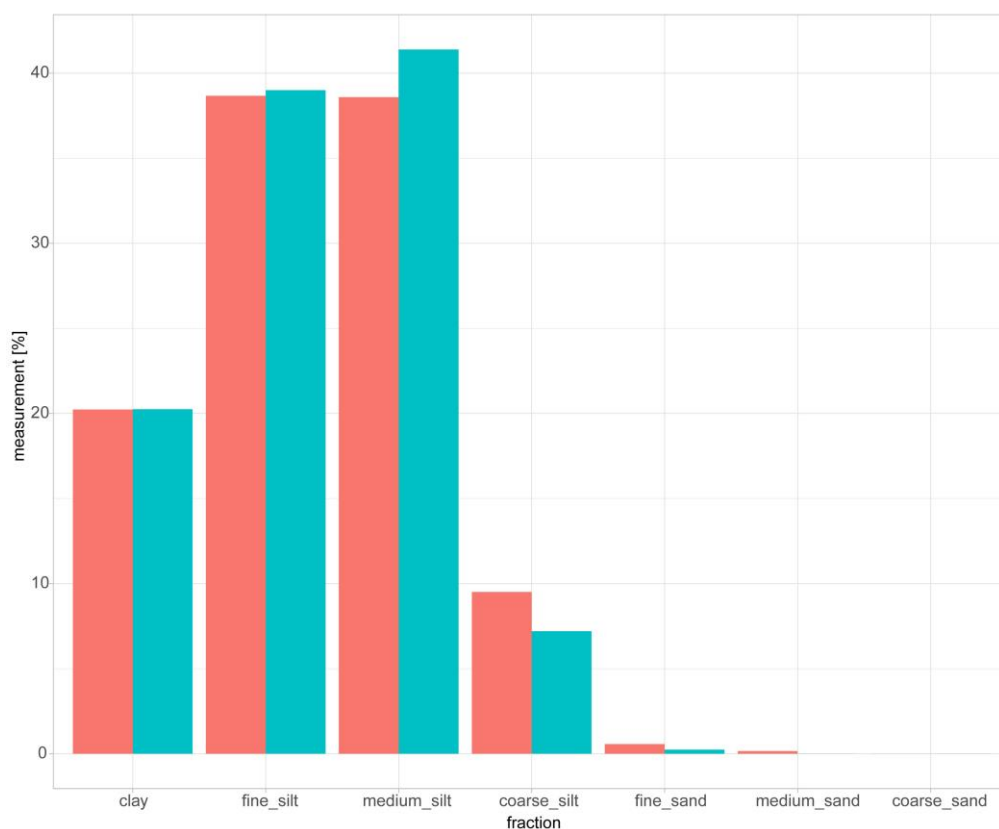


**Figure 7: Results of replicate measurements with (red) and without (green) the removal of carbonates during preparation.**



## 7 Synthesis

Sedimentary and geochemical processes have been analysed at four different lake sites in southern Greece. Lakes as potential geoarchives in southern Greece are very few, as most Greek lakes are situated in the W and NW of the country (Zacharias et al., 2002), and thus this study makes a significant contribution to add new palaeolimnological archives to a region, where the coverage is sparse but cultural heritage is rich.

All investigated lake sites may be classified as karstic lakes, but they also show considerable differences. Concerning the size, Trichonida is the deepest and largest natural lake in Greece, while Stymphalia is a very shallow and the last remaining natural lake on the Peloponnese peninsula. Pheneos and Kaisari on the contrary are palaeolakes and no assumptions about their former lake parameters were made. The lakes also differ in their location above sea level; while the three Peloponnesian lakes are situated in a mountainous region at 400 – 700 m a.s.l., Trichonida is located in the lowland at 10 m a.s.l., but receives its sediment load partly from a ca. 1,800 m high mountain ridge to the NE.

The four lake sites were investigated with the same set of proxies to facilitate the comparability of the data. Such a multi-archive approach seemed promising and was discussed in Appendix II.

### 7.1 Evaluation of the suitability of the investigated karstic lakes as palaeoenvironmental archives

The three Peloponnesian lakes are all located in poljes. As poljes have played an important role in land use activity at least since Antiquity (Vött et al., 2009) and as Lake Stymphalia was already successfully cored in 2010 (Appendix I), the choice to investigate the two unexamined palaeolakes in the neighbouring poljes for palaeoenvironmental development appeared obvious and reasonable. Another advantage was the relatively straightforward acquisition of drill cores from these study sites; as the lakes were drained and the sites were easily accessible with a land-based coring system (Appendix II).

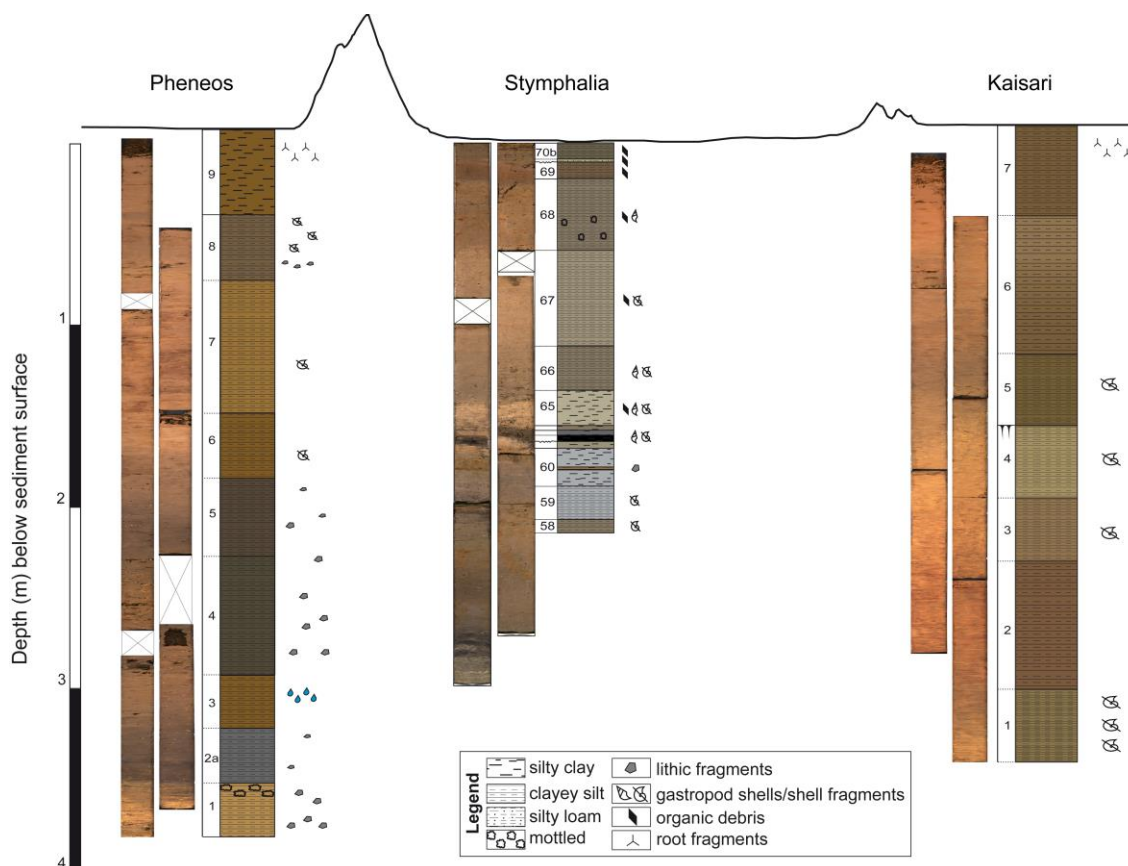


**Figure 8:** Sediment cores from the three polje sites on the NE Peloponnese. Images for both parallel cores and the derived lithological sequences are shown. Above, the elevation profile stretching over 25 km is indicated. Dimensions are not to scale.

Following (Birks and Birks, 2006), a careful selection of the study site, which is suitable to investigate the research aims, is an essential foundation for a successful research project. However, the challenge is that „[e]very lake had its own sedimentological character, and one never knew what to expect when daylight exposed the content of the corer [...] it was still impossible to foresee what would emerge from the bottom of each new lake“ (Björck, 2019).

In case of Pheneos and Kaisari, the intensive agricultural use of the polje floors disturbed approximately the upper 50 cm of the sequences (figure 8), making this section useless for palaeoenvironmental reconstruction for the last ca. 500 – 700 years. Additionally, the episodic desiccation of the polje floors, potentially influencing the sediment geochemistry post hoc, complicated the proxy interpretation (Appendix II).

For Lake Trichonida, extensive planning activities beforehand and a modification of the coring equipment to handle the required lake depth was conducted to ensure the successful coring. Though, due to the comparatively high sedimentation rate of 1.68 mm/yr, compared to

<0.5 mm/yr in Pheneos and 0.5 – 0.8 mm/yr in Kaisari, the cored sequence covered a shorter time span than previously targeted.

We found that proxies, that are successfully applied from other lake sediment studies, may not be directly applicable in these karst poljes. Pollen preservation is extremely low in Lake Stymphalia, due to alkaline and potentially periodical/seasonal dessication of the lake. Studying the geochemistry is considered a useful procedure that allows to obtain palaeoenvironmental proxies from these sites, but the proxies should be evaluated for each site individually before being interpreted as palaeoenvironmental indicators (Appendix II).

To conclude, karstic lakes generally provide suitable geoarchives for the area, but the choice of proxies may be limited, and they need to be revised site-specifically.

## **7.2 Radiocarbon dating in a limestone rich environment**

A robust age-depth model is substantial to derive age information from the sediment sequence and plot the proxy values accordingly. However, in carbonate-rich, organic-poor sediments radiocarbon dating reaches its limit.

For this study, it was discovered that impurities of reworked carbon from the surrounding lake catchment of Stymphalia introduced into the humin fraction caused a shift in the radiocarbon ages of bulk sediment alkali residue towards significantly too old ages (a detailed explanation is given in Appendix I). It necessitated a careful examination of all available radiocarbon dates, followed by a profound modelling in order to obtain stable age-depth models (Appendix I, II, III). This challenge proved to be highly advantageous for the development and refinement of the dating approach.

Contrary to studies, where chronologies were constructed by simple linear regression models, Bayesian statistics, using adaptive Markov chain Monte Carlo implementation, were applied here using rbacon modelling on a combination of numeric dates and relative age information, including historical dates – if available (Appendix I, III). Due to the considerable number of datings in Stymphalia and Asea, extensive modelling based on the youngest and most reliable dates and including historic age information lead to the construction of robust age-depth models (Appendix I, II). For Trichonida, the bulk sediment samples could be completely excluded from the final model, as sufficient organic macro remains could be retrieved from the cores. Furthermore, a tephra layer and the depth designation for the appearance of corn from an earlier pollen study gave two independent age indications (Bottema, 1982) that could be used for reference. At Pheneos and Kaisari, organic macro-remains were absent and thus dating had to be

conducted exclusively on bulk sediment. Additionally, it has only been conducted on the alkali residue fraction. Given the results from Stymphalia, we suppose now that the humic acid fraction would yield more reliable results in this environment. Erosional gaps could not be identified from the sediment lithology, but the palaeoenvironmental interpretation revealed that both sites sporadically dried out in the past; thus, a continuous sedimentation cannot be taken for granted. We have established age-depth models for these two sites to the best of our knowledge and have compared them to the more profound chronologies from Stymphalia and Asea to assess their reliability, which generally supported them (Appendix II).

In summary, it is more likely that the calculated age-depth models for the investigated sites deviate towards too old ages than the opposite. Due to the organic-poor and carbonate-rich environment, dating karstic lakes remains challenging and requires a cautionary approach. If one needs to date bulk sediment due to the absence of better organic material, it is crucial to assess the potential reservoir effect and it may be beneficial to evaluate the usability of both the alkali residue and the humic acid fraction. Additionally, the *rbacon* modelling allows to include different types of age indications and it has been shown that the integration of historical dates enhances the reliability of the model. Owing to the baseline conditions, our radiocarbon-based chronologies still include a considerable uncertainty range of around 100 – 200 years and do not allow to draw conclusions on cause-and-effect mechanisms between humans and their environment (Blaauw et al., 2019). But the sophisticated chronological modelling developed into an essential part of this work and brought us several steps closer to robust and reliable age-depth modelling.

### **7.3 The application of PCA as a suitable tool in palaeolimnology**

Principal Component Analysis (PCA) was applied to the XRF elemental data for each study site (Appendix I – III) in order to reduce a multivariate dataset to a limited number of meaningful parameters and to detect trends in the dataset.

The resulting patterns were in agreement with existing knowledge about geochemistry in sediments. Strong correlations between Sr and Ca were obtained, which was expected since both elements were present in the carbonate fraction. On the other hand, high covariance between terrigenous minerals (Ti, Al, K, Rb, Zr) showed the similar behaviour of elements within the clastic fraction. A close correlation of Fe with the terrigenous minerals for all lakes showed that they had very similar downcore patterns. We thus assumed that Fe variation was mainly controlled by terrigenous sediment input and that precipitation during redox changes was of minor importance at these sites (Naeher et al., 2013). High correlations between Ti and Si for the

Peloponnesian sites implied that the input of biogenic silica, notably through diatom abundances, was low.

For all lakes, the factor loading of PC1 spanned between carbonates and terrigenous material. Although slightly different elemental compositions were analysed or site-specific effects appeared, the distributions of the loadings were always similar. Thus, we concluded (1) that the geochemistry in these karstic lakes was generally comparable, (2) that PC1 could be used as a summary proxy representing the most meaningful variations in the lake ecosystem, and (3) that the scores of PC1 could be interpreted as a proxy for hydrological changes in the lake catchment.

The methodological proceeding of applying a PCA to a multivariate dataset can be extended to additional continuous or discrete parameters. It needs to be considered, however, that the dataset with the lowest resolution predefines the resolution of the results and, depending on the research questions, it seems reasonable to predominantly add high resolution datasets such as colours (RGB, L\*a\*b) or other continuously scanned parameters (e.g. magnetic susceptibility).

There is a natural tendency to consider one proxy more reliable or more informative than another and hence subconsciously give greater weight to it (Birks and Birks, 2006). A PCA represents a more objective technique to reduce a large dataset to a few meaningful variables. In this study, it was shown for all lake sites that the relationship between carbonates and terrigenous elements was presented on the first ordination (PC1). Based on this multivariate analysis, it seemed reasonable to give a greater weight to proxies such as the  $\log(\text{Rb}/\text{Sr})$  ratio that mirror the same relation.

XRF core scan data are affected by the closed-sum effect, meaning that they sum up to a constant (Filzmoser et al., 2009; Löwemark et al., 2011). An increase in one element inevitably leads to a decrease in another, which may bias the correlation of different elements. In a strictly statistical sense, an application of a principle component analysis to such a dataset is not valid without an appropriate data transformation (Filzmoser et al., 2009). However, in the research community a PCA analysis on XRF data is widely performed and accepted (e.g. Giralt et al., 2011; Katrantsiotis et al., 2018; Poraj-Górska et al., 2017; Rydberg et al., 2016; Schreiber et al., 2014). While other studies suggest alternative statistical approaches, such as log-scale transformation (Aitchison and Greenacre, 2002; Weltje and Tjallingii, 2008), isometric logratio transformation (Filzmoser et al., 2009), or independent component analysis (Ön et al., 2017).

Our results showed that the curve progressions of the PC1 scores and the  $\log(\text{Rb}/\text{Sr})$  ratio were extremely similar for every lake and the resulting palaeoenvironmental interpretations were identical (Appendix I – III). Thus, the log-scale ratio validated the PCA results. Or considered

from a different angle, the PCA on a multivariate dataset facilitated the decision, which log-ratio to interpret in order to obtain the most meaningful results. Care was taken to ensure that both proxies were shown to satisfy researchers of both sides. According to the current state of research, a combined approach of both statistical methods seems to be an adequate proceeding to handle the multivariable dataset.

#### **7.4 Exploring and identifying the causes of landscape transformation in sediment cores**

The most important driving factors of hydrological and geomorphological processes are climatic changes and anthropogenic land-use. It is thus essential, though challenging, to differentiate anthropogenic from climatic impacts on landscape development.

In the scope of this study, a special focus was placed on the identification of different influential factors on the selected palaeoenvironmental archives. For Stymphalia, comparatively extensive archaeological and historical information on past human settlement activity existed, leading to the description of an intensive interconnection of human action and natural forcings in the catchment for the analysed period (last 2,500 years). Such abundant archaeological information was completely lacking for the Kaisari polje and only very sparsely available for Pheneos. Hence, for the comparison of neighbouring sites (Appendix II), PC1, as a summary proxy of the respective XRF elemental data, was used as the main proxy for changes in hydrology and erosion processes. Similar signals at all or at several sites were interpreted as climatic changes, while site-specific changes were interpreted as spatially limited, local effects, including differing topographic factors as well as human activity.

As the limnological conditions at Lake Trichonida strongly differed from the other sites, a larger influence of natural (climatic) forcings on the proxy record was detected and thus Appendix III concentrates more specifically on the analysis of a climatic archive in the traditional sense. It was carefully concluded that this large and deep lake, where the coring spot is further away from the anthropogenic activity onshore, has a higher potential of detecting supra-regional and palaeoclimatic signals.

To conclude, human impact on the landscape was observed at all study sites with varying intensity during different time periods, being most explicit and effective within the last century. In most cases, it remains challenging to unambiguously decipher climatic from anthropogenic impact. However, within the scope of this thesis, three different proceedings have been applied to contribute to the achievement of this ambitious target:

(1) an interdisciplinary collaboration with partners from archaeology and history compiling the different proxies and information within one study (Appendix I; Haldon et al., 2018; Izdebski et al., 2016),

(2) a multi-archive approach using the same methodological proceeding on several lake archives from the same region to compare the site-specific manifestations against regional-scale climatic or environmental changes (Appendix II; Roberts et al., 2016),

(3) and hypothesis-based modelling, going through different options and weighing the likelihood or being able to exclude impossible scenarios (Appendix I, II, V; Knitter et al., 2019).

## **7.5 Scales of transformation – synthesis in the scope of the CRC1266**

In this chapter, the question of „scales of transformation“ in the scope of the CRC 1266 agenda, the subproject design within the collaborative research centre, as well as the interdisciplinary collaboration within the subproject shall be reviewed.

For this study, as for most studies in palaeoenvironmental research, it was decided to investigate proxies from lake sediment cores for their dynamics and interactions over time and set the results into a wider spatio-temporal context (Blaauw et al., 2019). In the thesis presented here as part of the E1 subproject, the environmental dimension of the concept was dominating, as it understood processes of transformation mainly as dynamics and fluctuations in lake ecosystems on different spatial and temporal scales. It was supplemented with project internal and external expertise from the humanities and social sciences, notably archaeology (brought together in Appendix I, II, V).

### **7.5.1 Investigated scales of transformation**

Different levels of spatial and temporal scales were tackled within this thesis. Proxy signals are spatially influenced by micro, meso, and macro scale forcings (Appendix II). Local, site-specific dynamics can differ significantly from regional or overregional averages. The varying signals may be linked to a mixture of human, environmental and climatic forcing factors.

Archive-related, spatial scale is also of influence concerning the size of the studied lakes, lake catchments, and lake depth. This dimension of spatial scale is a strong influential parameter on the formation of the sediment sequences. It is not trivial to compare proxy signals from small and shallow Lake Stymphalia to developments at the large and deep Lake Trichonida, as different processes will influence and alter the geochemical proxies in the sediment. For shallow Lake Stymphalia, for example, it appeared that for understanding the palaeohydrology, the extension

of the lake area was of higher importance than the lake depth (Appendix I). For deep Lake Trichonida, variation in the stratification and mixing of the lake water is more decisive for the geochemical composition of the sediment than for example changes in water depth (Appendix III). Since lake sediments accumulate over time, spatial depth is likewise a proxy for time and thus spatial and temporal scales in these archives are strongly interconnected.

On a temporal scale, proxy variations were reconstructed for each lake site for varying time periods and the temporal resolution of the proxy data is a decisive factor for the choice of an appropriate and meaningful scale of comparison (Birks et al., 2012). The largest scale, the shortest period respectively, was investigated in Appendix V, while the smallest scale, the longest period respectively, was covered in Appendix VI. The proxies presented in Appendix I – III have a comparable scale, although Appendix II covers a longer time period.

When speaking about temporal scales, the term „event“ is of high importance. We follow the definition of Chapman (2018), derived from a natural science perspective, and understand „event“ as an initial trigger of major significance that has profound and long-lasting effects. This may be a quick, short-term natural event, such as a volcanic eruption, which is followed by a period of colder climatic conditions e.g. the LALIA (Büntgen et al., 2016, Appendix I) or also a human induced event, such as the construction of the Hadrianic Aqueduct that is followed by long lasting changes in the lake ecosystem (Appendix I). Chapman (2018) points out that the „actual timescale of the initial trigger [...] remains mysterious“ and a chronological definition of such a „trigger event“ is lacking. He brings the example of the 8.2 event, which is a widely applied term that actually refers to an interval of approximately 600 years. If something may be classified as an event, it is largely a question of perspective and proportion. When concentrating on the Holocene or even longer time scales, this denotation for a 600-year-long period may be appropriate and justified, while this is certainly not the case, when analysing a 1,000 years time slice. Appendix III discusses the classification of the coloured sedimentary units in TR11 as event layers versus reactions to short-term trigger events.

### **7.5.2 Reflection on interdisciplinary collaboration**

Traditional research within a single discipline often resulted in conclusions about simple causal relationships, but manifold, mutual interactions between climate, environmental changes and human societies demand interdisciplinary research to enhance the understanding of the complex interrelationships (Holmgren et al., 2016).



Izdebski et al. (2016) identify major methodological prerequisites and pitfalls of interdisciplinary collaboration in palaeoenvironmental sciences and suggest solutions to the most common challenges. Their implementation within this project is examined in the following. Successful interdisciplinary collaborations need integrated, effective research strategies and operable methodologies (Haldon et al., 2018; Izdebski et al., 2016). According to Izdebski et al. (2016), interdisciplinary research strategies should be set up from the very beginning and four specific points of concern should be addressed to facilitate the collaboration: project design, terminologies, publication cultures, and research impact (Izdebski et al., 2016). The implementation of the first two is critically reviewed in the following.

### *Project design*

On a spatial scale, the NE Peloponnese and the region around the Gulf of Corinth were selected as study area for the reasons outlined in chapter 1. From an archaeological point of view, this was an extremely large research area and in the course of the research, certain focus areas needed to be set within the region (Appendix V; Kessler, in prep.). From a natural scientists perspective, this was a rather limited research area. Climatic signals, as observed from the proxies, needed to be compared to other archives beyond the study area, from the Peloponnese, Greece, the Balkan or the eastern Mediterranean region to evaluate and integrate the new archives into the existing pattern. By this means, a close connection between the proxy signal at Lake Trichonida and the overarching atmospheric North Atlantic Oscillation pattern (NAO) could be identified (Appendix III). Furthermore, the investigated geoarchives were intentionally selected from an area where human presence was known. On one hand this allowed to study possible links between natural and anthropogenic forcings and on the other hand this complicated the interpretation and the attribution of the proxy signals to a specific, prevailing forcing factor (Appendix I, II).

On a temporal scale, the disintegration of the Mycenaean civilisation at the end of the late Bronze Age and the formation of the polis culture during the Early Iron Age (ca. 3,200 – 2,800 BP / 1,250 to 850 BC) was the given focus of the research in the E1 subproject. Archaeologists specialise in cultural periods and thus cover proportionally shorter time spans than natural scientists. However, in the process of research for this thesis, it became clear that the analysis of unknown limnic sediments for such a specific, geologically very short time slice is challenging if not impossible. The landscape development at Lake Stymphalia could be reconstructed but for a much younger time sequence than the projected Bronze Age / Iron Age transition (Appendix I). The sediment sequence retrieved from Lake Trichonida did not fully reach the Bronze Age / Iron

Age transition (Appendix III), and the chronological uncertainties at Pheneos and Kaisari only allowed for hypotheses on general trends during this epoch but do not allow for clear conclusions on cause-and-effect relations between climate and humans (Appendix II).

The traditional historians' approach is to study only the societal impact of climate change, while natural scientist often tend to follow a deterministic, climate-centred perspective (Izdebski et al., 2016). An interdisciplinary approach towards the topic allows to study more complex questions (Haldon et al., 2018), e.g. dealing with social vulnerability and resilience to environmental stressors (Appendix V) or distinguishing climatic impact on human societies from other variables (Appendix I, II). Izdebski et al. (2016) term this a post-processual turn and call for the critical evaluation of mono-causal explanations and potential causal links. Our interdisciplinary study on Lake Stymphalia leads to this conclusion; the geoarchive displays a close connection of climatic and anthropogenic impacts and none of these factors should be regarded as mono-causal for the transformation observed in the lake ecosystem.

### Terminologies

Izdebski et al. (2016) assert that every discipline uses a specific rhetoric, jargon, and language, which may cause misunderstandings or hamper collaboration. To achieve fruitful collaboration, they suggest to communicate the data „in the most straightforward way“ (Izdebski et al., 2016).

One option to do so in the scope of this PhD project was the development of the graphical modelling of the landscape transformation sequence at Lake Stymphalia that comes along without the usage of language (chapter 6.1).

Furthermore, in the palaeoenvironmental context, terminology also concerns the differing mode of expressing time, for example using the BC/AD versus the BP notation, or climate periods (Late Holocene) versus cultural periods (Late Bronze Age) (Izdebski et al. (2016); chapter 4.3.1). To achieve a mutual understanding, all scientists participating in interdisciplinary research need to be aware of the differences in the temporal notions. When an interdisciplinary readership should be addressed, it is recommended to use both time notations (e.g. Appendix I). Furthermore, when speaking of periods, we always added a numeric age information to them and abstained from using abbreviations.

Concerning the line of argumentation, the aim in humanities is to offer possible narratives about the human past, while natural scientists often present bare, numerical data with the goal to prove a hypothesis (Izdebski et al., 2016). In this research project, we tried to combine both approaches by presenting numerical data and different possible hypotheses and scenarios for palaeohydrological fluctuations related to landscape development merging into a narrative of the most plausible progression (Appendix I).

### *Synthesis*

Within the scope of the CRC 1266 E1 project, some progress has been made to improve interdisciplinary collaboration. Awareness raising for the pitfalls in interdisciplinary collaboration was successful. Significant progress has been made in terms of using a common language and communicating findings in a way that is understandable for members from different disciplines. The development of collaborative models (Appendix V, chapter 6.1) was identified as one approach to strengthen interdisciplinary research and communication. The conceptual use of narratives was adopted when discussing natural scientific results (e.g. Appendix I) and is considered as beneficial to assess different hypothesis and to facilitate the mutual understanding. This should be further developed and strengthened in future interdisciplinary collaboration.

## 8 Prospects for further research

This chapter presents options for follow up research at the investigated sites as well as possibilities of transfer of the applied methodological proceeding to other, unexplored study sites.

Especially for the Pheneos polje, I see a high potential for follow-up studies. It may be worth attempting to improve the chronology for palaeolake Pheneos, i.a. by additionally dating the humic acid fraction of the samples and/or by sieving the sediment for datable organic remains. Future studies could involve the investigation of transects of multiple sediment cores through the eastern and western bay of the polje, ideally in direct connection with archaeological fieldwork or at least geophysical surveys. This may lead to refined hypotheses on the varying lake extension and level, potential human hydraulic-engineering measures as proclaimed by Knauss (1990), and the co-existence of the human settlement and the lake. The use of remote sensing images and spatial data analysis may likewise lead to additional information on the development of the lake basin. Geomorphologically, the young (modern) sinkhole development observed in the western bay of the Pheneos polje emphasise rapid, recent landscape changes that are also worth investigating in detail. Nevertheless, the desiccation processes in the more recent past will always constitute an obstacle to palaeoenvironmental reconstructions and thus, over longer time scales, Lake Stymphalia is the better palaeoclimatic archive for the region.

The polje is assumed to be filled with 160 m of clay-rich, homogeneous sediments as geophysical prospections in the 1980s suggest (Morfis and Zojer, 1986). This would provide a valuable long-term record of Quaternary palaeoenvironmental development. The analysis of the 15.5 m sediment sequence, cored in 2010, would be a promising and enlightening starting point for future investigations. The sequence seems to cover at least the last 30,000 years, as first, still unpublished radiocarbon dates suggest. The drilling of longer sediment sequences and further investigations are additionally favoured for Lake Trichonida. As it was shown that the geochemical signal clearly reflected variation in the NAO pattern (Appendix III), it would be valuable to prolong the record further into the past. Additional research revealed that the East Atlantic/West Russia teleconnection causes a similiar climatic pattern in Greece (Barnston and Livezey, 1987; Krichak and Alpert, 2005; Lim, 2015) and it seems conceivable that this signal may also be recorded in the sediment sequence. However, no palaeo-reconstruction of this insufficiently studied atmospheric circulation system was found that could have been compared to our proxies. More research on this topic would be advantageous in order to close this gap and to gain a better understanding of the interconnection of different climatic patterns that shaped the past climatic conditions over Greece. Furthermore, the TR11 core was taken from the deep, central

part of the lake and would be ideally suited for pollen studies (Birks and Birks, 2006), to complement the old, low resolution findings by Bottema (1982). Additional studies on biotic proxies, i.a. diatoms, which would give additional evidence for changes in the mixing pattern, may also be beneficial on this core. However, studying fossil diatoms in Greece seems not to be evident and the preservation conditions may not be ideal; hence, it has rarely been performed up to now (Katrantsiotis et al., 2015).

For the NE Peloponnese, pollen analysis would give valuable insights on vegetation and land use changes and may support or refine the erosion scenario depicted in Appendix I. They may also help to address questions of spatial scales as they can be transported long-distance or derived more locally, directly from the lakeside. The assumed lake level changes and episodic dessication of the lakes (Appendix I, II) were notably based on geochemical proxies and should be further investigated e.g. by using micropalaeontological analyses. Obtaining additional, independent proxies, i.e. from stable isotope, charcoal, or biomarker analyses and comparing them to the inorganic geochemical signals may be a useful and desirable complement for further analysis phases. However, exploratory works have shown that this is a difficult task in this environment.

It was shown that variations in the colour of the sediment with depth can provide a meaningful overview of changes in the sedimentary processes and environmental conditions during deposition (Appendix III, IV). Although it is quick and cheap to obtain high resolution colour data, its potential remains largely unexploited at present and an intensified application in the future seems beneficial, independent from the coring location.

Besides, when investigating a limnic archive, the coring location needs to be selected carefully (Birks and Birks, 2006). Palaeoclimate reconstructions are often based on a single core location, but intra-lake or intra-regional variability may influence the signal and ideally one would use multiple coring sites or multiple archives to reconstruct climatic parameters. The latter may be particularly useful, when catchment specific variations should be compared or – quite the opposite – levelled out to focus on the overregional signal.

The applied multi-archive, multi-proxy approach provided high-resolution datasets, suitable for palaeoenvironmental reconstruction and landscape transformation at different lake sites. However, it needs to be considered that each limnic archive may react differently to climatic fluctuations and that the varying combination of natural and anthropogenic factors has different effects on the lake ecosystem, producing different geochemical signals in the sediments. It is thus of high importance to understand the respective lake ecosystem and revise the proxy signal(s) accordingly before the interpretation.

It is suggested to integrate the palaeoenvironmental information in archaeological or historical research more intensively. The within-project combination of different archives, notably environmental proxies from the lake sediments with archaeological finds and historical sources, such as information on settlement activity, shows high potential in more accurately reconstructing palaeoenvironmental forcing factors within the catchment area (Appendix I) and calls for further interdisciplinary collaboration. Questions concerning human resilience and vulnerability, such as how and to what extent did climate change affect human behaviour or activity and inverse questions on how and when did humans start to lastingly affect and influence their environment, are of high importance in the ongoing climate debate and should be intensified.

## 9 Conclusion

Southern Greece is a region that is rich in archaeological sites, but still relatively sparse in palaeoenvironmental archives. To fill this gap, this thesis adds new proxy records from four lacustrine archives to the dataset and contributes to an improved understanding of landscape transformation in southern Greece during the Late Holocene.

The main outcomes of this work can be summarised as follows. Sedimentary processes in (palaeo)lakes Stymphalia, Kaisari, Pheneos, and Trichonida have been analysed using geochemical, sedimentary and statistical methods. Chronologies were established by intensive modelling using Bayesian statistics on radiocarbon dates, supplemented by historical dates, stratigraphic information, and a tephra layer. An intercomparison of different models strengthened their plausibility. This approach allowed to cope with dating challenges, which occurred due to old carbon effects. High-resolution XRF and colour scanning yielded detailed, continuous records for each studied lake site. A comparison with discrete measurements, such as TIC, TOC, TOC/TN, XRD, and GSD data, confirmed that the XRF scanning-derived elemental ratios provide valuable information and can be used as palaeoenvironmental proxies. At each lake site, the  $\log(\text{Rb}/\text{Sr})$  ratio was identified as the most valuable ratio and allowed to reconstruct changes in the palaeohydrological conditions. The application of a principal component analysis supported the single-proxy and proxy-ratio-results and presented a useful tool to identify patterns in the large and complex datasets. The first principal component (PC1) was understood as a summary proxy and its comparison to the  $\log(\text{Rb}/\text{Sr})$  showed extremely high correlations.

By applying this multi-archive approach, progress was achieved in differentiating signals on different spatial scales and to separate natural from anthropogenic impact on the landscape. That way, the sediment cores from Lake Stymphalia revealed the strong influence of the Hadrianic Aqueduct construction on the ecosystem, for instance, while the cores from Lake Trichonida showed that the palaeohydrological fluctuations were considerably influenced by changes in the North Atlantic Oscillation pattern. Comparisons with other palaeoclimatic records from Greece generally supported the findings.

Studying lake sediments as geoarchives is a key to understanding palaeoenvironmental changes, which may have had social causes or implications. The impact of palaeoclimatic variability on ancient societies is intensively discussed in the research community, notably for the Bronze Age / Iron Age transition. Existing geoarchives provide heterogeneous results for the respective period with a tendency towards drier conditions (Appendix II). All our records showed climatic variation for the respective period, but none of them indicated any abrupt, incisive

environmental or climatic event that would mono-causally explain the rapid demise of the Myceneans and other Late Bronze Age societies. In combination with the results of Appendix I and V, we conclude that climatic variation may have been one factor in a multi-causal network, but its role should not be overestimated and socio-economic factors seem to be of higher importance.

To conclude, the investigated lacustrine archives offer valuable contributions to a better understanding of palaeoenvironmental transformation in southern Greece during the Late Holocene. The findings emphasise that an intercomparison of multiple proxies and multiple archives as well as a close interdisciplinary collaboration hold the potential to disentangle natural and anthropogenic influences, which is also of high relevance in studies on vulnerability and anthropogenic climate change. The investigation area has a great potential for future studies that may reveal new insights into the human-environmental interrelationship, particularly when taking advantage of interdisciplinary consilience.



## References

- ad-hoc Arbeitsgruppe Boden, 2005. *Bodenkundliche Kartieranleitung*. E. Schweizerbart'sche Verlagbuchhandlung, Hannover.
- Aitchison, J., Greenacre, M., 2002. Biplots of compositional data. *J. R. Stat. Soc. Ser. C Appl. Stat.* 51, 375–392. doi:10.1111/1467-9876.00275
- Albrecht, C., Hauffe, T., Schreiber, K., Trajanovski, S., Wilke, T., 2009. Mollusc Biodiversity and Endemism in the Potential Ancient Lake Trichonis, Greece. *Malacologia* 51, 357–375. doi:10.4002/040.051.0209
- Avramidis, P., Geraga, M., Lazarova, M., Kontopoulos, N., 2013. Holocene record of environmental changes and palaeoclimatic implications in Alykes Lagoon, Zakynthos Island, western Greece, Mediterranean Sea. *Quat. Int.* 293, 184–195. doi:10.1016/j.quaint.2012.04.026
- Barnston, A.G., Livezey, R.E., 1987. Classification, Seasonality and Persistence of Low-Frequency Atmospheric Circulation Patterns. *Mon. Weather Rev.* 115, 1083–1126. doi:10.1175/1520-0493(1987)115<1083:CSAPOL>2.0.CO;2
- Barrett, S., Starnberger, R., Tjallingii, R., Brauer, A., Spötl, C., 2017. The sedimentary history of the inner-alpine Inn Valley, Austria: extending the Baumkirchen type section further back in time with new drilling. *J. Quat. Sci.* 32, 63–79. doi:10.1002/jqs.2924
- Bell, R.E., McNeill, L.C., Bull, J.M., Henstock, T.J., Collier, R.E.L., Leeder, M.R., 2009. Fault architecture, basin structure and evolution of the Gulf of Corinth rift, central Greece. *Basin Res.* 21, 824–855. doi:10.1111/j.1365-2117.2009.00401.x
- Benito, G., Macklin, M.G., Zielhofer, C., Jones, A.F., Machado, M.J., 2015. Holocene flooding and climate change in the Mediterranean. *Catena* 130, 13–33. doi:10.1016/j.catena.2014.11.014
- Berglund, B.E., 2003. Human impact and climate changes - Synchronous events and a causal link? *Quat. Int.* 104, 7–12. doi:10.1016/s1040-6182(02)00144-1
- Bintliff, J.L., 2012. *The Complete Archaeology of Greece, from Hunter-Gatherers to the Twentieth Century AD*. Blackwell-Wiley, Oxford, New York.
- Birks, H.H., Birks, H.J.B., 2006. Multi-proxy studies in palaeolimnology. *Veg. Hist. Archaeobot.* 15, 235–251. doi:10.1007/s00334-006-0066-6
- Birks, H.J.B., Lotter, A.F., Juggins, S., Smol, J.P., 2012. The March Towards the Quantitative Analysis of Palaeolimnological Data, in: Birks, H.J.B., Lotter, A.F., Juggins, S., Smol, J.P. (Eds.), *Tracking Environmental Change Using Lake Sediments*. Dordrecht, pp. 3–17.
- Björck, S., 2019. Ice, water and sediments: a cold, wet and muddy account of a very fun life in science. *J. Paleolimnol.* 62, 89–103. doi:10.1007/s10933-019-00073-5
- Blaauw, M., 2010. Methods and code for “classical” age-modelling of radiocarbon sequences. *Quat. Geochronol.* 5, 512–518. doi:10.1016/j.quageo.2010.01.002
- Blaauw, M., Christen, J.A., 2011. Flexible paleoclimate age-depth models using an autoregressive gamma process. *Bayesian Anal.* 6, 457–474. doi:10.1214/11-BA618
- Blaauw, M., Christen, J.A., Aquino-López, M.A., 2019. A Review of Statistics in Palaeoenvironmental Research. *J. Agric. Biol. Environ. Stat.* doi:10.1007/s13253-019-00374-2

- Bloemsmma, M.R., 2015. Development of a Modelling Framework for Core Data Integration using XRF Scanning. Dissertation, Delft University. Uitgeverij BOXPress, 's-Hertogenbosch.
- Bloemsmma, M.R., Zabel, M., Stuut, J.B.W., Tjallingii, R., Collins, J.A., Weltje, G.J., 2012. Modelling the joint variability of grain size and chemical composition in sediments. *Sediment. Geol.* 280, 135–148. doi:10.1016/j.sedgeo.2012.04.009
- Bottema, S., 1982. Palynological Investigations in Greece with Special Reference to Pollen as an Indicator of Human Activity. *Palaeohistoria* 24, 257–288.
- Boyd, M., 2015. Speleothems in Warm Climates: Holocene records from the Caribbean and Mediterranean. Dissertation, Stockholm University. Stockholm.
- Boyle, J.F., 2000. Rapid elemental analysis of sediment samples by isotope source XRF. *J. Paleolimnol.* 23, 213–221. doi:10.1023/A:1008053503694
- Bradley, R.S., 2015. *Paleoclimatology: Reconstructing Climates of the Quaternary*, 3rd ed. Academic Press, Oxford et al.
- Bronk Ramsey, C., 2008a. Deposition models for chronological records. *Quat. Sci. Rev.* 27, 42–60. doi:10.1016/j.quascirev.2007.01.019
- Bronk Ramsey, C., 2008b. Dealing with outliers and offsets in radiocarbon dating. *Radiocarbon* 57, 217–235.
- Büntgen, U., Myglan, V.S., Ljungqvist, F.C., McCormick, M., Cosmo, N. Di, Sigl, M., Jungclaus, J., Wagner, S., Krusic, P.J., Esper, J., Kaplan, J.O., Vaan, M.A.C. De, Luterbacher, J., Wacker, L., Tegel, W., Kirilyanov, A. V., 2016. Cooling and societal change during the Late Antique Little Ice Age from 536 to around 660 AD. *Nat. Geosci.* 9, 231–237. doi:10.1038/NGEO2652
- Chapman, J., 2018. Climatic and human impact on the environment?: A question of scale. *Quat. Int.* 496, 3–13. doi:10.1016/j.quaint.2017.08.010
- Cohen, A.S., 2003. *Paleolimnology: the history and evolution of lake systems*, 1st ed. Oxford University Press, Oxford.
- Croudace, I.W., Löwemark, L., Tjallingii, R., Zolitschka, B., 2019a. High resolution XRF core scanners: A key tool for the environmental and palaeoclimate sciences. *Quat. Int.* 514, 1–4. doi:10.1016/j.quaint.2019.05.038
- Croudace, I.W., Löwemark, L., Tjallingii, R., Zolitschka, B., 2019b. Current perspectives on the capabilities of high resolution XRF core scanners. *Quat. Int.* 514, 5–15. doi:10.1016/j.quaint.2019.04.002
- Croudace, I.W., Rindby, A., Rothwell, R.G., 2006. ITRAX: description and evaluation of a new multi-function X-ray core scanner. *New Tech. Sediment Core Anal.* 51–63. doi:10.1144/GSL.SP.2006.267.01.04
- Croudace, I.W., Rothwell, R.G., 2015. *Micro-XRF Studies of Sediment Cores, Tracking Environmental Change Using Lake Sediments. Volume 2: Physical and Geochemical Methods, Developments in Paleoenvironmental Research*. Springer Netherlands, Dordrecht. doi:10.1007/978-94-017-9849-5
- Dimitriou, E., Zacharias, I., 2006. Quantifying the rainfall-water level fluctuation process in a geologically complex Lake catchment. *Environ. Monit. Assess.* 119, 491–506. doi:10.1007/s10661-005-9039-y
- Drake, B.L., 2012. The influence of climatic change on the Late Bronze Age Collapse and the

- Greek Dark Ages. *J. Archaeol. Sci.* 39, 1862–1870. doi:10.1016/j.jas.2012.01.029
- Emmanouilidis, A., Unkel, I., Triantaphyllou, M., Avramidis, P., 2019. Late-Holocene coastal depositional environments and climate changes in the Gulf of Corinth, Greece. *The Holocene* 095968361987579. doi:10.1177/0959683619875793
- en.climate-data.org, 2019. Agrinio Climate [WWW Document]. URL <https://en.climate-data.org/europe/greece/agrinio/agrinio-6245/> (accessed 1.7.20).
- Erath, G., 1999. Archäologische Funde im Becken von Pheneos, in: Tausend, K. (Ed.), *Pheneos Und Lousoi. Untersuchungen Zu Geschichte Und Topographie Nordostarkadiens*. Frankfurt am Main, pp. 199–237.
- Filzmoser, P., Hron, K., Reimann, C., 2009. Principal components analysis for compositional data with outliers. *Environmetrics* 20, 621–632. doi:10.1002/env.966
- Finné, M., Bar-Matthews, M., Holmgren, K., Sundqvist, H.S., Liakopoulos, I., Zhang, Q., 2014. Speleothem evidence for late Holocene climate variability and floods in Southern Greece. *Quat. Res. (United States)* 81, 213–227. doi:10.1016/j.yqres.2013.12.009
- Finné, M., Holmgren, K., Shen, C.-C., Hu, H.-M., Boyd, M., Stocker, S., 2017. Late Bronze Age climate change and the destruction of the Mycenaean Palace of Nestor at Pylos. *PLoS One* 12, e0189447. doi:10.1371/journal.pone.0189447
- Finné, M., Holmgren, K., Sundqvist, H.S., Weiberg, E., Lindblom, M., 2011. Climate in the eastern Mediterranean, and adjacent regions, during the past 6000 years - A review. *J. Archaeol. Sci.* 38, 3153–3173. doi:10.1016/j.jas.2011.05.007
- Finné, M., Weiberg, E., 2018. Climate Change and Ancient Societies : Facing up to the Challenge of Chronological Control. *Stud. Glob. Archaeol.* 23.
- Finné, M., Woodbridge, J., Labuhn, I., Roberts, C.N., 2019. Holocene hydro-climatic variability in the Mediterranean: A synthetic multi-proxy reconstruction. *The Holocene* 29, 847–863. doi:10.1177/0959683619826634
- Fuchs, M., Lang, A., Wagner, G.A., 2004. The history of Holocene soil erosion in the Phlious Basin, NE Peloponnese, Greece, based on optical dating. *The Holocene* 14, 334–345. doi:10.1191/0959683604hl710rp
- Gawthorpe, R.L., Leeder, M.R., Kranis, H., Skourtsos, E., Andrews, J.E., Henstra, G.A., Mack, G.H., Muravchik, M., Turner, J.A., Stamatakis, M., 2018. Tectono-sedimentary evolution of the Plio-Pleistocene Corinth rift, Greece. *Basin Res.* 30, 448–479. doi:10.1111/bre.12260
- Geiger, R., 1954. *Klassifikation der Klimate nach W. Köppen*, Landolt-Bö. ed. Springer, Berlin.
- Giralt, S., Rico-Herrero, M.T., Vega, J.C., Valero-Garcés, B.L., 2011. Quantitative climate reconstruction linking meteorological, limnological and XRF core scanner datasets: The Lake Sanabria case study, NW Spain. *J. Paleolimnol.* 46, 487–502. doi:10.1007/s10933-011-9509-x
- Gogou, A., Triantaphyllou, M., Xoplaki, E., Izdebski, A., Parinos, C., Dimiza, M., Bouloubassi, I., Luterbacher, J., Kouli, K., Martrat, B., Toreti, A., Fleitmann, D., Rousakis, G., Kaberi, H., Athanasiou, M., Lykousis, V., 2016. Climate variability and socio-environmental changes in the northern Aegean (NE Mediterranean) during the last 1500 years. *Quat. Sci. Rev.* 136, 209–228. doi:10.1016/j.quascirev.2016.01.009
- Goslar, T., Czernik, J., 2000. Sample preparation in the Gliwice Radiocarbon Laboratory for AMS <sup>14</sup>C dating of sediments. *Geochronometria* 18, 1–8.

- Goslar, T., Czernik, J., Goslar, E., 2004. Low-energy  $^{14}\text{C}$  AMS in Poznań Radiocarbon Laboratory, Poland. *Nucl. Instruments Methods Phys. Res. Sect. B Beam Interact. with Mater. Atoms* 223–224, 5–11. doi:10.1016/j.nimb.2004.04.005
- Griffiths, H.I., Kryštufek, B., Reed, J.M., 2013. *Balkan Biodiversity: Pattern and Process in the European Hotspot*. Springer Science & Business Media.
- Grootes, P.M., Nadeau, M.-J., Rieck, A., 2004.  $^{14}\text{C}$ -AMS at the Leibniz-Labor: radiometric dating and isotope research. *Nucl. Instruments Methods Phys. Res. Sect. B Beam Interact. with Mater. Atoms* 223–224, 55–61. doi:10.1016/j.nimb.2004.04.015
- Haenssler, E., Nadeau, M.J., Vött, A., Unkel, I., 2013. Natural and human induced environmental changes preserved in a Holocene sediment sequence from the Etoliko Lagoon, Greece: New evidence from geochemical proxies. *Quat. Int.* 308–309, 89–104. doi:10.1016/j.quaint.2012.06.031
- Haldon, J., Mordechai, L., Newfield, T.P., Chase, A.F., Izdebski, A., Guzowski, P., Labuhn, I., Roberts, N., 2018. History meets palaeoscience: Consilience and collaboration in studying past societal responses to environmental change. *Proc. Natl. Acad. Sci.* 115, 201716912. doi:10.1073/pnas.1716912115
- Heiri, O., Lotter, A.F., Lemcke, G., 2001. Loss on ignition as a method for estimating organic and carbonate content in sediments: reproducibility and comparability of results. *J. Paleolimnol.* 25, 101–110. doi:10.1023/A:1008119611481
- Heymann, C., Nelle, O., Dörfler, W., Zagana, H., Nowaczyk, N., Xue, J., Unkel, I., 2013. Late Glacial to mid-Holocene palaeoclimate development of southern Greece inferred from the sediment sequence of Lake Stymphalia (NE-Peloponnese). *Quat. Int.* 302, 42–60. doi:10.1016/j.quaint.2013.02.014
- Holmgren, K., Gogou, A., Izdebski, A., Luterbacher, J., Sicre, M.A., Xoplaki, E., 2016. Mediterranean Holocene climate, environment and human societies. *Quat. Sci. Rev.* 136, 1–4. doi:10.1016/j.quascirev.2015.12.014
- Hughes, R., Weiberg, E., Bonnier, A., Finné, M., Kaplan, J., 2018. Quantifying Land Use in Past Societies from Cultural Practice and Archaeological Data. *Land* 7, 9. doi:10.3390/land7010009
- IPCC, 2013. Summary for Policymakers, in: Stocker, T.F., Qin, D., Plattner, G.-K., Tignor, M., Allen, S.K., Boschung, J., Nauels, A., Xia, Y., Bex, V., Midgley, P.M. (Eds.), *Climate Change 2013: The Physical Science Basis. Contribution of Working Group I to the Fifth Assessment Report of the Intergovernmental Panel on Climate Change*. Cambridge University Press, Cambridge, United Kingdom, and New York, NY, USA.
- Izdebski, A., Holmgren, K., Weiberg, E., Stocker, S.R., Büntgen, U., Florenzano, A., Gogou, A., Leroy, S.A.G., Luterbacher, J., Martrat, B., Masi, A., Mercuri, A.M., Montagna, P., Sadori, L., Schneider, A., Sicre, M.A., Triantaphyllou, M., Xoplaki, E., 2016. Realising consilience: How better communication between archaeologists, historians and natural scientists can transform the study of past climate change in the Mediterranean. *Quat. Sci. Rev.* 136, 5–22. doi:10.1016/j.quascirev.2015.10.038
- Jenkins, R., 1999. *X-Ray Fluorescence Spectroscopy*, 2nd editio. ed. Wiley & Sons, New York.
- Jenkins, R., De Vries, J., 1970. *X-ray spectrometry*. Macmillan, London.
- Kaniewski, D., Guiot, J., Van Campo, E., 2015. Drought and societal collapse 3200years ago in

- the Eastern Mediterranean: A review. *Wiley Interdiscip. Rev. Clim. Chang.* 6, 369–382. doi:10.1002/wcc.345
- Kaniewski, D., Marriner, N., Cheddadi, R., Morhange, C., Bretschneider, J., Jans, G., Otto, T., Luce, F., Van Campo, E., 2019. Cold and dry outbreaks in the eastern Mediterranean 3200 years ago. *Geology* 47, 933–937. doi:10.1130/g46491.1
- Kaniewski, D., Van Campo, E., Guiot, J., Le Burel, S., Otto, T., Baeteman, C., 2013. Environmental Roots of the Late Bronze Age Crisis. *PLoS One* 8, 1–10. doi:10.1371/journal.pone.0071004
- Katrantsiotis, C., Kylander, M.E., Smittenberg, R.H., Yamoah, K.K.A., Hättstrand, M., Avramidis, P., Strandberg, N.A., Norström, E., 2018. Eastern Mediterranean hydroclimate reconstruction over the last 3600 years based on sedimentary n-alkanes, their carbon and hydrogen isotope composition and XRF data from the Gialova Lagoon, SW Greece. *Quat. Sci. Rev.* 194, 77–93. doi:10.1016/j.quascirev.2018.07.008
- Katrantsiotis, C., Norström, E., Holmgren, K., Risberg, J., Skelton, A., 2015. High-resolution environmental reconstruction in SW Peloponnese, Greece, covering around the last c. 6000 years: Evidence from Agios Floros fen, Messenian plain. *The Holocene* 0959683615596838-. doi:10.1177/0959683615596838
- Katrantsiotis, C., Norström, E., Smittenberg, R.H., Finne, M., 2019. Climate changes in the Eastern Mediterranean over the last 5000 years and their links to the high-latitude atmospheric patterns and Asian monsoons. *Glob. Planet. Change* 175, 36–51. doi:10.1016/j.gloplacha.2019.02.001
- Keaveney, E.M., Reimer, P.J., 2012. Understanding the variability in freshwater radiocarbon reservoir offsets: a cautionary tale. *J. Archaeol. Sci.* 39, 1306–1316. doi:10.1016/j.jas.2011.12.025
- Kessler, T., 2020. Kontaktdimensionen. Früheisenzeitliche Keramik am Golf von Korinth. in preparation.
- Knapp, A.B., Manning, S.W., 2016. Crisis in Context: The End of the Late Bronze Age in the Eastern Mediterranean. *Am. J. Archaeol.* 120, 99. doi:10.3764/aja.120.1.0099
- Knauss, J., 1990. Der Graben des Herakles im Becken von Pheneos und die Vertreibung der stymphalischen Vögel. *MDAI(A)* 105, 52.
- Knitter, D., Brozio, J.P., Dörfler, W., Duttman, R., Feeser, I., Hamer, W., Kirleis, W., Müller, J., Nakoinz, O., 2019. Transforming landscapes: Modeling land-use patterns of environmental borderlands. *The Holocene* 29, 1572–1586. doi:10.1177/0959683619857233
- Kokinou, E., Kamberis, E., Vafidis, A., Monopolis, D., Ananiadis, G., Zelilidis, A., 2005. Deep seismic reflection data from offshore Western Greece: A new crustal model for the Ionian Sea. *J. Pet. Geol.* 28, 185–202. doi:10.1111/j.1747-5457.2005.tb00079.x
- Konert, M., Vandenberghe, J., 1997. Comparison of laser grain size analysis with pipette and sieve analysis: A solution for the underestimation of the clay fraction. *Sedimentology* 44, 523–535. doi:10.1046/j.1365-3091.1997.d01-38.x
- Köppen, W., 1936. *Das geographische System der Klimate*, Gebrüder B. ed. Berlin.
- Koussouris, T.S., Diapoulis, A.C., 1982. The aquatic vegetation of a large deep and oligotrophic lake (Lake Trichonis, western Greece). *Thalassographica* 5(2), 33–40.
- Krichak, S.O., Alpert, P., 2005. Decadal trends in the east Atlantic-west Russia pattern and

- Mediterranean precipitation. *Int. J. Climatol.* 25, 183–192. doi:10.1002/joc.1124
- Libby, W.F., Anderson, E.C., Arnold, J.R., 1949. Age determination by radiocarbon content: World-wide assay of natural radiocarbon. *Science* (80- ). 109, 227–228. doi:10.1126/science.109.2827.227
- Lim, Y.K., 2015. The East Atlantic/West Russia (EA/WR) teleconnection in the North Atlantic: climate impact and relation to Rossby wave propagation. *Clim. Dyn.* 44, 3211–3222. doi:10.1007/s00382-014-2381-4
- Lolos, Y.A., 2011. Land of Sikyon. Archaeology and History of a Greek City-state, *Hesperia Supplement*. American School of Classical Studies at Athens, Princeton, NJ.
- Longman, J., Ersek, V., Veres, D., Salzmann, U., 2017. Detrital events and hydroclimate variability in the Romanian Carpathians during the mid-to-late Holocene. *Quat. Sci. Rev.* 167, 78–95. doi:10.1016/j.quascirev.2017.04.029
- Löwemark, L., Bloemsma, M.R., Croudace, I., Daly, J.S., Edwards, R.J., Francus, P., Galloway, J.M., Gregory, B.R.B., Huang, J.S., Jones, A.F., Kylander, M., Löwemark, L., Luo, Y., Maclachlan, S., Ohlendorf, C., Patterson, R.T., Pearce, C., Profe, J., Reinhardt, E.G., Stranne, C., Tjallingii, R., Turner, J.N., 2019. Practical guidelines and recent advances in the Itrax XRF core-scanning procedure. *Quat. Int.* 514, 16–29. doi:10.1016/j.quaint.2018.10.044
- Löwemark, L., Chen, H.F., Yang, T.N., Kylander, M., Yu, E.F., Hsu, Y.W., Lee, T.Q., Song, S.R., Jarvis, S., 2011. Normalizing XRF-scanner data: A cautionary note on the interpretation of high-resolution records from organic-rich lakes. *J. Asian Earth Sci.* 40, 1250–1256. doi:10.1016/j.jseaes.2010.06.002
- Lucke, B., Lucke, B., Sprafke, T., Lucke, B., Sprafke, T., 2015. Correlation of soil color, redness ratings, and weathering indices of *Terrae Calcis* along a precipitation gradient in northern Jordan, in: *Erlanger Geographische Arbeiten Band 42*. pp. 53–68.
- Malvern Instruments, L., 2007. Mastersizer 2000 - user manual (No. MAN0384 Issue 1.0). Worcestershire, UK.
- Mayewski, P.A., Rohling, E.E., Curt Stager, J., Karlén, W., Maasch, K.A., Meeker, L.D., Meyerson, E.A., Gasse, F., van Kreveld, S., Holmgren, K., Lee-Thorp, J., Rosqvist, G., Rack, F., Staubwasser, M., Schneider, R.R., Steig, E.J., 2004. Holocene Climate Variability. *Quat. Res.* 62, 243–255. doi:10.1016/j.yqres.2004.07.001
- McNeill, L.C., Shillington, D.J., Carter, G.D.O., Everest, J.D., Gawthorpe, R.L., Miller, C., Phillips, M.P., Collier, R.E.L., Cvetkoska, A., De Gelder, G., Diz, P., Doan, M.-L., Ford, M., Geraga, M., Gillespie, J., Hemelsdaël, R., Herrero-Bervera, E., Ismaiel, M., Janikian, L., Kouli, K., Le Ber, E., Li, S., Maffione, M., Mahoney, C., Machlus, M.L., Michas, G., Nixon, C.W., Oflaz, S.A., Omale, A.P., Panagiotopoulos, K., Pechlivanidou, S., Sauer, S., Seguin, J., Sergiou, S., Zakharova, N. V., Green, S., 2019. High-resolution record reveals climate-driven environmental and sedimentary changes in an active rift. *Sci. Rep.* 9, 3116. doi:10.1038/s41598-019-40022-w
- McNeill, L.C., Shillington, D.J., Carter, G.D.O., Everest, J.D., Le Ber, E., Collier, R.E., Cvetkoska, A., De Gelder, G., Diz, P., Doan, M.L., Ford, M., Gawthorpe, R.L., Geraga, M., Gillespie, J., Hemelsdaël, R., Herrero-Bervera, E., Ismaiel, M., Janikian, L., Kouli, K., Li, S., Machlus, M.L., Maffione, M., Mahoney, C., Michas, G., Miller, C., Nixon, C.W., Oflaz, S.A., Omale, A.P., Panagiotopoulos, K., Pechlivanidou, S., Phillips, M.P., Sauer, S., Seguin, J., Sergiou,

- S., Zakharova, N.V., 2019. Corinth Active Rift Development. Proceedings of the International Ocean Discovery Program, Proceedings of the International Ocean Discovery Program. International Ocean Discovery Program, College Station, TX, USA. doi:10.14379/iodp.proc.381.2019
- Meyers, P.A., 2003. Applications of organic geochemistry to paleolimnological reconstructions: A summary of examples from the Laurentian Great Lakes. *Org. Geochem.* 34, 261–289. doi:10.1016/S0146-6380(02)00168-7
- Meyers, P.A., Ishiwatari, R., 1993. Lacustrine organic geochemistry-an overview of indicators of organic matter sources and diagenesis in lake sediments. *Org. Geochem.* 20, 867–900. doi:10.1016/0146-6380(93)90100-P
- Middleton, G.D., 2010. The Collapse of palatial society in LBA Greece and the postpalatial period.
- Mingram, J., Negendank, J.F.W., Brauer, A., Berger, D., Hendrich, A., Köhler, M., Usinger, H., 2007. Long cores from small lakes - Recovering up to 100 m-long lake sediment sequences with a high-precision rod-operated piston corer (Usinger-corer). *J. Paleolimnol.* 37, 517–528. doi:10.1007/s10933-006-9035-4
- Mook, W.G., van der Plicht, J., 1999. Reporting <sup>14</sup>C activities and concentrations. *Radiocarbon* 41, 227–239. doi:10.1017/S0033822200057106
- Moretti, I., Sakellariou, D., Lykousis, V., Micarelli, L., 2003. The Gulf of Corinth: An active half graben? *J. Geodyn.* 36, 323–340. doi:10.1016/S0264-3707(03)00053-X
- Morfis, A., Zojer, H., 1986. Karst Hydrogeology of the Central and Eastern Peloponnesus (Greece). *Steir. Beitr. zur Hydrogeol.* 37/38, 1–301.
- Müller, J., Kirleis, W., 2019. The concept of socio-environmental transformations in prehistoric and archaic societies in the Holocene: An introduction to the special issue. *The Holocene.* doi:10.1177/0959683619857236
- Munsell, A.H., 2000. Munsell Soil Color Charts. Munsell Color, Grand Rapids.
- Murray, M.R., 2002. Is laser particle size determination possible for carbonate-rich lake sediments? *J. Paleolimnol.* 27, 173–183. doi:10.1023/A:1014281412035
- Naeher, S., Gilli, A., North, R.P., Hamann, Y., Schubert, C.J., 2013. Tracing bottom water oxygenation with sedimentary Mn/Fe ratios in Lake Zurich, Switzerland. *Chem. Geol.* 352, 125–133. doi:10.1016/j.chemgeo.2013.06.006
- Nanou, E.-A., Zagana, E., 2018. Groundwater Vulnerability to Pollution Map for Karst Aquifer Protection (Ziria Karst System, Southern Greece). *Geosciences* 8, 125. doi:10.3390/geosciences8040125
- Nieto-Moreno, V., Martínez-Ruiz, F., Giralt, S., Jiménez-Espejo, F., Gallego-Torres, D., Rodrigo-Gámiz, M., García-Orellana, J., Ortega-Huertas, M., De Lange, G.J., 2011. Tracking climate variability in the western Mediterranean during the Late Holocene: A multiproxy approach. *Clim. Past* 7, 1395–1414. doi:10.5194/cp-7-1395-2011
- Norström, E., Katrantsiotis, C., Smittenberg, R.H., Kouli, K., 2017. Chemotaxonomy in some Mediterranean plants and implications for fossil biomarker records. *Geochim. Cosmochim. Acta* 219, 96–110. doi:10.1016/j.gca.2017.09.029
- Ön, B.B., Akçer-Ön, S., Özeren, S.M., Eriş, K.K., Greaves, A.M., Çağatay, N.M., 2017. Climate proxies for the last 17.3 ka from Lake Hazar (Eastern Anatolia), extracted by independent component analysis of  $\mu$ -XRF data. *Quat. Int.* doi:10.1016/j.quaint.2017.08.066

- Papastergiadou, E.S., Retalis, A., Kalliris, P., Georgiadis, T., 2007. Land use changes and associated environmental impacts on the Mediterranean shallow Lake Stymfalia, Greece. *Hydrobiologia* 584, 361–372. doi:10.1007/s10750-007-0606-9
- Perşoiu, A., Onac, B.P., Wynn, J.G., Blaauw, M., Ionita, M., Hansson, M., 2017. Holocene winter climate variability in Central and Eastern Europe. *Sci. Rep.* 7, 1–8. doi:10.1038/s41598-017-01397-w
- Poraj-Górska, A.I., Żarczyński, M.J., Ahrens, A., Enters, D., Weisbrodt, D., Tylmann, W., 2017. Impact of historical land use changes on lacustrine sedimentation recorded in varved sediments of Lake Jaczno, northeastern Poland. *Catena* 153, 182–193. doi:10.1016/j.catena.2017.02.007
- Psomiadis, D., Dotsika, E., Albanakis, K., Ghaleb, B., Hillaire-Marcel, C., 2018. Speleothem record of climatic changes in the northern Aegean region (Greece) from the Bronze Age to the collapse of the Roman Empire. *Palaeogeogr. Palaeoclimatol. Palaeoecol.* 489, 272–283. doi:10.1016/j.palaeo.2017.10.021
- QGIS Development Team, 2019. QGIS Geographic Information System. Open Source Geospatial Foundation Project.
- R Core Team, 2019. R: A language and environment for statistical computing. R Foundation for Statistical Computing, Vienna, Austria, Austria.
- Ramsey, M.H., Potts, P.J., Webb, P.C., Watkins, P., Watson, J.S., Coles, B.J., 1995. An objective assessment of analytical method precision: comparison of ICP-AES and XRF for the analysis of silicate rocks. *Chem. Geol.* 124, 1–19. doi:10.1016/0009-2541(95)00020-M
- Reimer, P.J., Bard, E., Bayliss, A., Beck, J.W., Blackwell, P.G., Ramsey, C.B., Buck, C.E., Cheng, H., Edwards, R.L., Friedrich, M., Grootes, P.M., Guilderson, T.P., Haflidason, H., Hajdas, I., Hatté, C., Heaton, T.J., Hoffmann, D.L., Hogg, A.G., Hughen, K.A., Kaiser, K.F., Kromer, B., Manning, S.W., Niu, M., Reimer, R.W., Richards, D.A., Scott, E.M., Southon, J.R., Staff, R.A., Turney, C.S.M., van der Plicht, J., 2013. IntCal13 and Marine13 Radiocarbon Age Calibration Curves 0–50,000 Years cal BP. *Radiocarbon* 55, 1869–1887. doi:10.2458/azu\_js\_rc.55.16947
- Richter, T.O., Van Der Gaast, S., Koster, B., Vaars, A., Gieles, R., De Stigter, H.C., De Haas, H., Van Weering, T.C.E., 2006. The Avaatech XRF Core Scanner: Technical description and applications to NE Atlantic sediments. *Geol. Soc. Spec. Publ.* 267, 39–50. doi:10.1144/GSL.SP.2006.267.01.03
- Roberts, N., Allcock, S.L., Arnaud, F., Dean, J.R., Eastwood, W.J., Jones, M.D., Leng, M.J., Metcalfe, S.E., Malet, E., Woodbridge, J., Yiğitbaşıoğlu, H., 2016. A tale of two lakes: a multi-proxy comparison of Lateglacial and Holocene environmental change in Cappadocia, Turkey. *J. Quat. Sci.* 31, 348–362. doi:10.1002/jqs.2852
- Roberts, N., Eastwood, W.J., Kuzucuoğlu, C., Fiorentino, G., Caracuta, V., 2011. Climatic, vegetation and cultural change in the eastern Mediterranean during the mid-Holocene environmental transition. *The Holocene* 21, 147–162. doi:10.1177/0959683610386819
- Roberts, N., Moreno, A., Valero-Garcés, B.L., Corella, J.P., Jones, M., Allcock, S., Woodbridge, J., Morellón, M., Luterbacher, J., Xoplaki, E., Türkeş, M., 2012. Palaeolimnological evidence for an east-west climate see-saw in the Mediterranean since AD 900. *Glob. Planet. Change* 84–85, 23–34. doi:10.1016/j.gloplacha.2011.11.002



- Roberts, N., Woodbridge, J., Bevan, A., Palmisano, A., Shennan, S., Asouti, E., 2017. Human responses and non-responses to climatic variations during the last Glacial-Interglacial transition in the eastern Mediterranean. *Quat. Sci. Rev.* 184, 47–67. doi:10.1016/j.quascirev.2017.09.011
- Rydberg, J., Lindborg, T., Sohlenius, G., Reuss, N., Olsen, J., Laudon, H., 2016. The Importance of Eolian Input on Lake-Sediment Geochemical Composition in the Dry Proglacial Landscape of Western Greenland. *Arctic, Antarct. Alp. Res.* 48, 93–109. doi:10.1657/aaar0015-009
- Ryzak, M., Bieganski, A., 2010. Determination of particle size distribution of soil using laser diffraction - comparison with areometric method. *Int. Agrophysics* 24, 177–181.
- Schreiber, N., Garcia, E., Kroon, A., Ilsøe, P.C., Kjær, K.H., Andersen, T.J., 2014. Pattern recognition on X-ray fluorescence records from Copenhagen lake sediments using principal component analysis. *Water, Air, Soil Pollut.* 225. doi:10.1007/s11270-014-2221-5
- Shillington, D.J., McNeill, L.C., Carter, G.D.O., 2019. Expedition 381 Preliminary Report: Corinth Active Rift Development 381. doi:10.14379/iodp.pr.381.2019
- Siani, G., Paterne, M., Arnold, M., Bard, E., Métivier, B., Tisnerat, N., Bassinot, F., 2000. Radiocarbon Reservoir Ages in the Mediterranean Sea and Black Sea. *Radiocarbon* 42, 271–280. doi:10.1017/S0033822200059075
- Skoulikidis, N.T., Bertahas, I., Koussouris, T., 1998. The environmental state of freshwater resources in Greece (rivers and lakes). *Environ. Geol.* 36, 1–17. doi:10.1007/s002540050315
- Staubwasser, M., Weiss, H., 2006. Holocene climate and cultural evolution in late prehistoric–early historic West Asia. *Quat. Res.* 66, 372–387.
- Storti, F., Balsamo, F., 2010. Particle size distributions by laser diffraction: sensitivity of granular matter strength to analytical operating procedures. *Solid Earth* 1, 25–48. doi:10.5194/se-1-25-2010
- Stuiver, M., Reimer, P.J., 1993. Extended 14 C Data Base and Revised CALIB 3.0 14 C Age Calibration Program. *Radiocarbon* 35, 215–230. doi:10.1017/S0033822200013904
- Tausend, K., 1999. Die Siedlungen im Gebiet von Pheneos, in: Tausend, K. (Ed.), *Pheneos Und Lousoi. Untersuchungen Zu Geschichte Und Topographie Nordostarkadiens*. Frankfurt am Main, pp. 331–342.
- Taymaz, T., Yilmaz, Y., Dilek, Y., 2007. The geodynamics of the Aegean and Anatolia: introduction. *Geol. Soc. London, Spec. Publ.* 291, 1–16. doi:10.1144/SP291.1
- Thompson, J.D., 2005. *Plant Evolution in the Mediterranean*. Oxford University Press. doi:10.1093/acprof:oso/9780198515340.001.0001
- Tjallingii, R., Röhl, U., Kölling, M., Bickert, T., 2007. Influence of the water content on X-ray fluorescence coresampling measurements in soft marine sediments. *Geochemistry, Geophys. Geosystems* 8, 1–12. doi:10.1029/2006GC001393
- Unkel, I., 2019. Nature and Perception of a Greek Landscape : Stymphalos, in: Haug, A., Käppel, L., Müller, J. (Eds.), *Past Landscapes. The Dynamics of Interaction between Society, Landscape and Culture*. Sidestone Press, Leiden, pp. 311–322.
- Unkel, I., Heymann, C., Nelle, O., Zagana, E., 2011. Climatic influence on Lake Stymphalia during the last 15 000 years, in: Lambrakis, N., Stournaras, G., Katsanou, K. (Eds.),

- Advances in the Research of Aquatic Environment. Springer Berlin Heidelberg, Berlin, Heidelberg, pp. 75–82. doi:10.1007/978-3-642-19902-8\_8
- Unkel, I., Schimmelmann, A., Shriner, C., Forsén, J., Heymann, C., Brückner, H., 2014. The environmental history of the last 6500 years in the Asea Valley (Peloponnese, Greece) and its linkage to the local archaeological record. *Zeitschrift für Geomorphol. Suppl. Issues* 58, 89–107. doi:10.1127/0372-8854/2014/S-00160
- Vött, A., Brückner, H., Zander, A.M., May, S.M., Mariolakos, I., Lang, F., Fountoulis, I., Dunkel, A., 2009. Late Quaternary evolution of Mediterranean poljes – the Vatos case study (Akarnania, NW Greece) based on geo-scientific core analyses and IRSL dating. *Zeitschrift für Geomorphol.* 53, 145–169. doi:10.1127/0372-8854/2009/0053-0145
- Voudouris, K., Mavrommatis, T., Antonakos, A., 2007. Hydrologic balance estimation using GIS in Korinthia prefecture, Greece. *Adv. Sci. Res.* 1, 1–8. doi:10.5194/asr-1-1-2007
- Walsh, K., Brown, A.G., Gourley, B., Scaife, R., 2017. Archaeology, hydrogeology and geomorphology in the Stymphalos valley. *J. Archaeol. Sci. Reports* 15, 446–458. doi:10.1016/j.jasrep.2017.03.058
- Warke, S.F., Fohlmeister, J., Schröder-Ritzrau, A., Constantin, S., Spötl, C., Gerdes, A., Esper, J., Frank, N., Arps, J., Terente, M., Riechelmann, D.F.C., Mangini, A., Scholz, D., 2018. Reconstruction of late Holocene autumn/winter precipitation variability in SW Romania from a high-resolution speleothem trace element record. *Earth Planet. Sci. Lett.* 499, 122–133. doi:10.1016/j.epsl.2018.07.027
- Weiberg, E., Bevan, A., Kouli, K., Katsianis, M., Woodbridge, J., Bonnier, A., Engel, M., Finné, M., Fyfe, R., Maniatis, Y., Palmisano, A., Panajiotidis, S., Roberts, N., Shennan, S., 2019. Long-term trends of land use and demography in Greece: A comparative study. The Holocene 095968361982664. doi:10.1177/0959683619826641
- Weiberg, E., Unkel, I., Kouli, K., Holmgren, K., Avramidis, P., Bonnier, A., Dibble, F., Finné, M., Izdebski, A., Katrantsiotis, C., Stocker, S.R., Andwinge, M., Baika, K., Boyd, M., Heymann, C., 2016. The socio-environmental history of the Peloponnese during the Holocene: Towards an integrated understanding of the past. *Quat. Sci. Rev.* 136, 40–65. doi:10.1016/j.quascirev.2015.10.042
- Weiss, B., 1982. The decline of Late Bronze Age civilization as a possible response to climatic change. *Clim. Change* 4, 173–198. doi:10.1007/BF02423389
- Weltje, G.J., Bloemsa, M.R., Tjallingii, R., Heslop, D., Röhl, U., Croudace, I.W., 2015. Prediction of Geochemical Composition from XRF Core Scanner Data: A New Multivariate Approach Including Automatic Selection of Calibration Samples and Quantification of Uncertainties, in: *Micro-XRF Studies of Sediment Cores.* pp. 507–534. doi:10.1007/978-94-017-9849-5\_21
- Weltje, G.J., Tjallingii, R., 2008. Calibration of XRF core scanners for quantitative geochemical logging of sediment cores: Theory and application. *Earth Planet. Sci. Lett.* 274, 423–438. doi:10.1016/j.epsl.2008.07.054
- Weninger, B., Clare, L., Rohling, E., Bar-Yosef, O., Böhner, U., Budja, M., Bundschuh, M., Feurdean, A., Gebe, H.G., Jöris, O., Linstädter, J., Mayewski, P., Mühlenbruch, T., Reingruber, A., Rollefson, G., Schyle, D., Thissen, L., Todorova, H., Zielhofer, C., 2009. The Impact of Rapid Climate Change on Prehistoric Societies during the Holocene in the

- Eastern Mediterranean. *Doc. Praehist.* 36, 7. doi:10.4312/dp.36.2
- Xoplaki, E., González-Rouco, J.F., Gyalistras, D., Luterbacher, J., Rickli, R., Wanner, H., 2003a. Interannual summer air temperature variability over Greece and its connection to the large-scale atmospheric circulation and Mediterranean SSTs 1950-1999. *Clim. Dyn.* 20, 537–554. doi:10.1007/s00382-002-0291-3
- Xoplaki, E., González-Rouco, J.F., Luterbacher, J., Wanner, H., 2003b. Mediterranean summer air temperature variability and its connection to the large-scale atmospheric circulation and SSTs. *Clim. Dyn.* 20, 723–739. doi:10.1007/s00382-003-0304-x
- Xoplaki, E., Luterbacher, J., Burkard, R., Patrikas, I., Maheras, P., 2000. Connection between the large-scale 500 hPa geopotential height fields and precipitation over Greece during wintertime. *Clim. Res.* 14, 129–146. doi:10.3354/cr014129
- Xoplaki, E., Luterbacher, J., Wagner, S., Zorita, E., Fleitmann, D., Preiser-Kapeller, J., Sargent, A.M., White, S., Toreti, A., Haldon, J.F., Mordechai, L., Bozkurt, D., Akçer-Ön, S., Izdebski, A., 2018. Modelling Climate and Societal Resilience in the Eastern Mediterranean in the Last Millennium. *Hum. Ecol.* 1–17. doi:10.1007/s10745-018-9995-9
- Zacharias, I., Bertachas, I., Skoulikidis, N., Koussouris, T., 2002. Greek Lakes: Limnological overview. *Lakes Reserv. Res. Manag.* 7, 55–62. doi:10.1046/j.1440-1770.2002.00171.x
- Zolitschka, B., Francus, P., Ojala, A.E.K., Schimmelmann, A., 2015. Varves in lake sediments - a review. *Quat. Sci. Rev.* 117, 1–41. doi:10.1016/j.quascirev.2015.03.019



# Appendix I



## **2,500 years of anthropogenic and climatic landscape transformation in the Stymphalia polje, Greece**

Joana Seguin<sup>1\*</sup>, John L. Bintliff<sup>2</sup>, Pieter M. Grootes<sup>1,3,4</sup>, Thorsten Bauersachs<sup>5</sup>, Walter Dörfler<sup>3,6</sup>, Christian Heymann<sup>1,3</sup>, Sturt W. Manning<sup>7</sup>, Samuel Müller<sup>8</sup>, Marie-Josée Nadeau<sup>4</sup>, Oliver Nelle<sup>1,3,9</sup>, Peter Steier<sup>10</sup>, Jan Weber<sup>5</sup>, Eva-Maria Wild<sup>10</sup>, Eleni Zagana<sup>11</sup>, Ingmar Unkel<sup>1,3</sup>

<sup>1</sup>Institute for Ecosystem Research, Christian-Albrechts-University, Olshausenstraße 75, 24118 Kiel, Germany

<sup>2</sup>Department of Archeology, Edinburgh University, Teviot Place, EH8 9AG, United Kingdom

<sup>3</sup>Graduate School, “Human Development in Landscapes”, Christian-Albrechts-University, Leibnizstr. 3, 24118 Kiel, Germany

<sup>4</sup>National Laboratory for Age Determination, NTNU Vitenskapsmuseet, 7491 Trondheim, Norway

<sup>5</sup>Institute of Geosciences, Department of Organic Geochemistry, Christian-Albrechts-University Kiel, Ludewig-Meyn-Straße 10, 24118 Kiel, Germany

<sup>6</sup>Institute of Pre- and Protohistoric Archaeology, Christian-Albrechts-University, Johanna-Mestorf-Straße 2-6, 24118 Kiel, Germany

<sup>7</sup>Cornell Tree-Ring Laboratory, Department of Classics, Cornell University, Ithaca NY 14853-3201, USA

<sup>8</sup>Institute of Geosciences, Department of Paleooceanography & Paleoclimate, Christian-Albrechts-University, Ludewig-Meyn-Straße 10, 24118 Kiel, Germany

<sup>9</sup>Tree-ring Lab, Landesamt für Denkmalpflege im Regierungspräsidium Stuttgart, Fischersteig 9, D-78343 Hemmenhofen, Germany

<sup>10</sup>VERA-Laboratorium, Währinger Straße 17, Kavalierstrakt, 1090 Wien, Austria

<sup>11</sup>Department of Geology, University of Patras, Rio 26500 Patras, Greece

\*Corresponding author: [jseguin@ecology.uni-kiel.de](mailto:jseguin@ecology.uni-kiel.de)

### **Origin**

This manuscript was accepted for publication in Quaternary Science Reviews.

The published journal article can be accessed via

<https://doi.org/10.1016/j.quascirev.2019.04.028>.

© 2019. This manuscript version is made available under the CC-BY-NC-ND 4.0 license

<http://creativecommons.org/licenses/by-nc-nd/4.0/>

## **Keywords**

*Late Holocene; Palaeoclimatology; Palaeolimnology; Eastern Mediterranean; Greece; Geochemistry; Sedimentology; XRF; GDGT; Late Antique Little Ice Age*

## **Abstract**

Lacustrine sediments generally record landscape development in the lake's catchment area controlled by palaeoclimatic and human induced changes. To improve our understanding on the anthropogenic and climatic influences on landscape development in Southern Greece for the last 2,500 years, we report a 2 m-long, continuous high-resolution sedimentary record from shallow Lake Stymphalia (Peloponnese, Greece). Our proxies record climatically as well as anthropogenically induced landscape changes, influencing the lake area and lake depth.

The Classical-Hellenistic era reflects a moderate, stable Mediterranean climate with low sedimentation rates. The parallel existence of the highly populated, major ancient city of Stymphalos, on the contemporary lake edge, doesn't seem to have caused lasting alterations in the record. The construction of the Hadrianic Aqueduct in the Roman era, ca. 130 AD, however causes an influential transformation in the lake development. It has a lasting effect on the lake hydrology as well as the vulnerability of this ecosystem. During Late Roman times, 5<sup>th</sup> to 6<sup>th</sup> century cal AD, the abandonment of the aqueduct combined with cooler climate conditions allows lake levels to recover. A phase of very high climatic instability was identified for the subsequent Early Byzantine (EB) period, during the 7<sup>th</sup> and 8<sup>th</sup> century cal AD. For this period, the later phase of the Late Antique Little Ice Age (LALIA), our proxies indicate further cooling and highly fluctuating water availability in a rather small lake area. The Middle Byzantine (MB) Period (9<sup>th</sup>-12<sup>th</sup> century AD) is characterized by an over fivefold increase in sedimentation rates. Since local population was still well below Classical levels, we explain this singular period through an interaction of modest increase in land use but marked by careless management of deforested areas, warm and wet climatic conditions during the Medieval Warm Period and long-term effects of



vulnerability caused by the aqueduct construction. Probably during this phase, the lake level rose through unparalleled sedimentary infill to flood and bury a significant part of the Lower Town of the abandoned ancient city. The Late Byzantine Period (13<sup>th</sup> and 14<sup>th</sup> century AD) sees core evidence for erosion of established, non-vegetated soils (high magnetic susceptibility), in a period of almost total depopulation. In the subsequent Ottoman era (late 15<sup>th</sup> – early 19<sup>th</sup> centuries AD) local settlement made only slight recovery, the climatic conditions seem less stable during the Little Ice Age (LIA) and the lake seasonally and later periodically starts to dry up, cumulating in a longer dry phase at the end of the 19<sup>th</sup> century AD, when agricultural activity on the polje floor was possible. The conclusion conforms with recent modelling of environmental change, critical of mono-causation, rather focussing on complex interactions of human and natural factors in the inception of landscape transformation.

## **1. Introduction**

The Late Holocene in southern Greece is shaped by a strong interaction of climatic changes with natural and anthropogenic landscape transformations. Although there is an increasing number of studies demonstrating the complex interrelationship between climate and societies, it often remains challenging to decipher the influence of climatic change versus human activities in environmental records. Palaeoclimatologists have developed reconstructions of climate change in the Mediterranean region during the Holocene, covering cultural periods back to the Neolithic, when humans became sedentary and the interrelationship between climatic fluctuations and human activity grew in importance (Finné et al., 2011; Magny and Magny, 2013; Meriam et al., 2017; Palmisano et al., 2019, 2017; Roberts et al., 2016).

Recent studies have suggested that important climatic shifts in the Late Holocene coincide with major changes in Mediterranean cultural history (Butzer, 2012; Drake, 2012; Kaniewski et al., 2013; Langgut et al., 2013; Staubwasser and Weiss, 2006; Weninger et al., 2009). However, many archaeologists and historians have been critical of naïve use of climate change as a forcing factor in the socio-cultural development of the region due to the lack of both high-resolution terrestrial palaeoclimate data in a solid chronology framework and simple forcing-and-response

mechanisms (Haldon et al., 2018). Hence, there is a strong need for closer interdisciplinary collaboration on research questions dealing with human-environmental interaction and societal response to climatic changes (Bintliff, 2012a, 2002; Casana, 2008; Izdebski et al., 2016a; Knapp and Manning, 2016; Sadori et al., 2008).

Climate reconstructions from lake sediment archives in the Eastern Mediterranean are still relatively scarce and the climate patterns often seem less well constrained compared to the Western Mediterranean (Gogou et al., 2016; Luterbacher et al., 2012, McCormick et al., 2012). In particular, the last 2,500 years have been studied less frequently or with lower resolution in palaeoenvironmental records although this time period is of major relevance for the development of Greek society (Finné et al., 2011; Sadori et al., 2016; Xoplaki et al., 2016a). Recently, Büntgen et al. (2016) identified a cold phase in Eurasia lasting from 536 to 660 AD based on high-resolution tree ring records and named it Late Antique Little Ice Age (LALIA). This overlaps with the latter part of the European Migration Period (4<sup>th</sup> – 7<sup>th</sup> century AD; Moschen et al., 2011), an interval of widespread migration movements into the Roman Empire, which saw considerable societal changes, including the collapse of the Western Roman Empire, the transformation of the Eastern Roman Empire into the Byzantine state, the collapse of the Sasanian Empire, the expansion of Slavic-speaking peoples in central and eastern Europe and the Justinian Plague (Moschen et al., 2011). Due to these significant societal changes and its negative impacts on European civilisations, this wider period is also referred to as the “Dark Age[s]” (Brooke, 2014; Büntgen et al., 2016; Helama et al., 2017a; McCormick et al., 2012). While there is considerable archaeological information from the Greek Mainland, including the Peloponnese Peninsula, for human activities during the last two millennia (Bintliff, 2012b; Izdebski et al., 2016b), high resolution palaeoclimate records for this period are rare (Atherden and Hall, 1994; Finné et al., 2011; Izdebski et al., 2016; Jahns, 1993). In a recent review of the currently available climate records from the Mediterranean for the last two millennia, Luterbacher et al. (2012) state that the existing climate proxies often express varying trends, even within the same region. All of this demonstrates the need for further interdisciplinary, high-resolution studies on landscape development in the Eastern Mediterranean.

With the intention of addressing this gap and limited dataset, we here provide a detailed palaeoenvironmental reconstruction of the last 2,500 years from Lake Stymphalia, the only remaining natural perennial lake in the Peloponnese. We discuss the environmental changes in the catchment in relation to the human history known from the area in order to distinguish anthropogenic from climatic developments imprinted into the sedimentary record. The potential expression of the LALIA in Southern Greece is investigated in order to improve our understanding of the societal and environmental history of this area during this period of rapid climate fluctuations. Excavations at Ancient Stymphalos by the Canadian Institute in Greece since 1983 provide the archaeological groundwork to reconstruct human activity in the area (cf. section 3.6). As a karst polje without surficial outflow represents on the one hand a continuous sediment sink and on the other hand has always been considered as an important location for agriculture and farming in the Mediterranean area (Vött et al., 2009), Lake Stymphalia represents an excellent archive to study a combination of climatically as well as anthropogenically induced environmental changes. The differentiation between human and climate induced factors behind environmental changes, however, is not always trivial and several causes may provoke the same response in the sedimentary record. For example, reduction in the amount of water available in Lake Stymphalia may result from either: (1) a decrease in precipitation; (2) an increase in evaporation; (3) changes in the thawing period and variations in the discharge related to snowmelt; (4) inferred or recorded human channelling of the water from the source; (5) increased water usage of lake water for agricultural purposes. To get a better idea of the complete picture, we take into account several different palaeoenvironmental proxies, traditional and well-established ones as well as new and innovative proxies. As far as available, we included archaeological or historical evidence and when we can still not be certain of the process causing a signal in the record, we provide a selection of possible scenarios.

## **2. Study area**

Lake Stymphalia (Λίμνη Στυμφαλία) (37.85° N, 22.46° E), is a shallow karstic lake located in the north-eastern Peloponnese (Greece; Figure 1 and 3-A). It is described in detail by Heymann et al.

(2013). Sediment material is only received from surface runoff and torrential rivers originating from karst springs, which depend on the amount of precipitation that is brought mainly in winter and early spring (Figure 2). On the polje floor, the karstified limestone is covered by argillaceous sediments of up to 160 m thickness (Morfis and Zojer, 1986). Presently, Lake Stymphalia is the largest remaining mountain lake in the Peloponnese, protected by the NATURA 2000 network (Heymann et al., 2013; Morfis and Zojer, 1986, Papastergiadou et al., 2007).

Modern climatic conditions are described in Heymann et al. (2013) and Morfis and Zojer (1986). In a recent publication, Nanou and Zagana (2018) indicate a mean annual precipitation of 850 mm and ranges from 719 to 1656 mm for the time period 1975–2015, confirming high inter-annual variation.

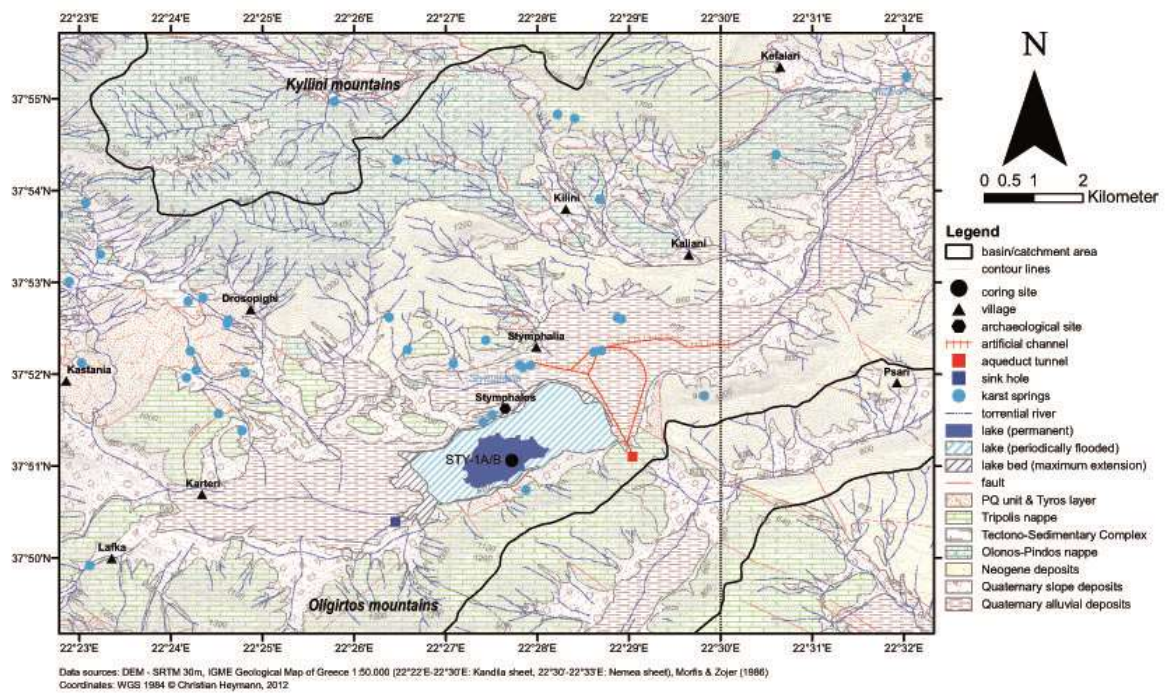


**Figure 1. Topographic and geological map. The Stymphalia basin with its drainage system and the approximate catchment area are shown. The map was created using ESRI ArcGIS 10.**

Based on daily precipitation data recorded between 1949 and 2011 at the meteorological station Driza-Stymphalia (37.8699° N, 22.4643° E, Greek Special Secretariat for Water, Ministry of Environment and Energy), we calculated the mean annual precipitation at  $618\pm 201$  mm over the respective period; this occurs mainly from October to February (Figure 2). In April 2017, we installed a small datalogger (Tinytag Plus 2) close to the fountain house of ancient Stymphalos to measure daily temperatures and relative humidity, which provided the monthly temperature values shown in Figure 2.

The lake's surface area may have varied substantially throughout time and there is evidence for seasonal desiccation (Walsh et al., 2017). Since the 19<sup>th</sup> century, the lake occasionally dried out completely, which in the mid-20<sup>th</sup> century allowed it occasionally to function as a aircraft runway (hence the reason for its local nickname “aerodromio” (airport)). In recent times, Lake Stymphalia fell dry during the early 1990s and was used for agricultural purposes (Papastergiadou et al., 2007). For several reasons, we do not assume any extreme lake level rise at Lake Stymphalia, at least not during the last 2,500 years, although local archaeological and historical records indicate significant variation in the height and extent of the lake since Classical times: (1) there is no evidence of rocky, barren beach deposits in Stymphalia comparable to those described by Knauss (1990) from the neighbouring Pheneos polje, where an exceptionally high lake level was artificially induced by Ottoman troops during the Greek liberation battle in the 19<sup>th</sup> century; (2) Stymphalia has three discharge possibilities, the large natural sinkhole in the Southwest of the polje, a smaller sinkhole in the North (Morfis and Zojer, 1986) and the Hadrianic Aqueduct built around 130 AD; (3) the Cistercian Zaraka Monastery, the best preserved Frankish monastic site in Greece (Campbell, 2018), was built in the first half of the 13<sup>th</sup> century AD on the relatively flat valley floor, about 2 m above and 1 km distant from the present day lake shore, with no sign of later flooding. However, a major part of the Lower Town of ancient Stymphalos city has been submerged and silted since the Early Roman era and currently lies under sediments (Williams, 2005), induced by a rise of the lake bottom of only few metres since the founding of that town.

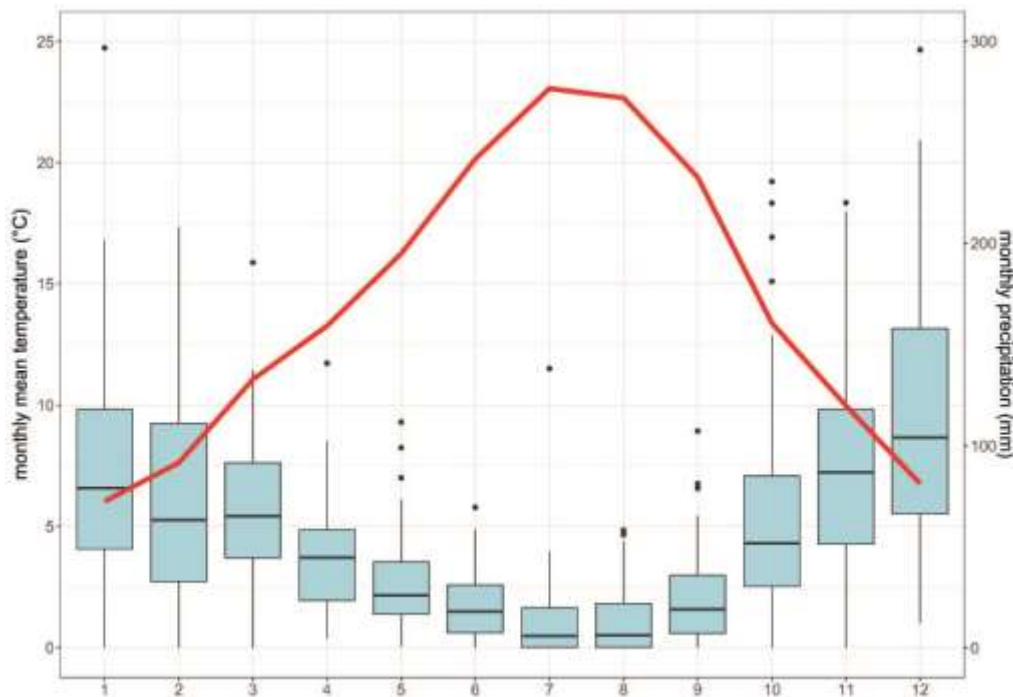


*Figure 2. Modern air temperature and precipitation for the Stymphalia basin. The mean monthly temperature for the station Driza-Stymphalia (37.8699 °N, 22.4643 °E, 622 m a.s.l.) for the period 1950 – 2011 (red line) and boxplots for the monthly precipitation are shown from January (1) to December (12).*

### 3. Materials and Methods

#### 3.1 Sediment cores

Field and initial laboratory work were mostly conducted in 2010 and 2011 and have been described in detail by Heymann et al. (2013). Three overlapping sediment core pairs of different lengths (STY-1, STY-2, and STY-3) were retrieved. The 16-m-long composite core STY-1 is the most complete and here, we discuss the upper 208 cm of it in detail (units 59 – 70b; Table 1), that cover approximately the last 2,500 years based on the updated age-depth-model described below which records both natural and anthropogenic influences. The lower limit was set at the upper sedimentary boundary of unit 58. We use the following proxies measured and described by Heymann et al. (2013): lithology, sediment structure, Munsell color (Munsell, 2000), grain size distribution, total carbon (TC), total inorganic carbon (TIC), total nitrogen (TN), magnetic susceptibility (Nowaczyk, 2001; Nowaczyk et al., 2002), and X-ray fluorescence (XRF) measurement (see section 3.3 below).

### **3.2 Dating technique**

The age control of the sediment cores was based on accelerator mass spectrometry (AMS) radiocarbon ( $^{14}\text{C}$ ) measurements performed at four different laboratories. For radiocarbon dating, 24 core samples and 3 surface samples have been taken and, as visible organic remains were almost absent from the core, mainly bulk sediments were used for dating (Table 2). The combined dating results lead to a time scale substantially different from the one published by Heymann et al. (2013). We present the construction of the time scale in detail in the following section 4.2. Throughout the paper, the year 1950 AD is used as year 0 BP (Mook and Plicht, 1999).

### **3.3 Elemental composition: X-ray fluorescence measurements**

Non-destructive X-ray fluorescence (XRF) measurements using energy dispersive fluorescence radiation on split core surfaces were performed with an Avaatech XRF Core Scanner, using a Rhodium X-ray source. The scanning parameters are the same as described by Heymann et al. (2013). The scan resolution of the upper 5 m of core STY-1A and overlapping intervals of core STY-1B was 1 mm with an exposure time of 10 s at 10 kV and 15 s at 30 kV, respectively. We selected 13 elements (10 kV: Al, Si, S, Cl, K, Ca, Ti, Mn, Fe; 30 kV: Zn, Rb, Sr, Zr) for a detailed analysis of their presence across the sediment sequence and their palaeo-environmental and -climatic significance ( $n = 4961$ ). Elements with low intensities ( $< 300$  total counts) which are less reliable (Tjallingii et al., 2007) were excluded. The XRF scanning results represent element intensities in total counts per second (tcps) which mainly depend on element concentration, but also on matrix effects, physical properties, sample geometry, and hardware settings of the scanner (Tjallingii et al., 2007). We chose to plot the XRF scanning results as log-ratios that can be interpreted as changes in relative concentration of an element pair, to avoid statistical analysis of data sensitive to the closed-sum effect and asymmetric element ratios (Weltje and Tjallingii, 2008). As we were applying the R software (R Core Team, 2017) for plotting, natural logarithms with base  $e$  ( $\log$ ) were applied by default. To assess the normalized elemental data in a palaeo-environmental and -climatic context, we compare relative changes of one element to another, rather than using absolute changes in element concentration.

### 3.4 Organic analysis: Lipid extraction and GDGT analysis

The interval 152 – 191 cm has been sampled at an average resolution of 0.5 cm from the sediment core STY-1A. Generally, five mm-thick sediment slices were taken, but for some exceptions, the spacing was varied due to the lithology. The sediments were lyophilized for 24 h and ground to a fine powder using a solvent-cleaned agate pestle and mortar. Subsequently, an aliquot (3.6-8.1 g) of each homogenized sediment was extracted using an ASE 200 (Dionex, USA) at a temperature of 75 °C and a pressure of  $5.0 \times 10^6$  Pa. Each sample was extracted for 20 min using a solvent mixture of dichloromethane (DMC)/methanol (MeOH) (9:1, v/v). The bulk of solvent was removed by rotary evaporation and the obtained total lipid extract (TLE) dried under a gentle stream of nitrogen. An aliquot (0.7-1.0 mg) of each TLE was separated into an apolar and a polar fraction using a small Pasteur pipette filled with activated aluminum oxide (3.5 cm) as stationary phase. The apolar fractions were eluted with 4 ml *n*-hexane/DCM (9:1, v:v) and the polar fractions with 4 ml DCM:MeOH (1:1, v/v), respectively. The polar fractions (containing isoprenoid and branched glycerol dialkyl glycerol tetraethers (GDGTs)) were dried under nitrogen, re-dissolved in *n*-hexane:2-propanol (99:1, v/v) to a concentration of 2 mg/ml and passed through a 0.45 µm polytetrafluoroethylene (PTFE) filter (Macherey-Nagel, Germany) prior to analysis.

GDGTs were measured using an Alliance 2695 HPLC system (Waters, UK) following the analytical protocol described by Hopmans et al. (2016), which allows the separation of 5- and 6-methyl branched GDGTs. The HPLC system was equipped with two Waters BEH HILIC silica columns (2.1 x 150 mm; 1.7 µm particle size) and a guard column of the same material, which were all maintained at 30 °C. Target compounds were eluted with a flow rate of 0.2 ml/min starting isocratically with 82 % eluent A (*n*-hexane) and 18 % eluent B (*n*-hexane:2-propanol (9:1, v/v)) for 25 min. A linear gradient was set to 65 % eluent A and 35 % eluent B in 25 min, followed by a linear gradient to 0 % eluent A and 100 % eluent B in 30 min. Re-equilibration of the column to initial conditions with 82 % eluent A and 18 % eluent B was within the following 20 min. Detection of isoprenoid and branched GDGTs was achieved using a Micromass ZQ single quadrupole mass spectrometer (MS) equipped with an atmospheric pressure chemical ionization (APCI) interface operated in positive ion mode. MS conditions were as detailed in Weidenbach



et al. (2017). The methylation index  $MBT'_{5Me}$ , a proxy that was developed to reconstruct absolute temperatures, was calculated using only 5-methyl isomers according to De Jonge et al. (2014) with roman numerals corresponding to GDGT structures displayed in the supplementary online material (SOM 5).

$$MBT'_{5Me} = (Ia + Ib + Ic) / (Ia + Ib + Ic + IIa + IIb + IIc + IIIa) \quad (1)$$

The branched-over-isoprenoid tetraether (BIT) index, indicating the relative input of terrestrial organic matter, was calculated as given in Hopmans et al. (2004) using the combined peak areas of the 5- and 6-methyl isomers of the branched GDGTs:

$$BIT \text{ Index} = (Ia + IIa + IIa' + IIIa + IIIa') / (Ia + IIa + IIa' + IIIa + IIIa' + IV) \quad (2)$$

### 3.5 Statistical data processing

We applied statistical approaches such as correlations and multivariate analyses, including principal component analyses (PCA) using the R software (R Version 3.4.2; R Core Team, 2017) to investigate the covariance of the different chemical elements of the sediment core.

For the geochemical data, cleaning of the dataset, i.e. the removal of explicit outliers and filling of missing values by spline interpolation was done manually prior to statistical processing. Correlation coefficients of elemental log-ratios can give an insight into the coupling/decoupling of elements over time. Hence, the relationships between different elemental ratios were explored calculating Pearson correlation coefficients, if normal distribution of the data existed (tested with the Shapiro-Wilk-test), or alternatively, Spearman rank-based correlation was applied. Furthermore, we applied PCA to the original XRF elemental dataset to objectively describe similarities and differences between the elements and to identify the main environmental processes that influence the composition of the lake sediment. The aim of the PCA is to reduce a high dimensional dataset to a very limited amount of meaningful and uncorrelated variables, so called components or factors, that still explain most of the variance in the data set (Filzmoser et

al., 2009). Here, the loadings indicate the contribution of each element to the respective principle component (PC). Not all element records in our dataset are normally distributed, and some show a pronounced skewness. As PCA requires a Gaussian distribution of the data, the dataset was standardized, i.e. z-normalized to a mean of zero ( $\mu = 0$ ) and a standard deviation of one ( $\sigma = 1$ ) for each parameter. In this way, we also avoid overestimating elements with extremely high counts (mainly calcium and iron) in order to equally weight the different parameters. Subsequently, PCA based on the correlation matrix was applied using the function *prcomp* from the R stats package. This approach also includes an orthogonal rotation of the components, which may facilitate the interpretation of the scores and loadings. We abstained from the application of intensive smoothing of the dataset to avoid any further approximation of the data.

### **3.6 Archaeological data**

Regional surveys in the area started in 1982. From 1983 to 2012, the site of Ancient Stymphalos was excavated under the auspices of the Canadian Institute in Greece, however the publication of the finds has still not been completed. For the present study, no further excavation or archaeological data collection have been conducted, as the focus was on the palaeoenvironmental investigation. Instead, already existing, published data have been gathered (Bintliff, 2012b; Brown and Walsh, 2017a; Lolos, 1997; Panagiotopoulos, 1985; Philippson, 1892; Schaus, 2014; Walsh et al., 2017; Williams, 1996, 1984a, 1984b, 1983, 2005, 2003, Williams et al., 2002, 1998, 1997; Williams and Cronkite Price, 1995; Williams and Gouley, 2005) and consulted for information on human activity in the Stymphalia Polje.

As empirical data collections from archaeological and palaeoenvironmental archives are traditionally very different, juxtaposition of these different kinds of (quantitative) proxies can be challenging (Palmisano et al., 2017) and only a small number of studies try to bring them together (Palmisano et al., 2019; Weiberg et al., 2016). Weiberg et al. (2016) provide continuous quantitative data on settlements from archaeological information during the last 8000 years on the Peloponnese Peninsula. As it is the only quantitative proxy currently available, we use it as

indication of settlement intensity, also in the Stymphalia Polje, and refined it from local archaeological information.

## 4. Results

### 4.1 Lithology

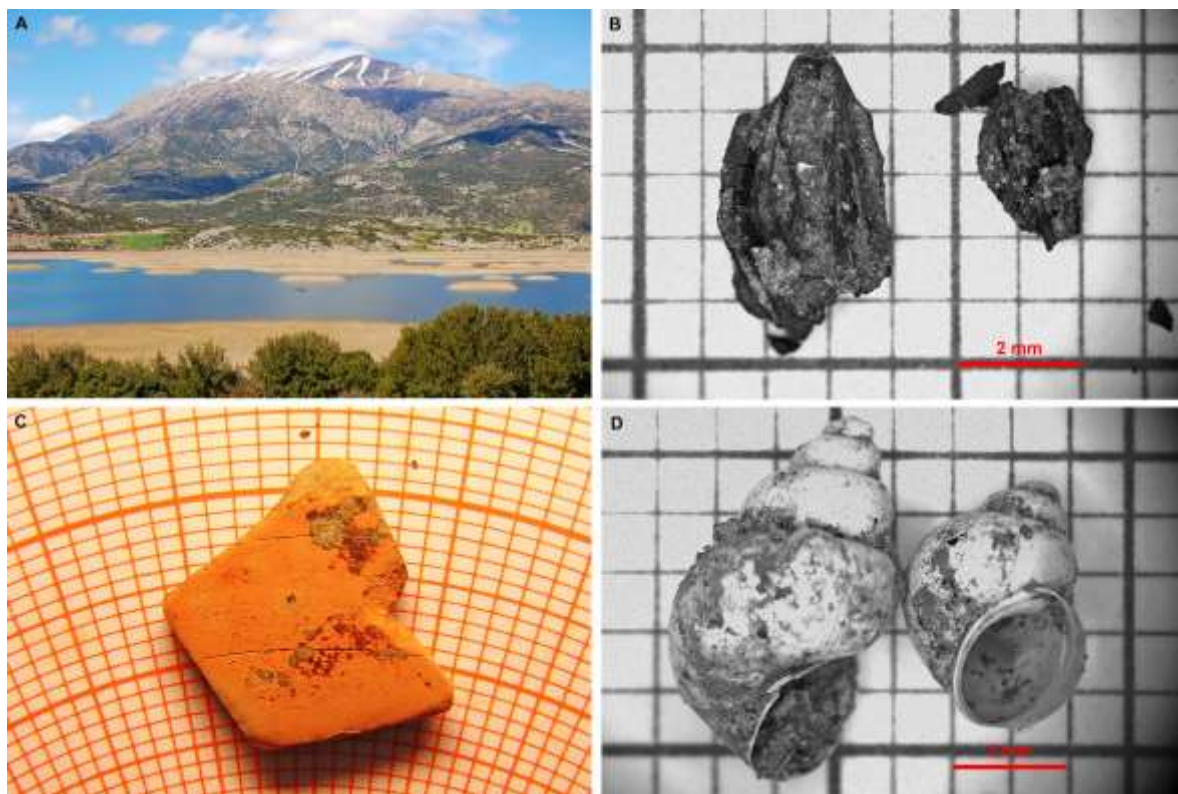


**Figure 3.** Photos of Lake Stymphalia and sample material. (A) Photo of Lake Stymphalia taken from the southern shore during coring campaign in 2010 with Mt. Ziria in the background (coring platform in the centre for scale). (B) *Crataegus* seed (VERA-6258) found at 165 cm depth (masterscale) in core STY-1A. (C) Ceramic shard dated to 5th century BC found at 205 cm depth (masterscale) in core STY-3B. (D) *Bythinia* sp. shell sample.

**Table 1. Sedimentary units of the uppermost 208 cm of core STY-1. The soil type classification follows the German Arbeitsgruppe Boden (2005). (UB = upper boundary, G = gradational, E = erosional, S = sharp)**

Core Depth [cm]	Sediment Unit	Munsell Color	Soil Type	Description
0–9	70b	5Y 4/2	Ut4	Olive gray clayey silt with organic fragments decreasing to the top
9–10.5	70a	5Y 5/3	Lu	Olive fine sand with silt, medium sand-sized mineral grains, and organic fragments (UB=G)
10.5–20	69	10YR 4/3	Ut4	Very compact brown clayey silt with some organic fragments, irregular down-cutting to 12 cm, (UB=S)
20–59	68	7.5YR 5/4	Ut4	Brown clayey silt with minor silt content, some shells and organic fragments, oxidized root channels (UB=S)
59–112	67	2.5Y 5/2	Ut4	Grayish brown clayey silt with shell fragments (gastropods), becoming lighter towards top, organic fragments, oxidized root channels (UB=G)
112–136.5	66	2.5Y 5/2	Ut4	Grayish brown clayey silt with higher sand content, shells, and shell fragments (gastropods) decreasing to the top, (UB=G)
136.5–156.5	65	2.5Y 6/2	Tu4	Light brownish gray silty clay with higher sand content with shells and shell fragments (gastropods), organic content, organic fragments decrease to the top (UB=G)
156.5–158.5	64	2.5Y 5/2	Tu3	Grayish brown silty clay with some shell fragments, and organic content (UB=S)
158.5–161	63	5Y 4/1	Tu4	Dark gray silty clay with higher sand content, with shells and shell fragments (gastropods) (UB=S)
161–164	62	5Y 2.5/1	Tu4	Black layer of silty clay with shells, and shell fragments (gastropods) (UB=G)
164–167.5	61	5Y 6/2- 5Y 5/1	Tu3	Light olive gray silty clay with higher sand content, shell fragments (gastropods), and organic content, intercalated with gray clay, upper boundary irregular (UB=E?); at 167.5 cm and 166 cm: 2 mm-thick fine to medium sand laminae; at 165 cm: 3 mm-thick fine to medium sand laminae
167.5–189	60	10YR 5/1	Tu4	Gray silty clay with coarse sand- to gravel-sized clastic fragments and organic content, both increasing to the top, (UB=S); at 180 cm: thin coarse grained oxidized orange layer, at 183.5 cm, 182 cm, 177 cm and 176.5 cm: carbonatic, coarse sand-sized clastic fragments, oxidized; at 173 cm: carbonatic, gravel-sized clastic fragment, oxidized
189–208	59	10YR 5/1	Ut4	Gray clay with some silt, shell fragments (gastropods), and organic content, shell fragments increase until 201 cm then decrease, organic content increases to the top (UB=G); at 201 cm: layer with partly intact shells

Building upon the stratigraphy presented by Heymann et al. (2013), the uppermost 208 cm of core STY-1 are subdivided into 20 stratigraphic units (No. 59 – 70b, Table 1, Figure 4) based on sedimentological properties (e.g. colour, texture, macro remains). None of the units is laminated nor are there visual, sedimentological indicators of short-term cyclic beddings. The sediment sequence has a fine texture and is generally composed of a varying mixture of clay (mean = 27%) and silt (mean = 70%), containing 0 – 4 % sand with the exception of units 63 and 70a, in which 7.5 % and 17 % of sand were recorded (SOM 3).

Munsell (2000) colours in the upper 161 cm of the core range from olive to greyish brown and are generally brighter than in the lower part, which is also evident in the distance of the respective RGB colours to each other (Figure 4, Table 1). Organic debris and roots are generally small and scarce. Below 164 cm, darker greyish colours dominate and shell fragments of *Bythinia sp.* (Figure 3-D) and *Valvata sp.* gastropods are more frequent. A distinct black layer (unit 62), ranging from 164 – 161 cm, separates the upper brownish units from the lower more greyish units. TIC values range between 0.8 to 8.0 wt% and correlate well with Ca counts (Figure 4, Figure SOM 2). The TOC content varies from 1.2 to 6.4 wt% and is 3.0 wt% in the black layer (Figure 4, SOM 2). While TIC values are lower in units 59 and 60 compared to the upper part, the TOC content does not show any obvious differences between these two. The blackish unit 62 exhibits a singularly high magnetic susceptibility (MS) peak (SI = 3000). For the rest of the depicted core sequence, MS constantly fluctuates around a median of 70.27 (mean = 103.68). The upper brownish units 68 and 69 dispose of persistently higher MS values.

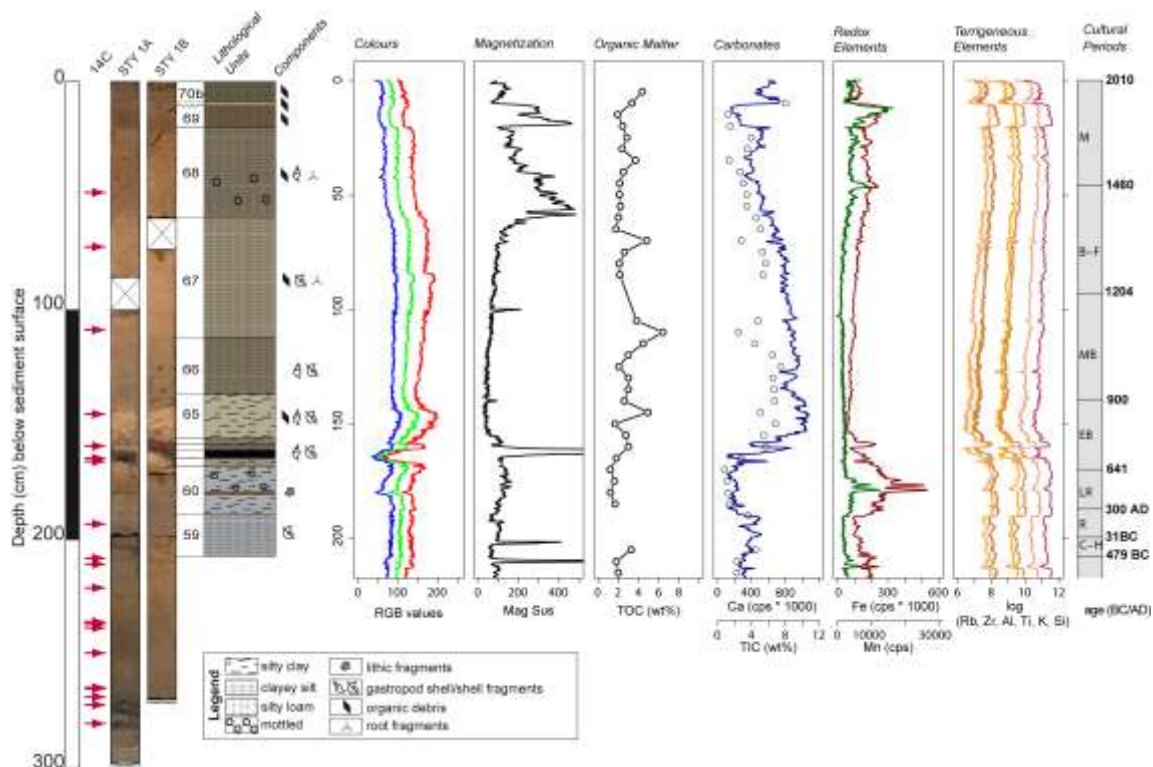


**Figure 4.** STY-1 composite core log with lithological units for the upper 208 cm (left) and overview of different proxies plotted against depth. Depths where samples for 14C dating were taken from STY-1A are indicated with red arrows. The only sample taken from the parallel core (VERA-6383) at 161 cm is additionally marked on the STY-1B core picture with a red dot. RGB color values (blue, green, red), magnetic susceptibility, TOC, TIC (black) and counts per second of Calcium (darkblue), Iron (darkred) and Manganese (green), as well as log-values of Rubidium, Aluminum, Zirconium, Titanium, Potassium, and Silicon (from left to right) are plotted against depth. For orientation, boxes with cultural periods and ages (BC/AD) at the respective transition boundaries to the right (for abbreviations of cultural periods see Table 3). For interpretation of the references to color, the reader is referred to the web version of this article.

## 4.2 Core chronology

### 4.2.1 Radiocarbon dates

From the uppermost 324 cm of the parallel cores STY-1A and STY-1B (units 48–70), 24 samples for radiocarbon dating have been taken. Although our focus is on the uppermost 208 cm recording anthropogenic influences, the age model was calculated for a longer interval in order to construct a solid model and avoid boundary effects (Figure 5). The sedimentological analysis of the core sequence gave no indications for any hiatus or erosional discontinuities; hence, a continuous, even if sometimes very low sedimentation is assumed (Figure 6).

To determine the time at which specific layers in a sediment core were deposited, we need to isolate organic material from the time of sedimentation that is either terrestrial or has a known reservoir age. The challenge in dating sediments is that they contain a small fraction of old carbon, eroded and transported with the mineral fraction, in addition to limnic and terrestrial material from the time of deposition. Furthermore, sediments are open systems, so dissolved and colloidal carbon may be introduced at a later point in time. The standard Acid-Alkali-Acid (AAA) chemical pretreatment, commonly used in radiocarbon dating, aims to remove potentially mobile contaminating acid and alkali soluble organic compounds. If no recognizable macrofossils can be found, dating the remaining insoluble fraction (humic fraction) is the best candidate to provide a useful sedimentation age in organic rich sediments (organic content of the residue >1 %) (Grootes et al., 2004). A check on the age inhomogeneity of organic carbon in the sediment can be obtained by dating not only the insoluble residue, but also the organic material removed by alkali extraction. Acidification of this alkali extract precipitates the humic acid fraction. This fraction often dates younger than the insoluble residue since it may contain contaminating younger compounds and is less likely to receive a contribution from recalcitrant reworked carbon compounds. In case of an age difference between the humic acids and the humin, the humins are most likely to indicate the approximate time of sedimentation for organic rich sediments. For organic poor sediments the fraction of old reworked carbon, which is often around 0.1 %, is no longer negligible and can lead to measured humin ages that may be thousands of years too old (Grootes et al., 2004). In the eastern Mediterranean, it has been observed in a number of cases that humic acids extracted from samples appear not to offer appreciably different  $^{14}\text{C}$  ages and so likely derive from the sample in question or contemporaneous material (Wild et al., 2013).

In total, 45 radiocarbon measurements were made on these 26 samples (Table 2). Alkali residue, humic acids, shell carbonates, and repeats of some fractions were measured at four different AMS- $^{14}\text{C}$  facilities, the Leibniz-Laboratory for Radiometric Dating and Isotope Research at Kiel University (KIA), the Beta Analytic Radiocarbon Dating Laboratory Miami (BETA), the VERA Laboratory at Vienna University, and the Poznań Radiocarbon Laboratory at Adam Mickiewicz University (POZ).

Due to the limestone rich environment containing a high amount of “old” carbon, a large hard water effect may be expected for limnic organics. Together with an influx of fresh and reworked old terrestrial organics this makes radiocarbon dating of the sediment challenging (Finné et al., 2011).

Table 2 shows sometimes large differences between results from different fractions and laboratories. Carbonate of the *Bythinia* gastropod shells at 141 cm dates at least 700 years older than organic samples above and below it indicating the expected large hard water effect. A *Ranunculus aquatilis* specimen, which grows subaqueously and was sampled live in 2015, provides an apparent age of  $657 \pm 29$  years (PMC 92.15 or  $F^{14}C$  0.92146; VERA-6256, Table 2) that after comparison with the Jungfrauoch atmospheric  $^{14}C$  record (Hammer and Levin, 2017) yields a reservoir age of  $810 \pm 30$   $^{14}C$  years. This is in good agreement with the carbonate result at 141 cm and slightly higher than the reservoir age of  $600 \pm 10$  years applied by Heymann et al. (2013). The ten KIA results for the alkali residue give, as expected considering the low organic carbon content of 0.19 to 0.83 % of this fraction, unreasonably old ages and should not be used in the time scale construction. Recognizable terrestrial plant remains are largely absent from the core, except for one single *Crataegus* seed, which was found at 165 cm depth (masterscale) in core STY-1A, yielding an age of  $1237 \pm 35$   $^{14}C$  years (690 – 870 cal AD; VERA-6258; Figure 3-B). The humic acid result for KIA42912 of  $1355 \pm 23$  yr BP at 164 cm is only 118 years older. This small difference indicates that the humic acid fraction is largely of terrestrial origin as opposed to the limnic material with 800-year reservoir effect. Ages obtained on the humic acid fractions may thus better indicate the time of deposition with a reservoir effect in the range 100 to 200 years. This reservoir effect will however vary with the balance between limnic and terrestrial organics supplied to the lake and there is no reason to assume that it was constant in the past. Hence, this is an inherently problematic issue and we can only employ the current situation as a guide and try to estimate the recent reservoir age (as we do below).



#### 4.2.2 Bayesian age model

The *Crataegus* seed and a ceramic fragment (Figure 3-C) – the latter was found at 205 cm depth (masterscale) in core STY-3B and was identified as non-Attic, late or sub-Archaic and dated approximately to 500 BC  $\pm$  50 years (ceramic classification: Bernhard Schmaltz, Kiel University, personal communication) –serve as “golden spikes” in the age-depth-model. For the ceramic shard, ca. 500 BC is considered a *terminus post quem*, the earliest possible date when the shard may have found its way into the lake; most likely it continued to exist as part of a decorative bowl for a while before it broke apart and then at some later point in time was deposited in the lake. A piece of charred organic matter from 324 cm depth, dated at 7708  $\pm$  35 <sup>14</sup>C yr BP (KIA42913) and with a combustion yield of 32.5 % carbon, which proves its high organic matter content, sets the lower limit of the age-depth-model (ADM).

Bayesian age-depth-modelling was performed using the R package Rbacon (v.2.3; Blaauw and Christen, 2011) as well as the software OxCal 4.2 (Bronk Ramsey, 2009; Bronk Ramsey and Lee, 2013; Ramsey, 2008), both using IntCal13 as the terrestrial calibration curve (Reimer et al., 2013).

*Table 2. List of radiocarbon samples taken from Lake Stymphalia parallel cores STY-1A and STY-1B. Lab-Codes: KIA – Kiel; VERA – Vienna; Poz – Poznan; BETA – Beta Analytics. The sample numbers refer to the sampling depth before adjusting the field-based correlations between individual core sections in the laboratory to a master depth scale. Indicated <sup>14</sup>C ages are unmodelled ages giving the 68.2 % calendar dating probability. Indicated IntCal13 ages are cal BP ages modelled with rcarbon using the IntCal13 calibration dataset (Reimer et al., 2013). Notes: Dates marked with an asterisk have been excluded from age-depth modelling. <sup>1)</sup> calculated from CO<sub>2</sub> pressure. <sup>2)</sup> Fraction of sample material after respective pre-treatment. <sup>3)</sup> calibrated 1 $\sigma$ -age ranges without reservoir correction (following page)*

sample no.	analysis no.	sample material	sample fraction	C weight <sup>1</sup> [mg]	C content in this fraction <sup>2</sup> [%]	$\delta^{13}\text{C}$ [‰]	<sup>14</sup> C age $\pm 1\sigma$ [BP]	IntCal13 [cal BP] <sup>3</sup>	depth [cm]
LSR-01	KIA 42322	Reed	Alkali residue				>1950		0*
STY-1/0	KIA 44002	Green Algae	Alkali residue				280 $\pm$ 20	299 – 421	0*
STY-res-03	VERA-6256	<i>Ranunculus aquatilis</i>	ABA			-25.2 $\pm$ 1.1	657 $\pm$ 29	565 – 664	0*
STY-1/32	KIA44003	Bulk sediment	Alkali residue	1.58	0.42	-22.74 $\pm$ 0.16	3174 $\pm$ 29	3370 – 3443	32*
STY-1A/050	VERA-6380_1	Bulk sediment	TOC			-25.0 $\pm$ 0.9	1557 $\pm$ 38	1406 – 1521	50
	VERA-6380_2	Bulk sediment	TOC			-23.8 $\pm$ 0.8	1568 $\pm$ 37	1413 – 1521	50
	VERA-6380HS_2	Bulk sediment	Humic acids			-23.7 $\pm$ 0.9	1575 $\pm$ 38	1415 – 1522	50
STY-1/52	KIA45954	Bulk sediment	Alkali residue	1.57	0.27	-21.40 $\pm$ 0.16	2184 $\pm$ 28	2146 – 2302	52*
STY-1A/072	KIA47446	Bulk sediment	Alkali residue	3.12	0.44	-25.25 $\pm$ 0.10	2171 $\pm$ 20	2134 – 2299	72*
	KIA47446	Bulk sediment	Alkali residue	3.12	0.44	-24.50 $\pm$ 0.19	2225 $\pm$ 20	2161 – 2310	72*
	KIA47446	Bulk sediment	Humic acids	1.52	0.07	-25.28 $\pm$ 0.23	1285 $\pm$ 35	1184 – 1273	72
STY-1/92.5	KIA44004	Bulk sediment	Alkali residue	2.55	0.31	-23.77 $\pm$ 0.17	2935 $\pm$ 25	3045 – 3157	107*
STY-1A/100	VERA-6382_1	Bulk sediment	TOC			-26.2 $\pm$ 0.8	1419 $\pm$ 36	1298 – 1342	114
	VERA-6382_2	Bulk sediment	TOC			-25.3 $\pm$ 0.8	1444 $\pm$ 36	1304 – 1357	114
	VERA-6382HS_2	Bulk sediment	Humic acids			-23.9 $\pm$ 0.8	1419 $\pm$ 37	1297 – 1342	114
STY-1A/127	VERA-6381_30	<i>Bithynia sp.</i>	Carbonate		30% etched	-11.7 $\pm$ 0.7	2091 $\pm$ 34	2005 – 2113	141*
	VERA-6381_50	<i>Bithynia sp.</i>	Carbonate		50% etched	-12.1 $\pm$ 0.7	2258 $\pm$ 35	2183 – 2338	141*
STY-1B/161	VERA-6383_1	Bulk sediment	TOC			-26.4 $\pm$ 0.8	1553 $\pm$ 35	1403 – 1520	161
	VERA-6383_2	Bulk sediment	TOC			-28.8 $\pm$ 0.8	1516 $\pm$ 36	1350 – 1515	161
	VERA-6383HS_2	Bulk sediment	Humic acids			-23.4 $\pm$ 0.7	1441 $\pm$ 35	1304 – 1354	161
STY-1/149.5	KIA42912	Bulk sediment	Alkali Residue	1.62	0.35	-24.94 $\pm$ 0.21	3285 $\pm$ 30	3478 – 3559	164*
	KIA42912	Bulk sediment	Humic acids	2.21	0.69	-27.22 $\pm$ 0.19	1355 $\pm$ 23	1281 – 1298	164
STY-1A/150	VERA-6258	<i>Crataegus sp.</i>	ABA			-26.8 $\pm$ 0.6	1237 $\pm$ 35	1089 – 1258	165
STY-1A/180	VERA-6259	Bulk sediment	TOC			-33.5 $\pm$ 2.1	2125 $\pm$ 31	2054 – 2148	195
	VERA-6259HS	Bulk sediment	Humic acids			-42.8 $\pm$ 6.9	2174 $\pm$ 37	2124 – 2303	195
STY-1A/207	KIA47448	Bulk sediment	Alkali Residue				5720 $\pm$ 40	6447 – 6560	207*
	KIA47448	Bulk sediment	Humic acids				3170 $\pm$ 30	3987 – 4136	207
STY-1A/210	Poz-96329	Bulk sediment	Alkali residue	6.36	4.2	-26.2	2310 $\pm$ 35	2316 – 2353	210
STY-1A/220	Poz-96330	Bulk sediment	Alkali residue	2.25	1.8	-26.5	3850 $\pm$ 40	4159 – 4395	220
STY-1A/216	VERA-6260	Bulk sediment	TOC			-37.0 $\pm$ 1.2	3809 $\pm$ 39	4098 – 4280	236
	VERA-6260HS	Bulk sediment	Humic acids			-26.8 $\pm$ 0.8	3937 $\pm$ 33	4298 – 4434	236
STY-1/216.5	KIA44005	Bulk sediment	Alkali Residue	6.03	0.83	-24.77 $\pm$ 0.25	4020 $\pm$ 30	4439 – 4521	236*
	KIA44005	Bulk sediment	Humic acids	2.09	0.41	-24.03 $\pm$ 0.22	3563 $\pm$ 29	3832 – 3899	236
STY-1A/238	Poz-96331	Bulk sediment	Alkali residue	5.46	7.4	-24.8	3335 $\pm$ 35	3485 – 3630	238

STY-1A/248	Poz-96325	Bulk sediment	Alkali residue	5.16	2.4	-26.2	4180 ± 40	4630 – 4829	248
STY-1/246.5	KIA44006	Bulk sediment	Alkali Residue	2.89	0.29	-27.00 ± 0.13	6350 ± 40	7185 – 7408	266*
	KIA44006	Bulk sediment	Humic acids	1.95	0.28	-26.22 ± 0.15	4837 ± 34	5486 – 5606	266
STY-1A/247	VERA-6261	Bulk sediment	TOC			-27.2 ± 0.7	4600 ± 35	5295 – 5444	267
	VERA-6261HS	Bulk sediment	Humic acids			-40.7 ± 1.6	4631 ± 36	5312 – 5446	267
STY-1A/250	VERA-6262	Bulk sediment	TOC			-23.1 ± 3.1	4829 ± 38	5485 – 5603	270
	VERA-6262HS	Bulk sediment	Humic acids			-26.6 ± 1.6	4877 ± 29	5590 – 5642	270
STY-1A/253	VERA-6263	Bulk sediment	TOC			-25.9 ± 1.7	4791 ± 31	5481 – 5587	273
	VERA-6263HS	Bulk sediment	Humic acids			-23.7 ± 0.9	4841 ± 36	5486 – 5640	273
STY-1A/280	KIA45955	Bulk sediment	Alkali Residue	1.77	0.19	-25.89 ± 0.19	7178 ± 39	7961 – 8013	280*
	KIA45955	Bulk sediment	Humic acids				6025 ± 35	6798 – 6925	280
STY-1A/300	KIA42913	Charcoal	Alkali Residue	1.76	32.5	-27.6 ± 0.1	7708 ± 35	8450 – 8538	324

The final age-depth-model (STY\_25) was constructed with Rbacon in an iterative process based on several key assumptions and offers a best plausible interpretation: (1) The age of the core top is set at 2010 cal AD, the year of coring. The age determinations for the *Crataegus sp.* seed and the ceramic shard serve as reliable, solid anchor points. The charcoal sample at 324 cm likewise gives a reliable result for the bottom of the model. (2) If there are multiple dates for one depth derived from the same carbon fraction, they have been combined to one value using the *R\_combine* function in OxCal. Otherwise, the fact of having a higher quantity of datings for a certain depth would have influenced the modelling by assuming a higher credibility for these samples. (3) As the *Bythinia sp.* shell samples (VERA-6381\_30, VERA-6381\_50) delivered different ages, depending on the degree of etching, they were excluded from the age-model (Figure 5 marked in light blue). (4) Based on the assessment of alkali residue ages versus humic acid ages outlined above, the generally younger humic acid ages were regarded as more plausible and the considerably older KIA alkali residue ages were excluded from modelling (Figure 5 marked in red). (5) As outlined in section 4.2.1, the reservoir correction was set to  $200 \pm 100$  years for all bulk sediment samples because of the age difference between the *Crataegus* seed ( $1237 \pm 35$   $^{14}\text{C}$  years) and the adjacent KIA42912 humic acid sample ( $1355 \pm 23$   $^{14}\text{C}$  years). To take the uncertainty of varying reservoir effects into account, we assigned a relatively high standard deviation of  $\pm 100$  years to the reservoir correction (the table can be found in SOM 1). (6) Finally, the construction of the Hadrianic Aqueduct, a cultural event that took place around 130 AD (Lolos, 1997), indicated in the sediment core among others by a strong and abrupt increase in the Fe content due to oxidation processes (see section 5.3.2), was taken into account in the modelling process. In the following, all proxies are plotted against the mean calendar age estimates of model STY\_25. Calibrated years are denoted as cal BC/AD, due to the focus of this paper on cultural and climatic aspects of the last 2,500 years (Mook and Plicht, 1999). The applied cultural chronology (Table 3) is based on Bintliff (2012) and Weiberg et al. (2016).

Based on the age-depth-model, we calculated the sedimentation rate in the lower part to be approx. 0.2 mm/yr. It rises slightly to 0.4 mm/yr at 195 cm and strongly increases to more than 2 mm/yr at 165 cm. For the uppermost 50 cm, a lowering of the sedimentation rate to 0.7 mm/yr was calculated (Figure 6). This pattern of sedimentation largely resembles that of carbonate content and Ca (Figure 4) and hence supports the age-depth-model.

Note that the age-depth-model published by Heymann et al. (2013), which was based on fewer radiocarbon dates for the respective core sequence, is outdated. The discovery of the *Crataegus* seed (VERA-6258) and the improved modelling approach presented here require a substantial shift – to more recent ages – in the dates and associations compared with the published data of Heymann et al. (2013).

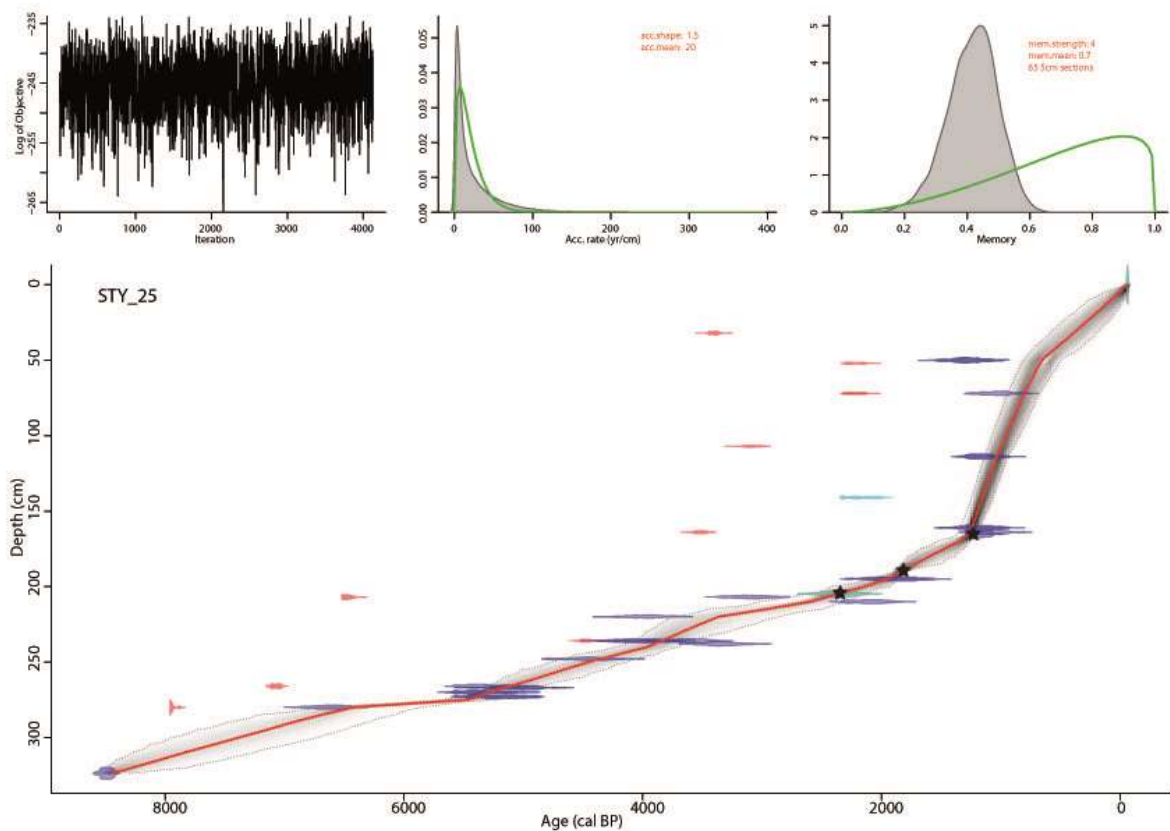


**Figure 5. Age-depth model STY\_25 from rbacon for 324 cm of STY-1. The red dashed line represents the weighted mean. Black dashed lines represent minimum and maximum ranges (95% confidence interval). The red (Alkali residue) and the light blue (Carbonate shells) dates have been treated as outliers and have been excluded from the modelling processes. The black stars highlight the anchor points ceramic shard, aqueduct, and *Crataegus* seed (cf. details in section 4.2). For interpretation of the references to color, the reader is referred to the web version of this article.**

### 4.3 Geochemical Proxies

Our palaeoclimate record consists of continuous XRF core-log measurements of 13 chemical elements, augmented with discrete measurements of grain size, TOC, TIC, and TN contents as well as isoprenoid and branched GDGT distributions.

The sediment is dominated by calcium (Ca, 67.3 % of all considered total counts), caused by autochthonous calcium carbonate precipitation in the lake and allochthonous limestone weathering in the catchment. Iron (Fe, 14.7 %) and silicon (Si, 8.6 %) were the elements with the second and third most abundant counts, respectively. The elements Rb, K, Zr, Ti, Si, and Al all show extremely high correlations ( $\rho_{sp} > 0.9$ ) throughout the sequence due to their common allochthonous origin from siliciclastic rocks in the catchment such as schists and breccias (Figure 4).

Gastropod shells in core STY-1B1 in the depth interval 84.4 – 105.4 cm made it difficult to obtain the smooth, planar core surface needed for reliable XRF analysis (Bloemsma et al., 2018; Tjallingii, 2006; Tjallingii et al., 2007). As a result some element counts deviated from those in the other core sections, showing larger oscillation and leading to artefacts at the section boundaries (Figure 7).

Four element ratios were determined that show trends which can be interpreted as suitable palaeoenvironmental proxies (cf. section 5.1). The generally negative  $\log(\text{Rb}/\text{Sr})$  ratios (Figure 7) in our record (varying between -0.18 to -3.29) indicate the dominance of carbonates compared to siliciclastic material in the lake's catchment, which is dominated by limestone karst. Relatively higher values of the Rb/Sr ratio occur in units with low carbonate content.

As stated by Heymann et al. (2013), we use the  $\log(\text{Zr}/\text{Rb})$  ratio as a grain size proxy; higher values are linked to the coarser, silt-sized fraction, while low values refer to fine, clayey mineral input. The mean is 0.44 and the median is 0.41. There is a considerable shift in the data around 700 cal AD and afterwards the variability in the ratio is considerably larger than in the first half of the sequence (Figure 7). The  $\log(\text{Mn}/\text{Fe})$  ratio fluctuates between -5.0 to -3.0 and highest variation can be seen for the period 500 to 1000 cal AD. As Fe show a high correlation with other terrestrial elements ( $\rho_{sp}$  for Fe and Ti = 0.92), it is mainly related to allochthonous input and hence the potential use of the Fe/Mn ratio as an indicator of redox conditions in the water column needs to be applied with caution. The  $\log(\text{Sr}/\text{Ca})$  ratio (Figure 7) is consistently negative and varies between -4.6 to -2.8. Between 350 to 700 cal AD, we see the highest variation.

We additionally applied a principal component analysis (PCA) to the dataset of the 13 selected geochemical elements in order to reduce the dimensions and summarize the data structure. The scree test suggests using the first three factors, as the first (PC1), second (PC2) and third principal component (PC3) account for about 79 % of the variance in the dataset (SOM 4). We only apply PC1,

taking into account 52.9 % of the variance. The loadings provide information on the influence of the chemical elements on the respective component. While PC1 is tied to Ca and Sr at the negative end and to all the other elements at the positive end, PC2 is negatively related to Zr and Si, while the other elements show positive loadings (SOM 4). Consequently, PC1 can be interpreted as an axis that spans between carbonate rich samples (Ca, Sr) on the negative end and mineral rich assemblages indicated by positive values. These divergent elemental compositions are likewise reflected in the Rb/Sr ratio. A Spearman correlation between  $\log(\text{Rb/Sr})$  and PC1 hence leads to an extremely high correlation ( $\rho_{\text{sp}} = -0.968$ ,  $p < 0.05$ ). This similarity is also apparent in the high degree of alignment between the curve progressions in Figure 7, as they show the same temporal responses. It can thus be concluded that PC1 for the STY-1 XRF dataset represents a suitable summary proxy for chemical weathering. In addition, the results of the PC1 confirm the applicability of Rb/Sr as a palaeoenvironmental proxy, because it covers the most important fluctuations in the complete dataset.

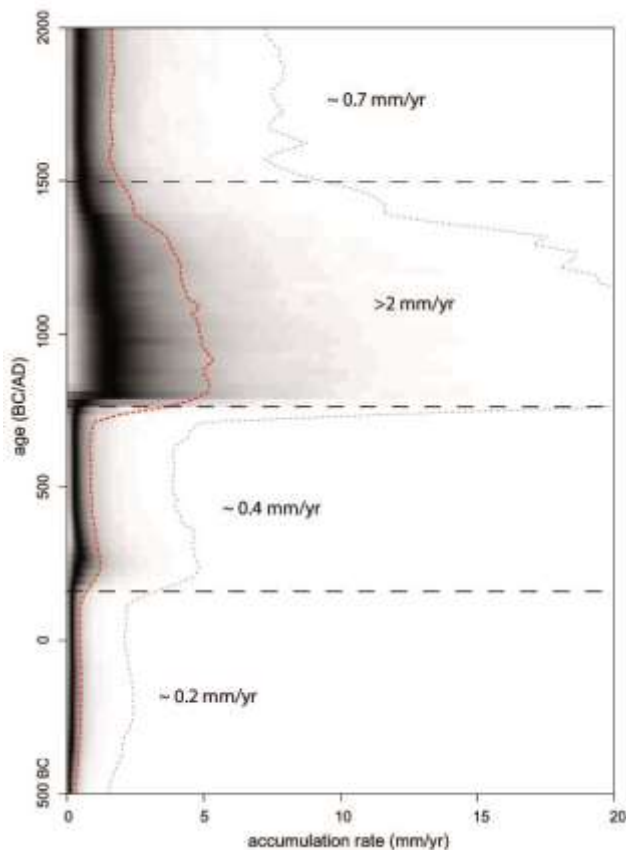


*Figure 6. Sediment accumulation rate (mm/yr) over the last 2,500 years. Dashed, horizontal lines broadly indicate 4 phases with differing sedimentation rates and the approximated average sedimentation rate within this phase.*

#### **4.4 GDGT distributions**

Both isoprenoid and branched GDGTs were ubiquitously present in the investigated interval with the latter dominating the GDGT pool. This is also expressed in generally high BIT values varying between 0.95 and 0.98 (data not shown). Highest  $MBT'_{5Me}$  values of about 0.60, reflecting higher mean annual air temperatures (MAATs), are found at 200 cal AD, after which  $MBT'_{5Me}$  values decrease by about 0.13 over the next 200 years, yielding a minimum  $MBT'_{5Me}$  of 0.47 at 390 cal AD. Subsequently, the  $MBT'_{5Me}$  increases over the next 140 years and stays relatively invariant with values between 0.52 and 0.53 in the interval from 535 to 660 cal AD. A second minimum of 0.47 occurred at 690 cal AD followed by an increase in temperature expressed by an increase in the  $MBT'_{5Me}$  value of about 0.52 shortly after. The  $MBT'_{5Me}$  value decreased to an absolute minimum of about 0.45 at 710 cal AD followed by a rapid increase to 0.53 around 720 cal AD (Figure 8).

### **5. Discussion**

#### **5.1 Geochemical ratios**

The geochemical elements obtained from XRF analysis are shown and interpreted as log-ratios to circumvent the closed-sum effect and to obtain a signal that is relatively easy to interpret for palaeoenvironmental variation (Löwemark et al., 2011; Weltje and Tjallingii, 2008). Selected element ratios are explained and discussed in the following.

The rubidium-strontium (Rb/Sr) ratio is commonly applied as a proxy for weathering intensity in the catchment (Chen et al., 1999; Jin et al., 2006; Xu et al., 2010). Rb has an allochthonous source and can replace potassium (K) in the crystal lattice of clay minerals. It enters the lake environment with silicates and K-rich minerals. Sr can have an allochthonous or autochthonous origin and is thus introduced either from carbonate weathering in the catchment or from precipitation of  $SrCO_3$ , as substitute for Ca, within the lake (Cohen, 2003; Koinig et al., 2003). Precipitation of  $SrCO_3$  also increases by evaporative concentration in lakes, a process which often happens during a lowering of the lake level due to dry and warm climate conditions (Heymann et al., 2013). Hence, high Rb/Sr values in lake sediments may generally be interpreted as enhanced erosion of siliciclastic material under cooler and wetter climatic conditions and enhanced catchment precipitation, while low Rb/Sr values indicate warmer and drier conditions with evaporation-driven carbonate precipitation in the lake (Heymann et al., 2013; Unkel et al., 2014). As the period presented in this paper shows a strong imprint of human activity in the polje, the Rb/Sr ratio cannot unequivocally be linked to climatic variations and firstly reflects the balance between carbonates and clastic components. For the period



presented here, the Rb/Sr ratio can instead be interpreted as proxy for water availability and lake size. High Sr and low Rb/Sr values indicate high water availability dissolving carbonates from the limestone bedrock and precipitating in the lake during warm summers, while high Rb and high Rb/Sr values are present in phases with less water availability and thus a smaller lake area, where terrestrial detritus is more easily eroded up to the depocentre of the lake. The proxy does not indicate whether these processes occur naturally or are human induced.

For the strontium-calcium (Sr/Ca) ratio, some authors associate higher values in stalagmites with lower levels of recharge into the karstic aquifer during dry climate conditions (Cruz et al., 2007). Other authors explain higher Sr concentrations with enhanced biogenic carbonate precipitation compared to detrital carbonates, because the Sr partition coefficient ( $K_{DSr}$ ) for biogenic carbonate is much greater than that for inorganic carbonates (Hodell et al., 2008). We here follow the interpretation of Hodell et al. (2008) and interpret higher Sr/Ca ratios as more biogenic carbonate precipitation in the lake and lower values as more inorganic, detrital carbonate input from the catchment.

Iron (Fe) and manganese (Mn) concentrations correspond among others to oxidation processes within the lake. The Mn/Fe ratio is often interpreted as an indicator for redox conditions (Davison, 1993; Heymann et al., 2013). In the water column,  $Fe^{2+}$  is less stable than  $Mn^{2+}$  and precipitates earlier. Thus, low (high) Mn/Fe values are considered to indicate anoxic (oxic) conditions, often visible by greyish-blue (brownish-red) sediments (Koinig et al., 2003; Unkel et al., 2014). Besides redox conditions, pH changes affect the ratio, as more Mn is mobilized when pH is decreasing. Hence, low (high) Mn/Fe values may also indicate acidic (alkaline) conditions. In periods of high productivity, intensive degradation of organic matter leads to oxygen depletion and acidic condition and may also be reflected in higher TOC values (Koinig et al., 2003). If the variability of Fe is closely related to allochthonous input, this suggests that Fe mainly originates from terrestrial sources and the use of the Mn/Fe ratio as an indicator of redox conditions in the water column may be limited (Naehrer et al., 2013). As Fe and inert Ti show a high correlation ( $S_{rho}$ : 0.86) at Lake Stymphalia, we assume that Fe mainly originates from terrestrial sources and interpret the Mn/Fe proxy with caution only in phases when both elements show clear signals.

The ratio of allochthonous Rb versus zircon (Zr) is widely used as grain-size proxies, as Rb is associated with clay minerals, while Zr is mainly associated with coarser grain material (Chen et al., 2006; Cuven et al., 2010; Dypvik and Harris, 2001; Koinig et al., 2003; Kylander et al., 2011). In the Stymphalia record, Zr is linked to the silt-sized fraction and Rb is strongly linked to the clay mineral assemblage suggesting no K-feldspar source contribution (Heymann et al., 2013).

*Table 3. Cultural chronology of southern Greece from Classical to Late Medieval. The chronology is based on Weiberg et al. 2016, Bintliff, 2012; Manning, 2010.*

Time (BC/AD)	Period	Event	Abbreviation
AD 1204 – 1460	Byzantine and Frankish/Late Medieval	Start: Frankish conquest of Constantinople.	B-F
AD 900 – 1204	Middle Byzantine/Medieval	Start: Consolidation of the Roman (Byzantine) power in the southern Balkans.	MB
AD 641 – 842	Early Byzantine/Early Medieval	Start: Death of Emperor Heraclius and the collapse of the Late Roman political order.	EB
AD 300 – 641	Late Antiquity/Late Roman	Start: Founding of the city of Constantinople and the parting of ways between the Western and Eastern parts of the Roman Empire.	LR
31 BC – AD 300	Roman	Start: Destruction of Corinth and end of Achaian war.	R
323 – 31 BC	Hellenistic	Start: Death of Alexander	H
479 – 323 BC	Classical	Start: Greek victory over the Persians in the battle of Plataea; Persian invasion of Greece repelled.	C

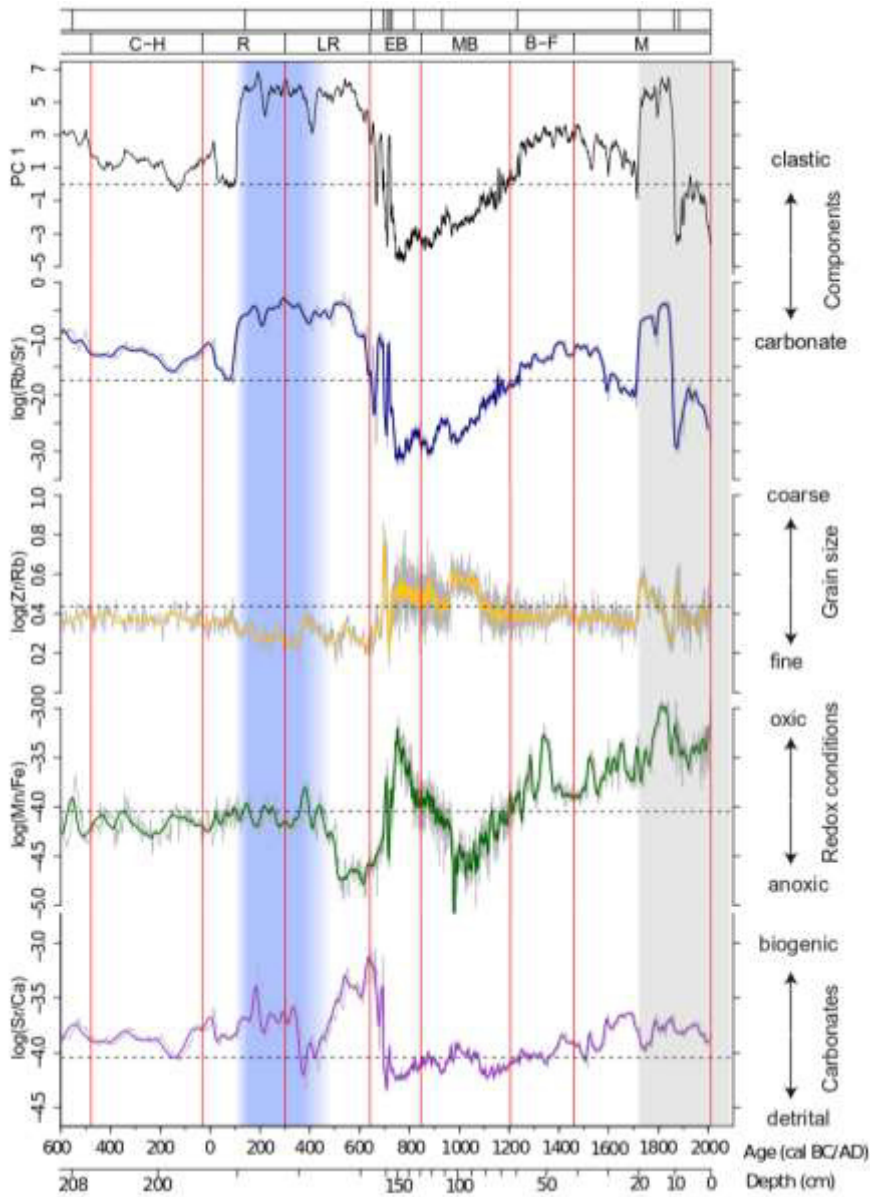


Figure 7. Selected elemental ratios depict paleoenvironmental changes at Lake Stymphalia for the last 2,500 years. The log-normalized ratios plotted in grey are based on the Avaatech XRF counts per second measured on STY-1. Colored lines were calculated with a 5-point moving window. Dashed horizontal lines mark the respective mean values for the whole dataset. PC1 and Rb/Sr indicate changes in the material composition. Zr/Rb is used as a grain size proxy. Mn/Fe hints to redox conditions in the bottom water. Sr/Ca explains the origin of the carbonates. Arrows to the right explain how to read the proxies. All proxies are plotted against age (cal BC/AD). Approximate depth scale (cm) is included for comparison. The upper boxes above the graph show the lithological units. The lower boxes and vertical red lines refer to the transitions between Greek cultural boundaries as specified in Weiberg et al. (2016; cf. Table 3). The blue vertical bar shades the approximate period of the functioning of the Hadrianic Aqueduct (130 – max 500 AD). Values in the grey shaded area (>1720 cal AD) need to be interpreted with caution due to strong anthropogenic alteration. For interpretation of the references to color, the reader is referred to the web version of this article.

## 5.2 General palaeoenvironmental interpretations

The lack of lamination throughout the entire core sequence indicates that the water level has never been considerably higher than at present over any long time period as would be necessary to allow for water column stratification and repress complete mixing of the water column (Zolitschka et al., 2015). A generally low water level is also supported by the presence of *Bythinia sp.* (Figure 3-D) and *Valvata sp.* shells or shell fragments throughout most of the sediment sequence (Figure 4). Both organisms are gastropods living in well oxygenized, shallow waters and swamps, and are often found, e.g., in the reed belt of shallow lakes in the Balkans (Tom Wilke, pers. comm. 2015; Davies, 2008). Their presence in Lake Stymphalia thus indicates a generally molluscan favourable environment with well-mixed, oxygenized conditions within a small, permanent and constantly shallow freshwater lake even within the blackish units 62 and 63 (Davies, 2008; Mischke et al., 2017).

The different shades of colour in the sediment sequence indicate varying depositional conditions. While the lower part of the core shows signs of low sedimentation under water-logged conditions, the brownish colours of the upper part indicate increased erosion, a higher input of terrigenous material and short periods of desiccation, e.g. during summer (Figure 4).

The grain size distribution in lake sediments provides information on the erosion, transport and accumulation mechanisms of material from the source to the lake. The compact, fine-grained silty clay and clayey silt units in this sequence point to a dominance of chemical weathering in the catchment. In a water balance calculated by Morfis and Zojer (1986), more than half of the water discharge volume is ascribed to underground inflow, suggesting the importance of mineral transport in dissolution, mainly concerning the carbonates.

Four main sedimentation phases can be distinguished over the last 2,500 years (Figure 6). During Classical-Hellenistic times, the sedimentation rate is approx. 0.2 mm/yr. It slightly increases to about 0.4 mm/yr during the Roman Period. Interestingly, this is on a comparable scale to the sedimentation rates calculated from colluvia in the neighbouring Phlious basin (Fuchs et al., 2004). Around 800 cal AD, we see a strong increase in the sedimentation to >2 mm/yr lasting for approximately 300 years and then gradually decreasing to the top; and for the last 500 years it is calculated at 0.7 mm/yr (Figure 6). Walsh et al. (2017) report a mean accumulation rate of 1.7 mm/yr for their Stymphalian sediment cores recovered from the lakeshore.

The MBT<sub>5Me</sub> proxy provides a means to quantify temperature variations over time (De Jonge et al., 2014). As no regional lake temperature calibration for the MBT<sub>5Me</sub> is currently available and the only other calibrations available for tropical East African lakes (Russel et al., 2018) and alkaline Chinese lakes (Dang et al., 2018) yield temperature estimates for Lake Stymphalia that are much higher than

the 20<sup>th</sup> century data from the meteorological station at Driza-Stymphalia, and are thus highly unrealistic, we prefer to discuss relative temperature trends instead of reporting absolute temperatures (Figure 8). Additionally, we do not address the question of variation between autochthonous and allochthonous sources in the sediment composition, which likely affects the palaeothermometer. As lipid biomarker analysis in Greece is still at an early stage (Gogou et al., 2016; Katrantsiotis et al., 2018; Norström et al., 2018), we assume the full potential of this method is not yet achieved, and only provide a first tentative interpretation. However, we included this dataset with the aim to contribute to the further development of this method.

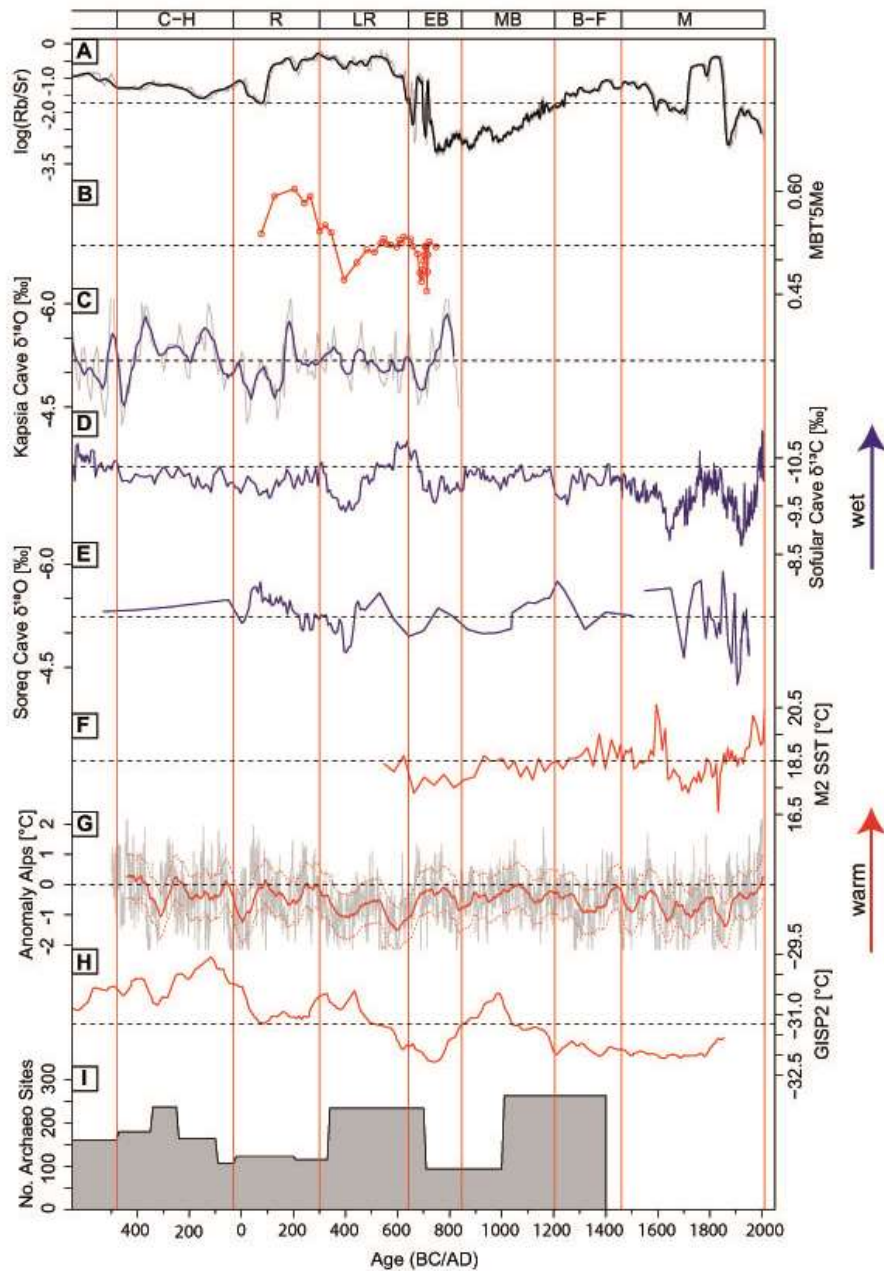


**Figure 8:** Comparison of Lake Stymphalia climate proxies ( $\log(\text{Rb}/\text{Sr})$ , A) and MBT'5Me (B) to other regional (C-F) and supra-regional/global climate archives (G-H) and the number of archaeological sites on the Peloponnese (I) for the last 2,500 years. (C) Finné et al., 2014 (inverted); (D) Fleitmann et al., 2009 (inverted); (E) Bar-Matthews et al., 1999 (inverted); (F) Gogou et al., 2016; (G) Büntgen et al., 2011; (H) Alley, 2004 (I) Weiberg et al., 2016; Blue proxies reflect precipitation or humidity; higher water availability is plotted towards the top. Red proxies reflect absolute or relative temperature. Warmer temperatures are plotted towards the top. Dashed horizontal lines mark the mean values for the respective dataset. Boxes and vertical red lines represent transitions between Greek cultural boundaries as specified in Weiberg et al. (2016) and Table 3. For interpretation of the references to color, the reader is referred to the web version of this article.

### 5.3 The socio-environmental history

#### 5.3.1 Classical-Hellenistic and Early Roman Periods (479 BC – 130 AD; unit 59)

Archaeological investigations and palaeoecological findings postulate agricultural activity in the Stymphalia catchment from the Early Neolithic onwards (Walsh et al., 2017; Williams, 2005). Thus, variations in the analysed sediment sequence most likely reflect both natural as well as anthropogenic changes in the landscape.

During Archaic to Middle Hellenistic times (600-250 BC), the city of Stymphalos was flourishing, accommodating ca. 2,500 people plus potentially another 500 people in the rural surroundings (Williams, 2005, 2003; Karambinis personal communication). Williams (2005, 2003) describes a large, fortified wealthy city for the 5<sup>th</sup> to 3<sup>rd</sup> century BC; the florescence of the city was associated with the maximum regional population and land use unrepeated until the later 20<sup>th</sup> century AD. Excavations in the Lower Town by Williams, a large part of which lies in the lake flats, have revealed that the archaeology is covered by at least 1 m of fine-grained colluvial sediments deposited into a shallow freshwater environment overlying the abandoned buildings, while the house foundations extend below the modern water level. Clearly, the lake during this urban phase must have been further out into the current lake bed, and at a significantly lower level.

The geochemical records for this urban period (lithological unit 59) are all very stable (Figure 7). The absence of major fluctuations points to a phase of rather stable environmental conditions. Greyish clayey silt with a slightly black mottled appearance and a high content of shell fragments suggests that the sediments were continuously water-logged at that time.

The finding of a larger ceramic shard at 205 cm in core STY-3B (Figure 3-C) as well as a small amount of tiny ceramic particles in STY-1B prove human presence at this depth, during the 6<sup>th</sup> to 5<sup>th</sup> century BC. The shard was embedded in a fine matrix, indicating slow, regular and constant accumulation excluding any extreme event such as a debris flow or strong erosion induced by land-use management which would have required a coarser matrix, whilst the Zr/Rb ratio shows consistently fine sediment. The low sedimentation rate (~ 0.2 mm/yr) for this period further confirms this assumption (Figure 6). On that basis, we assume that the ceramic was deposited under regular, stable sedimentation conditions and it was thus also considered a *terminus post quem* for the surrounding sediment. It is striking, that despite high levels of local population and inferred maximal land use in the surroundings of the lake, unparalleled until the late 19<sup>th</sup> century AD, no larger disturbances can be found in the sediment core. Clearly, on the one hand, farming and pastoralism were practised in ways that protected the landscape from significant erosion, and on the other hand,

reconstructions of contemporary climate in Classical-Hellenistic Greece suggest stable climate conditions unlikely to destabilize the land surface (Finné et al., 2011).

In later Hellenistic into Early Roman times (locally 250 BC – 100 AD) the city shrank and then lost its city status, becoming a far smaller settlement which by Middle Roman times (200-400 AD) may have been little more than a village (Williams, 2003). This demographic decline in Stymphalia is in agreement with decreasing settlement activity from the Peloponnese (cf. Figure 8-I; Weiberg et al., 2016).

Around the beginning of the Roman period, we observe a slight shift in the grain size of the sediment core towards even finer silty clay. This matches the archaeological data indicating that land use was more restricted. During this period, land use will have declined on a massive scale and natural vegetation cover may have spread again, stabilizing the soils, limiting surface weathering, and leading to less detrital input. The sedimentation rate is lowest around 0 – 100 cal AD which suggests a largely abandoned land use and a recolonization of the landscape by stabilizing natural vegetation such as scrub and woodland that hinders the soils from eroding. However, the TOC/TN values for this period are incomplete and pollen is not well-enough preserved in the sediments to support this indication.

It can be considered that during Classical, Hellenistic and the first two centuries of the Early Roman period, inhabitants of the Stymphalia polje practised sustainable agro-pastoralism that didn't cause a lasting imprint in the lake. For this period, the lake seems to have been steady in size and the ecosystem seems to have been resilient and in equilibrium as no large disturbances have been recorded.

### **5.3.2 Later Early to Late Roman Period (ca. 130 – 641 AD; unit 60)**

From approximately the first two centuries of Early Roman times onwards, only a very small settlement is known in the catchment of Stymphalia and the impact on the landscape is assumed to have been small (Williams, 2003). A slight increase in population might be recorded for Late Roman times (400-650 AD), indicated among others by the finding of graves dated to the late 4<sup>th</sup> and 5<sup>th</sup> century (Williams, 2003; Williams et al., 2002); but in the former city and in the wider region it will have been a fraction of the population development seen in the climax era of Archaic to Middle Hellenistic times. For the Peloponnese, a higher settlement activity is also reported by Weiberg et al. (2016) for the time span 350 – 700 AD (Figure 8-I).

All geochemical elements measured from the sediment core show an abrupt change in the measured counts at 189 cm (140 cal AD). While the carbonates Ca, Sr as well as the TIC content drop



considerably, the terrigenous elements (Rb, Zr, Al, Ti, K, Si) increase sharply and stay constant at higher level for several centuries, with the exception of a small dip at 180 cm (360 cal AD). This very sudden shift at 189 cm, clearly seen in Mn and Fe counts (Figure 4) is interpreted as a direct consequence of the building of the imperial, Hadrianic aqueduct. Around 130 AD the Hadrianic aqueduct was built over a distance of 84 km from the spring of Driza to the ancient city of Corinth in order to extend the latter city's water supply (Lolos, 1997; Unkel et al., 2011). In the natural state, underground discharge from the Stymphalia catchment would drain first into the lake, mainly being fed by two sources, and then by subterranean sinkholes into the Gulf of Argos to the SE (Morfi and Zojer, 1986), but with the help of tunnels and bridges, the engineers of the time redirected the bulk of the water to the NE. Ancient Corinth, as the capital of the Roman province of southern Greece, was flourishing at that time, and although water supply in the city was generally sufficient for the basic needs of the citizens, it is assumed that the Corinthians wanted the additional water source for elaborate water infrastructure features such as fountains and bath complexes (Lolos, 1997). The construction of the aqueduct meant a huge impact for the Stymphalia lake system. As response to the water being diverted directly from the spring of Driza to the aqueduct, the lake area shrank drastically and the lake level became lower. This explains the sudden shift in the geochemical elements at 189 cm (Figures 4 and 7).

The sedimentation rate was at a minimum at the beginning of the aqueduct construction project and reached a small local maximum of approximately 0.5 mm/yr between 200 to 300 cal AD (Figure 6), contemporaneous with the zenith of the aqueduct. We assume that the increase in sedimentation rate can best be explained by the diminishing lake area; the coring spot in the depocentre of the lake would have been closer to the shores and thus more terrigenous material would reach its position. Throughout the existence of the aqueduct during the Roman and Late Roman Period, carbonate content in the system is considerably lower and we hardly find any gastropod and shell fragments here, while detrital input of terrigenous elements is highest, indicating that material input was dominantly allochthonous.

Additionally, a strong increase in Fe is visible over the running time of the aqueduct, peaking at 178.9 cm and 176.8 cm (ca. 380–440 cal AD). Here, we find a coarser grained, oxidized, orange layer, clearly visible in the high Fe content as well as in the RGB colour together with a peak in Zr/Rb (Figures 4 and 7). Sedimentologically, the orange colour and the high Fe content point towards oxidation and precipitation of Fe-hydroxide. It seems plausible that the lake area continuously shrank over time and by the end of the 4<sup>th</sup> century AD, the lake seasonally or periodically dried up allowing for oxidation to take place. Several proxies point towards a very small lake, desiccating and oxidizing

conditions around 400 cal AD, which can be ascribed to the draw off of water discharges for the aqueduct. When we compare the Stymphalia dataset to other archives for the Eastern Mediterranean, e.g. the  $\delta^{18}\text{O}$  and  $\delta^{13}\text{C}$  stable isotope data from Kapsia Cave, Peloponnese (Finné et al., 2014), Soreq Cave, Israel (Orland et al., 2009), and Sofular Cave, Turkey respectively (Fleitmann et al., 2009; Göktürk et al., 2011), we do not see a consistent picture, but rather regionally diverse expressions (Luterbacher et al., 2012; Manning, 2013a; Roberts et al., 2012). Around 400 AD however, most proxies tend to indicate slightly drier conditions (Figure 8-C,D,E) and it is thus possible that the dry conditions in Lake Stymphalia at that time may have additionally been influenced by a climatic factor. Conditions change during the 5<sup>th</sup> century AD, when relatively more Sr is precipitated within the lake and additionally the Mn/Fe ratio points towards more anoxic conditions suggesting that the lake was continuously waterlogged again. Historical information indicate that during the 3<sup>rd</sup> to 4<sup>th</sup> century AD maintenance was carried out to keep the aqueduct working, while during the 5<sup>th</sup> century AD, the Hadrianic Aqueduct was abandoned and partially collapsed, associated with a significant decline in the size and prosperity of Corinth (Hammond, 2015; Lolos, 1997). The beginning of the long-term abandonment of the aqueduct – which was actually not re-activated until the 1880s (Morfis and Zojer, 1986) – coincides with the changes in the sediment geochemistry. After the collapse of the aqueduct, more water stayed in the basin and the lake was refilling. The Fe content is continuously decreasing again and it seems as if the lake system that had been disturbed and unbalanced by the construction of the aqueduct was trying to retrieve its equilibrium state. The Rb/Sr ratio, which was relatively constant since the construction of the aqueduct, starts to decrease around 540 cal AD, parallel to when Mn/Fe reaches its minimum. Temporally, this coincides with two large volcanic eruptions in 536 AD and probably in 540 AD, which caused atmospheric dimming and contributed to a cold spell in the Northern Hemisphere. A climatic connection, concomitant with cooler conditions at Lake Stymphalia, seems possible and could be consistent with the age-depth-modelling for this phase. The period 500–650 cal AD, depicting high Sr/Ca values and low Mn/Fe ratios, emphasizes constantly waterlogged conditions. As the Mn/Fe ratio during this period shifts to more anoxic conditions, we conclude that Lake Stymphalia was probably (slightly) deeper and less well ventilated. One possible explanation could be that wind intensity during this phase was lower causing less frequent mixing of the whole water body and the sediment surface. Another scenario would be that the target surface for the wind might have been lower due to protection by vegetation cover, e.g. like a pronounced reed belt as it can be found around the lake today. Sr/Ca shows its highest peak in the record here, pointing to an increased supply of biogenic carbonate material. This is supported by a high amount of shells and shell fragments. The gastropods must have developed under constant water

conditions. It can thus be concluded that during the 6<sup>th</sup> and early 7<sup>th</sup> century cal AD considerably higher amounts of water reached the Stymphalia polje enabling the extension of the lake area. As the aqueduct was not working anymore and human influence in the area is very low at that time, the water supply can be primarily associated with the reintroduction of water from the lake's main source, the Driza spring. Additional effects of changes in precipitation and temperature may have influenced this turn; reconstructions from the Eastern Mediterranean however do not show a homogeneous pattern. The Sofular Cave proxies show considerable higher precipitation at this time (Fleitmann et al., 2009; Göktürk et al., 2011), while data from Soreq Cave is interpreted as showing a decrease in precipitation for the 2<sup>nd</sup> to 7<sup>th</sup> century AD (Göktürk et al., 2011; Luterbacher et al., 2012). In their review of climatic changes during and after the Roman Empire 100 BC – 800 AD, McCormick et al. (2012) state that precipitation in France and central Europe became exceptionally variable between 250 and 650 AD. They see a warming trend in the 4<sup>th</sup> century AD, while the 6<sup>th</sup> century is characterized by generally cooler conditions, crop failures and the Justinian Plague (541 AD onwards), a devastating epidemic outbreak in the Mediterranean, as well as droughts and heat events, a high number of famines and cold winters in the Middle East (600–724 AD) (McCormick et al., 2012).

During the Roman Period, we initially see crucial human influence on the lake ecosystem with the building of the aqueduct, followed by a period, when the proxies seem to respond to climatic influences again, however more sensitively than before, which may be ascribed to the unbalancing caused by natural rebound of the hydrographic system once the aqueduct ceased to function.

### **5.3.3 The Early Byzantine Period (641-842 AD; units 61 – 65)**

During the Early Byzantine and the early part of the Middle Byzantine very low population and very limited land use are expected for the Stymphalia basin in the context of generally low settlement activity in the Peloponnese and Greece generally (Bintliff, 2012a; Weiberg et al., 2016; Figure 8-I). The plague in the Eastern Mediterranean began in 541 AD and recurred several times until ca. 800 AD (Benovitz, 2014; Izdebski et al., 2016b; Little, 2007), causing major depopulation for the Stymphalia area. The Migration Period in Greece is most prominent in the 8<sup>th</sup> century AD, when Slavic colonisation spread to the Peloponnese, taking in some of the land emptied by the lost local population. Although recognition of Slavic sites is highly problematic (just two cemeteries have been excavated in the Peloponnese), and surviving Greek populations in the countryside are hard to detect since much of their material culture continues Late Roman forms, the evidence overall points to a

demographic low point in Greek rural landscapes (Bintliff, 2012b). Dated churches confirm the delay in population recovery until the 10<sup>th</sup> century AD (Sigalos, 2004).

For the 7<sup>th</sup> and early 8<sup>th</sup> century cal AD (156.5 – 167.5 cm, unit 61 – 64) we see high variability in the sediment core and all geochemical proxies (Figure 4). As human activity is considered to be low, as outlined above, it can be assumed during this period that fluctuations in the sediment are primarily attributed to natural climatic and environmental changes rather than to anthropogenic influence. Four very thin but lithologically different units (unit 61 – 64) have been identified in this phase. As gastropods are present throughout all phases, we assume the constant existence of a lake, however with varying extent. The short but intense fluctuations indicate that after the vast disruption from building the aqueduct, the lake system had not fully recovered and regained its balance, but was highly vulnerable and new environmental changes led to significant repercussions in the ecosystem. Unit 61, dating to the second half of the 7<sup>th</sup> century, contains light olive grey material with a higher amount of coarse material and only few shell fragments (Table 1). It contains a sharp Ca peak, higher than in the units below but lower than in unit 65 and above. High Zr counts indicate coarser grain size most likely due to more intense erosion or strong precipitation events in the lake's catchment. Vegetation cover or a potential reed belt around the lake must have been low or absent, allowing the coarser material to reach the coring spot. Unit 62 again is rather fine grained, has a high amount of terrigenous elements and the lowest Ca counts of the analysed core sequence. The *Crataegus* seed, dated to ca. 780 AD, was found within this unit (modelled to 690 cal AD). The most characteristic features of this unit are its black colour and the high magnetic susceptibility values (>30x higher than the median). The blackish colour may indicate organic matter and anoxic conditions, supported by a very low Mn/Fe ratio. Unit 63, is also black, but consists of considerably coarser material, a high amount of intact shells and shell fragments and shows a strong Fe peak. What can clearly be observed here is a sudden, strong increase in the sedimentation rate to over 2 mm/yr that continues with a slightly decreasing trend for the following centuries. The variable and rapidly changing Zr/Rb proxy, reflecting grain size fluctuations, implies a vulnerable environment with quick changes in water availability. The intensity of variation of the geochemical proxies in units 61–64 is unparalleled through the entire sequence at Lake Stymphalia, even stronger than during the Pleistocene/Holocene transition (Heymann et al., 2013).

The period between approximately 100 to 750 cal AD was specifically investigated using the distribution of branched GDGTs MBT<sub>5Me</sub> to gain information on relative temperature fluctuations, because it is known as a period of significant temperature variations (Büntgen et al., 2016). The relative  $\Delta$ MAAT variation (Figure 8-B) based on the MBT<sub>5Me</sub> lipids suggests relatively warm

conditions in Stymphalia during the 2<sup>nd</sup> to 3<sup>rd</sup> century cal AD followed by a strong cooling trend at the beginning of the Late Roman period and coldest temperatures around 400 and again later around 700 cal AD. This first cold phase is parallel to the decrease in rainfall described from the Middle East (Göktürk et al., 2011; Orland et al., 2009), and also aligns with  $\delta^{18}\text{O}$  inferred drier conditions observed in the Kapsia Cave (Finné et al., 2014) and the Soreq Cave (Bar-Matthews et al., 1999). Within the error margin of the age-depth-model, the MBT<sub>5Me</sub>-reconstructed relative MAAT variation is also largely in agreement with a previously reported cooling in the 6<sup>th</sup> and 7<sup>th</sup> century AD based on dendrochronological data from the French Alps and the Russian Altai described by Büntgen et al. (2016) and referred to as the “Late Antique Little Ice Age” (LALIA, Figure 8-G). As possible triggers, Büntgen et al. (2016) suggest high volcanic activity and low solar forcing. In a recent review paper, Helama et al. (2017) describe a longer period of cold conditions between 400 and 765 AD termed “Dark Ages Cold Period” (DACP). However, we here follow the terminology of Büntgen et al. (2016) and abstain from using the term DACP (Büntgen et al., 2017; Helama et al., 2017b), as the latter is not only culturally pejorative, but it can also easily be confused with the Greek Dark Ages at the Bronze Age/Iron Age transition (Drake, 2012), which for the same cultural reasons are more frequently referred to as the Early Iron Age or (Proto-) Geometric and Archaic Period (Bintliff, 2012b; Weiberg et al., 2016). For the temporal extension of the cold LALIA period as reflected in our Stymphalia record, we would however rather follow Helama et al. (2017), as our brGDGT-inferred relative temperature record shows continuously colder temperatures until the beginning of the 8<sup>th</sup> century as compared to the 2<sup>nd</sup> century cal AD. Izdebski et al. (2016) also report colder climate conditions during the Late Antiquity for Anatolia and the Levant and add that the coldest decade most probably covered the time of the devastating pandemic known as the “Justinian plague” (541 AD). Büntgen et al. (2016) also consider the LALIA as one influential factor on “crop failure, famine and plague, as well as a possible trigger for political, societal and economic turmoil”. During this period, described as the “rural agrarian system of Antiquity” (Izdebski et al. 2016), the people in the Eastern Mediterranean were strongly depending on cereal cultivation, viticulture and arboriculture, activities that are generally vulnerable to climatic fluctuations. The rapid drop in temperatures may have strongly increased their vulnerability, made them less resilient and more fragile to social crises. More pertinently, as occurred in the early years of the 17<sup>th</sup> century during the LIA, closely spaced and even contiguous severe drought years may have caused historically significant unrest/collapse of normal agrarian adaptive systems (Manning, 2018; White, 2013).

The situation in the eastern Roman Empire during the 6<sup>th</sup> and 7<sup>th</sup> centuries AD is described as showing “signs of hydroclimatic difficulties” and drier conditions that seemed to have prevailed until the 8<sup>th</sup>

century AD (Manning, 2013b; McCormick et al., 2012). The onset of the Late Antique cooling in the 7<sup>th</sup> and 8<sup>th</sup> century AD is described by McCormick et al. (2012) as a period of “deep transformations”. This phase of high climatic instability in the Eastern Mediterranean is contemporaneous to the period of high instability and very varying conditions seen in Lake Stymphalia.

The core sequence reflecting the second half of the Early Byzantine Period, unit 65, comprises bright clayey silt containing some sand and a considerable amount of gastropod shells. Ca content is highest compared to the lower core sequence and the Sr/Ca ratio indicates mainly detrital input due to enhanced limestone weathering intensity. Strong chemical weathering may be explained by episodes of warm and wet climate conditions (Jin et al., 2001). Strong precipitation events may account for the influx of coarser material in unit 62, together with chemical changes. The continuing effects of the LALIA climatic fluctuation may be responsible, given the very low human impact. The notable rise in sedimentation after 780 cal AD and on till the 14<sup>th</sup> century AD begins in what Büntgen et al. (2011) as well as Bradley et al. (2016) term “Medieval Quiet Period”, a period of reduced climate variability between 700 and 1000 AD. With the exception of the Mn/Fe ratio, which points towards decreasing oxic conditions and thus less intense mixing conditions, our proxies also show comparatively few fluctuations within that period, but that may also be explained by low human activity in a more stable land-cover. Although evidence for population changes in the Stymphalos Polje are so far not studied for the entire Early Byzantine period, wider evidence from the Peloponnese and other parts of Greece suggest low population and levels of land use throughout the era. The onset of increased sedimentation seem to mark the earliest phase of the Early Medieval Warm era, but this in itself would not seem sufficient to account for the increased influx of erosion products, which is lacking in the Greco-Roman eras under similar climatic conditions.

#### **5.3.4 Middle Byzantine Period (842 – 1204 AD; units 66 – 67)**

In the 9<sup>th</sup> century AD, southern Greece is re-integrated into the Byzantine Empire (Xoplaki et al., 2016a). From Middle Byzantine (MB) times onwards, we see a gradual rise in population and a revival of agricultural use across the study region, reaching its climax after 1150 cal AD (Figure 8-I; Bintliff, 2012b; Williams, 2005; Xoplaki et al., 2016b). Xoplaki et al. (2016) define the 12<sup>th</sup> century AD as a “most prosperous period for southern Greece, with high agricultural productivity” and a relatively resilient society.

The steady increase in terrigenous elements (Figure 4), consequently an increase in Rb/Sr (Figure 7) and the sustained high sedimentation rate (Figure 6) from the 11<sup>th</sup> century until approximately 1400

cal AD would fit increasing human impact. While the Zr/Rb ratio showed only minor fluctuations before ca. 700 cal AD, the ratio strongly oscillates within this period starting in the mid-8<sup>th</sup> century, which could suggest enhanced human activity, land use, and erosion of soils with varying grain sizes. The silt content increases from 63 % in unit 64 to 79 % in unit 68 (SOM 3). The coarsening of the particles could potentially be linked to more intensified land use, such as herding, agricultural activity or deforestation loosening the soil and destabilizing the slopes, although the archaeologists believe that during this period the area was largely covered by forest (Campbell, 2018). Contrary to the Late Roman period, we do not consider that the lake area was small during the MB time, allowing more coarse-grained material to reach the depocentre, because we see high carbonate content here, which demands chemical weathering due to the presence of water and a rather large lake surface for summer evaporation to be more effective. Additionally, more allogenic organic matter is washed in and preserved, as seen by higher TOC and TOC/TN values at 145 cm (4.9% and 39.6 respectively) or 110-115 cm (6.4% and 43.6 respectively; SOM 2). For the analysed sequence, TOC/TN ratios usually fluctuate between 10 and 20 (mean = 17.6), which suggests significant mixing of terrestrial and aquatic organic matter (Meyers, 2003). In the MB period, the amount of terrestrial organic matter dominates, while the high sedimentation rates may contribute to the comparatively better preservation of the organic matter as the sediment buries it before it can be completely decomposed. While in unit 66 we still find intact gastropod shells, unit 67 only contains shell fragments and additionally root fragments, suggesting the reworked nature of the material and vegetation growth. The increase in detrital terrestrial material input is likewise visible in PC1 and Rb/Sr (Figure 7). As Ca and Sr still have high values, although decreasing over time, we would expect intensive chemical weathering and high evaporation, thus generally warm and wet conditions. The archaeological and historical evidence for Greece clearly indicate an increasing rate of demographic growth and land intake between the 9<sup>th</sup> and the 12<sup>th</sup> centuries (Bintliff, 2012b; Xoplaki et al., 2016b). That this took place within a climate phase, which was warm and moist according to current climate reconstructions, was a very positive background to a new political stability in the countryside. Other high resolution climate proxies for this period are still rather sparse (Xoplaki et al., 2016b), but SSTs from M2 in the Aegan Sea (Figure 8-F; Gogou et al., 2016) also record increasingly warmer temperatures for this phase starting from 900 AD up to the 14<sup>th</sup> century.

However since demographic levels are well below those of Classical-Hellenistic times, and by inference the extent of landscape in intensive use, the unparalleled erosion into the lake, seen by the high sedimentation rate, must imply either strong precipitation events, or effective evaporation from a large and shallow water body, or non-investigated more localised and very destructive deforestation

and modes of farming and herding in the immediate catchment of the lake, than prevailed throughout Greco-Roman times.

### **5.3.5 Late Byzantine-Frankish Period (1204 – 1460 AD; units 67 – 68)**

The uppermost part of sedimentary unit 67 and the lower part of 68 cover the era of Crusader occupation and parallel Byzantine control of different parts of the Peloponnese, before the Ottoman conquest of the mid-15<sup>th</sup> century. Since the 13<sup>th</sup> to early 14<sup>th</sup> centuries show dramatic contrasts both in the archaeological and historical record, as in the core evidence, to the period of the late 14<sup>th</sup> into mid-15<sup>th</sup> centuries, we shall discuss these separately.

For the 13<sup>th</sup> century the high sedimentation rate which had commenced already in Middle Byzantine times is maintained, but with a visible slowing down. The continued increase in Rb/Sr points to more terrigenous influence and Mn/Fe suggests that the lake continued to become shallower and/or well mixed, reaching its most oxic state in the first half of the 13<sup>th</sup> century, which coincides with societal changes in the catchment.

Although we do not expect any major change in regional demography and land use, the Stymphalos lakeside has a truly exceptional history in the 13<sup>th</sup> century, since it was chosen for the foundation of a Cistercian monastery, located above and slightly inland of the ancient city site (Campbell, 2018). In general, such establishments favoured areas with high agro-pastoral potential but remote from major population centres. They emphasized manual labour by the monks and advanced farming techniques, but the assistance of local labour (lay-brothers) required the existence of nearby settlements. We can expect intensive use of the landscape around the monastery but rather good management of local ecology. That erosion into the lake continued but at a declining rate may indicate new clearance initiatives near the coring site but maybe slightly greater ecological care than in the preceding period of settlement. However, the Zaraka monastery existed for only less than one century and due to the age uncertainties in the sediment core outlined above, it is not possible to draw conclusive links between changes in the sediment sequence and monastery activities. We conclude here that the climatic regime for this century marks the highpoint of the early Medieval Warm period, remaining as favourable to settlement and land use as in previous centuries.

In the second half of the Late Byzantine-Frankish (B-F) era, there is strong societal transformation. The collapse of Frankish power leaves the Peloponnese in Byzantine control, and the monastery at Stymphalos is abandoned. Furthermore, in the mid-14<sup>th</sup> century, the Black Death produces a massive reduction in European populations, while a period of colder climatic conditions lasting into the 15<sup>th</sup>



century, a first phase of the Little Ice Age, was reconstructed from the Alps (Büntgen et al., 2011). Although this climatic period is associated with increased precipitation in temperate Europe, the effects in the southern parts of Europe may have been temperature and rainfall decline (Magny et al., 2007).

The latter part of the B-F period is covered by sedimentary unit 68, which shows a more brownish colour and considerably high magnetic susceptibility (MS) values suddenly increasing by a factor of 4 around 1400 cal AD and this continues into the first part of the early Post-Medieval period (Figure 4). High magnetic susceptibility indicates that these sections contain a higher amount of terrigenous material that may be magnetized, especially ferromagnetic elements such as magnetite or maghemite (Lucke and Sprafke, 2015). Fe counts are elevated but not as high as during the Late Roman period (Figure 4). Contrary to the material eroded in early centuries, it seems likely that the sediments eroded at this period were stored locally as colluviums or on terraces before, where processes of soil formation took place before they were finally deposited in the lake. This would likewise explain the strong rise in the magnetic susceptibility followed by a declining trend; upper layers with most intensive development of soil formation and highest MS values eroded first. The loss of soil from abandoned fields following the phase of the Black Death is also described from Macedonia (Gogou et al., 2016).

Throughout Greece, the 14<sup>th</sup> to early 15<sup>th</sup> centuries is a period of large-scale depopulation in the countryside, associated with a devastating plague, prolonged episodes of warfare between Franks, Byzantine and the expanding power of the Ottoman Turks, and colder climatic conditions (Bintliff, 2012b; Finné et al., 2011). After the abandonment of the Zaraka monastery in the mid-14<sup>th</sup> century, we have only minor archaeological traces of human settlement in the region at the ancient city site and the former monastery until archival records from 1700 AD (Campbell, 2018; Williams, 2005). In agreement with better-documented trends elsewhere in Greece (Bintliff, 2012b), we expect very low populations and widespread abandonment of cultivated land in the 14<sup>th</sup> to early 15<sup>th</sup> centuries, coinciding with the core trends just discussed. Hence, the highly magnetized sediments eroding into the lake probably mark the erosion of deserted, non-vegetated fields during an unstable and generally colder climate, perhaps with shorter but more powerful precipitation events.

### **5.3.6 Ottoman to Modern times (1460 – 2010 AD; units 68 – 70)**

With the Ottoman conquest of the Peloponnese in mid-15<sup>th</sup> century, we enter a new phase of local settlement history, so we shall first discuss the relevant evidence up until the end of the 18<sup>th</sup> century

AD, associated with the upper three-quarters of sediment unit 68. The age-depth-model for the uppermost 50 cm of the core has high uncertainties and the calculated ages are probably slightly too old. Thus, we rather combine the geochemical signals with known historical dates.

The Ottoman authorities were proactive in Greece in encouraging the resettlement of abandoned fields and villages (Bintliff, 2012b; Kiel, 1997, 1987), in particular inviting Albanian farmers and pastoralists to recolonise the Greek regions, including the Stymphalos district, where the modern villages mostly take their origin from this population movement. In Central Greece, repopulation began in the late 14<sup>th</sup> century and led to settlement growth into the late 16<sup>th</sup> century. The later inception of repopulation in the Peloponnese occurred within the late 15<sup>th</sup> into 16<sup>th</sup> century. This era falls within the generally colder and locally potentially drier Little Ice Age period and posed problems to the population for prosperous land use (White, 2013). The rate of sediment deposition into the lake continues to decrease up to the 16<sup>th</sup> century and stays at a rather constant level of ca. 0.7 mm/yr until the core top. Throughout unit 68, this is accompanied by a parallel fall-off in magnetized material, indicating that less soil material is eroded. Additionally, a refinement of the material is observed as shown by the Zr/Rb ratio. We suggest this marks stabilisation of an almost empty landscape by vegetation, scrub or emerging young woodland and only minor human impact.

Central Greek populations were to collapse dramatically from the late 16<sup>th</sup> into the 18<sup>th</sup> century. The demographic recovery which had begun much later in the Peloponnese, would also have been reversed at this time. The failure of central government, the peak of the Little Ice Age, and devastating warfare between the Ottomans and Venice were the major factors (Bintliff, 2012b). As a result, the first census figures for villages in the Stymphalos district ca. 1700 AD show very low levels, with 50 or less inhabitants per village for almost all settlements in the Stymphalos district (the successor to the ancient city and medieval monastery, the village of Stymphalia, has 52; Panagiotopoulos, 1985). Brown and Walsh (2017) see a drastic decrease in clastic sedimentation (Cu, Zn, Fe, Ti) and an increase in Ca in the upper 72 cm of their sediment cores taken from the lake shore, which they interpret as a lake level becoming constantly shallower and drying out repeatedly. However, their chronology needs to be regarded with caution, as it is not well anchored in the uppermost part. In contrast to these results, we see the opposite elemental trend in our sediment record, a constant increase in terrigenous elements (Rb, Zr, Al, Ti, K, Si) for the upper 156.5 cm (with the exception of unit 69 – 70) and a decreasing carbonate content (Ca and Sr). TOC and TOC/TN values for this period are low, indicating, as the Mn/Fe ratio implies strongly oxic conditions, that organic matter input in this section was strongly decomposed and not preserved. Unit 68 contains shell fragments of *Bythinia sp.* proving that a lake, however shallow, existed at that time. In addition, the sediment in unit 68 is

orange mottled with iron oxides hinting oxygen supply and desiccation. This leads to the conclusion that a small, shallow lake existed for most of the year and periodically dried out in summer. Thus, although the geochemical argumentation is different, we come to a similar conclusion as Brown and Walsh (2017) that the lake bottom became shallower over time and since approximately 1500 AD may have periodically dried out.

The uppermost units 69 and 70, covering the Early Modern era of the 18<sup>th</sup> to 20<sup>th</sup> century cal AD, need to be regarded with caution. We see very strong, abrupt changes and we assume that the material was altered post-hoc; for example due to desiccation, some material might have been eroded or due to agricultural activity on the lake bottom, it may have been anthropogenically reworked and first soil formation processes may have set in. According to Walsh et al. (2017) the lake dried up completely over several years in the recent and was even used as a landing strip. This is known from historical sources and brought the lake its nickname “aerodromio”, airport (Walsh et al., 2017). The desiccation, compaction and anthropogenic drainage can also be seen in the sedimentological record; unit 69 (dated to ca. 1720 – 1860 cal AD) is very dense and compact and contains a sudden, abrupt increase in terrigenous elements, especially in Rb and K, typical clay elements; this increase in clay can also be seen in the Mastersizer data. Zr/Rb firstly indicates a shift to coarser material and then a refining within the unit. The TOC content in this section is low, only increasing in unit 70 above, indicating that enough oxygen was present in this section to decompose the organic matter. An increase in Mn, Fe and MS suggests first soil formation processes; gastropods are absent here. All these proxies indicate that in the 19<sup>th</sup> century the lake has repeatedly fallen dry. Furthermore, there is historical evidence that the authorities in the Corinth region re-activated the aqueduct in the 1880s to irrigate their local farmland (Morfis and Zojer, 1986), giving one explanation why less water reached the lake. Although the sinkhole at the southern shore has been isolated from regular outflow since the 19<sup>th</sup> century (Walsh et al., 2017), no larger flooding events are visible in the core apart from the more coarse grained unit 70a (at 9 cm, dated to ca. 1880 cal AD). During the late 19<sup>th</sup> and early 20<sup>th</sup> century, agricultural production in the polje strongly expanded. The population of this district, as over the rest of the Peloponnese, grew exponentially; Philippson (1892) lists village sizes in the Stymphalos district that are 10 to 15 times those of the same communities two hundred years earlier (Stymphalos has now 808 inhabitants). This did not simply mean sustainable subsistence and minor commercial agriculture as during Classical-Hellenistic times (cf. section 5.3.1), but rather industrialized primary production for the global market with the help of farming machines (Kourelis, 2018), which would also explain the strong compaction of the soil. The shift from the colder LIA climate to a more typical

Mediterranean climate over this same period, starting in the 19<sup>th</sup> century AD based on SSTs in M2 (Figure 8-F; Gogou et al., 2016), was highly positive for the observed agricultural take-off.

The thin unit 70a, characterized by a high amount of sand particles probably indicates a strong precipitation event with surface run-off refilling the lake and feeding in coarser grained material into the centre of the lake that accumulated in the plain during the dry period; reed vegetation holding back the material was probably absent by then.

Unit 70b may be characteristic for today's conditions; high TOC, average TIC and Ca counts as well as moderate terrigenous input. The lake is perennial, but depending on the season it can vary considerably in size. The polje is intensively used for agricultural purposes. For the second half of the 20<sup>th</sup> century, land use has also been analysed by Papastergiadou et al. (2007); wet-meadows and open water areas declined considerably while reed beds and irrigated agricultural land spread out. The use of fertilizers reinforces the reed growth and most likely affects the faunal populations.

## **6. Conclusion**

The geochemical and sedimentological analyses of the Stymphalia lake sequence show a complex interlinking of natural variability and anthropogenic influence on the lake over the last 2,500 years. Water supply to the lake was not constant over time and the land cover in the catchment must have changed substantially in relation to climate fluctuations, intensity of land-use and human occupation phases that influenced the sedimentary conditions. The lake level and particularly the lake area have fluctuated considerably over the last 2,500 years including shorter periods of entire desiccation, more frequently occurring in the younger phase. No evidence for a very high lake level comparable with the neighbouring Pheneos polje has been found in the sediment sequence; we are continuously dealing with a shallow lake system here.

Stable climatic conditions and sustainable agro-pastoralism prevailed during Classical Hellenistic times. Major alteration in the lake's hydrological cycle occurred with the construction of the Early Roman Hadrianic Aqueduct around 130 AD, which increased the vulnerability of the ecosystem and, even after its failure, probably had a long-lasting impact on ecosystem reactions to climatic changes during the following centuries. We interpret this event as a trigger for the highly sensitive reaction to climatic variations during the LALIA period in the 6<sup>th</sup> to 8<sup>th</sup> century AD. The Lake Stymphalia data indicate that the Late Roman to Early Byzantine Period in southern Greece is associated with a shift to several cold periods of varying durations, strong variation in water availability and a generally more unstable climatic context. Although anthropogenic influence was chronologically limited, it

represents a significant element in understanding long-term reactions in the sediment core that were mainly linked to water availability. For the period 9<sup>th</sup> to 17<sup>th</sup> century, the age-depth-model implies higher uncertainties; however, we see a phase of higher sedimentation and carbonate precipitation during warm and wet conditions within the Medieval Warm Period roughly until the 15<sup>th</sup> century and indications for colder conditions during the Little Ice Age. The last 200 years are strongly shaped by desiccation and human activity.

Land use intensity and vegetation cover were in a fluctuating dialectic with temperature and precipitation changes in the degree and nature of surface erosion. These conclusions agree with recent modelling of environmental change, critical of mono-causation, rather focussing on complex interactions of human and natural factors in the inception of landscape transformation (Bintliff, 2002; Casana, 2008). Pollen analysis would lead to an additional value, supporting our hypotheses or further classifying the land use activities, however pollen preservation in the core sequence was inadequate for any detailed analysis. The close interdisciplinary collaboration between natural scientists and archaeologists in this research field was highly beneficial and offers a more holistic interpretative approach. In the near future, independent sedimentary records from other sedimentary archives in adjacent valleys shall offer additional insights on the reconstruction of climatic changes and associated human impact interaction in the NE Peloponnese.

### **Acknowledgements**

Funded by the Deutsche Forschungsgemeinschaft (DFG, German Research Foundation - Projektnummer 2901391021 – SFB 1266). The positions of Joana Seguin and Jan Weber are funded by the DFG through the Collaborative Research Centre “SFB 1266”. The position of Christian Heymann was funded by the DFG through the Graduate School “Human Development in Landscapes” at Christian-Albrechts-University. The authors acknowledge insights into the archaeology coupled with the history of the lake and the Hadrianic aqueduct from Hector Williams, Malcom Wagstaff, and Iannis Lolos. We kindly thank Tom Wilke (Georg-August-University Göttingen) for the determination of the mollusc species, Jesse Kalwij (Christian-Albrechts-University Kiel) for the determination of the plant species, and Bernhard Schmaltz (Christian-Albrechts-University Kiel) for the classification of the ceramic fragment. In alphabetical order, we kindly thank our following colleagues and students for their invaluable support in the field and in the laboratory: Mathias Bahns, Kimon Christanis, Sophia Dazert, Giorgos Floros, Elke Hänßler, Görkim Oskay,

Giorgos Savalas, Marcus Schütz, and Stavros Vrachliotis. We also thank two anonymous reviewers and Neil Roberts as editor for their valuable and constructive comments on the manuscript. The project was carried out with the relevant permits from the Greek Authorities.

## References

- ad-hoc Arbeitsgruppe Boden, 2005. *Bodenkundliche Kartieranleitung*. E. Schweizerbart'sche Verlagbuchhandlung, Hannover.
- Alley, R.B., 2004. *GISP2 Ice Core Temperature and Accumulation Data*. Boulder CO, USA.
- Atherden, M.A., Hall, J.A., 1994. Holocene pollen diagrams from Greece. *Hist. Biol. An Int. J. Paleobiol.* 9, 117–130.
- Bar-Matthews, M., Ayalon, A., Kaufman, A., Wasserburg, G.J., 1999. The Eastern Mediterranean paleoclimate as a reflection of regional events: Soreq cave, Israel. *Earth Planet. Sci. Lett.* 166, 85–95.
- Benovitz, N., 2014. The Justinianic plague: evidence from the dated Greek epitaphs of Byzantine Palestine and Arabia. *J. Rom. Archaeol.* 27, 487–498. doi:10.1017/S1047759414001378
- Bintliff, J.L., 2012a. Environmental degradation and the decline of ancient complex societies in the Mediterranean region, in: Bertonecello, F., Braemer, F. (Eds.), *Variabilités Environnementales, Mutations Sociales. Nature, Intensités, Échelles et Temporalités Des Changements*. XXXIIIe Rencontres Internationales d'archéologie et d'histoire d'Antibes. Antibes, pp. 213–220.
- Bintliff, J.L., 2012b. *The Complete Archaeology of Greece, from Hunter-Gatherers to the Twentieth Century AD*. Blackwell-Wiley, Oxford, New York.
- Bintliff, J.L., 2002. Time, process and catastrophism in the study of Mediterranean alluvial history: A review. *World Archaeol.* 33, 417–435. doi:10.1080/00438240120107459
- Blaauw, M., Christen, J.A., 2011. Flexible paleoclimate age-depth models using an autoregressive gamma process. *Bayesian Anal.* 6, 457–474. doi:10.1214/11-BA618
- Bloemsma, M., Croudace, I., Daly, J.S., Francus, P., Galloway, J.M., Gregory, B.R.B., Steven Huang, J.-J., Jones, A.F., Kylander, M., Löwemark, L., Luo, Y., Maclachlan, S., Ohlendorf, C., Patterson, R.T., Pearce, C., Profe, J., Reinhardt, E.G., Stranne, C., Tjallingii, R., Turner, J.N., 2018. Practical guidelines and recent advances in the Itrax XRF core-scanning procedure. *Quat. Int.* doi:10.1016/j.quaint.2018.10.044
- Bradley, R.S., Wanner, H., Diaz, H.F., 2016. The Medieval Quiet Period. *The Holocene* 26, 990–993. doi:10.1177/0959683615622552
- Bronk Ramsey, C., 2009. Bayesian Analysis of Radiocarbon Dates. *Radiocarbon* 51, 337–360.
- Bronk Ramsey, C., Lee, S., 2013. Recent and Planned Developments of the Program OxCal. *Radiocarbon* 55.
- Brooke, J.L., 2014. *Climate Change and the Course of Global History: A Rough Journey*. Cambridge University Press, New York.
- Brown, A.G., Walsh, K., 2017a. Societal stability and environmental change: Examining the archaeology-soil erosion paradox. *Geoarchaeology* 32, 23–35. doi:10.1002/geoa.21611

- Brown, A.G., Walsh, K., 2017b. Societal stability and environmental change: Examining the archaeology-soil erosion paradox. *Geoarchaeology* 32, 23–35. doi:10.1002/geo.21611
- Büntgen, U., Myglan, V.S., Ljungqvist, F.C., McCormick, M., Cosmo, N. Di, Sigl, M., Jungclauss, J., Wagner, S., Krusic, P.J., Esper, J., Kaplan, J.O., Vaan, M.A.C. De, Luterbacher, J., Wacker, L., Tegel, W., Kirilyanov, A. V., 2016. Cooling and societal change during the Late Antique Little Ice Age from 536 to around 660 AD. *Nat. Geosci.* 9, 231–237. doi:10.1038/NGEO2652
- Büntgen, U., Myglan, V.S., Ljungqvist, F.C., McCormick, M., Di Cosmo, N., Sigl, M., Jungclauss, J., Wagner, S., Krusic, P.J., Esper, J., Kaplan, J.O., de Vaan, M.A.C., Luterbacher, J., Wacker, L., Tegel, W., Solomina, O.N., Nicolussi, K., Oppenheimer, C., Reinig, F., Kirilyanov, A. V., 2017. Reply to “Limited Late Antique cooling.” *Nat. Geosci.* 10, 243–243. doi:10.1038/ngeo2927
- Büntgen, U., Tegel, W., Nicolussi, K., McCormick, M., Frank, D., Trouet, V., Kaplan, J.O., Herzig, F., Heussner, K.-U.K.-U., Wanner, H., Luterbacher, J., Esper, J., 2011. 2500 Years of European Climate Variability and Human Susceptibility. *Science* (80-. ). 331, 578–582. doi:10.1126/science.1197175
- Butzer, K.W., 2012. Collapse, environment, and society. *Proc. Natl. Acad. Sci.* 109, 3632–3639. doi:10.1073/pnas.1114845109
- Campbell, S., 2018. Overview of the Site, Daily Life, and Small Finds, in: Campbell, S. (Ed.), *The Cistercian Monastery of Zaraka, Greece*. Western Michigan University, p. 259.
- Casana, J., 2008. Mediterranean valleys revisited: Linking soil erosion, land use and climate variability in the Northern Levant. *Geomorphology* 101, 429–442. doi:10.1016/j.geomorph.2007.04.031
- Chen, J., An, Z., Head, J., 1999. Variation of Rb/Sr Ratios in the Loess-Paleosol Sequences of Central China during the Last 130,000 Years and Their Implications for Monsoon Paleoclimatology. *Quat. Res.* 51, 215–219. doi:10.1006/qres.1999.2038
- Chen, J., Chen, Y., Liu, L., Ji, J., Balsam, W., Sun, Y., Lu, H., 2006. Zr/Rb ratio in the Chinese loess sequences and its implication for changes in the East Asian winter monsoon strength. *Geochim. Cosmochim. Acta* 70, 1471–1482. doi:10.1016/j.gca.2005.11.029
- Cohen, A.S., 2003. *Paleolimnology: the history and evolution of lake systems*, 1st ed. Oxford University Press, Oxford.
- Cruz, F.W., Burns, S.J., Jercinovic, M., Karmann, I., Sharp, W.D., Vuille, M., 2007. Evidence of rainfall variations in Southern Brazil from trace element ratios (Mg/Ca and Sr/Ca) in a Late Pleistocene stalagmite. *Geochim. Cosmochim. Acta* 71, 2250–2263. doi:10.1016/j.gca.2007.02.005
- Cuven, S., Francus, P., Lamoureux, S.F., 2010. Estimation of grain size variability with micro X-ray fluorescence in laminated lacustrine sediments, Cape Bounty, Canadian High Arctic. *J. Paleolimnol.* 44, 803–817. doi:10.1007/s10933-010-9453-1
- Davies, P., 2008. *Snails: Archaeology and Landscape Change*, Oxbow. ed.
- Davison, W., 1993. Iron and manganese in lakes. *Earth Sci. Rev.* 34, 119–163. doi:10.1016/0012-8252(93)90029-7
- De Jonge, C., Hopmans, E.C., Zell, C.I., Kim, J.-H., Schouten, S., Sinninghe Damsté, J.S., 2014. Occurrence and abundance of 6-methyl branched glycerol dialkyl glycerol tetraethers in soils: Implications for palaeoclimate reconstruction. *Geochim. Cosmochim. Acta* 141, 97–112. doi:10.1016/j.gca.2014.06.013

- Drake, B.L., 2012. The influence of climatic change on the Late Bronze Age Collapse and the Greek Dark Ages. *J. Archaeol. Sci.* 39, 1862–1870. doi:10.1016/j.jas.2012.01.029
- Dypvik, H., Harris, N.B., 2001. Geochemical facies analysis of fine-grained siliciclastics using Th/U, Zr/Rb and (Zr + Rb)/Sr ratios. *Chem. Geol.* 181, 131–146. doi:10.1016/S0009-2541(01)00278-9
- Filzmoser, P., Hron, K., Reimann, C., 2009. Principal components analysis for compositional data with outliers. *Environmetrics* 20, 621–632. doi:10.1002/env.966
- Finné, M., Bar-Matthews, M., Holmgren, K., Sundqvist, H.S., Liakopoulos, I., Zhang, Q., 2014. Speleothem evidence for late Holocene climate variability and floods in Southern Greece. *Quat. Res. (United States)* 81, 213–227. doi:10.1016/j.yqres.2013.12.009
- Finné, M., Holmgren, K., Sundqvist, H.S., Weiberg, E., Lindblom, M., 2011. Climate in the eastern Mediterranean, and adjacent regions, during the past 6000 years - A review. *J. Archaeol. Sci.* 38, 3153–3173. doi:10.1016/j.jas.2011.05.007
- Fleitmann, D., Cheng, H., Badertscher, S., Edwards, R.L., Mudelsee, M., Göktürk, O.M., Fankhauser, A., Pickering, R., Raible, C.C., Matter, A., Kramers, J., Tüysüz, O., 2009. Timing and climatic impact of Greenland interstadials recorded in stalagmites from northern Turkey. *Geophys. Res. Lett.* 36, L19707. doi:10.1029/2009GL040050
- Fuchs, M., Lang, A., Wagner, G.A., 2004. The history of Holocene soil erosion in the Phlious Basin, NE Peloponnese, Greece, based on optical dating. *The Holocene* 14, 334–345. doi:10.1191/0959683604hl710rp
- Gogou, A., Triantaphyllou, M., Xoplaki, E., Izdebski, A., Parinos, C., Dimiza, M., Bouloubassi, I., Luterbacher, J., Kouli, K., Martrat, B., Toreti, A., Fleitmann, D., Rousakis, G., Kaberi, H., Athanasiou, M., Lykousis, V., 2016. Climate variability and socio-environmental changes in the northern Aegean (NE Mediterranean) during the last 1500 years. *Quat. Sci. Rev.* 136, 209–228. doi:10.1016/j.quascirev.2016.01.009
- Göktürk, O.M., Fleitmann, D., Badertscher, S., Cheng, H., Edwards, R.L., Leuenberger, M., Fankhauser, A., Tüysüz, O., Kramers, J., 2011. Climate on the southern Black Sea coast during the Holocene: implications from the Sofular Cave record. *Quat. Sci. Rev.* 30, 2433–2445.
- Grootes, P.M., Nadeau, M.J., Rieck, A., 2004. 14C-AMS at the Leibniz-Labor: Radiometric dating and isotope research. *Nucl. Instruments Methods Phys. Res. Sect. B Beam Interact. with Mater. Atoms* 223–224, 55–61. doi:10.1016/j.nimb.2004.04.015
- Haldon, J., Mordechai, L., Newfield, T.P., Chase, A.F., Izdebski, A., Guzowski, P., Labuhn, I., Roberts, N., 2018. History meets palaeoscience: Consilience and collaboration in studying past societal responses to environmental change. *Proc. Natl. Acad. Sci.* 115, 201716912. doi:10.1073/pnas.1716912115
- Hammer, S., Levin, I., 2017. Monthly mean atmospheric  $\Delta 14 \text{CO}_2$  at Jungfraujoch and Schauinsland from 1986 to 2016. doi:10.11588/data/10100
- Hammond, M.D., 2015. Late Roman Ceramics from the Panayia Field, Corinth. University of Missouri.
- Helama, S., Jones, P.D., Briffa, K.R., 2017a. Dark Ages Cold Period: A literature review and directions for future research. *The Holocene* 16, 095968361769389. doi:10.1177/0959683617693898
- Helama, S., Jones, P.D., Briffa, K.R., 2017b. Limited Late Antique cooling. *Nat. Geosci.* 10, 242–



243. doi:10.1038/ngeo2926

- Heymann, C., Nelle, O., Dörfler, W., Zagana, H., Nowaczyk, N., Xue, J., Unkel, I., 2013. Late Glacial to mid-Holocene palaeoclimate development of southern Greece inferred from the sediment sequence of Lake Stymphalia (NE-Peloponnese). *Quat. Int.* 302, 42–60. doi:10.1016/j.quaint.2013.02.014
- Hodell, D.A., Channell, J.E.T., Curtis, J.H., Romero, O.E., Röhl, U., 2008. Onset of “Hudson Strait” Heinrich events in the eastern North Atlantic at the end of the middle Pleistocene transition (~640 ka)? *Paleoceanography* 23, n/a-n/a. doi:10.1029/2008PA001591
- Hopmans, E.C., Schouten, S., Sinninghe Damsté, J.S., 2016. The effect of improved chromatography on GDGT-based palaeoproxies. *Org. Geochem.* 93, 1–6. doi:10.1016/j.orggeochem.2015.12.006
- Hopmans, E.C., Weijers, J.W., Schefuß, E., Herfort, L., Sinninghe Damsté, J.S., Schouten, S., 2004. A novel proxy for terrestrial organic matter in sediments based on branched and isoprenoid tetraether lipids. *Earth Planet. Sci. Lett.* 224, 107–116. doi:10.1016/j.epsl.2004.05.012
- Izdebski, A., Pickett, J., Roberts, N., Waliszewski, T., 2016a. The environmental, archaeological and historical evidence for regional climatic changes and their societal impacts in the Eastern Mediterranean in Late Antiquity. *Quat. Sci. Rev.* 136, 189–208. doi:10.1016/j.quascirev.2015.07.022
- Izdebski, A., Pickett, J., Roberts, N., Waliszewski, T., 2016b. The environmental, archaeological and historical evidence for regional climatic changes and their societal impacts in the Eastern Mediterranean in Late Antiquity. *Quat. Sci. Rev.* 136, 189–208. doi:10.1016/j.quascirev.2015.07.022
- Jahns, S., 1993. On the Holocene vegetation history of the Argive Plain (Peloponnese, southern Greece). *Veg. Hist. Archaeobot.* 2, 187–203. doi:10.1007/bf00198161
- Jin, Z., Cao, J., Wu, J., Wang, S., 2006. A Rb/Sr record of catchment weathering response to Holocene climate change in Inner Mongolia. *Earth Surf. Process. Landforms* 31, 285–291. doi:10.1002/esp.1243
- Jin, Z., Wang, S., Shen, J., Zhang, E., Li, F., Ji, J., Lu, X., 2001. Chemical weathering since the little ice age recorded in lake sediments: A high-resolution proxy of past climate. *Earth Surf. Process. Landforms* 26, 775–782. doi:10.1002/esp.224
- Kaniewski, D., Van Campo, E., Guiot, J., Le Burel, S., Otto, T., Baeteman, C., 2013. Environmental Roots of the Late Bronze Age Crisis. *PLoS One* 8, 1–10. doi:10.1371/journal.pone.0071004
- Katrantsiotis, C., Kylander, M.E., Smittenberg, R., Yamoah, K.K.A., Hättestrand, M., Avramidis, P., Strandberg, N.A., Norström, E., 2018. Eastern Mediterranean hydroclimate reconstruction over the last 3600 years based on sedimentary n-alkanes, their carbon and hydrogen isotope composition and XRF data from the Gialova Lagoon, SW Greece. *Quat. Sci. Rev.* 194, 77–93. doi:10.1016/J.QUASCIREV.2018.07.008
- Kiel, M., 1997. The rise and decline of Turkish Boeotia, 15th-19th century, in: Bintliff, J.L. (Ed.), *Recent Developments in the History and Archaeology of Central Greece. Tempus Reparatum*, Oxford, pp. 315–358.
- Kiel, M., 1987. Population growth and food production in 16th century Athens and Attica according to the Ottoman Tahrir Defters, in: Bacque-Grammont, J.-L., van Donzel, E. (Eds.), *Proceedings of the VIth Cambridge CIEPO Symposium. The Divit Press, Istanbul-Paris-Leiden*, pp. 115–133.

- Knapp, A.B., Manning, S.W., 2016. Crisis in Context: The End of the Late Bronze Age in the Eastern Mediterranean. *Am. J. Archaeol.* 120, 99. doi:10.3764/aja.120.1.0099
- Knauss, J., 1990. Der Graben des Herakles im Becken von Pheneos und die Vertreibung der stymphalischen Vögel 105.
- Koinig, K.A., Shotyk, W., Lotter, A.F., Ohlendorf, C., Sturm, M., 2003. 9000 years of geochemical evolution of lithogenic major and trace elements in the sediment of an alpine lake – the role of climate, vegetation, and land- use history. *J. Paleolimnol.* 30, 307–320. doi:10.1023/A:1026080712312
- Kourelis, K., 2018. Zaraka Surrounded: The Archaeology of Settlements in the Peloponnesian Countryside, in: Campell, S. (Ed.), *The Cistercian Monastery of Zaraka, Greece*. Western Michigan University, pp. 193–213.
- Kylander, M.E., Ampel, L., Wohlfarth, B., Veres, D., 2011. High-resolution X-ray fluorescence core scanning analysis of Les Echets (France) sedimentary sequence: new insights from chemical proxies. *J. Quat. Sci.* 26, 109–117. doi:10.1002/jqs.1438
- Langgut, D., Finkelstein, I., Litt, T., 2013. Climate and the Late Bronze Collapse: New Evidence from the Southern Levant. *Tel Aviv* 40, 149–175. doi:10.1179/033443513X13753505864205
- Little, L.K. (Ed.), 2007. *Plague and the End of Antiquity - The Pandemic of 541-750*.
- Lolos, Y.A., 1997. The Hadrianic Aqueduct of Corinth. *Hesperia* 66, 271–314.
- Löwemark, L., Chen, H.F., Yang, T.N., Kylander, M., Yu, E.F., Hsu, Y.W., Lee, T.Q., Song, S.R., Jarvis, S., 2011. Normalizing XRF-scanner data: A cautionary note on the interpretation of high-resolution records from organic-rich lakes. *J. Asian Earth Sci.* 40, 1250–1256. doi:10.1016/j.jseaes.2010.06.002
- Lucke, B., Sprafke, T., 2015. Correlation of soil color, redness ratings, and weathering indices of Terrae Calcis along a precipitation gradient in northern Jordan, in: *Erlanger Geographische Arbeiten*. pp. 53–68.
- Luterbacher, J., García-Herrera, R., Akcer-On, S., Allan, R., Alvarez-Castro, M.-C., Benito, G., Booth, J., Büntgen, U., Cagatay, N., Colombaroli, D., Davis, B., Esper, J., Felis, T., Fleitmann, D., Frank, D., Gallego, D., Garcia-Bustamante, E., Glaser, R., Gonzalez-Rouco, F.J., Goosse, H., Kiefer, T., Macklin, M.G., Manning, S.W., Montagna, P., Newman, L., Power, M.J., Rath, V., Ribera, P., Riemann, D., Roberts, N., Sicre, M.-A., Silenzi, S., Tinner, W., Tzedakis, P.C., Valero-Garcés, B., van der Schrier, G., Vannièrè, B., Vogt, S., Wanner, H., Werner, J.P., Willett, G., Williams, M.H., Xoplaki, E., Zerefos, C.S., Zorita, E., 2012. A Review of 2000 Years of Paleoclimatic Evidence in the Mediterranean, in: Lionello, P. (Ed.), *The Climate of the Mediterranean Region*. Elsevier, pp. 87–185. doi:10.1016/B978-0-12-416042-2.00002-1
- Magny, M., de Beaulieu, J.L., Drescher-Schneider, R., Vannièrè, B., Walter-Simonnet, A.V., Miras, Y., Millet, L., Bossuet, G., Peyron, O., Brugiapaglia, E., Leroux, A., 2007. Holocene climate changes in the central Mediterranean as recorded by lake-level fluctuations at Lake Accesa (Tuscany, Italy). *Quat. Sci. Rev.* 26, 1736–1758. doi:10.1016/j.quascirev.2007.04.014
- Magny, M., Magny, M., 2013. The Holocene central Europe: A comment on Bleicher. doi:10.1177/0959683613483627
- Manning, S.W., 2018. Some Perspectives on the Frequency of Significant, Historically Forcing Drought and Subsistence Crises in Anatolia and Region, in: Holt, E. (Ed.), *Water and Power in Past Societies: IEMA Proceedings, Volume 7*. State University of New York Press, Albany, pp. 279–295.

- Manning, S.W., 2013a. The Roman World and Climate: Context, Relevance of Climate Change, and Some Issues, in: Harris, W.V. (Ed.), *The Ancient Mediterranean Environment between Sciences and History*. Brill, Leiden, pp. 103–170.
- Manning, S.W., 2013b. The Roman World and Climate: Context, Relevance of Climate Change, and Some Issues, in: *The Ancient Mediterranean Environment between Science and History*.
- McCormick, M., Büntgen, U., Cane, M.A., Cook, E.R., Harper, K., Huybers, P., Litt, T., Manning, S.W., Mayewski, P.A., More, A.F.M., Nicolussi, K., Tegel, W., 2012. Climate Change during and after the Roman Empire: Reconstructing the Past from Scientific and Historical Evidence. *J. Interdiscip. Hist.* 43, 169–220. doi:10.1162/JINH\_a\_00379
- Meriam, E.O., Aurélia, H., Héléne, L., Volkan, K., Jacqueline, V.A., Gilles, L., Olivier, D., Sabine, S., 2017. Soil erosion in relation to land-use changes in the sediments of Amik Lake near Antioch antique city during the last 4 kyr. *The Holocene* 1–15. doi:10.1177/0959683617715702
- Meyers, P.A., 2003. Applications of organic geochemistry to paleolimnological reconstructions: A summary of examples from the Laurentian Great Lakes. *Org. Geochem.* 34, 261–289. doi:10.1016/S0146-6380(02)00168-7
- Mischke, S., Ginat, H., Al-Saqarat, B.S., Faershtein, G., Porat, N., Braun, P., Rech, J.A., 2017. Fossil-Based Reconstructions of Ancient Water Bodies in the Levantine Deserts, in: *Quaternary of the Levant*. pp. 381–390. doi:10.1017/9781316106754.045
- Mook, W.G., Plicht, J. Van Der, 1999. REPORTING 14C ACTIVITIES AND CONCENTRATIONS Willem. *Radiocarbon* 41, 227–239. doi:10.1017/S0033822200057106
- Morfis, A., Zojer, H., 1986. Karst Hydrogeology of the Central and Eastern Peloponnesus (Greece). *Steir. Beitr. zur Hydrogeol.* 37/38, 1–301.
- Moschen, R., Kühl, N., Peters, S., Vos, H., Lücke, A., 2011. Temperature variability at Dürres Maar, Germany during the Migration Period and at High Medieval Times, inferred from stable carbon isotopes of *Sphagnum* cellulose. *Clim. Past* 7, 1011–1026. doi:10.5194/cp-7-1011-2011
- Munsell, A.H., 2000. *Munsell Soil Color Charts*. Munsell Color, Grand Rapids.
- Naeher, S., Gilli, A., North, R.P., Hamann, Y., Schubert, C.J., 2013. Tracing bottom water oxygenation with sedimentary Mn/Fe ratios in Lake Zurich, Switzerland. *Chem. Geol.* 352, 125–133. doi:10.1016/j.chemgeo.2013.06.006
- Nanou, E.-A., Zagana, E., 2018. Groundwater Vulnerability to Pollution Map for Karst Aquifer Protection (Ziria Karst System, Southern Greece). *Geosciences* 8, 125. doi:10.3390/geosciences8040125
- Norström, E., Katrantsiotis, C., Finné, M., Risberg, J., Smittenberg, R.H., Bjursäter, S., 2018. Biomarker hydrogen isotope composition ( $\delta D$ ) as proxy for Holocene hydroclimatic change and seismic activity in SW Peloponnesus, Greece. *J. Quat. Sci.* 33, 563–574. doi:10.1002/jqs.3036
- Nowaczyk, N.R., 2001. Logging of Magnetic Susceptibility, in: Last, W.M. (Ed.), *Tracking Environmental Change Using Lake Sediments*. Kluwer Academic Publishers, Dordrecht, pp. 155–170. doi:10.1007/0-306-47669-X\_8
- Nowaczyk, N.R., Minyuk, P., Melles, M., Brigham-Grette, J., Glushkova, O., Nolan, M., Lozhkin, A. V., Stetsenko, T. V., M. Andersen, P., Forman, S.L., 2002. Magnetostratigraphic results from impact crater Lake El'gygytgyn, northeastern Siberia: a 300 kyr long high-resolution terrestrial palaeoclimatic record from the Arctic. *Geophys. J. Int.* 150, 109–126. doi:10.1046/j.1365-246X.2002.01625.x

- Orland, I.J., Bar-Matthews, M., Kita, N.T., Ayalon, A., Matthews, A., Valley, J.W., 2009. Climate deterioration in the Eastern Mediterranean as revealed by ion microprobe analysis of a speleothem that grew from 2.2 to 0.9??ka in Soreq Cave, Israel. *Quat. Res.* 71, 27–35. doi:10.1016/j.yqres.2008.08.005
- Palmisano, A., Bevan, A., Shennan, S., 2017. Comparing archaeological proxies for long-term population patterns : An example from central Italy Comparing archaeological proxies for long-term population patterns : An example from central Italy. *J. Archaeol. Sci.* 87, 59–72. doi:10.1016/j.jas.2017.10.001
- Palmisano, A., Woodbridge, J., Roberts, N., Bevan, A., Fyfe, R., Shennan, S., Cheddadi, R., Greenberg, R., Kaniewski, D., Langgut, D., Leroy, S.A., Litt, T., Miebach, A., 2019. Holocene landscape dynamics and long-term population trends in the Levant. *The Holocene* 095968361982664. doi:10.1177/0959683619826642
- Panagiotopoulos, V., 1985. *Plithismos kai Oikismoi tis Peloponnisou*, Commercial. ed. Athens.
- Papastergiadou, E.S., Retalis, A., Kalliris, P., Georgiadis, T., 2007. Land use changes and associated environmental impacts on the Mediterranean shallow Lake Stymfalia, Greece. *Hydrobiologia* 584, 361–372. doi:10.1007/s10750-007-0606-9
- Philippson, A., 1892. *Der Peloponnes. Versuch einer Landeskunde auf geologischer Grundlage; Nach Ergebnissen eigener Reisen.* Verlag von R. Friedländer und Sohn, Berlin.
- R Core Team, 2017. *R: A language and environment for statistical computing.* R Foundation for Statistical Computing, Vienna, Austria, Austria.
- Ramsey, C.B., 2008. Deposition models for chronological records. *Quat. Sci. Rev.* 27, 42–60. doi:10.1016/j.quascirev.2007.01.019
- Reimer, P.J., Bard, E., Bayliss, A., Beck, J.W., Blackwell, P.G., Ramsey, C.B., Buck, C.E., Cheng, H., Edwards, R.L., Friedrich, M., Grootes, P.M., Guilderson, T.P., Hafllidason, H., Hajdas, I., Hatté, C., Heaton, T.J., Hoffmann, D.L., Hogg, A.G., Hughen, K.A., Kaiser, K.F., Kromer, B., Manning, S.W., Niu, M., Reimer, R.W., Richards, D.A., Scott, E.M., Southon, J.R., Staff, R.A., Turney, C.S.M., van der Plicht, J., 2013. IntCal13 and Marine13 Radiocarbon Age Calibration Curves 0–50,000 Years cal BP. *Radiocarbon* 55, 1869–1887. doi:10.2458/azu\_js\_rc.55.16947
- Roberts, N., Allcock, S.L., Arnaud, F., Dean, J.R., Eastwood, W.J., Jones, M.D., Leng, M.J., Metcalfe, S.E., Malet, E., Woodbridge, J., Yiğitbaşıoğlu, H., 2016. A tale of two lakes: a multi-proxy comparison of Lateglacial and Holocene environmental change in Cappadocia, Turkey. *J. Quat. Sci.* 31, 348–362. doi:10.1002/jqs.2852
- Roberts, N., Moreno, A., Valero-Garcés, B.L., Corella, J.P., Jones, M., Allcock, S., Woodbridge, J., Morellón, M., Luterbacher, J., Xoplaki, E., Türkeş, M., 2012. Palaeolimnological evidence for an east-west climate see-saw in the Mediterranean since AD 900. *Glob. Planet. Change* 84–85, 23–34. doi:10.1016/j.gloplacha.2011.11.002
- Sadori, L., Giraudi, C., Masi, A., Magny, M., Ortu, E., Zanchetta, G., Izdebski, A., 2016. Climate, environment and society in southern Italy during the last 2000 years. A review of the environmental, historical and archaeological evidence. *Quat. Sci. Rev.* 136, 173–188. doi:10.1016/j.quascirev.2015.09.020
- Sadori, L., Zanchetta, G., Giardini, M., 2008. Last Glacial to Holocene palaeoenvironmental evolution at Lago di Pergusa (Sicily, Southern Italy) as inferred by pollen, microcharcoal, and stable isotopes. *Quat. Int.* 181, 4–14.
- Schaus, G.P. (Ed.), 2014. *Symphalos: The Acropolis Sanctuary, Volume 1.* University of Toronto

Press.

- Sigalos, E., 2004. Housing in Medieval and Post-Medieval Greece. *Br. Archaeol. Reports Int. Ser.*
- Staubwasser, M., Weiss, H., 2006. Holocene climate and cultural evolution in late prehistoric–early historic West Asia. *Quat. Res.* 66, 372–387.
- Tjallingii, R., 2006. Application and quality of X-Ray Fluorescence core scanning in reconstructing late Pleistocene NW African continental margin sedimentation patterns and paleoclimate variations. *Dep. Geosci. Univ. Bremen* 1–114.
- Tjallingii, R., Röhl, U., Kölling, M., Bickert, T., 2007. Influence of the water content on X-ray fluorescence corescanning measurements in soft marine sediments. *Geochemistry, Geophys. Geosystems* 8, 1–12. doi:10.1029/2006GC001393
- Unkel, I., Heymann, C., Nelle, O., Zagana, E., 2011. Climatic influence on Lake Stymphalia during the last 15 000 years, in: *Advances in the Research of Aquatic Environment*. Springer Berlin Heidelberg, Berlin, Heidelberg, pp. 75–82. doi:10.1007/978-3-642-19902-8\_8
- Unkel, I., Schimmelfmann, A., Shriner, C., Forsén, J., Heymann, C., Brückner, H., 2014. The environmental history of the last 6500 years in the Asea Valley (Peloponnese, Greece) and its linkage to the local archaeological record. *Zeitschrift für Geomorphol. Supplement*. doi:10.1127/0372-8854/2014/S-00160
- Vött, A., Brückner, H., Zander, A.M., May, S.M., Mariolagos, I., Lang, F., Fountoulis, I., Dunkel, A., 2009. Late Quaternary evolution of Mediterranean poljes – the Vatos case study (Akarnania, NW Greece) based on geo-scientific core analyses and IRSL dating. *Zeitschrift für Geomorphol.* 53, 145–169. doi:10.1127/0372-8854/2009/0053-0145
- Walsh, K., Brown, A.G., Gourley, B., Scaife, R., 2017. Archaeology, hydrogeology and geomorphology in the Stymphalos valley. *J. Archaeol. Sci. Reports* 15, 446–458. doi:10.1016/j.jasrep.2017.03.058
- Weiberg, E., Unkel, I., Kouli, K., Holmgren, K., Avramidis, P., Bonnier, A., Dibble, F., Finn??, M., Izdebski, A., Katrantsiotis, C., Stocker, S.R., Andwinge, M., Baika, K., Boyd, M., Heymann, C., 2016. The socio-environmental history of the Peloponnese during the Holocene: Towards an integrated understanding of the past. *Quat. Sci. Rev.* 136, 40–65. doi:10.1016/j.quascirev.2015.10.042
- Weidenbach, K., Nickel, L., Neve, H., Alkhnbashi, O.S., Künzel, S., Kupczok, A., Bauersachs, T., Cassidy, L., Tholey, A., Backofen, R., Schmitz, R.A., 2017. Methanosarcina Spherical Virus, a Novel Archaeal Lytic Virus Targeting Methanosarcina Strains. *J. Virol.* 91, e00955-17. doi:10.1128/JVI.00955-17
- Weltje, G.J., Tjallingii, R., 2008. Calibration of XRF core scanners for quantitative geochemical logging of sediment cores: Theory and application. *Earth Planet. Sci. Lett.* 274, 423–438. doi:10.1016/j.epsl.2008.07.054
- Weninger, B., Clare, L., Rohling, E., Bar-Yosef, O., Böhner, U., Budja, M., Bundschuh, M., Feurdean, A., Gebe, H.G., Jöris, O., Linstädter, J., Mayewski, P., Mühlenbruch, T., Reingruber, A., Rollefson, G., Schyle, D., Thissen, L., Todorova, H., Zielhofer, C., 2009. The Impact of Rapid Climate Change on Prehistoric Societies during the Holocene in the Eastern Mediterranean. *Doc. Praehist.* 36, 7. doi:10.4312/dp.36.2
- White, S.A., 2013. *The Climate of Rebellion in the Early Modern Ottoman Empire*, Cambridge. ed. Cambridge.

- Wild, E.M., Steier, P., Fischer, P., Höflmayer, F., 2013. 14C Dating of Humic Acids from Bronze and Iron Age Plant Remains from the Eastern Mediterranean. *Radiocarbon* 55, 599–607. doi:10.2458/azu\_js\_rc.55.16450
- Williams, E.H., 1983. Stymphalos: A Planned City of Ancient Arcadia. *Echos du Monde Class. = Class. Views* 27, 194–205.
- Williams, H., 2005. Excavations at Stymphalos. Preliminary Reports 1983 - 2005. *Museion*.
- Williams, H., 2003. The Exploration of Ancient Stymphalos, 1982 - 2002 397–411.
- Williams, H., 1996. Excavations at Stymphalos, 1995. *Echos du Monde Class. = Class. Views* 40, 75–98.
- Williams, H., 1984a. Investigations at Stymphalos. *Échos du monde Class. = Class. Views* 26, 215–224.
- Williams, H., 1984b. Investigations at Mytilene and Stymphalos. *Échos du monde Class. = Class. Views* 169–183.
- Williams, H., Cronkite Price, S.-M., 1995. Excavations at Stymphalos, 1994. *Échos du monde Class. = Class. Views* 39, 1–22.
- Williams, H., Gouley, B., 2005. The Fortifications of Stymphalos. *Mouseion* III, 5, 213–259.
- Williams, H., Schaus, G., Cronkite Price, S.-M., Gourley, B., Hagerman, C., 1998. Excavations at Ancient Stymphalos, 1997. *Echos du Monde Class. = Class. Views* 42, 261–319.
- Williams, H., Schaus, G., Cronkite Price, S.-M., Gourley, B., Lutomsky, H., 1997. Excavations at Ancient Stymphalos, 1996. *Echos du Monde Class. = Class. Views* 41, 23–73.
- Williams, H., Schaus, G., Gourley, B., Cronkite Price, S.-M., Sherwood, K.D., Lolos, Y., 2002. Excavations at Ancient Stymphalos, 1999–2002. *Mouseion* 2, 135–187. doi:10.1353/mou.2002.0016
- Xoplaki, E., Fleitmann, D., Luterbacher, J., Wagner, S., Haldon, J.F., Zorita, E., Telelis, I., Toreti, A., Izdebski, A., 2016a. The Medieval Climate Anomaly and Byzantium: A review of the evidence on climatic fluctuations, economic performance and societal change. *Quat. Sci. Rev.* 136, 229–252. doi:10.1016/j.quascirev.2015.10.004
- Xoplaki, E., Fleitmann, D., Luterbacher, J., Wagner, S., Haldon, J.F., Zorita, E., Telelis, I., Toreti, A., Izdebski, A., 2016b. The Medieval Climate Anomaly and Byzantium: A review of the evidence on climatic fluctuations, economic performance and societal change. *Quat. Sci. Rev.* 136, 229–252. doi:10.1016/j.quascirev.2015.10.004
- Xu, H., Liu, B., Wu, F., Dasch, E., Liu, C., Zhang, J., Li, C., Chen, J., An, Z., Head, J., Chen, J., An, Z., Liu, L., Ji, J., Yang, J., Chen, Y., Jin, Z., Cao, J., Wu, J., Wang, S., Xu, H., Liu, X., An, Z., Hou, Z., Dong, J., Xu, H., Ai, L., Tan, L., An, Z., Xu, H., Hou, Z., An, Z., Liu, X., Dong, J., Pang, J., Huang, C., Zhang, Z., Li, F., Xie, C., Pan, G., Xu, H., Hou, Z., Ai, L., Tan, L., 2010. Spatial and temporal variations of Rb/Sr ratios of the bulk surface sediments in Lake Qinghai. *Geochem. Trans.* 11, 3. doi:10.1186/1467-4866-11-3
- Zolitschka, B., Francus, P., Ojala, A.E.K., Schimmelmänn, A., 2015. Varves in lake sediments - a review. *Quat. Sci. Rev.* 117, 1–41. doi:10.1016/j.quascirev.2015.03.019

**Supplementary Information** is linked to the online version of the paper at [www.journals.elsevier.com/quatarnary-science-reviews](http://www.journals.elsevier.com/quatarnary-science-reviews). This file contains Supplementary Graphs and Supplementary Tables (see SOM list for details).

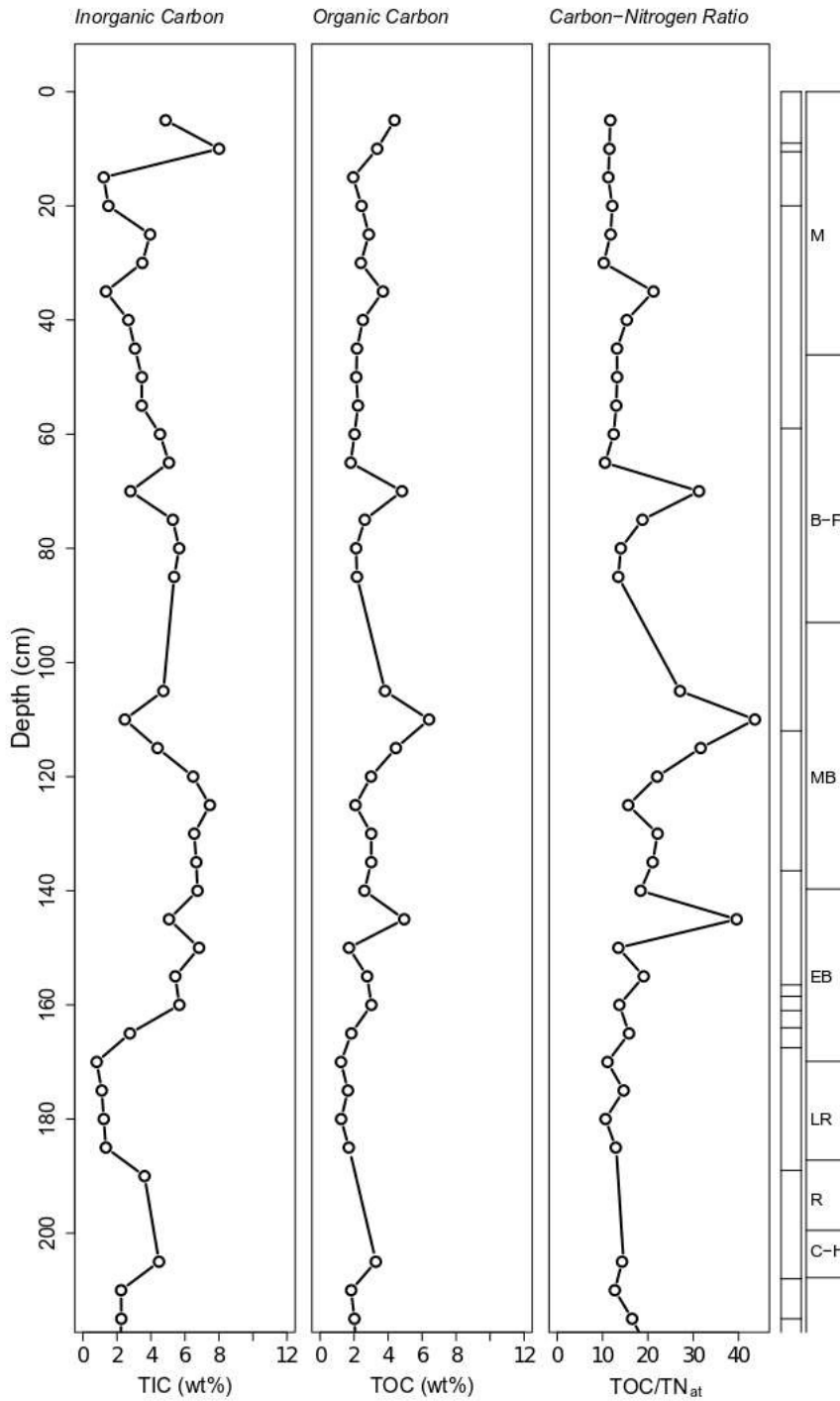
### **Supplementary Online Material**

*SOM 1. Input table as applied for Rbacon modelling of STY\_25. Column 2 indicates the uncalibrated C14 ages for radiocarbon ages or the calender ages for historical dates. Column 3 mainly shows measurement uncertainties (always  $\pm$ ) or defined errors for historical dates. The depth unit for column 4 is cm. Column 5 indicates the applied calibration curve (cc=0 for none - applied for calender dates or cal BP, cc=1 for northern hemisphere terrestrial material which is calibrated with IntCal13. Column 6 and 7 indicate the mean and error of core-wide age offsets, namely reservoir effects. Comments in the last column were excluded from modelling and only have a documentation purpose to improve the readability (following page).*

Lab_No	14C_age	error	depth	cc	delta.R	delta.STD	Comment
surface	-60	5	0	0	0	0	
VERA-6380HS-combine	1608	20	50	1	200	100	# OxCal
VERA-6380-combine	1537	19	50	1	200	100	# OxCal
KIA47446_HS	1285	35	72	1	200	100	
VERA-6382HS_2	1419	37	114	1	200	100	
VERA-6382-combine	1432	26	114	1	200	100	# OxCal
VERA-6383HS_2	1441	35	161	1	200	100	
VERA-6383-combine	1535	26	161	1	200	100	# OxCal
KIA42912_HS	1355	23	164	1	200	100	
VERA-6258	1237	35	165	1	0	0	# Crataegus
Aqueduct	1820	20	189	0	0	0	# Aqueduct building 130 AD
VERA-6259-combine	2071	20	195	1	200	100	
VERA-6259HS-combine	2206	22	195	1	200	100	
Ceramic	2350	100	205	0	0	0	# 5th century BC
KIA47448_HS	3170	30	207	1	200	100	
Poz-96329	2310	35	210	1	200	100	
Poz-96330	3850	40	220	1	200	100	
VERA-6260	3809	39	236	1	200	100	
VERA-6260HS	3937	33	236	1	200	100	
KIA44005_HS	3563	29	236	1	200	100	
Poz-96331	3335	35	238	1	200	100	
Poz-96325	4180	40	248	1	200	100	
KIA44006_HS	4837	34	266	1	200	100	
VERA-6261	4600	35	267	1	200	100	
VERA-6261HS	4631	36	267	1	200	100	
VERA-6262	4829	38	270	1	200	100	
VERA-6262HS	4877	29	270	1	200	100	
VERA-6263-combine	4674	21	273	1	200	100	# OxCal
VERA-6263HS-combine	4790	22	273	1	200	100	# OxCal
KIA45955_HS	6025	35	280	1	200	100	
KIA42913	7708	35	324	1	0	0	# Charcoal



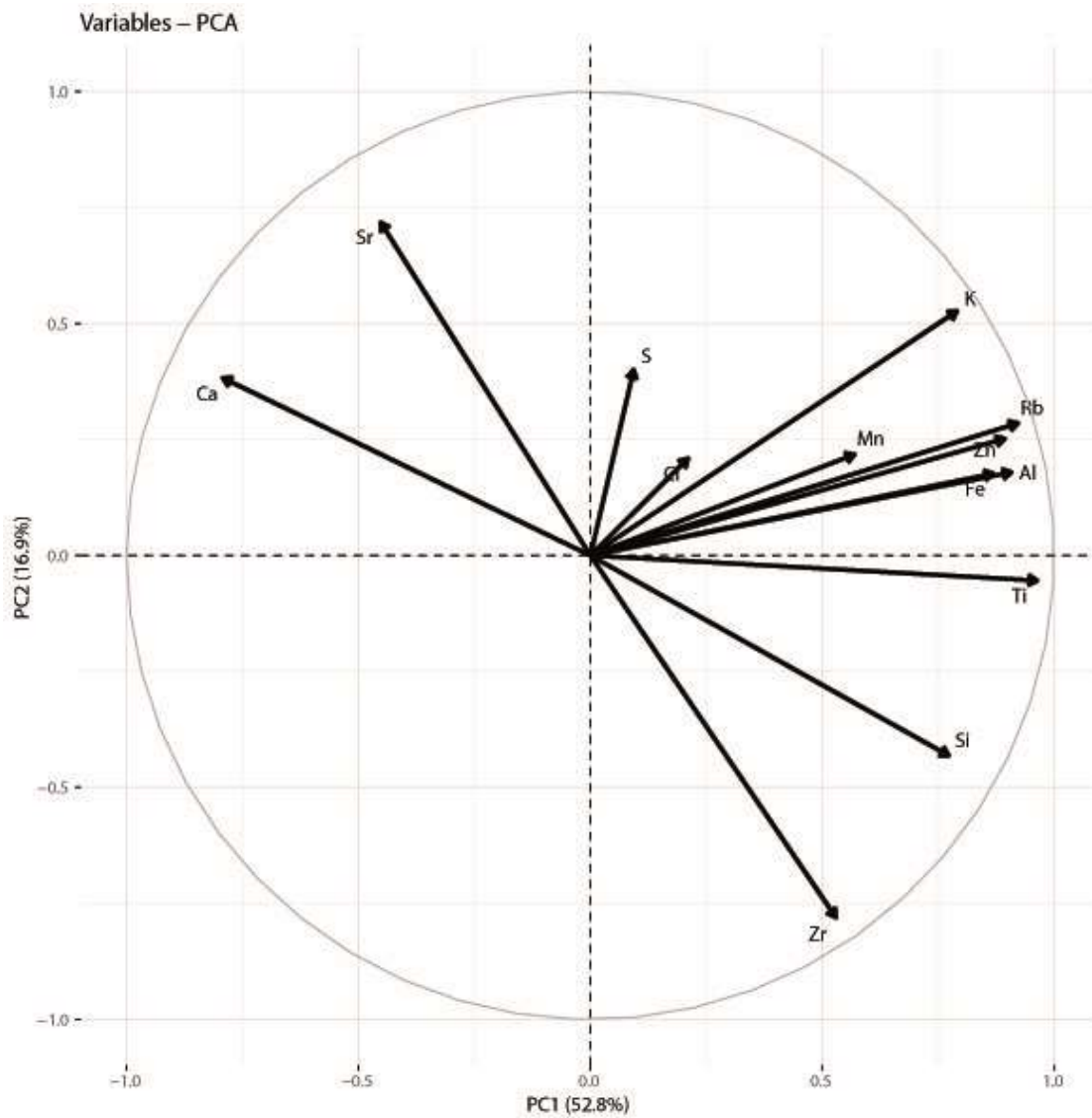
**SOM 2. TIC, TOC and TOC/TN (atomic masses) plotted against depth. The boxes to the right show the lithological units and the Greek cultural phases as specified in Weiberg et al. (2016; cf. Table 3).**



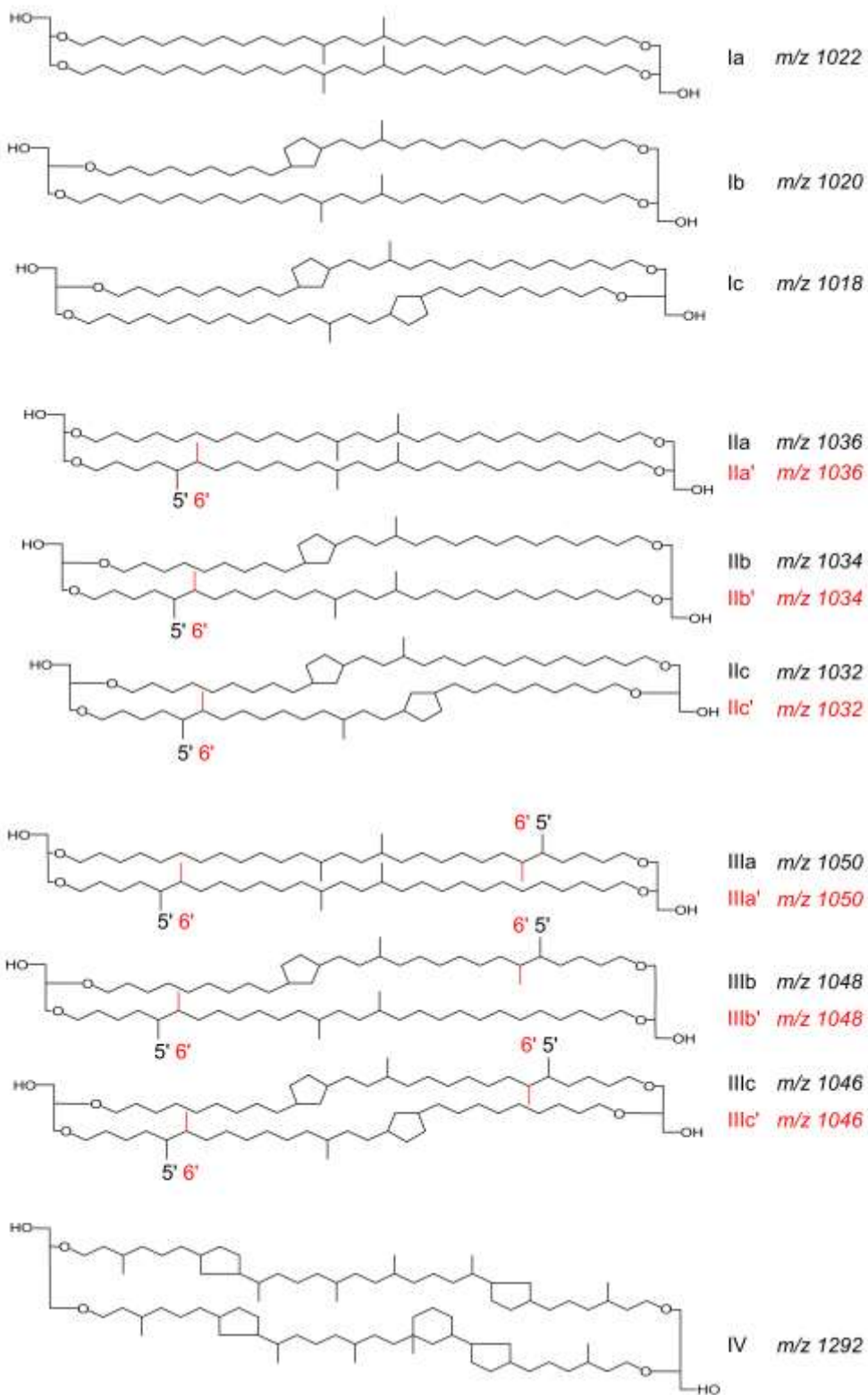
**SOM 3. Table of grain size measurements for every sediment unit. The fraction classes and the soil type classification follow the German Arbeitsgruppe Boden (2005).**

Depth [cm]	Sediment Unit	Clay [%]	Fine Silt [%]	Medium Silt [%]	Coarse Silt [%]	Fine Sand [%]	Medium Sand [%]	Coarse Sand [%]	Soil Type
5	70b	22,43	39,47	34,30	3,13	0,66	0,00	0,00	Ut4
10	70a	24,33	28,84	22,71	6,91	6,45	7,67	3,08	Lu
15	69	23,73	35,06	35,72	5,06	0,43	0,00	0,00	Ut4
40	68	20,45	36,02	37,11	6,24	0,18	0,00	0,00	Ut4
65	67	21,87	38,54	35,11	4,41	0,07	0,00	0,00	Ut4
124	66	24,68	35,79	30,72	7,03	1,62	0,14	0,00	Ut4
144	65	27,19	34,29	27,92	7,84	2,73	0,03	0,00	Tu4
158	64	37,33	38,42	20,76	3,43	0,06	0,00	0,00	Tu3
159	63	27,05	30,90	23,53	10,98	4,95	2,58	0,02	Tu4
163	62	31,25	34,34	23,92	7,00	1,69	1,80	0,00	Tu4
165	61	39,57	32,57	19,60	5,43	1,42	1,42	0,00	Tu3
179	60	29,96	42,25	26,06	1,62	0,03	0,06	0,00	Tu4
204	59	24,03	37,54	32,13	5,67	0,46	0,15	0,01	Ut4

**SOM 4. Principle Components Analysis of XRF data. Plot of the 13 included element variables as defined by the first two principal components of the PCA. The PC1 accounts for 52.8% and PC2 for 16.9% of the observed variability.**



**SOM 5. GDGTs structures.**



# Appendix II



# **Inter-comparison of palaeoenvironmental records from four lacustrine archives on the Peloponnese (Greece) over the last 5,000 years**

Joana Seguin<sup>1\*</sup>, Pavlos Avramidis<sup>2</sup>, Annette Haug<sup>3</sup>, Torben Kessler<sup>3</sup>, Arndt Schimmelmann<sup>4</sup>,  
Ingmar Unkel<sup>1</sup>

<sup>1</sup>Institute for Ecosystem Research, Kiel University, Olshausenstraße 75, 24118 Kiel, Germany

<sup>2</sup>Department of Geology, University of Patras, Rio 26504 Patras, Greece

<sup>3</sup>Institute for Classical Archaeology, Kiel University, Johanna-Mestorf-Str. 5, 24118 Kiel, Germany

<sup>4</sup>Department of Earth and Atmospheric Sciences, Indiana University, 1001 E 10<sup>th</sup> Street, Bloomington, IN 47405-1405, USA

\*Corresponding author: jseguin@ecology.uni-kiel.de

## **Keywords**

*Palaeoenvironment; palaeolimnology; multi-archive; geographical scales; XRF analysis; sedimentology; Late Holocene*

## **Highlights**

- Multi-proxy investigation of Mid to Late Holocene hydrological development from four (palaeo)lake sediment sequences
- Notable transformation in hydrological regime points towards drier conditions around 3,200 cal BP
- High regional to local variability of palaeoclimatic proxies across the Peloponnese peninsula

## **Abstract**

High quantity and quality of geoarchives are needed to successfully connect palaeoenvironmental reconstructions with socio-environmental and cultural transformations in a geographically heterogeneous region such as the Peloponnese. However, high-resolution palaeoclimatic and palaeoenvironmental archives from southern Greece are still relatively sparse or discontinuous. Here, we present two new archives from NE Peloponnese palaeolakes of Pheneos and Kaisari. Along with datasets from Lake Stymphalia and the Asea valley, we perform a multi-archival

approach by applying the same set of sedimentological and geochemical, and statistical analyses to all four lacustrine archives.

We provide continuous proxy evidence for hydrological variations and environmental changes for the last 5,000 years, since the beginning of the Bronze Age and Early Helladic Period (5,050 BP or 3,100 BC) in Greece. We hereby focus on different spatial scales to estimate the validity range of the proxy signals. On a meso-scale level, high conformance and generally similar reactions and trends are evident in the proxies across all sites; e.g., a drying trend is detected during the transition phase from the Late Bronze age to the Early Iron age (ca. 3,200 – 2,800 cal BP). Although all our geoarchives show evidence for drier phases, their timing and duration display considerable variance. Additionally, we see notable differences that may be explained on a micro-scale level by site-specific variations in individual ecosystem responses owing to various forcing factors.

The high regional geographical diversity within the Peloponnese combined with the variation in our data testify that any hypothetical mono-causal connection between palaeoenvironmental changes in a single geoarchive and contemporaneous societal transformations across the Peloponnese would be an oversimplification.

## **1. Introduction**

The Eastern Mediterranean can be considered as a region of high importance for palaeoenvironmental research, as it experienced a long history of cultural development and human-environmental interaction throughout the Mid to Late Holocene (Izdebski et al., 2016; Roberts et al., 2011).

Mid to Late Holocene environmental archives often provide records on palaeoenvironmental changes containing a combination of natural climatic and anthropogenic signals, which are often not easy to disentangle. From southern Greece and the Peloponnese, high-resolution environmental archives covering this time period are still relatively sparse or often discontinuous (Finné et al., 2011; Gogou et al., 2016; Luterbacher et al., 2012, McCormick et al., 2012, Atherden and Hall, 1994; Izdebski et al., 2016; Jahns, 1993).



Lake sediments record macro-scale climatic changes as well as local, catchment-specific processes (Roberts et al., 2008). However, each lake responds differently to global, regional or local influences, depending on its size and catchment settings (Meyers and Lallier-Vergès, 1999). To distinguish local from regional or even hemispheric climatic signals, a combination of a larger number of geoarchives and an analysis of multiple proxies seems more promising (Finné et al., 2019).

Although there is an increasing number of studies on Eastern Mediterranean palaeoenvironmental archives that has been published most recently (Emmanouilidis et al., 2018, 2019; Finné et al., 2017; Katrantsiotis et al., 2018, 2019; Masi et al., 2018; Rothacker et al., 2018), they do not provide a uniform picture of the climatic and environmental changes through the Mid to Late Holocene, and sometimes they are inconsistent with archaeological or historical data (Finné et al., 2019). Most reconstructions of Holocene climatic variations in the Mediterranean are based on one single palaeoenvironmental archive, leading to very heterogeneous and often even divergent results when being compared to each other (Finné et al., 2011; Luterbacher et al., 2012). This calls for the need for not only multi-proxy approaches on one palaeoenvironmental archive, but for multi-archive approaches that use the same methods and proxies at different study sites.

Here, we present a combined approach of four lake sediment archives from the northeastern and central Peloponnese (Greece), namely from Lake Stymphalia and from the valleys of Asea, Pheneos, and Kaisari (Fig. 1), which hosted lakes of different extent in the past. Human presence in the study area is proven since Neolithic times, but has been relatively sparse and widely unexplored except for the Classical Hellenistic period and the last 200 years (Seguin et al., 2019; Walsh et al., 2017). Due to its mountainous topography with elevations of up to 2400 m only few kilometres away from the coast, the Peloponnese displays a high climatic heterogeneity with significant precipitation and temperature gradients from west to east and from the coast to the mountain ranges. Hence, palaeoclimate records across the Peloponnese are prone to reveal different patterns on a spatially comparatively limited scale (Katrantsiotis et al., 2019). Given the proximity of our selected palaeoenvironmental archives to each other and the similar geological and geomorphological setting, we suppose that they experienced similar meso-scale climatic

conditions (<50 km distance). We investigate each archive with the same analytical tools to reveal the differences and similarities in the proxy records that help us to disentangle local (micro-scale) from regional (meso-scale) signals. A concordance in the course of the same proxy at the different sites would suggest that the proxy reflects an overarching signal of regional environmental or climatic change (macro-scale). If the proxy shows no agreement between the sites, this may hint towards local site-specific effects or a mismatching of the data due to dating uncertainties (Roberts et al., 2016). Earlier studies on Lake Stymphalia (Heymann et al., 2013; Seguin et al., 2019) showed that the lake reacted sensitively to environmental and hydrological changes as well as to human disturbances notably during the last 2,500 years. A sediment core from the Asea valley provided a record on the hydrological variability in the area of the last 6,500 years (Unkel et al., 2014), however in lower resolution than the Stymphalia record. We here compare these already published records with two new sediment sequences from palaeolakes Pheneos and Kaisari for the last 5,000 years, which are covered in all four records. That way, we arrive at a more profound picture of the environmental and climatic history of the Peloponnese, going beyond the capabilities of a single lake record alone.

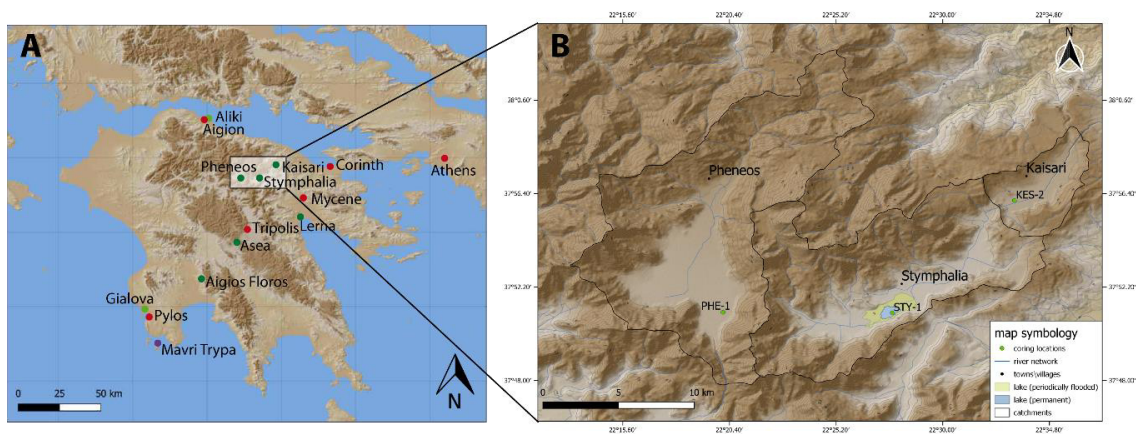


**Figure 1: Map of the study area in the NE Peloponnese. (A) Overview of the Peloponnese. Lacustrine (lagoonal) archives are indicated in (light) green, archaeological sites and cities, mentioned in the paper, are indicated in red, speleothem archives occur in purple. (B) Topographic map of the poljes. Coring sites are indicated by green dots and settlements, the sites and poljes are named after, by black dots. Black lines trace the surface hydrological catchments. Contour lines are drawn in increments of 100.**

## 2. Regional setting

The three karst poljes Pheneos, Stymphalia, and Kaisari surround the limestone massif of Mt. Ziria/Kyllini (2374 m) in the south (Fig. 1). The Asea basin is located in central Arcadia, close to Tripolis (Peloponnese) and about 50 km south of Stymphalia.

The Stymphalia Polje, extending approximately 13 km from west to east, is located at 600 m above sea level. It comprises Lake Stymphalia, the only remaining natural permanent lake of the Peloponnese (37.85° N, 22.46° E) as well as the archaeological site of the Hellenistic town of Stymphalos (Walsh et al., 2017; Williams, 1983, 2005). Formerly, Lake Stymphalia was drained via one main sinkhole (*katavothre*), which was encased in concrete in the 19<sup>th</sup> century (Morfis and Zojer, 1986). Nowadays, water is discharged via the Hadrianic aqueduct, built around 130 AD and reactivated in the 19<sup>th</sup> century, and it is pumped away for agricultural purposes. Lake level and notably lake size varied considerably over time (Seguin et al., 2019). The total catchment area, excluding subsurface water flow of the Ziria karst system (Nanou and Zagana, 2018), is today approximately 217 km<sup>2</sup>, divided into the larger Stymphalia catchment (~182 km<sup>2</sup>) and the smaller Kaisari catchment in the NE (~35 km<sup>2</sup>), which were hydrologically connected in the early 20<sup>th</sup> century AD by an artificial tunnel (Knauss, 1990; Morfis and Zojer, 1986).

The latter is relatively small, stretching ca. 7 km from SW to NE direction, and we here term it Kaisari Polje (37.93° N, 22.55° E, ca. 730 m a.s.l.), as it contains the village of Kesario/Kaisari (Καϊσάρτιο; Fig. 1). Morfis and Zojer (1986) address it as part of the Stymphalia Polje and call it valley of Klimenti, which is the village north of Kesario/Kaisari. Differing from the situation in Stymphalia and Pheneos, the Kaisari Polje is entirely situated in Neogene marls and conglomerates (Morfis and Zojer, 1986) and receives its water from a more homogeneous catchment. It contained a small lake in former times, which was drained in the 1880s for agricultural purposes.

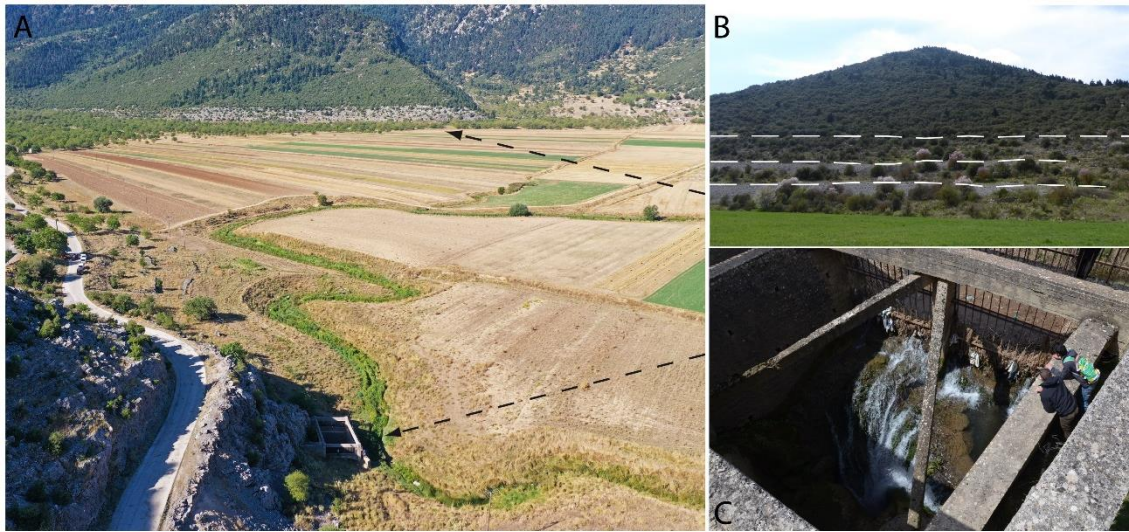


**Figure 2: Photos of the Pheneos Polje. (A) Aerial perspective with southwestward view on the eastern bay of the Pheneos Polje used for agricultural purposes. (B) Side view on shore lines in the eastern bay close to Amigdalía. (C) Top-down view into the eastern katavothre contained in a concrete construction. The metal grille allows the discharge of water and prevents blockage. To the right, humans for scale. (photos: J. Seguin, 2017; I. Unkel, 2019).**

To the west of the Stymphalia Polje, crossing the Geronteion Pass in the Mavrovouni mountain ridge (rising up to 1,600 m), the Pheneos Polje (37.85° N, 22.33° E) is located at approx. 700 m a.s.l.. It is 28 km long and max. 13 km wide, with a catchment area of approximately 235 km<sup>2</sup> (Knauss, 1990; Morfis and Zojer, 1986). The ancient site of Archea Pheneos at the NW end of the polje (Fig. 1) was mainly inhabited during the Middle Helladic (ca. 4,050 – 3,650 BP/2,100 – 1,700 BC).

Geologically, the Stymphalia and Pheneos poljes are located in the limestone and dolomite dominated Gavrovo-Tripoli and Olonos-Pindos geotectonic zones, where karst features are abundant. Outcrops of the metamorphic phyllite-quartzite series, Neogene and Pleistocene conglomerates and marls, schists and Quaternary deposits can be found mainly in the west and southwest (IGME, 1982, 1970; Morfis and Zojer, 1986). Morfis and Zojer (1986) divide the Pheneos polje into an eastern and a western bay. It consists of two main hydro-tectonic systems containing 87 springs and seven sinkholes, which would drain the water (Morfis and Zojer, 1986). In this karstic environment, subsurface flow is of high importance for the hydrological system (Nanou and Zagana, 2018). Today, no perennial Lake Pheneos exists anymore and the water drains through trenches to the eastern katavothre (Fig. 2A). Most katavothres were

anthropogenically regulated and the polje floor is no longer inundated thus creating more space for agricultural land. Only during wet winter months, a small ephemeral/seasonal lake may develop in the western bay (Morfis and Zojer, 1986). Nowadays, the eastern katavothre is surrounded by a concrete construction to prevent it from blocking (Fig. 2C), but there are narratives and reports recounting that it was blocked in the past more than once, causing the lake level to rise up considerably (Knauss, 1990). Knauss (1990) refers to different historical scholars who report inundations and high lake level stands as well as complete desiccation of the polje. In the more recent past during the Ottoman Period, the drainage system was purposely blocked in the 1820s leading to a 39 km<sup>2</sup> large and 42.5 m deep lake, which was re-opened by an earthquake in 1834 (Knauss, 1990).

Contrary to the geomorphologically closed poljes, the Asea valley represents a natural thoroughfare and the rivers drain into the Ionian Sea. Geologically, it belongs to the Tripolis zone, characterised by carbonate rocks and some clastic flysch (IGME, 2002, 1992; Morfis and Zojer, 1986; Unkel et al., 2014).

### 3. Materials and methods

The methods presented here were equally applied to the sediment cores from Stymphalia (STY1) and Asea (Asea-1), which we compare in the following to the new cores from Pheneos (PHE1) and Kaisari (KES2). Detailed information on the methods concerning Stymphalia and Asea can be found in Heymann et al. (2013), Seguin et al. (2019), and Unkel et al. (2014) (Table 1).

*Table 1. Overview of coring sites discussed in this study. The elevation is indicated in meters above sea level.*

ID	Location	Core Acronym	Coordinates	Elevation [m a.s.l.]	Catchment Size	Presented Core Length
1	Stymphalia	STY1	37.84944° N, 22.46056° E	610	182 km <sup>2</sup>	324 cm
2	Kaisari	KES2	37.94558° N, 22.57641° E	730	35 km <sup>2</sup>	350 cm
3	Pheneos	PHE1	37.85114° N, 22.33510° E	710	235 km <sup>2</sup>	390 cm
4	Asea	Asea-1	37.37603° N, 22.26592° E	630		500 cm

### **3.1 Sediment coring**

Fieldwork at the former lake sites of Kaisari and Pheneos was conducted in spring 2017. At the time of coring, both sites were drained and covered by pastures and non-vegetated field, thus being accessible for land-based vibracore drilling. Following a test coring using an open system (A cores), two parallel cores (B and C) for each site with a vertical offset of 50 cm were retrieved in one-meter-sections of 55 mm diameter using inliner-tubes deployed in a piston corer (Stitz type). PHE1 (37.85114° N, 22.33510° E) was cored in the eastern bay of the Pheneos Polje in proximity to the eastern katavothre. Two corings were taken from the Kaisari Polje and we here present results from KES2 (37.94558° N, 22.57641° E), which is assumed to have been closer to the former lake depocentre. The sediment cores were kept in their sealed inline PVC tubes and transported to Kiel University (Germany), where they were stored at +4° C in a cooler.

### **3.2 Sedimentology and geochemistry**

After the cores from Pheneos and Kaisari had been split longitudinally in the laboratory, lithology, sediment texture, structure, and colour according to Munsell soil colour charts (Munsell, 2000) were recorded. A master depth scale was established for each site based on compilation of overlapping parallel cores. The core sections were visually correlated on distinct marker layers where possible and fine-tuning was done in a second step based on the RGB values.

The surfaces of the archive half cores were scraped clean and digitally photographed using a line-scan camera (resolution: 143 pixels \*cm<sup>-1</sup>). The same half cores were analysed geochemically via non-destructive X-ray fluorescence (XRF) scans using an Avaatech XRF Core Scanner with a rhodium X-ray source. The defined overlapping intervals in the parallel cores were scanned in two runs with 10 kV (exposure time of 10s at 750µA) and 30 kV (exposure time of 20s at 2 mA, using a Pd-thick filter) at a resolution of 5 mm. Combining the data into a continuous sequence as well as data quality assurance were done in R version 3.5.1 (R Core Team, 2019).

We selected ten elements measured in all cores (10 kV: Al, Si, K, Ca, Ti, Mn, Fe; 30 kV: Rb, Sr, Zr) for detailed analyses along the sediment sequence. The XRF scanning results are expressed as semi-quantitative element intensities in total counts per second (tcps). Relative changes of one element to another are analysed by natural logarithmic (log) ratios of elemental pairs and are used

and interpreted as proxies for palaeo-environmental variation to minimise measurement variation caused by sample geometry, physical properties and the closed-sum effect (Weltje and Tjallingii, 2008). For each lake ecosystem, these proxies need to be understood and validated individually (Xu et al., 2010). While in more arid or semi-arid regions, input of more terrigenous detritus may be attributed to drier periods with less vegetation cover, higher soil instability and vulnerability, the same geochemical signal in more temperate regions may indicate wetter periods with strong precipitation events triggering more erosion.

We here use the Rb/Sr ratio, which reflects the variation between siliciclastic-rich and carbonate-rich material in the sediment. It is used as a proxy for weathering intensity (Chen et al., 1999; Jin et al., 2006; Katrantsiotis et al., 2019; Xu et al., 2010). Rb replaces K in feldspars and is associated with an increase in physical erosion of terrigenous material from the catchment during wetter periods (Kylander et al., 2011). Sr is linked to authigenic carbonate precipitation, which occurs mainly during warmer and drier phases with intensive evaporation (Yanhong et al., 2006). In the following, a high (low)  $\log(\text{Rb/Sr})$  ratio is interpreted as indicating rather cold/wet (warm/dry) conditions. The same relationship can be visualised by using the  $\log(\text{Ca/Ti})$  ratio (Croudace and Rothwell, 2015; Kylander et al., 2011).

The  $\log(\text{Zr/Rb})$  ratio is used as grain size proxy, because high amounts of potassium (K) and rubidium (Rb) are generally associated with clay minerals, while zirconium (Zr) occurs in very coarse silt or sand grains (Chen et al., 2006; Cuven et al., 2010; Dypvik and Harris, 2001; Kylander et al., 2011). We used discrete grain size measurements to reconcile the ratio, which is used in the following to indicate changes in grain size coupled with transport processes and erosion intensity.

For discrete samples from KES2 and PHE1, the grain size distribution of the fine matrix (<2 mm) was measured on dried samples at 30 cm intervals along the cores using a laser-particle-analyser, Malvern Mastersizer 2000. The samples were pre-treated with hydrogen peroxide ( $\text{H}_2\text{O}_2$ ) to remove the organic matter and the dispersant agent sodium pyrophosphate ( $\text{Na}_4\text{P}_2\text{O}_7$ ) was added to avoid aggregation of particles. At least one measurement was conducted per previously identified lithological unit. The grain size distribution was categorised according to the DIN EN

ISO 14688-1 nomenclature. The results are indicated in vol%. Adjacent to the grain size samples, samples for carbon and nitrogen analyses were taken at the same intervals. The concentrations of total carbon (TC), total inorganic carbon (TIC), and total nitrogen (TN) were determined on dried and powdered samples using a Euro EA (elemental analyser). We calculated total organic carbon (TOC) concentrations in dry sediment by subtracting TIC from TC. The TOC/TN ratio was calculated to indicate the origin of the sedimentary organic matter. While values for autochthonous organic matter, such as algal biomass, are low, generally ranging between 4 and 10, land-plant organic matter eroded into the lake shows values higher than 10 and vascular plants even higher than 20 (Meyers, 2003).

### **3.3 Radiocarbon dating**

The radiocarbon dates used here from Stymphalia are published in Seguin et al. (2019), those from Asea in Unkel et al. (2014). The chronologies of the new sediment cores from Pheneos and Kaisari (Table 2) are based on accelerator mass spectrometry (AMS) radiocarbon ( $^{14}\text{C}$ ) measurements performed at the Poznań Radiocarbon Laboratory. Bulk sediment samples were taken for dating using the alkali residue fraction, due to the absence of discrete organic macroremains. Tephra layers supporting the chronology could not be found in the sediments and have so far not been reported in southern Greece for the Mid to Late Holocene in this area (Zanchetta et al., 2011). The age-depth models were produced using rbacon (Blaauw and Christeny, 2011) with respect to the IntCal13 calibration curve (Reimer et al., 2013) without any reservoir correction (Fig. 3). All dates are indicated as calibrated calendar years before present (cal BP), where ‘present’ is defined as AD 1950 with  $1\sigma$ -uncertainty ranges according to Mook and van der Plicht (1999).

### **3.4 Statistical data processing**

All statistical analyses, diagrams and figures were compiled using the open-source programme R (R Version 3.4.2; (R Core Team, 2019)). We applied statistical approaches such as Spearman rank-based correlations (Spearman’s rho) and multivariate analyses, including principal component



analyses (PCA) to investigate the covariation of the different chemical elements in each sediment core and to compare the different sites with one another. A PCA reduces the dimensions of the elemental dataset and helps to identify the main processes influencing the chemical composition of each lake sediment. We standardised our datasets prior to analysis and applied the *prcomp* function from the R stats package.

For the geochemical data, cleaning of the dataset, i.e. the removal of explicit outliers and re-filling of the missing values by linear interpolation was done manually prior to statistical processing. Voids in the sediment, e.g. in PHE1 and in the topmost part, were not filled with interpolated data.

## **4. Results**

### **4.1 Core chronologies and Bayesian modelling**

Poor preservation of organic matter and the high amount of reworked material and inorganic carbon content present a considerable challenge for precise  $^{14}\text{C}$  dating in the semi-arid Mediterranean (Grootes et al., 2004; Vaezi et al., 2019; Walsh et al., 2019). As human decisions may have a strong influence on the age-depth modelling, we present our dating proceeding in detail in the following. If not stated otherwise, mean ages were extracted and used for representation and interpretation of the geochemical proxies.

#### ***Pheneos***

For the Pheneos sequence, we calculated the age-depth model PHE\_03 based on 8 samples (Table 2) for the complete master core of 390 cm (Fig. 3).

The analysis of the sediment sequence gave no indications for hiati or erosional discontinuities and thus a continuous sedimentation was assumed. The lithology of the upper half of the core however seems different and most probably reflects higher input of terrestrial material. Four samples in this section (PHE075 – PHE149) all show an age reversal of up to 3,000 years, indicating contamination by old detrital carbon (Seguin et al., 2019), and were hence excluded from the modelling process.

On average, the sedimentation rate for the whole sequence was calculated at approximately 0.37 mm/yr, being lowest between 4,500 – 6,500 cal BP with ca. 0.16 mm/yr, slightly increasing to 0.32 mm/yr between ca. 4,800 – 3,300 cal BP, and further increasing to ca. 0.53 mm/yr during the last 3,000 years.

### ***Kaisari***

For the Kaisari sequence, four bulk samples were used (Table 2) along the 350 cm core covering a time span of 6,500 years (Fig. 3). During the sedimentological analysis of the core sequence, no indications for hiati or erosional discontinuities were found and hence we assumed a continuous sedimentation.

Based on the age-depth model KES2\_01, we calculated the average sedimentation rate for KES2 to be approx. 0.54 mm/yr with a slightly higher accumulation rate (0.78 mm/yr) between 3,800 – 2,800 cal BP.

***Table 2. List of radiocarbon samples taken from PHE1 and KES2. The sampling depths refer to the master core. Indicated <sup>14</sup>C ages are unmodelled ages giving the 68.2 % calendar dating probability. Indicated IntCal13 ages are cal BP ages modelled with rcarbon using the IntCal13 calibration dataset (Reimer et al., 2013). Dates marked with an asterisk have been excluded from age-depth modelling. <sup>1)</sup> Amount of remaining sample material after respective pre-treatment. (following page)***

sample no.	core ID	analysis no.	sample material	sample fraction	C content in this fraction <sup>1</sup> [mgC]	conventional <sup>14</sup> C age $\pm 1\sigma$ [BP]	calibrated <sup>14</sup> C age [cal BP], 1 $\sigma$ -ranges	depth [cm]	remarks
KES103	KES-2c	Poz-95623	bulk sediment	alkali residue	>1.0	1515 $\pm$ 30	1350-1414 1465-1475 1510	103	
KES169	KES-2c	Poz-95624	bulk sediment	alkali residue	0.9	2775 $\pm$ 35	2799-2822 2843-2894	169	
KES240	KES-2c	Poz-95564	bulk sediment	alkali residue	0.4	3420 $\pm$ 35	2901-2924 3613-3706	240	
KES282	KES-2c	Poz-95625	bulk sediment	alkali residue	0.2	4530 $\pm$ 50	5059-5114 5117-5185 5215-5222	282	
KES332	KES-2c	Poz-95626	bulk sediment	alkali residue	>1.0	2825 $\pm$ 30	5238-5241 5266-5306 2879-2914 2916-2958	332*	broken vial - contaminated
PHE075	PHE-1b	Poz-95627	bulk sediment	alkali residue	0.5	4080 $\pm$ 40	4450-4465 4518-4625	75*	
PHE095	PHE-1c	Poz-98167	bulk sediment	alkali residue	>1.0	4890 $\pm$ 40	4764-4788 5595-5647	95*	
PHE128	PHE-1c	Poz-95628	bulk sediment	alkali residue	0.9	4850 $\pm$ 40	5489-5504 5582-5615	128*	
PHE149	PHE-1b	Poz-98169	bulk sediment	alkali residue	>1.0	4825 $\pm$ 30	5628-5642 5486-5508 5581-5600	149*	
PHE186	PHE-1c	Poz-95630	bulk sediment	alkali residue	0.8	3180 $\pm$ 35	3376-3413 3421-3445	186	
PHE225	PHE-1b	Poz-95565	bulk sediment	alkali residue	>1.0	4100 $\pm$ 30	4528-4626 4763-4789	225	
PHE-256	PHE-1b	Poz-106235	bulk sediment	alkali residue	0.5	5870 $\pm$ 40	4795 6656-6737	256	
PHE348	PHE-1b	Poz-95797	bulk sediment	alkali residue	0.2	8640 $\pm$ 60	9539-9634 9641-9660	348	

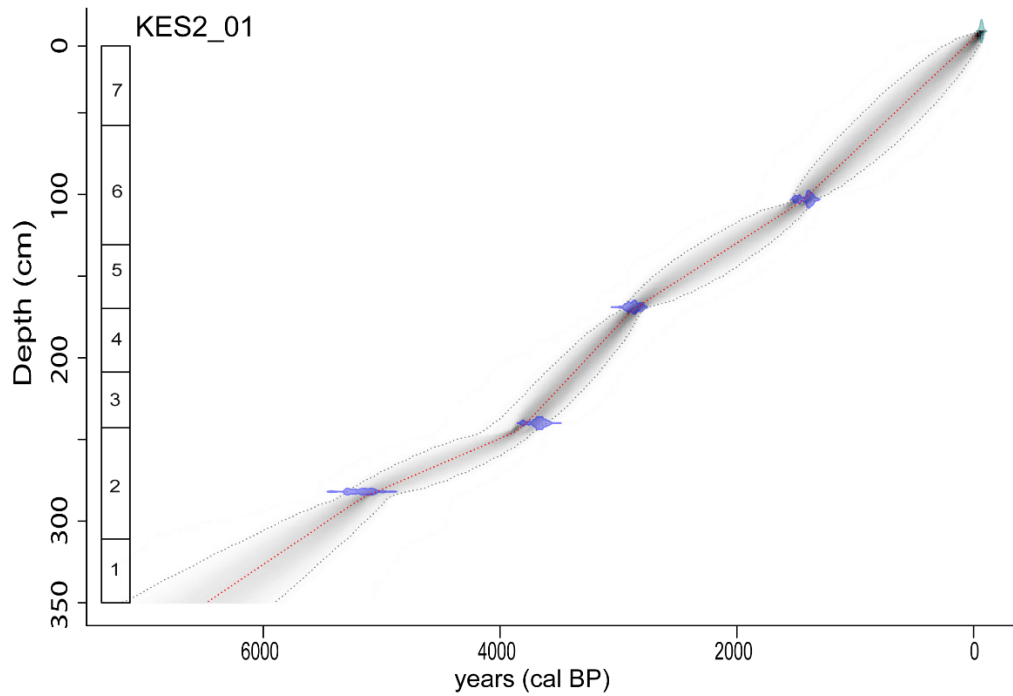
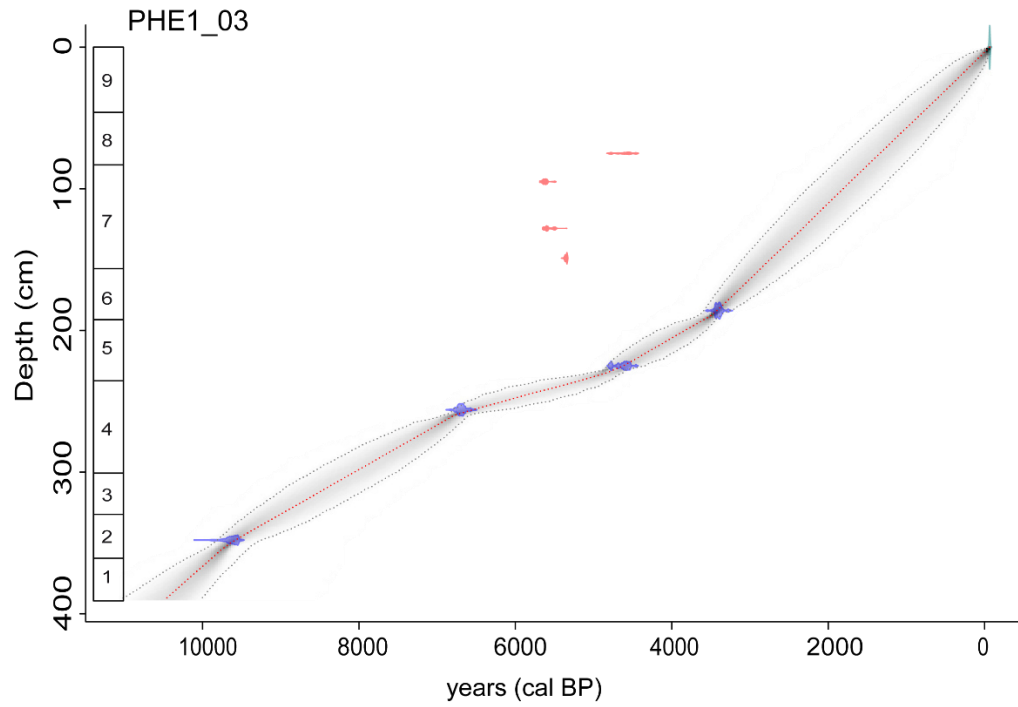


*Figure 3: Bayesian age-depth models for Pheneos (top) Kaisari (bottom). The models were constructed using the R package rbacon (Blaauw and Christen, 2011). The blue tie bars indicate the 14C age distributions (cf. Table 2). Outliers are plotted in red and were excluded from modelling. The greyscale of the line graph reflects the likelihood; the darker the more likely the model passes through that age. The red dotted line follows the mean ages.*

### *Asea*

The initial age-depth model published in Unkel et al. (2014) was calculated using Oxcal 4.1 and was based on IntCal09 (Reimer et al., 2009). Based on the most recent state of knowledge and for the sake of consistency in the inter-comparison, the model was updated using rbacon and calibrated using IntCal13 as calibration curve (Reimer et al., 2013).

Charcoal and plant remains from thirty sediment intervals were handpicked, pre-treated and radiocarbon dated by NOSAMS at Woods Hole Oceanographic Institution (cf. Table 1 in Unkel et al., 2014). For sample No. 229 and 236, dating was carried out only on charcoal material and these dates most likely give too old ages and were considered as outliers. Sample No. D, 233, and M contained root fragments penetrating the sediment post-hoc and thus give too young ages and were likewise considered as outliers. Three additional samples between 3.30 – 3.60 m depth (L, 235, N) yielded considerably younger ages than the rest. Unkel et al. (2014) explained this phenomenon by inadvertent dating of root material that had penetrated the sediment from above aiming to reach water stored on the aquitard horizon (greenish-grey units 2 – 3). They were also excluded from modelling. Due to this more sophisticated modelling approach, our new age-depth model shifted towards younger ages by up to 1,000 years compared to the Unkel-2014-model, especially during the third millennium cal BP (Suppl. Fig. 1). According to the new age-depth model (Asea\_9), the average sedimentation rate for Asea is calculated to 0.92 mm/yr. For the period 3,000 – 3,600 cal BP, the rate is considerably lower with approximately 0.3 mm/yr.

### *Stymphalia*

The data and modelling approach is described in detail in Seguin et al. (2019). It is based on 45 radiocarbon measurements on 26 samples, modelled with rbacon and calibrated using IntCal13 as calibration curve (Reimer et al., 2013). For bulk sediment samples, we regarded the humic acids fraction as providing more plausible results and we applied a reservoir correction of  $200 \pm 100$  years. Cultural events were additionally integrated into the modelling approach.

## **4.2 Lithostratigraphy and geochemistry**

### **4.2.1 Pheneos**

Core PHE1 stretches over 390 cm and nine lithological units (Fig. 4, Suppl. Fig. 2). The upper 19 cm are missing due to unconsolidated material and core compaction. Due to an unfortunate match of coring depths of parallel lower core segments, a void exists at 276 – 290 cm.

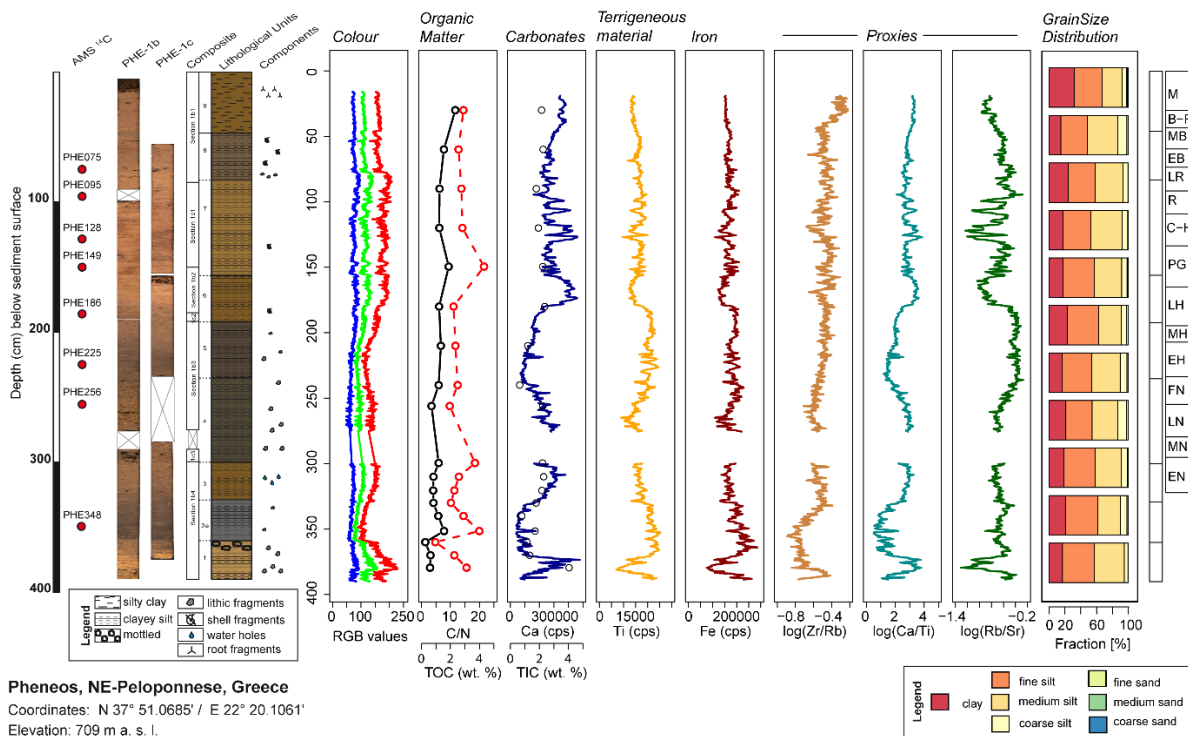


**Figure 4:** PHE1 composite core log with pictures, master core profile, lithological units and overview of different proxies plotted against depth. Depths where samples for  $^{14}\text{C}$  dating were taken are marked by red dots. From left to right: RGB colour values (blue, green, red), TOC (black line) and TOC/TN (red dotted line), TIC (circles) together with counts per second (cps) of calcium (darkblue line), titanium, iron, as well as log-ratios of Zr/Rb, Ca/Ti, Rb/Sr and granulometry are plotted against depth. For orientation, boxes with lithological units and cultural periods are plotted to the right (for abbreviations of cultural periods see Seguin et al., 2019; Weiberg et al., 2016).

Colours range from 10YR 3/1 to 10YR 5/3 with brown and dark yellowish brown colours dominating (Munsell, 2000). The lower part is generally darker than the upper half, except for the bright unit 1 (Fig. 4). Visible organic debris is absent except for some modern roots in the plough horizon (unit 9). Very few shell fragments were found in units 6 to 8. The TOC content varies between 0.2 wt. %, at the boundary between units 1 and 2, and 2.3 wt. % in the uppermost unit (cf. Fig. 4). The existence of numerous carbonate concretions within the rather fine matrix of the sediment in several intervals of the core is characteristic and points towards at least seasonal desiccation and initiation of soil formation. A higher number of carbonate concretions with diameters  $<0.5$  cm occurs in units 1 and 4. TIC (ranging from 0.6 to 4.0 wt. %) and Ca contents follow a similar trend, showing highest values in unit 1 and low values in units 2 and 5. Total nitrogen (TN) ranges from 0.04 to 0.16 wt. % with an average of 0.08 wt. %. The TOC/TN ratio ranges from 4.8 to 21.6 indicating varied mixing of aquatic

algae and terrestrial vascular plant material (Meyers, 2003). Units 2 and 4 show the lowest TOC/TN ratios suggesting a greater input of autochthonous aquatic algae.

The grainsize distribution ranges from fine to medium silt; it has a mean clay content of 20.4 %, a mean silt content of 78.1 % and a mean sand content of only 1.5 %. The uppermost unit 9 is of homogeneous brown colour and has an exceptionally high clay content >30 %, which may be linked to alteration and compression by agricultural use of the area. Due to this modern anthropogenic alteration, unit 9 is excluded from any palaeoenvironmental interpretation.

#### **4.2.2 Kaisari**

The core KES2 has a length of 350 cm, while the upper 34 cm of unconsolidated material are missing. Most analyses including XRF scanning exclude the upper 50 cm, as the material was too loose to meet the scanning prerequisites. KES2 was subdivided into seven lithological units (Fig. 5, Suppl. Fig. 3). No laminations are visible, all unit boundaries are gradual and do not show any sign of abrupt changes, hiatuses or event layers. Overall, the core looks very homogeneous; yellowish-brown to olive-brown colours (10YR 4/4 to 2.5Y 5/3) are dominant. Reddish mottled sections with a higher Fe content suggest that the coring spot periodically dried out and oxidation processes occurred. However, fractures, layers of gypsum or carbonate nodules, that could indicate desiccation or soil formation, are absent. With the beginning of unit 6, few patches of reddish material appear which suggests the selective input of reddish soils present in the catchment. Macro-remains are likewise largely absent except for some roots in the plough horizon (unit 7) and sporadic, small shell fragments in the lower part of the core. Intact gastropod shells – abundant in Lake Stymphalia – are absent here. The sediment sequence has a fine, silty texture composed of a varying mixture of clay (mean = 21.5 %) and silt (mean = 77.5 %); sand content was <1 %. TOC varies between 1.0 to 2.2 wt. %. TN is similar to Pheneos and ranges from 0.06 to 0.13 wt. % with an average of 0.09 wt. %. TOC/TN ratios are in the range of 14 – 27, which in contrast to Pheneos indicate a predominantly or exclusively terrestrial source of organic matter with a higher input of vascular plants (TOC/TN > 20) in unit 2 to 4.

The sediment sequence in Kaisari only shows very slight variations in the proxy record. The catchment as well as the transport distance from the slopes to the coring spot are much smaller and the input of terrestrial detritus thus higher compared to Pheneos or Stymphalia. Comparatively stable counts of terrigenous elements suggest that the input of clastic detritus was relatively constant during the Mid and Late Holocene, which is likewise supported by the rather stable sedimentation rate.

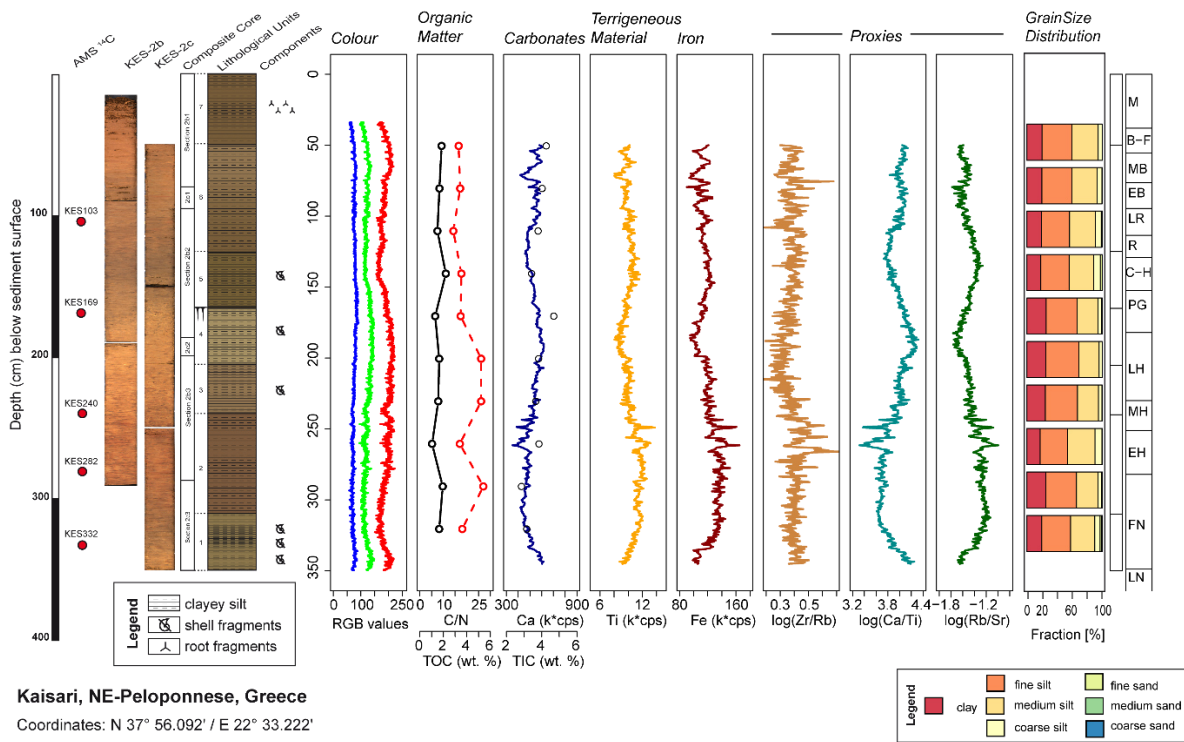


**Figure 5:** KES2 composite core log with pictures, master core profile, lithological units and overview of different proxies plotted against depth. Depths where samples for 14C dating were taken are marked by red dots. From left to right: RGB colour values (blue, green, red), TOC (black line) and TOC/TN (red dotted line), TIC (circles) together with counts per second (cps) of calcium (darkblue line), titanium, iron, as well as log-ratios of Zr/Rb, Ca/Ti, Rb/Sr and granulometry are plotted against depth. For orientation, boxes with lithological units and cultural periods are plotted to the right (for abbreviations of cultural periods see Seguin et al., 2019; Weiberg et al., 2016).

### 4.3 Statistical analyses of the geochemical data

For each study site, we applied a standardised and rotated principal component analysis (PCA) to the XRF geochemical element counts to reduce the dimensions that explain the variability in the dataset and the relationship between the different elements and their distribution within the sedimentary units. These principal components (PCs) do not have absolute units but reflect relative changes in the chemical composition over time.

We extracted the first three principal components (PC1 – PC3) for each site that account for >75 % of the variance in the respective dataset. Generally, the loadings of Ca and Sr in carbonates are closely bound together and point to one axis direction, while the loadings of elements such as Al, Fe, K, Rb, Si, Ti, and Zr in clastic material show a wider spread of directions, but largely point to the opposite direction of the carbonates (Fig. 6).



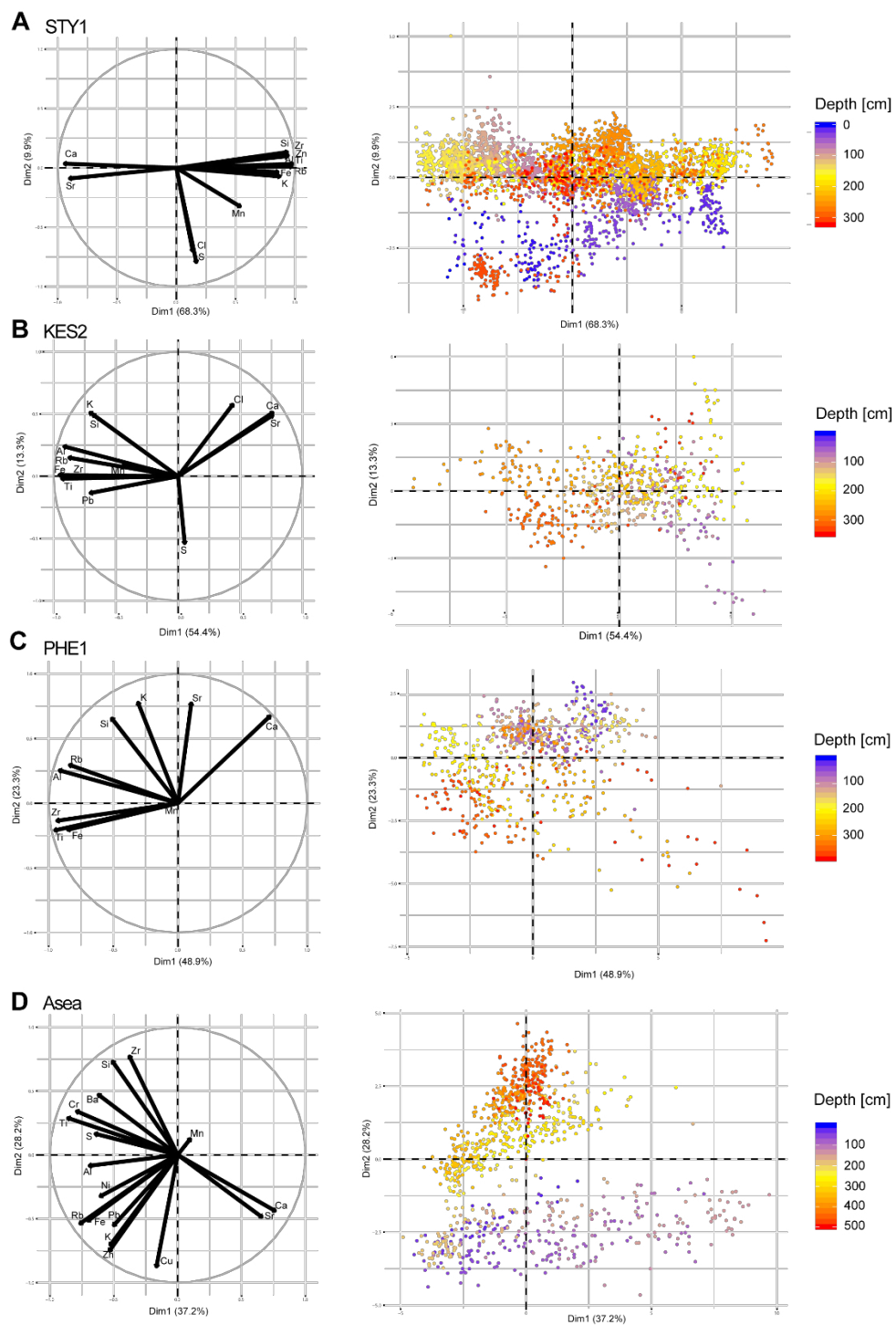


**Figure 6: Principal component analyses (PCA) for all study sites. (left) Variable correlation circles of PCA of the XRF data displaying correlation between PC1 (Dim1) on the x-axis and PC2 (Dim2) on the y-axis. (right) Distribution of sample points in the PC1–PC2-scatterplot for each site. The samples are coloured according to their depth in the**

*sediment core from purple (surface) to red (maximum depth). The point density for STY1 is highest, because data resolution is 1 mm. For the interpretation, the reader is referred to the text.*

For Stymphalia, PC1 explains >68% of the variance and is negatively associated with Ca and Sr and positively associated with elements in clastic materials. For Pheneos, Kaisari, and Asea, the relationship between carbonates and clastic material is similar but reversed on the axis; carbonates Ca and Sr are bound positively to PC1, while the other elements show negative loadings (Fig. 6). It is likewise apparent that in all cores, except parts of STY1, manganese plays a minor role in the first two components.

For all four study sites, PC1 always spans the axis between carbonate and siliciclastic assemblages and allows for the application as palaeoenvironmental proxy (Seguin et al., 2019). For each site, the PC1 compared to  $\log(\text{Rb}/\text{Sr})$  was plotted over time (Fig. 8) to demonstrate any similarity and to illustrate the highest fluctuations of geochemical proxies in the respective dataset.

## **5. Discussion**

Our analyses of the four sediment cores revealed considerable variation within the proxies, which shows that the landscape in NE Peloponnese has changed significantly over the last 5,000 years. All study sites represent shallow lacustrine environments that were not permanently waterlogged during the respective period, but rather show phases of periodic or episodic desiccation. Changes in water level and water availability may be attributed to climatic fluctuations as well as to human interference. Although Pheneos, Stymphalia, and Kaisari are located in immediate proximity and may have experienced the same climatic changes, the sedimentary facies vary significantly due to differences in catchment size, lake size and depth, and geology. Common features of all sites are a relatively low organic carbon content and the very low abundance of sand-sized particles within the grain size distribution. Noticeable differences between the three sites are the amount of gastropod shells, which are preserved in Stymphalia in a higher number than in the other two sites, the existence of carbonate nodules in Pheneos, which are lacking in Stymphalia, and the strongly mottled, oxidised, reddish sediment which characterizes Kaisari.

### **5.1 Palaeoenvironmental reconstruction of Kaisari and Pheneos**

The Pheneos sediment sequence retrieved so far covers the last 10,500 years, while the bottom of the Kaisari core (KES2) was dated to 6,500 cal BP. The former lakes at both sites show no signs of laminae or significant stratification, which would only develop in deep water along with suboxic to anoxic bottom-water conditions. Hence, this suggests high water level fluctuations, strong ventilation

and constant well-mixing of the water column leading to sufficient oxygen supply. Both lakes should have experienced at least periodic desiccation during the last 5,000 years, which is indicated by the absence of visible organic macro remains, the low TOC content, the carbonate nodules in Pheneos, the absence of black colouration in Kaisari, and the strongly mottled nature of the sediment in Kaisari. Both sites show evidences for shallow lacustrine environments.

In Pheneos, phases of blackish sediment colour and low Ca content indicate phases of lower evaporation and more permanent water saturation for the periods 9,900 – 9,000 cal BP (unit 2) and 5,100 – 3,600 cal BP (unit 5) (cf. Fig. 4). This is supported by the lowest measured TOC/TN ratio at 360 cm (9,900 cal BP), which is  $<7$  and thus indicates that the organic matter here has a predominantly aquatic origin (Meyers and Ishiwatari, 1993). It thus seems as if during these periods, generally colder and wetter conditions prevailed and the eastern Pheneos Bay was covered by a permanent lake. However, carbonate nodules, which are quite abundant in Pheneos in the lower two meters, possibly indicate desiccation, post-depositional alteration and/or initial soil formation processes (Unkel et al., 2014; Viehberg et al., 2018). High TOC/TN values of 18.5 around 8,000 cal BP (300 cm) and 21.6 around 2,700 cal BP (150 cm) show that the eastern Pheneos Bay received more terrestrial influence during these times and it is conceivable that, when the lake dried out during these periods, it may have led to the formation of carbonate concretions within pores of the buried sediment. During the last 3,300 years, the sediment structure looks more similar to KES2 and carbonate nodules are absent. We assume that during this period the eastern Pheneos Bay was mainly shaped by terrestrial influence and was not covered by a considerably deep lake for several centuries, facilitating the alternation between well-waterlogged and relatively dry environmental conditions. The rocky, barren beach and palaeo-shorelines (Fig. 2B) on the flanks in the southern part of the Pheneos basin, however, point towards higher lake level stands.

### ADM Comparison Peloponnese

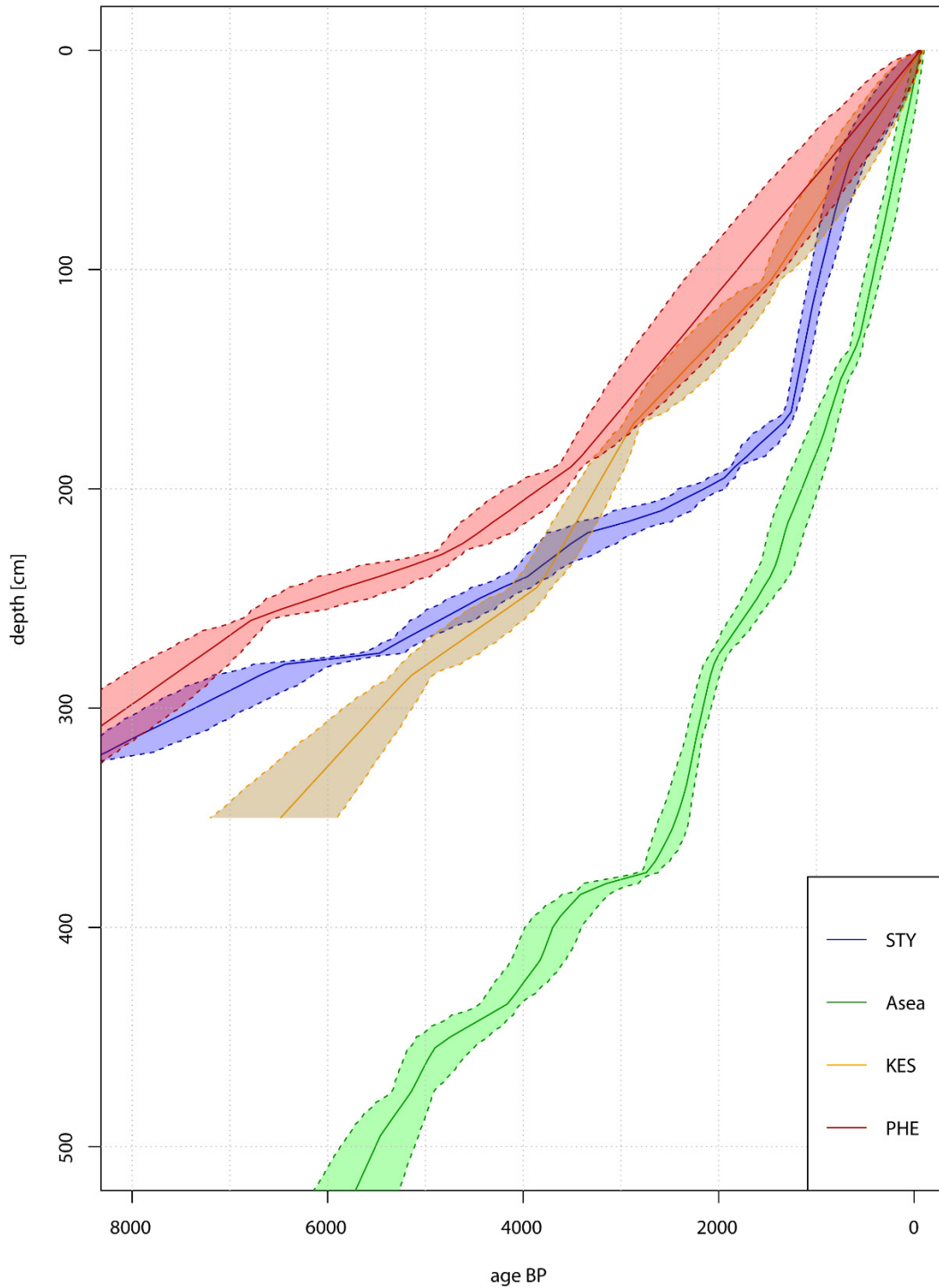


**Figure 7: Comparison of age-depth models for all study sites. Asea-1 (green) has a consistently higher sedimentation rate. For 6,500 – 3,500 cal BP, the sedimentation rate in STY1 (blue) and PHE1 (red) is similar and increases in younger times. For KES2 (yellow), the sedimentation rate stays relatively constant.**

Their age is unknown, but in combination with the historically reported high stands (Knauss, 1990) and the absence of patina on the boulders, we may assume that they were formed during shorter periods of high inundation in the more recent past. Yet, Pausanias, travelling through Greece in the 2<sup>nd</sup> century AD, already mentioned the existence of “mountains marks up to which, it is said, the water rose” (Paus. 8.14.1), which suggests that the existence of shorelines seems to be older than expected. A closer investigation of these features is needed to give more precise information on their morphology.

The grain size distribution in both cores is comparable to Lake Stymphalia. Fine-grained silty clay and clayey silt dominate both sequences. Sand is almost absent. Coarse matrix (>2 mm) is also absent with the exception of the carbonate nodules. No event layers can be identified and boundaries between the sedimentary units are exclusively gradual. Combined with the dominance of fine material, this indicates rather constant deposition of sediment under relatively stable or gradually changing conditions and excludes the existence of slumped units deposited during extreme precipitation events or earthquakes.

Changes in the geochemical proxies occur gradually; the most significant shift visible in all proxies occurs in Pheneos around 3,300 cal BP and in Kaisari around 3,100 cal BP. Due to the uncertainty ranges of the age-models (Fig. 7), these shifts can be regarded as contemporaneous. The input of terrigenous elements (Ti, Zr, K) drops, while carbonate content increases (Fig. 5). The reddish mottled sediment indicates the formation of iron oxides and episodic desiccation. This may be explained climatologically by warmer summers leading to more evaporation and carbonate precipitation and lower input of allochthonous sediment due to less intense precipitation. The change in Pheneos is rather abrupt, while in Kaisari the proxies depict a continuous shift (Fig. 8B,C). The temporal deviations at the two sites of  $\pm 100$  years lie within the range of the dating uncertainties and thus these changes may have occurred simultaneously.

In Pheneos, the Rb/Sr ratio shows significantly stronger fluctuations during the period 3,300 – 1,500 cal BP than before. A similar pattern can be observed in peaks in Ca within sedimentary unit 7 (Figs. 4, 8). This pattern may be interpreted as a lasting transformation in the ecosystem around 3,300 cal BP towards increased vulnerability of the system due to a larger instability of the lake level. The Ca peaks hereby indicate dry phases with strong authigenic carbonate precipitation. Historical sources also indicate strongly fluctuating lake levels in the eastern Pheneos Polje in younger times (Knauss, 1990); the existence of a large lake is reported for 1895 while a dry plain was present in 1901. These cannot be observed in the sediment sequence, as the poljes have been completely drained and used for agricultural purposes since the 1930s. Hence, the uppermost 46 – 50 cm in both sediment cores

show signs of ploughing (Figs. 4, 5, Suppl. Figs. 2, 3) and the palaeoenvironmental signal for the last 800 years in Pheneos and 700 years in Kaisari have thus been destroyed.

## 5.2 Comparison of the Peloponnesian study sites

A comparison of all four age-depth models (Fig. 7) shows a high resemblance for the ADMs for the three poljes surrounding Mt. Ziria, while the ADM for Asea shows a significantly higher sedimentation rate. While Stymphalia and Pheneos have similar sedimentation rates in the lower part (>3,800 cal BP), Kaisari shows an overall constant and slightly higher deposition rate, which can be ascribed to the softer and more easily erodible marl sediments in the catchment and the smaller lake size, where allochthonous detrital material from the slopes reaches the coring site more easily. In Stymphalia, a strong increase in the sedimentation rate related to anthropogenic activity was observed around 1,200 cal BP (Seguin et al., 2019). In Pheneos and Kaisari, the sedimentation rate over the last 3,000 years appears rather constant. However, in Pheneos, age constraints for the upper 185 cm are weak and human influence on the sedimentation rate in this phase may thus not be visible.

For all our study sites, the first principal component (PC1) explains the variation between carbonate-rich and mineral-rich assemblages (Fig. 6). We interpret these fluctuations as hydro-climatic variations. In a simplified manner, intensified carbonate precipitation occurs during warm and dry summers, while the input of clastic material may be enhanced during wetter periods (Katrantsiotis et al., 2018).

When we calculate Spearman correlations between PC1 and the  $\log(\text{Rb}/\text{Sr})$  ratio, they are consistently high for each site ( $r_{\text{STY}} = 0.97$ ,  $r_{\text{PHE}} = -0.77$ ,  $r_{\text{KES}} = -0.93$ ,  $r_{\text{ASEA}} = -0.77$ ). This stresses the significance of  $\log(\text{Rb}/\text{Sr})$  as an important palaeoenvironmental proxy in this environment (Seguin et al., 2019). We use PC1 as main palaeoenvironmental proxy in the following, as it represents all carbonate and siliciclastic elements by their loadings and thus is more representative than the  $\text{Rb}/\text{Sr}$  ratio, based on only two elements. An additional useful proxy is the  $\text{Ca}/\text{Ti}$  ratio, which also reflects the bipolar distribution between carbonate precipitation and terrigenous input ( $r_{\text{STY}} = -0.97$ ,  $r_{\text{PHE}} = 0.87$ ,  $r_{\text{KES}} = 0.91$ ,  $r_{\text{ASEA}} = 0.45$ ). For Asea however, this correlation is lower than between PC1 and the  $\log(\text{Rb}/\text{Sr})$  ratio, which may be explained by the disproportionate increase of Ca in the uppermost part due to post-depositional alteration and carbonate nodules (Unkel et al., 2014). This facies shift is also visible in the scatterplot (Fig. 6D), where the point cloud is clearly divided into two groups; the upper 160 cm are mainly controlled by carbonates, while the lower part mainly clusters in the quadrant with the terrigenous elements.

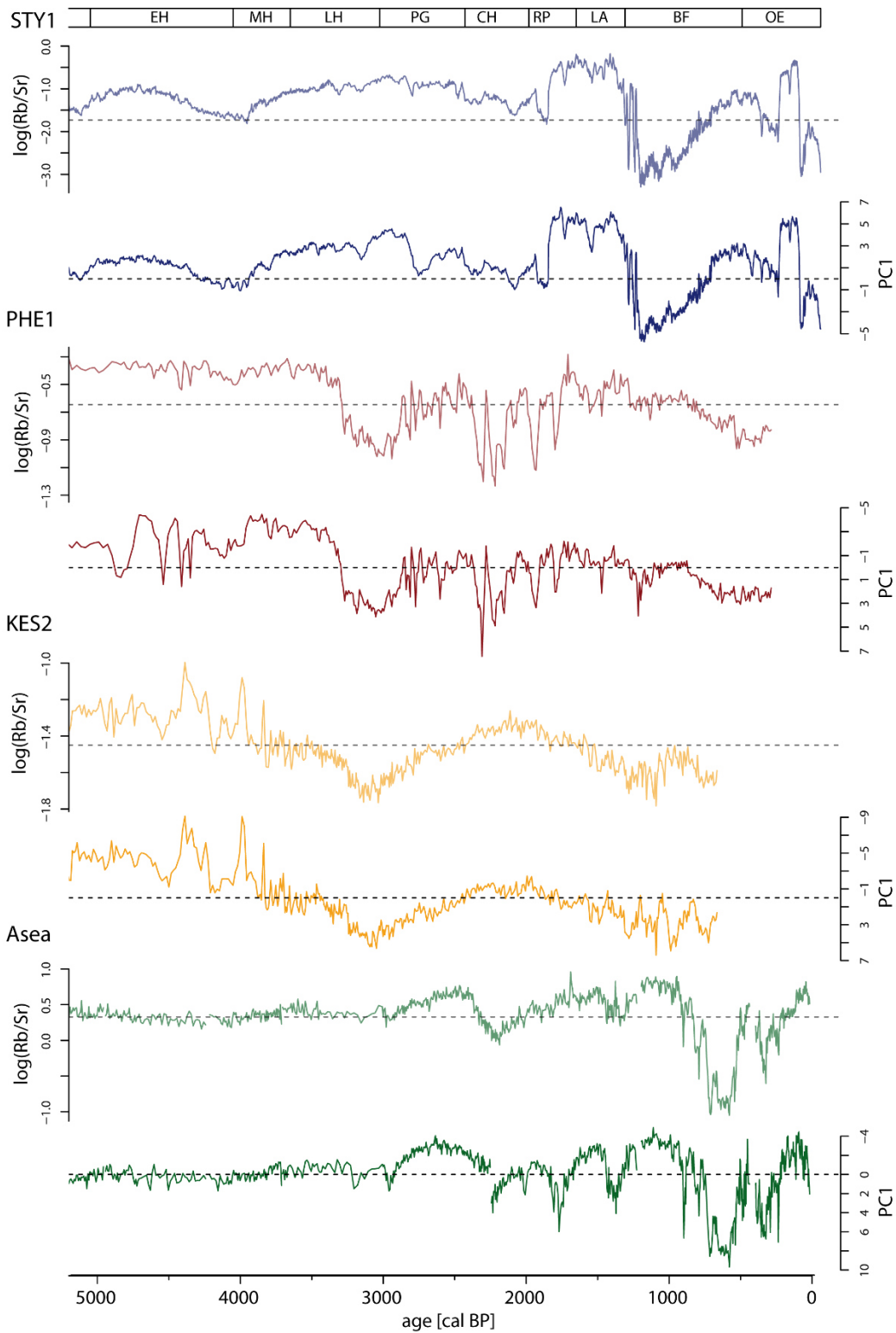


**Figure 8: Comparison of PC1 and Rb/Sr proxies for all study sites. For orientation, boxes with cultural periods are plotted on top. For the interpretation, the reader is referred to the text.**

In Stymphalia, the uppermost samples plot in the lower left quadrant (cf. Fig. 6A), showing a high importance of soluble elements of Ca, Sr, Cl, and S that most likely indicate increasing salinity and shallowing of the increasingly alkaline water body. The group of samples from the Late Neolithic (~300 cm depth) suggests that – geochemically speaking – the hydrological conditions at that time were similar.

The redox-sensitive elemental pair Mn/Fe is often used as a proxy for bottom water redox conditions and/or changes in the pH values (Davison, 1993; Koinig et al., 2003) and has been successfully applied in the past (Heymann et al., 2013; Unkel et al., 2014). For Lake Stymphalia, low Mn/Fe values were carefully interpreted to indicate more oxygen-depleted bottom water conditions during certain periods (Seguin et al., 2019). But as immobile Ti and Fe show very similar down core patterns and a high correlation in the three NE Peloponnesian archives ( $r_{PHE1} = 0.84$ ,  $r_{KES2} = 0.85$ ,  $r_{STY1} = 0.92$ ,  $r_{Asea} = 0.34$ ), we assume that in these catchments, Fe variation is mainly controlled by terrigenous sediment input rather than by redox changes (Naeyer et al., 2013). In Kaisari and Pheneos, measuring Mn proved to be challenging either due to the limits of XRF scanning or due to well-oxygenised conditions at the lake bottom during sediment deposition. In the PCA, Mn shows very little influence on the first two components and we thus abstain from interpreting Mn/Fe as palaeoenvironmental proxy.

### **5.3 The role of climate variability**

Changes in the proxies can be interpreted on different spatial and temporal scales. Micro-scale changes occur due to local forcings that only influence the lake catchment and hence are not visible in the neighbouring poljes. They may also hint towards anthropogenic activities in the respective valley. On a meso-scale, we may find regional, climatic similarities (<100 km) across the Peloponnese, while macro-scale changes can be linked to over-regional climatic phenomena.

On a spatiotemporal macro scale, Mayewski et al. (2004) identified several periods of rapid climate change (RCC) during the Holocene. The 4.2 ka event, a period of increased aridity and drought conditions in large parts of the Mediterranean (Finné et al., 2011; Isola et al., 2019; Kaniewski et al., 2018) and which has recently been set as time marker for the onset of the Late Holocene (Walker et al., 2019), is completely absent in Asea and not very distinct in the other three records (Fig. 8). In Stymphalia, Pheneos, and Kaisari, the PC1 may indicate a slight tendency towards drier conditions. Pheneos and Kaisari, however, show more prominent short-term fluctuations on a micro-scale level, which in turn could be related to overall drier conditions, leading to higher fluctuations in the respective lake levels. The following Mid Helladic to mid Late Helladic cultural period (ca. 4,050 –



3,300 cal BP) appears as a relatively stable phase in all environmental proxies. This is likewise supported by reconstructions from Lake Lerna (Katrantsiotis et al., 2019) and Aigios Floros (Norström et al., 2018), although they have a much lower resolution.

The RCC climate period from 3,500 – 2,500 cal BP (Mayewski et al., 2004) is characterised by pronounced but heterogeneous climatic shifts in many regions across the Mediterranean and Europe. Scaling up to the meso level, some authors see a significant climate event at 3,200 cal BP (3.2 ka event), and relate it to cultural changes at the end of the Greek Bronze Age (Drake, 2012; Finné et al., 2017; Kaniewski et al., 2013; Weiberg et al., 2016). While other studies find more evidence of a climatic shift around 2,800 cal BP (2.8 ka event; Neugebauer et al., 2015; van Geel et al., 2014), temporally related to the onset of the Greek Early Iron Age. The temporal and spatial diversity in the results of various studies shows that climatic changes proclaimed on a macro scale could be regionally very different and reveal very heterogeneous (local) conditions. This seems to be particularly the case during this time interval, while studies for other Holocene climate events, such as the 8.2 ka or the 4.2 ka events, reveal more homogeneous manifestations on the different scales (Bini et al., 2019; Isola et al., 2019; Zanchetta et al., 2016).

Around 3,300 – 3,200 cal BP, Pheneos and Kaisari show a strong increase, while Stymphalia and Asea show a smaller increase in Ca and Sr, indicating carbonate precipitation under drier conditions. The increase in Pheneos and Kaisari is gradual, peaking in 3,000 cal BP and then declining again until 2,800 – 2,600 cal BP. Asea and Stymphalia show two minor dry spells around 3,200 cal BP and 2,900 cal BP, which can be regarded as contemporaneous to Pheneos and Kaisari within the uncertainty ranges of the respective age models. Several proxies confirm this drying trend in Greece at the end of the Late Helladic period (Emmanouilidis et al., 2018; Finné et al., 2017; Katrantsiotis et al., 2018, 2019; Warken et al., 2018). While other studies indicate an overall drying trend for the 1<sup>st</sup> millennium BC with an incision of one wetter phase or two separate dry phases (Norström et al., 2018; Psomiadis et al., 2018). This juxtaposition of climate records shows that the end of the Greek Bronze Age was a period of high climatic instability, during which the majority of the records for southern Greece indicates a shift towards generally drier conditions, but when we also find high intra-regional variability (Finné et al., 2011). We reason that based on the heterogeneous data even on a meso scale, one needs to examine studies critically that draw a direct causal link between climate fluctuations and cultural decline. One needs to question if the resolution of the age constraints in a study really allows for conclusions concerning causes and effects in contemporaneous environmental and cultural developments. In the records presented here, we mostly see gradual changes in the environmental proxies for the last 5,000 years and conclude that climatic fluctuations in the NE

Peloponnese have not been as rapid or drastic to cause a societal downturn. Nevertheless, they may have been one factor in a multi-causal relationship and it seems that resilience or vulnerability of a society were other very decisive intrinsic factors that need to be taken into consideration (Izdebski et al., 2016; Weiberg et al., 2016).

Climate reconstruction for the last 2,500 years is more of a challenge in the four archives, as we see strong human impact or desiccation processes that additionally affect the geochemical proxies (Seguin et al., 2019; Unkel et al., 2014), but overall more arid conditions prevail in the area. During the Classical-Hellenistic period around 2,200 cal BP, when the Asea proxy starts to be influenced by pedogenic processes and the occurrence carbonate nodules (Unkel et al., 2014) which indicate desiccation, Lake Lerna shows its driest phase (Katrantsiotis et al., 2019) and also in Pheneos strong fluctuations in the Ca record point towards quickly changing, dry conditions (Fig. 9B). Stymphalia and Kaisari, on the contrary, show more stable conditions during this phase. PC1 in Kaisari is constantly above average and suggests episodic desiccation and overall drying conditions for the last 2,000 years (Fig. 9C). Over-regionally, this is in agreement with the modelling approach by Finné et al. (2019) and the records used herein (Fig. 9K).

#### **5.4 The role of human activity**

For the Peloponnese, the beginning of the Neolithic period, associated with sedentarism and development of agricultural activity, is set at 8,750 BP (Weiberg et al., 2016). The intensity and spatial distribution of human activities over this period however is highly variable. Archaeological evidence in the valleys presented here is limited to specific periods. Human activity within the lake catchments certainly had an impact on erosion processes and water availability (Seguin et al., 2019), but it is not always easy to differentiate clearly anthropogenic and natural drivers in the geochemical record of the sediment.

Anthropogenic influence is visible in Lake Stymphalia, notably the building of the Hadrianic aqueduct, and the interrelation is described in detail for the last 2,500 years by Seguin et al. (2019). The archaeological site of ancient Stymphalos has been identified on the northern shore of the lake, its earliest architectural remains dating to the 5<sup>th</sup> century BC ( $2,400 \pm 50$  BP; Kissas, 2013), while Mycenaean activity is attested only by some pottery sherds (Williams, 2013). Since Homer (Il. II, 608) mentions Stymphalos in the Catalogue of Ships, we might assume a settlement at least in the 8<sup>th</sup> century BC ( $2,700 \pm 50$  BP). Some possibly Geometric sherds from the western rim of the plain (Howell, 1970) corroborate the assumption.

In the Kaisari Polje, Mycenaean settlement activity is attested by pottery at the northern fringe of the plain (Lolos and Koskinas, 2011). The next archaeological evidence is just appearing in the Early Iron Age during Archaic and Classical times (Lolos and Koskinas, 2011), leaving human activity during the centuries in between quite obscure. We do not see any evidences for human activity in the sediment record. For Asea, we know about human activity due to an archaeological survey (Forsén and Forsén, 2003), but we do not have any clear indications to distinguish human and climate influences in the record (Unkel et al., 2014).

In the Pheneos Polje, Mycenaean and postpalatial (12<sup>th</sup> century BC / 3,100 ± 50 BP) pottery has been observed at ancient Pheneos, complemented by some possibly Geometric sherds that point to settlement activity at least since the 8<sup>th</sup> century BC (2,700 ± 50 BP; Howell, 1970; Tausend, 1999). A second site with Geometric pottery lies on the northern entry of the plain, on a small promontory above the Olbios riverbed (Erath, 1999). However, no further stratigraphical or architectural information has been gained. In contrast to the situation at ancient Pheneos, earlier occupation at this site seems to have ended already in prepalatial times (Late Helladic I, 16<sup>th</sup> century BC / 3,500 ± 50 BP). Although the archaeological evidence is not very abundant, we can assume that the Pheneos Polje was populated during the Late Bronze Age Early Iron Age Transition (ca. 3,150 – 2,650 BP).

In the sediment record of Pheneos, we see a considerable transformation around 3,300 cal BP (179.5 cm), apparent as a drop in terrigenous elements and an increase in carbonate content (Fig. 4), which may be interpreted climatically as a shift towards a drier and/or warmer phase. Although elements in siliciclastic material decrease in concentration, the accumulation rate indicates an increase in erosional input, potentially detrital carbonates, which may be explained by lower vegetational land cover in the catchment due to drier climate. This would be supported by the brighter yellowish-brown colour of the sequence and oxidised patches in the sediment, suggesting episodic desiccation. However, human-induced vegetation clearing may cause similar signals in the sediment and thus this shift may likewise be explained by anthropogenic forcing. According to Knauss (1990), Mycenaean constructed an artificial channel crossing the Pheneos Polje in order to control the Aroanius river and prevent it from flooding the southern and eastern plain (Knauss, 1990). He hypothesizes extensive Mycenaean hydro-engineering constructions according to which our coring spot would be located in a polder area that was subject to controlled flooding and could otherwise be used for agricultural purposes, as it is used today. However, such constructions have never been proven by archaeological excavations, even though water management practices could, to some extent, explain the abrupt shift visible in our geochemical proxies. A direct human influence on the sudden shift in the geochemical

proxies around 3,300 cal BP (14<sup>th</sup> century BC) in Pheneos cannot be confirmed, as archaeological evidence is lacking, but it cannot be excluded either.

### **5.5 The role of seismo-tectonic activity**

As the Peloponnese is a seismically very active region, local seismic activity needs to be considered as one possible influential factor on changes in the hydrological system over time (Weiberg et al., 2016). Norström et al. (2018) even hypothesize that seismic activity had an impact on the isotopic composition of the groundwater system in their study area in the SW Peloponnese. The southern coast of the Gulf of Corinth adjacent to the valleys of Pheneos, Stymphalia and Kaisari is subject to active faulting producing numerous earthquakes each year (Moretti et al., 2003). The best palaeo-seismic record available so far in the proximity of the studied poljes comes from the Aliko Lagoon near Aigion (Kontopoulos and Avramidis, 2003).

So far, we have not found any clear sedimentological or geochemical evidence in our records that we can undoubtedly relate to seismic events such as a structural offset in the sediment or abrupt coarse-grained detrital input. We also found no evidence of deep-water lake sediments, which would suggest a longer blocking of the sinkholes due to seismic activity. Pheneos and Stymphalia have several sinkholes at different locations along the polje margins. Hence, a complete and simultaneous blocking of all sinkholes by one seismic event is rather unlikely. Following the assumptions by Ghilardi et al. (2019) for the Messara plain on Crete, we may also assume for our studied period that the seismo-tectonic activity recorded for the Gulf of Corinth did not affect the inland, the poljes around Mt. Ziria, in the same intensity. More and detailed archaeo-seismological investigations would be needed to identify and date earthquakes in the study region and to investigate whether there was lasting seismo-tectonic influence on the karst hydrological system.

## **6. Conclusions**

Our comparative analysis of proxy responses between neighbouring lakes improved the validity of the palaeoclimatic interpretation compared to single-site studies such as Stymphalia and Asea. It closes some gaps between archaeological sites and palaeoenvironmental archives on the Peloponnese, as called for in the review on the socio-environmental history by Weiberg et al. (2016). However, a thorough understanding of site-specific environmental processes is essential prior to multi-site comparisons, as especially geochemical proxies may respond differently depending on the prevailing preservation, sedimentological, and ecological conditions. Furthermore, the verification of the proxy

interpretation by discrete, destructive methods accompanying non-destructive scanning techniques like XRF is highly recommended. The application of statistical tools, such as PCA, has proven to be useful, because they simplify the complex, multivariate relationships within a lake ecosystem and help to identify the importance of certain geochemical elements and visualise their coherences, here especially in the context of tracing sedimentation processes of carbonate versus siliciclastic material. Based on the geochemical analysis of the four study sites, we identified different phases when permanent lake water bodies existed at all sites, as well as phases when the lakes episodically or at least seasonally dried out. Our analyses showed that Kaisari has never been a deep permanent lake over the last 5,000 years, but regularly dried out. Due to its small size and the comparatively homogeneous catchment, it is not very suitable as a high-resolution palaeoenvironmental archive. In Pheneos, phases with a more permanent lake water body were identified for the Early and Mid-Holocene (9,900 – 9,000 cal BP and 5,100 – 3,600 cal BP), while the period in between can be described as a shallow lacustrine environment. Around the end of the Greek Bronze Age ( $\pm 3,000$  cal BP), a strong transition is observed in the proxies in Pheneos and Kaisari, indicating a shift towards drier conditions. Human impact cannot be excluded as an alternative explanation, but this requires more archaeological evidence in combination with palaeoenvironmental investigations. We did not see any dramatic shift in the proxies, which would hint towards rapid climatic changes with severe impact on the human population but we rather noticed gradual variations. We thus suggest that climatic changes may have been only one factor in a multi-causal interaction network that contributed to but did not cause social transformations.

Our study also shows that geoarchives in meso-scale proximity to each other show similar trends and respond generally in a similar way to climate variations on the next larger scale. However, the mountainous landscape and the specific karst morphology of the Peloponnese cause significant variations in the response of the archives to climate, environmental, and human forcings on a local valley scale. Hence, it would be too simplified to assume societal transformations like the Early Bronze Age II – III transition or the Late Bronze Age to Early Iron Age transition across the entire Peloponnese to be mainly induced by climatic changes like the 4.2 ka event or the 3.2 ka event. Additionally, the uncertainty ranges of radiocarbon-based chronologies, both in most geoarchives and in the archaeological record of the Peloponnese, of sometimes more than 100 years limit the extent to which conclusions on cause and effect within the interaction between humans and their environment can be drawn.

Research to better understand soil development and erosion processes in the research area is still ongoing and important to understand landscape development with respect to increasing anthropogenic

land use. As carbonates are clearly dominating this limestone rich area, it would be highly beneficial to distinguish calcite and aragonite, as well as allochthonous from authigenic carbonates to be able to give precise information on the genesis of the sediments. Further studies on the transformation of the landscape and land-use activities would additionally call for pollen analysis, although pollen preservation is extremely low or sometimes non-existent as test samples from Stymphalia have shown.

## **Appendices**

Supplementary data to this article can be found online

## **Data availability**

Primary data will be uploaded to PANGAEA after acceptance.

## **Funding**

This research was supported by the Collaborative Research Centre 1266 ‘Scales of Transformation – Human-environmental interaction in prehistoric and archaic societies’ of the German Research foundation (DFG, project number 2901391021).

## **Acknowledgements**

We kindly thank our following colleagues and students for their invaluable support in the field: Dimitris Bassukas, Alexandros Emmanouilidis, Konstantinos Nikolaou, and Jan Weber. Sophia Dazert and McKenzie Elliott are acknowledged for support and assistance during laboratory work. Special thanks to Thomas Birndorfer, who was instrumental in creating the map. The project was carried out with the relevant permits from Greek Authorities, the Institute of Geology and Mineral Exploration of Greece (IGME) and the Water Management Body of Decentralization Prefecture of Peloponnese-Western Greece and Ionian Islands.

## **Author Contributions**

JS made the lab work, statistical analyses, and interpretation of the data. JS wrote the manuscript with contributions from all authors, above all from IU and TK. IU and AH are project investigators and designed the project. PA supported the sampling and field campaigns of Pheneos and Kaisari and

contributed to the interpretations. TK and AH provided information on archaeological finds. AS contributed Asea data. All authors have read and approved the final version of the manuscript.

### **Declarations of interest**

The authors declare that they have no conflict of interest.

### **ORCID**

Joana Seguin: <https://orcid.org/0000-0002-4364-512X>

Pavlos Avramidis: <https://orcid.org/0000-0002-8204-970X>

Arndt Schimmelmann: <https://orcid.org/0000-0003-4648-5253>

Ingmar Unkel: <https://orcid.org/0000-0002-8940-1657>

### **References**

- ad-hoc Arbeitsgruppe Boden: Bodenkundliche Kartieranleitung, E. Schweizerbart'sche Verlagbuchhandlung, Hannover, 2005.
- Atherden, M.A., Hall, J.A.: Holocene pollen diagrams from Greece, *Hist. Biol.*, 9, 117–130, doi:10.1080/10292389409380493, 1994.
- Bini, M., Zanchetta, G., Perşoiu, A., Cartier, R., Català, A., Cacho, I., Dean, J.R., Di Rita, F., Drysdale, R.N., Finnè, M., Isola, I., Jalali, B., Lirer, F., Magri, D., Masi, A., Marks, L., Mercuri, A.M., Peyron, O., Sadori, L., Sicre, M.-A., Welc, F., Zielhofer, C., Brisset, E.: The 4.2 ka BP Event in the Mediterranean region: an overview, *Clim. Past*, 15, 555–577, doi:10.5194/cp-15-555-2019, 2019.
- Blaauw, M., Christeny, J.A.: Flexible paleoclimate age-depth models using an autoregressive gamma process, *Bayesian Anal*, 6, 457–474, doi:10.1214/11-BA618, 2011.
- Chen, J., An, Z., Head, J.: Variation of Rb/Sr Ratios in the Loess-Paleosol Sequences of Central China during the Last 130,000 Years and Their Implications for Monsoon Paleoclimatology, *Quat. Res.*, 51, 215–219, doi:10.1006/qres.1999.2038, 1999.
- Chen, J., Chen, Y., Liu, L., Ji, J., Balsam, W., Sun, Y., Lu, H.: Zr/Rb ratio in the Chinese loess sequences and its implication for changes in the East Asian winter monsoon strength, *Geochim.*

- Cosmochim. Acta, 70, 1471–1482, doi:10.1016/j.gca.2005.11.029, 2006.
- Croudace, I.W., Rothwell, R.G.: Micro-XRF Studies of Sediment Cores, Tracking Environmental Change Using Lake Sediments. Volume 2: Physical and Geochemical Methods, Developments in Paleoenvironmental Research, Springer Netherlands, Dordrecht, doi:10.1007/978-94-017-9849-5, 2015.
- Cuven, S., Francus, P., Lamoureux, S.F.: Estimation of grain size variability with micro X-ray fluorescence in laminated lacustrine sediments, Cape Bounty, Canadian High Arctic, J. Paleolimnol., 44, 803–817. doi:10.1007/s10933-010-9453-1, 2010.
- Davison, W.: Iron and manganese in lakes, Earth Sci. Rev., 34, 119–163, doi:10.1016/0012-8252(93)90029-7, 1993.
- Drake, B.L.: The influence of climatic change on the Late Bronze Age Collapse and the Greek Dark Ages, J. Archaeol. Sci., 39, 1862–1870, doi:10.1016/j.jas.2012.01.029, 2012.
- Dypvik, H., Harris, N.B.: Geochemical facies analysis of fine-grained siliciclastics using Th/U, Zr/Rb and (Zr + Rb)/Sr ratios, Chem. Geol., 181, 131–146, doi:10.1016/S0009-2541(01)00278-9, 2001.
- Emmanouilidis, A., Katrantsiotis, C., Norström, E., Risberg, J., Kylander, M., Sheik, T.A., Iliopoulos, G., Avramidis, P.: Middle to late Holocene palaeoenvironmental study of Gialova Lagoon, SW Peloponnese, Greece, Quat. Int., 476, 46–62, doi:10.1016/j.quaint.2018.03.005, 2018.
- Emmanouilidis, A., Unkel, I., Triantaphyllou, M., Avramidis, P.: Late Holocene coastal depositional environments and climate changes in Gulf of Corinth, Greece, The Holocene, <https://doi.org/10.1177/0959683619875793>, 2019.
- Erath, G.: Archäologische Funde im Becken von Pheneos, in: Pheneos Und Lousoi - Untersuchungen Zu Geschichte Und Topographie Nordostarkadiens, edited by: Tausend, K., Frankfurt am Main, 199–237, 1999.
- Finné, M., Holmgren, K., Shen, C.-C., Hu, H.-M., Boyd, M., Stocker, S.: Late Bronze Age climate change and the destruction of the Mycenaean Palace of Nestor at Pylos, PLoS One, 12, e0189447, doi:10.1371/journal.pone.0189447, 2017.
- Finné, M., Holmgren, K., Sundqvist, H.S., Weiberg, E., Lindblom, M.: Climate in the eastern Mediterranean, and adjacent regions, during the past 6000 years - A review, J. Archaeol. Sci., 38, 3153–3173, doi:10.1016/j.jas.2011.05.007, 2011.



- Finné, M., Woodbridge, J., Labuhn, I., Roberts, C.N.: Holocene hydro-climatic variability in the Mediterranean: A synthetic multi-proxy reconstruction, *The Holocene*, 29, 847–863, doi:10.1177/0959683619826634, 2019.
- Forsén, J., Forsén, B.: *The Asea Valley Survey. An Arcadian Mountain Valley from the Palaeolithic Period until Modern Times*, Paul Åströms Förlag, Stockholm, 2003.
- Ghilardi, M., Revelles, J., Glais, A., Theodorakopoulou, K., Theodoropoulou, T., Lespez, L., Longo, F., Rossi, A., Bellier, O., Benedetti, L., Fleury, J.: Reconstructing human-environment interactions in the western Messara Plain (Phaistos, Crete, Greece) from the emergence of city states to Byzantine times, *J. Archaeol. Sci. Reports*, 26, 101909, doi:10.1016/j.jasrep.2019.101909, 2019.
- Grootes, P.M., Nadeau, M.-J., Rieck, A.: 14C-AMS at the Leibniz-Labor: radiometric dating and isotope research, *Nucl. Instruments Methods Phys. Res. Sect. B Beam Interact. with Mater. Atoms*, 223–224, 55–61, doi:10.1016/j.nimb.2004.04.015, 2004.
- Heymann, C., Nelle, O., Dörfler, W., Zagana, H., Nowaczyk, N., Xue, J., Unkel, I.: Late Glacial to mid-Holocene palaeoclimate development of southern Greece inferred from the sediment sequence of Lake Stymphalia (NE-Peloponnese), *Quat. Int.*, 302, 42–60, doi:10.1016/j.quaint.2013.02.014, 2013.
- Howell, R.: A Survey of Eastern Arcadia in Prehistory, *Annu. Br. Sch. Athens*, 65, 79–127, doi:10.1017/S0068245400014702, 1970.
- Institute of Geology and Mineral Exploration of Greece (IGME): *Geological Map of Greece, 1:50000 (Sheet Kollinai)*, Athens, 2002.
- Institute of Geology and Mineral Exploration of Greece (IGME): *Geological Map of Greece, 1:50000 (Sheet Megalopolis)*, Athens, 1992.
- Institute of Geology and Mineral Exploration of Greece (IGME): *Geological Map of Greece, 1:50000 (Sheet Kandila)*, Athens, 1982.
- Institute of Geology and Mineral Exploration of Greece (IGME): *Geological Map of Greece, 1:50000 (Sheet Nemea)*, Athens, 1970.
- Isola, I., Zanchetta, G., Drysdale, R.N., Regattieri, E., Bini, M., Bajo, P., Hellstrom, J.C., Baneschi, I., Lionello, P., Woodhead, J., Greig, A.: The 4.2 ka event in the central Mediterranean: new data from a Corchia speleothem (Apuan Alps, central Italy), *Clim. Past*, 15, 135–151,

doi:10.5194/cp-15-135-2019, 2019.

- Izdebski, A., Pickett, J., Roberts, N., Waliszewski, T.: The environmental, archaeological and historical evidence for regional climatic changes and their societal impacts in the Eastern Mediterranean in Late Antiquity, *Quat. Sci. Rev.*, 136, 189–208, doi:10.1016/j.quascirev.2015.07.022, 2016.
- Jahns, S.: On the Holocene vegetation history of the Argive Plain (Peloponnese, southern Greece), *Veg. Hist. Archaeobot.*, 2, 187–203, doi:10.1007/bf00198161, 1993.
- Jin, Z., Cao, J., Wu, J., Wang, S.: A Rb/Sr record of catchment weathering response to Holocene climate change in Inner Mongolia, *Earth Surf. Process. Landforms*, 31, 285–291, doi:10.1002/esp.1243, 2006.
- Kaniewski, D., Marriner, N., Cheddadi, R., Guiot, J., Van Campo, E.: The 4.2ka BP event in the Levant, *Clim. Past*, 14, 1–29, doi:10.5194/cp-2018-82, 2018.
- Kaniewski, D., Van Campo, E., Guiot, J., Le Burel, S., Otto, T., Baeteman, C.: Environmental Roots of the Late Bronze Age Crisis, *PLoS One*, 8, 1–10, doi:10.1371/journal.pone.0071004, 2013.
- Katrantsiotis, C., Kylander, M.E., Smittenberg, R., Yamoah, K.K.A., Hättestrand, M., Avramidis, P., Strandberg, N.A., Norström, E.: Eastern Mediterranean hydroclimate reconstruction over the last 3600 years based on sedimentary *n*-alkanes, their carbon and hydrogen isotope composition and XRF data from the Gialova Lagoon, SW Greece, *Quat. Sci. Rev.*, 194, 77–93, doi:10.1016/j.quascirev.2018.07.008, 2018.
- Katrantsiotis, C., Norström, E., Smittenberg, R.H., Finne, M.: Climate changes in the Eastern Mediterranean over the last 5000 years and their links to the high-latitude atmospheric patterns and Asian monsoons, *Glob. Planet. Change*, 175, 36–51, doi:10.1016/j.gloplacha.2019.02.001, 2019.
- Kissas, K.: *Ancient Corinthia. From Prehistoric Times to the End of Antiquity*, Foinikas Publications, Athens, 2013.
- Knauss, J.: Der Graben des Herakles im Becken von Pheneos und die Vertreibung der stymphalischen Vögel, *MDAI(A)*, 105, 52, 1990.
- Koinig, K.A., Shotyk, W., Lotter, A.F., Ohlendorf, C., Sturm, M.: 9000 years of geochemical evolution of lithogenic major and trace elements in the sediment of an alpine lake – the role of climate, vegetation, and land-use history, *J. Paleolimnol.*, 30, 307–320,

doi:10.1023/A:1026080712312, 2003.

- Kontopoulos, N., Avramidis, P.: A late Holocene record of environmental changes from the Aliko lagoon, Egion, North Peloponnesus, Greece, *Quat. Int.*, 111, 75–90, doi:10.1016/S1040-6182(03)00016-8, 2003.
- Kylander, M.E., Ampel, L., Wohlfarth, B., Veres, D.: High-resolution X-ray fluorescence core scanning analysis of Les Echets (France) sedimentary sequence: new insights from chemical proxies, *J. Quat. Sci.*, 26, 109–117, doi:10.1002/jqs.1438, 2011.
- Lolos, Y.A., Koskinas, A.: *Land of Sikyon. Archaeology and History of a Greek City-state*, Hesperia Supplement, American School of Classical Studies at Athens, Princeton, NJ, 2011.
- Luterbacher, J., García-Herrera, R., Akcer-On, S., Allan, R., Alvarez-Castro, M.-C., Benito, G., Booth, J., Büntgen, U., Cagatay, N., Colombaroli, D., Davis, B., Esper, J., Felis, T., Fleitmann, D., Frank, D., Gallego, D., Garcia-Bustamante, E., Glaser, R., Gonzalez-Rouco, F.J., Goosse, H., Kiefer, T., Macklin, M.G., Manning, S.W., Montagna, P., Newman, L., Power, M.J., Rath, V., Ribera, P., Riemann, D., Roberts, N., Sicre, M.-A., Silenzi, S., Tinner, W., Tzedakis, P.C., Valero-Garcés, B., van der Schrier, G., Vannièrè, B., Vogt, S., Wanner, H., Werner, J.P., Willett, G., Williams, M.H., Xoplaki, E., Zerefos, C.S., Zorita, E.: A Review of 2000 Years of Paleoclimatic Evidence in the Mediterranean, in: *The Climate of the Mediterranean Region*, edited by: Lionello, P., Elsevier, 87–185. doi:10.1016/B978-0-12-416042-2.00002-1, 2012.
- Masi, A., Francke, A., Pepe, C., Thienemann, M., Wagner, B., Sadori, L.: Vegetation history and paleoclimate at Lake Dojran (FYROM/Greece) during the Late Glacial and Holocene, *Clim. Past*, 14, 351–367, doi:10.5194/cp-14-351-2018, 2018.
- Mayewski, P.A., Rohling, E.E., Curt Stager, J., Karlén, W., Maasch, K.A., Meeker, L.D., Meyerson, E.A., Gasse, F., van Kreveld, S., Holmgren, K., Lee-Thorp, J., Rosqvist, G., Rack, F., Staubwasser, M., Schneider, R.R., Steig, E.J.: Holocene Climate Variability, *Quat. Res.*, 62, 243–255, doi:10.1016/j.yqres.2004.07.001, 2004.
- Meyers, P.A.: Applications of organic geochemistry to paleolimnological reconstructions: A summary of examples from the Laurentian Great Lakes, *Org. Geochem.*, 34, 261–289, doi:10.1016/S0146-6380(02)00168-7, 2003.
- Meyers, P.A., Ishiwatari, R.: Lacustrine organic geochemistry-an overview of indicators of organic matter sources and diagenesis in lake sediments, *Org. Geochem.*, 20, 867–900, doi:10.1016/0146-6380(93)90100-P, 1993.

- Meyers, P.A., Lallier-Vergès, E.: Lacustrine sedimentary organic matter records of Late Quaternary paleoclimates, *J. Paleolimnol.*, 21, 345–372, 1999.
- Mook, W.G., van der Plicht, J.: Reporting  $^{14}\text{C}$  activities and concentrations, *Radiocarbon*, 41, 227–239, doi:10.1017/S0033822200057106, 1999.
- Moretti, I., Sakellariou, D., Lykousis, V., Micarelli, L.: The Gulf of Corinth: An active half graben?, *J. Geodyn.*, 36, 323–340, doi:10.1016/S0264-3707(03)00053-X, 2003.
- Morfis, A., Zojer, H.: Karst Hydrogeology of the Central and Eastern Peloponnesus (Greece), *Steir. Beitr. zur Hydrogeol.*, 37/38, 1–301, 1986.
- Munsell, A.H.: Munsell Soil Color Charts, Munsell Color, Grand Rapids, 2000.
- Naeher, S., Gilli, A., North, R.P., Hamann, Y., Schubert, C.J.: Tracing bottom water oxygenation with sedimentary Mn/Fe ratios in Lake Zurich, Switzerland, *Chem. Geol.*, 352, 125–133, doi:10.1016/j.chemgeo.2013.06.006, 2013.
- Nanou, E.-A., Zagana, E.: Groundwater Vulnerability to Pollution Map for Karst Aquifer Protection (Ziria Karst System, Southern Greece), *Geosciences*, 8, 125, doi:10.3390/geosciences8040125, 2018.
- Neugebauer, I., Brauer, A., Schwab, M.J., Dulski, P., Frank, U., Hadzhiivanova, E., Kitagawa, H., Litt, T., Schiebel, V., Taha, N., Waldmann, N.D.: Evidences for centennial dry periods at ~3300 and ~2800 cal. yr BP from micro-facies analyses of the Dead Sea sediments, *The Holocene*, 25, 1358–1371, doi:10.1177/0959683615584208, 2015.
- Norström, E., Katrantsiotis, C., Finné, M., Risberg, J., Smittenberg, R.H., Bjursäter, S.: Biomarker hydrogen isotope composition ( $\delta\text{D}$ ) as proxy for Holocene hydroclimatic change and seismic activity in SW Peloponnese, Greece, *J. Quat. Sci.*, 33, 563–574, doi:10.1002/jqs.3036, 2018.
- Psomiadis, D., Dotsika, E., Albanakis, K., Ghaleb, B., Hillaire-Marcel, C.: Speleothem record of climatic changes in the northern Aegean region (Greece) from the Bronze Age to the collapse of the Roman Empire, *Palaeogeogr. Palaeoclimatol. Palaeoecol.*, 489, 272–283, doi:10.1016/j.palaeo.2017.10.021, 2018.
- R Core Team: R: A language and environment for statistical computing, R Foundation for Statistical Computing, Vienna, Austria, 2019.
- Reimer, P.J., Baillie, M.G.L., Bard, E., Bayliss, A., Beck, J.W., Blackwell, P.G., Bronk Ramsey, C., Buck, C.E., Burr, G.S., Edwards, R.L., Friedrich, M., Grootes, P.M., Guilderson, T.P., Hajdas,

- I., Heaton, T.J., Hogg, A.G., Hughen, K.A., Kaiser, K.F., Kromer, B., McCormac, F.G., Manning, S.W., Reimer, R.W., Richards, D.A., Southon, J.R., Talamo, S., Turney, C.S.M., van der Plicht, J., Weyhenmeyer, C.E.: IntCal09 and Marine09 Radiocarbon Age Calibration Curves, 0–50,000 Years cal BP, *Radiocarbon*, 51, 1111–1150, doi:10.1017/S0033822200034202, 2009.
- Reimer, P.J., Bard, E., Bayliss, A., Beck, J.W., Blackwell, P.G., Ramsey, C.B., Buck, C.E., Cheng, H., Edwards, R.L., Friedrich, M., Grootes, P.M., Guilderson, T.P., Haflidason, H., Hajdas, I., Hatté, C., Heaton, T.J., Hoffmann, D.L., Hogg, A.G., Hughen, K.A., Kaiser, K.F., Kromer, B., Manning, S.W., Niu, M., Reimer, R.W., Richards, D.A., Scott, E.M., Southon, J.R., Staff, R.A., Turney, C.S.M., van der Plicht, J.: IntCal13 and Marine13 Radiocarbon Age Calibration Curves 0–50,000 Years cal BP, *Radiocarbon*, 55, 1869–1887, doi:10.2458/azu\_js\_rc.55.16947, 2013.
- Roberts, N., Allcock, S.L., Arnaud, F., Dean, J.R., Eastwood, W.J., Jones, M.D., Leng, M.J., Metcalfe, S.E., Malet, E., Woodbridge, J., Yiğitbaşıoğlu, H.: A tale of two lakes: a multi-proxy comparison of Lateglacial and Holocene environmental change in Cappadocia, Turkey, *J. Quat. Sci.*, 31, 348–362, doi:10.1002/jqs.2852, 2016.
- Roberts, N., Eastwood, W.J., Kuzucuoğlu, C., Fiorentino, G., Caracuta, V.: Climatic, vegetation and cultural change in the eastern Mediterranean during the mid-Holocene environmental transition, *The Holocene*, 21, 147–162, doi:10.1177/0959683610386819, 2011.
- Roberts, N., Jones, M.D., Benkaddour, A., Eastwood, W.J., Filippi, M.L., Frogley, M.R., Lamb, H.F., Leng, M.J., Reed, J.M., Stein, M., Stevens, L., Valero-Garcés, B., Zanchetta, G.: Stable isotope records of Late Quaternary climate and hydrology from Mediterranean lakes: the ISOMED synthesis, *Quat. Sci. Rev.*, 27, 2426–2441, doi:10.1016/j.quascirev.2008.09.005, 2008.
- Rothacker, L., Dosseto, A., Francke, A., Chivas, A.R., Vigier, N., Kotarba-Morley, A.M., Menozzi, D.: Impact of climate change and human activity on soil landscapes over the past 12,300 years, *Sci. Rep.*, 8, 247, doi:10.1038/s41598-017-18603-4, 2018.
- Seguin, J., Bintliff, J.L., Grootes, P.M., Bauersachs, T., Dörfler, W., Heymann, C., Manning, S.W., Müller, S., Nadeau, M.J., Nelle, O., Steier, P., Weber, J., Wild, E.M., Zagana, E., Unkel, I.: 2500 years of anthropogenic and climatic landscape transformation in the Stymphalia polje, Greece, *Quat. Sci. Rev.*, 213, 133–154, doi:10.1016/j.quascirev.2019.04.028, 2019.
- Tausend, K.: Die Siedlungen im Gebiet von Pheneos, in: Pheneos Und Lousoi. Untersuchungen Zu Geschichte Und Topographie Nordostarkadiens, edited by: Tausend, K., Frankfurt am Main,

331–342, 1999.

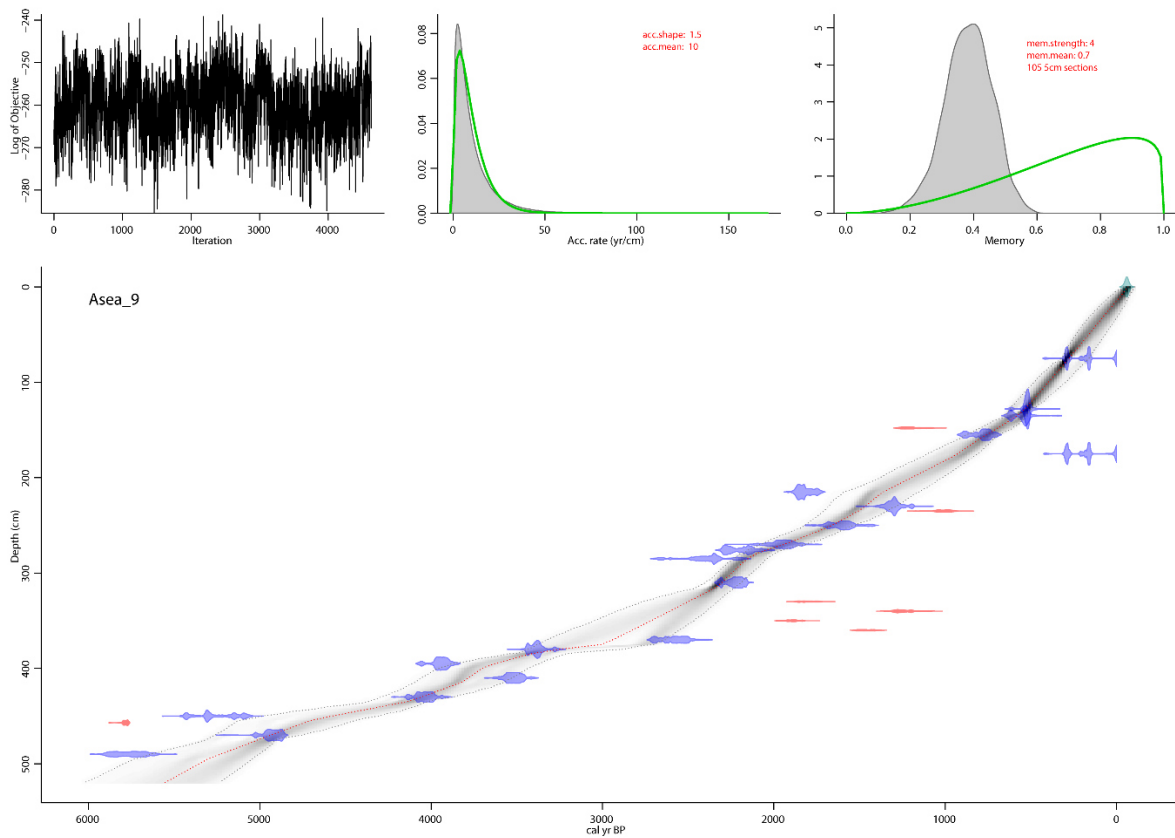
- Unkel, I., Schimmelmann, A., Shriner, C., Forsén, J., Heymann, C., Brückner, H.: The environmental history of the last 6500 years in the Asea Valley (Peloponnese, Greece) and its linkage to the local archaeological record, *Zeitschrift für Geomorphol. Suppl. Issues*, 58, 89–107, doi:10.1127/0372-8854/2014/S-00160, 2014.
- Vaezi, A., Ghazban, F., Tavakoli, V., Routh, J., Beni, A.N., Bianchi, T.S., Curtis, J.H., Kylin, H.: A Late Pleistocene-Holocene multi-proxy record of climate variability in the Jazmurian playa, southeastern Iran, *Palaeogeogr. Palaeoclimatol. Palaeoecol.*, 514, 754–767, doi:10.1016/j.palaeo.2018.09.026, 2019.
- van Geel, B., Heijnis, H., Charman, D.J., Thompson, G., Engels, S.: Bog burst in the eastern Netherlands triggered by the 2.8 kyr BP climate event, *The Holocene*, 24, 1465–1477, doi:10.1177/0959683614544066, 2014.
- Viehberg, F.A., Just, J., Dean, J.R., Wagner, B., Franz, S.O., Klasen, N., Kleinen, T., Ludwig, P., Asrat, A., Lamb, H.F., Leng, M.J., Rethemeyer, J., Milodowski, A.E., Claussen, M., Schäbitz, F.: Environmental change during MIS4 and MIS 3 opened corridors in the Horn of Africa for *Homo sapiens* expansion, *Quat. Sci. Rev.*, 202, 139–153, doi:10.1016/j.quascirev.2018.09.008, 2018.
- Walker, M., Head, M.J., Lowe, J., Berkelhammer, M., Björck, S., Cheng, H., Cwynar, L.C., Fisher, D., Gkinis, V., Long, A., Newnham, R., Rasmussen, S.O., Weiss, H.: Subdividing the Holocene Series/Epoch: formalization of stages/ages and subseries/subepochs, and designation of GSSPs and auxiliary stratotypes, *J. Quat. Sci.*, 34, 173–186, doi:10.1002/jqs.3097, 2019.
- Walsh, K., Berger, J.-F., Roberts, C.N., Vanniere, B., Ghilardi, M., Brown, A.G., Woodbridge, J., Lespez, L., Estrany, J., Glais, A., Palmisano, A., Finné, M., Verstraeten, G.: Holocene demographic fluctuations, climate and erosion in the Mediterranean: A meta data-analysis, *The Holocene*, 29, 864–885, doi:10.1177/0959683619826637, 2019.
- Walsh, K., Brown, A.G., Gourley, B., Scaife, R.: Archaeology, hydrogeology and geomorphology in the Stymphalos valley, *J. Archaeol. Sci. Reports*, 15, 446–458, doi:10.1016/j.jasrep.2017.03.058, 2017.
- Warren, S.F., Fohlmeister, J., Schröder-Ritzrau, A., Constantin, S., Spötl, C., Gerdes, A., Esper, J., Frank, N., Arps, J., Terente, M., Riechelmann, D.F.C., Mangini, A., Scholz, D.: Reconstruction of late Holocene autumn/winter precipitation variability in SW Romania from a high-resolution

- speleothem trace element record, *Earth Planet. Sci. Lett.*, 499, 122–133, doi:10.1016/j.epsl.2018.07.027, 2018.
- Weiberg, E., Unkel, I., Kouli, K., Holmgren, K., Avramidis, P., Bonnier, A., Dibble, F., Finné, M., Izdebski, A., Katrantsiotis, C., Stocker, S.R., Andwinge, M., Baika, K., Boyd, M., Heymann, C.: The socio-environmental history of the Peloponnese during the Holocene: Towards an integrated understanding of the past, *Quat. Sci. Rev.*, 136, 40–65, doi:10.1016/j.quascirev.2015.10.042, 2016.
- Weltje, G.J., Tjallingii, R.: Calibration of XRF core scanners for quantitative geochemical logging of sediment cores: Theory and application, *Earth Planet. Sci. Lett.*, 274, 423–438, doi:10.1016/j.epsl.2008.07.054, 2008.
- Williams, E.H.: Stymphalos: A Planned City of Ancient Arcadia, *Echos du Monde Class. = Class. Views* 27, 194–205, 1983.
- Williams, H.: Archaeological Investigations at Ancient Stymphalos, 1982–2008, in: *The Corinthia and the Northeast Peloponnese. Topography and History from Prehistoric Times until the End of Antiquity*, edited by: Kissas, K., Niemeier, W.D., Munich, 425–431, 2013.
- Williams, H.: *Excavations at Stymphalos, Preliminary Reports 1983 - 2005*, Museion, 2005.
- Xu, H., Liu, B., Wu, F., Dasch, E., Liu, C., Zhang, J., Li, C., Chen, J., An, Z., Head, J., Chen, J., An, Z., Liu, L., Ji, J., Yang, J., Chen, Y., Jin, Z., Cao, J., Wu, J., Wang, S., Xu, H., Liu, X., An, Z., Hou, Z., Dong, J., Xu, H., Ai, L., Tan, L., An, Z., Xu, H., Hou, Z., An, Z., Liu, X., Dong, J., Pang, J., Huang, C., Zhang, Z., Li, F., Xie, C., Pan, G., Xu, H., Hou, Z., Ai, L., Tan, L.: Spatial and temporal variations of Rb/Sr ratios of the bulk surface sediments in Lake Qinghai, *Geochem. Trans.*, 11, 3, doi:10.1186/1467-4866-11-3, 2010.
- Yanhong, W., Lücke, A., Zhangdong, J., Sumin, W., Schleser, G.H., Battarbee, R.W., Weilan, X.: Holocene climate development on the central Tibetan Plateau: A sedimentary record from Cuoe Lake, *Palaeogeogr. Palaeoclimatol. Palaeoecol.*, 234, 328–340, doi:10.1016/j.palaeo.2005.09.017, 2006.
- Zanchetta, G., Regattieri, E., Isola, I., Drysdale, R.N., Bini, M., Baneschi, I., Hellstrom, J.C.: The so-called “4.2 event” in the central Mediterranean and its climatic teleconnections, *Alp. Mediterr. Quat.*, 29, 5–17, 2016.
- Zanchetta, G., Sulpizio, R., Roberts, N., Cioni, R., Eastwood, W.J., Siani, G., Caron, B., Paterne, M.,

Santacroce, R.: Tephrostratigraphy, chronology and climatic events of the Mediterranean basin during the Holocene: An overview, *The Holocene*, 21, 33–52, doi:10.1177/0959683610377531, 2011.

## Supplementary Material

**Supplementary Material 1: Revised Bayesian age-depth model for Asea. The model was constructed using the R package rbacon (Blaauw and Christen, 2011). The blue tie bars indicate the  $^{14}\text{C}$  age distributions. Outliers are plotted in red and were excluded from modelling. The greyscale of the line graph reflects the likelihood; the darker the more likely the model passes through that age. The red dotted line follows the mean ages.**





**Supplementary Material 2: Sedimentary units of core PHE1. The soil type classification follows the German ad-hoc Arbeitsgemeinschaft Boden (2005). (UB = upper boundary, G = gradational).**

Core Depth [cm]	Sediment Unit	Unit Thickness [cm]	Munsell Color	Soil Type	Description
0–46	9	46	10YR 5/3 brown	Tu4	homogeneous brown, hardly mottled, well mixed, very compact, plough horizon, excluded from analysis
46–83	8	37	10YR 4/4 brown (slight greyish touch)	Ut3	similar to unit 7 without red colour, few shell fragments, fewer blackish mottles and more homogeneous than unit 7, blackish clasts at 83-73 cm, (UB = G)
83–156	7	73	10YR 4/3 brown	Ut4	slightly brighter than unit 6 but with reddish patches (decreasing towards top), slightly more blackish/charcoal flitter, few shell fragments (gastropods), absence of clasts - only fine matrix, (UB = very G)
156–192	6	36	10YR 4/3 brown	Ut4	yellow-grey-mottled, fine charcoal particles intensely visible up to 180 cm, absence of clasts - only fine matrix, very few shell fragments, (UB = G)
192–235	5	43	10 YR 3/2 very dark greyish brown	Ut3	sub-angular clasts of up to 1 cm diameter decreasing towards top, sediment getting brighter, continuous charcoal particles, very tiny shell fragments, (UB = G)
235–300	4	65	10 YR 4/3 dark yellowish brown	Ut4	fewer clasts but darker colour and larger than in unit 2+3, all clasts are subangular, colour is similar to unit 3 with lots of orange mottles and gets slightly darker towards top, continuous charcoal particles/slightly fewer than in unit 3, some very tiny shell fragments, (UB = very G)
300–329	3	29	10 YR 4/3 or 4/4 dark yellowish brown	Ut4	more abundant small, in situ formed carbonate nodules <55 mm than in unit 2, clay matrix but less clayey than in unit 2 - dull surface (similar to unit 2 but brighter colour), water holes at 3.28 and 3.23 m, orange patches e.g. 3.46 m, darker in central part of the unit, (UB = G)
329–360	2	31	10 YR 3/1 very dark grey	Ut4	clayey matrix, darkest unit, occasional orange spots (oxidation), occasional gravel clasts with max. 5 mm diameter, 346-360 cm: minor charcoal particles, (UB = G)
360–390	1	30	10YR 4/4 dark yellowish brown	Ut3	mix of grey-brown-yellow and white-orange-oxidized mottles, brightest unit, fine matrix with clasts and carbonate nodules of up to 1 cm diameter, clasts are subangular and unsorted, gravel content decreases upwards, increase in organic content (= black colour intensifies, charcoal flitter visible), fining upwards, (UB = G)

*Supplementary Material 3: Sedimentary units of core KES2. The soil type classification follows the German ad-hoc Arbeitsgemeinschaft Boden (2005). (UB = upper boundary, G = gradational)*

Core Depth [cm]	Sediment Unit	Unit Thickness [cm]	Munsell Color	Soil Type	Description
0–50	7	50	10YR 4/4 dark yellowish brown	Ut4	plough horizon, plant remains and roots in upper 15 cm visible, core segment strongly damaged - difficult to delimit boundaries, excluded from analysis
50–125	6	75	10YR 5/4 yellowish brown	Ut4	similar to unit 5 but black speckles become fewer, gets brighter towards top, less mottled, silt content increasing upwards, patches of red soil and brick/loam? (e.g. 1.10 m; 1.00 m; 0.87 m), unit becomes brighter towards top (UB = G)
125–165	5	40	2.5 Y 4/3 olive brown	Ut3	darker olive-grey colour, black speckles, higher organic content, strongly mottled, (UB = G)
165–205	4	40	2.5 Y 6/4 light yellowish brown	Ut4	brightest unit of the core, yellowish-beige colour, especially visible in 2c while 2b resembles more unit 3, unit has a very different morphostructure: matt, airy, very high carbonate content, (UB = seepage water shift?)
205–240	3	35	10YR 5/3 brown	Ut4	similar to unit 2 but less reddish instead more greyish colour, high carbonate content, few shell fragments (UB = G)
240–310	2	70	7.5 YR 4/4 brown	Ut4	reddish colour dominates, contains most black speckles in whole core sequence, very strongly mottled, very clayey adhesive but matt surface, no shell fragments visible, (UB = G)
310–350	1	40	2.5Y 5/3 light olive brown	Ut3	matrix beige-yellowish-greenish-gley shimmer with black and yellow-orange speckles, some shell fragments throughout the unit, black spots look finely dotted, (UB = G)

# Appendix III



# **A 2,600 years high-resolution climate record from Lake Trichonida (SW Greece)**

Joana Seguin<sup>1\*</sup>, Pavlos Avramidis<sup>2</sup>, Walter Dörfler<sup>3</sup>, Alexandros Emmanouilidis<sup>2</sup>, Ingmar Unkel<sup>1</sup>

<sup>1</sup>Institute for Ecosystem Research, Christian-Albrechts-University, Olshausenstraße 75, 24118 Kiel, Germany

<sup>2</sup>Department of Geology, University of Patras, Rio 26504 Patras, Greece

<sup>3</sup>Institute of Pre- and Protohistoric Archaeology, Christian-Albrechts-University, Johanna-Mestorf-Straße 2-6, 24118 Kiel, Germany

\*Corresponding author: jseguin@ecology.uni-kiel.de

## **Keywords**

*Palaeoclimate reconstruction; Eastern Mediterranean; Greece; Sedimentology; XRF; NAO*

## **Abstract**

This paper aims at reconstructing the palaeoclimatic changes during the last 2,600 years in southern Greece based on a proxy record from Lake Trichonida. For the first time, we provide a solid age-depth model and continuous geochemical data for the largest and deepest lake in Greece. We use XRF geochemical data supported by discrete measurements of XRD, grain size distribution, and organic matter content to investigate changes in the ecosystem and identify the major forcing mechanisms. A principal component analysis identifies the variation between carbonate rich and terrigenous material as the dominating process and we interpret it as depicting fluctuations in the hydrological conditions. The first principal component (PC1) shows a very strong correlation with  $\log(\text{Rb}/\text{Sr})$ . When comparing the PC1 summary proxy to independent proxies from the Balkan region, we find generally concurring patterns on a multi-decadal to centennial scale. We show that phases with wetter conditions at Lake Trichonida coincide with a more negative North Atlantic Oscillation (NAO) index, suggesting that the precipitation variability in southern Greece is linked to changes in the NAO atmospheric pattern, as one major driving force. A cluster analysis highlights the similarities in the sediment characteristics deposited during wetter phases, notably during 1850 – 1750 cal BP, 1500 – 1400 cal BP, ca. 1100 cal BP, and ca. 100 cal BP.

As human impact on the lake seems to be constantly present but marginal, the 2,600-year long sedimentary record of Lake Trichonida contributes to our understanding of late Holocene palaeohydrological changes in an important climatic transitional zone in the Eastern Mediterranean.

## **Zusammenfassung**

In diesem Artikel rekonstruieren wir paläoklimatische Veränderungen der vergangenen 2600 Jahre in Südgriechenland anhand von Proxies aus dem See Trichonida.

Erstmals stellen wir ein stabiles Alterstiefenmodell, sowie durchgängige, geochemische Daten für den größten griechischen See zur Verfügung. Wir verwenden XRF geochemische Daten, unterstützt durch diskrete XRD Messungen, Korngrößenverteilungen und Messungen des Organikgehalts, um Änderungen im Ökosystem zu untersuchen und deren Haupteinflussfaktoren zu ermitteln. Mittels einer Hauptkomponentenanalyse identifizieren wir die Schwankungen zwischen Carbonaten auf der einen und terrigenem Material auf der anderen Seite als dominierenden Prozess und interpretieren diese Schwankungen als Änderungen in den hydrologischen Gegebenheiten. Ein Vergleich der ersten Hauptkomponente (PC1), welche hohe Übereinstimmungen mit  $\log(\text{Rb}/\text{Sr})$  aufweist, mit unabhängigen Proxies anderer Studien aus der Balkanregion zeigt grundsätzlich übereinstimmende Muster auf multidekadischen bis hundertjährigen Zeitskalen. Wir zeigen, dass Phasen mit feuchteren Bedingungen im Einzugsgebiet des Sees Trichonida mit einem negativem NAO Index zusammenfallen, woraus sich schließen lässt, dass die Niederschlagsvariabilität in Südgriechenland zu einem Großteil von Veränderungen in dem Nordatlantischen Oszillationsmuster geprägt ist. Eine Clusteranalyse verdeutlicht die Ähnlichkeiten in den Eigenschaften der Sedimente, welche während feuchterer Phasen abgelagert wurden, insbesondere in den Zeiträumen 1850 – 1750 cal BP, 1500 – 1400 cal BP, ca. 1100 cal BP und ca. 100 cal BP.

Menschlicher Einfluss auf den See scheint kontinuierlich, jedoch marginal zu sein, so dass der 2600 Jahre abdeckende Sedimentkern zu unserem Verständnis natürlicher, spätholozäner paläohydrologischer Schwankungen in einer klimatisch wichtigen Übergangszone im östlichen Mittelmeer beiträgt.

## **1. Introduction**

Climatic changes and anthropogenic land-use are two of the most significant driving forces of hydrological and geomorphological processes. As the interaction and connectivity between humans, climate and environment are complex, it is necessary – though challenging – to differentiate anthropogenic from climatic impacts on landscape development over long timescales. Due to the long history of human-environmental interaction in the Mediterranean, the region is especially valuable for interdisciplinary studies on past climate variability and human activity (McCormick et al., 2012; Mercuri and Sadori, 2014; Roberts et al., 2011; Weiberg et al., 2016).

Greece is located in a transitional zone between the temperate climate and the Mediterranean climate. Different large-scale atmospheric circulation patterns influence the Greek and Eastern Mediterranean climate, such as the North Atlantic Oscillation (NAO), the Siberian High Pressure System, and the East Atlantic/West Russia (EA/WR) pattern, mainly in winter, as well as the South Asian Monsoon in summer (Barnston and Livezey, 1987; Xoplaki et al., 2003b, 2003a). However, the rugged topography with its strong relief gradients leads to quite a heterogeneous modulation of these large-scale teleconnection patterns on a local level, influencing for example the amount of mean annual precipitation (Xoplaki et al., 2003a).

In southern Greece, high-resolution environmental archives completely covering the last 2,600 years have been relatively sparse, often incomplete, or present divergent results (Finné et al., 2011, 2019; Katrantsiotis et al., 2019; Luterbacher et al., 2012), but the number of studies has been increasing recently (Emmanouilidis et al., 2018, 2019, Katrantsiotis et al., 2018, 2019, Seguin et al., 2019a, 2019b). For the last 2,600 years, a couple of major climatic phases and events have been identified for different regions across Europe, such as the Roman Warm Period (RWP, ca. 2200 – 1550 BP; Luterbacher et al., 2016; McCormick et al., 2012b; Morellón et al., 2016; Wilson et al., 2016), the Late Antique Little Ice Age or Migration Period (LALIA, ca. 1400 – 1600 BP; Büntgen et al., 2016; Helama et al., 2017)), the Medieval Climate Anomaly (MCA, ca. 1000 – 700 BP; Christiansen and Ljungqvist, 2017; Keigwin, 1996; Mangini et al., 2005), and the Little Ice Age (LIA, ca. 700 – 100 BP; Christiansen and Ljungqvist, 2017; Keigwin, 1996; Kelly and Ó Grada, 2014a). It seems however that their manifestations was spatially and temporally very different (Neukom et al., 2019) and local studies are needed to investigate the partly diverging characteristics.

In this article, we present a new sedimentological archive from Lake Trichonida. Our aims are (1) to obtain a solid age-depth model for the largest Greek lake, (2) to compile high-resolution geochemical records for palaeoclimatic reconstructions from Lake Trichonida, and (3) to study climatic trends in southern Greece and investigate major forcing mechanisms during the Late Holocene by comparing our results with independent palaeoclimate studies from the Balkan and the Eastern Mediterranean.

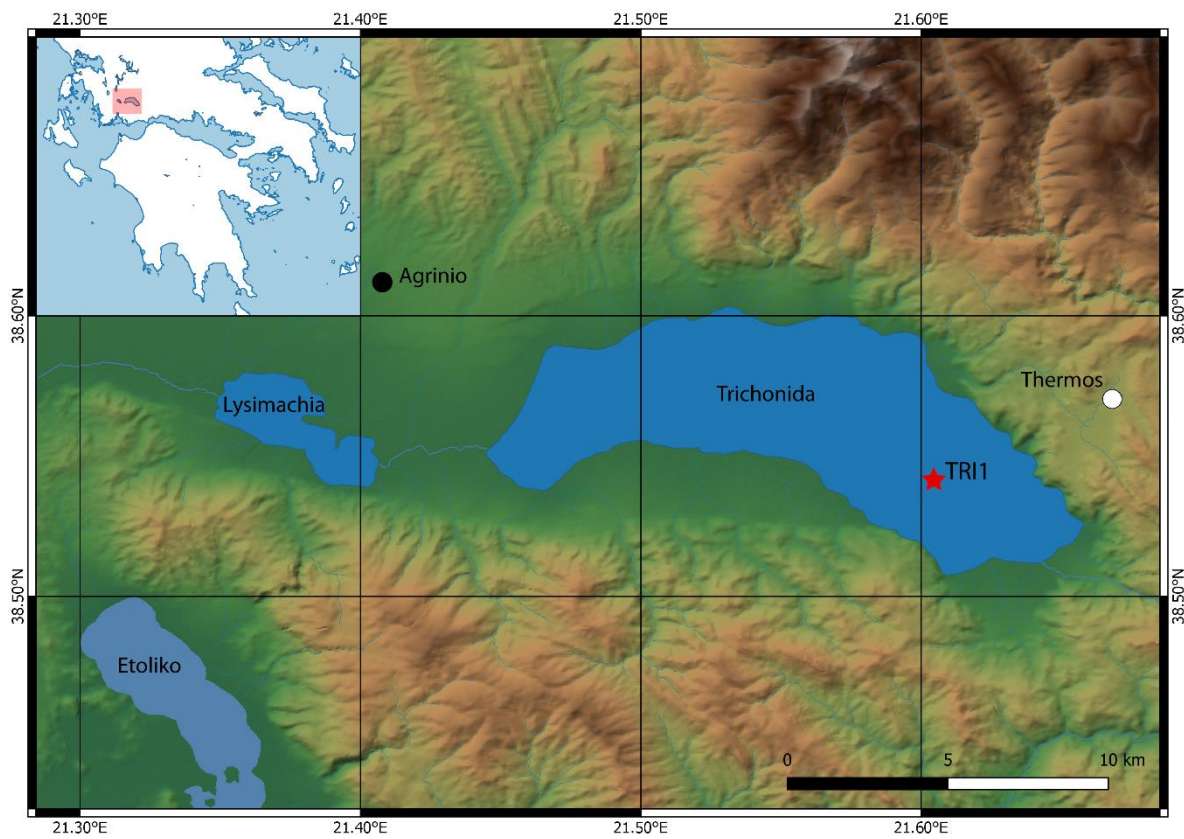


*Figure 1: Map of the study area. The coring site is indicated by a red star. The map was created using QGIS.*

## 2. Regional Setting

Lake Trichonida (Λίμνη Τριχωνίδα, or in old Greek “Trichonis”) (38.56° N, 21.55° E) is the deepest and largest natural lake in Greece, located in the region Aetolia-Acarmania (figure 1). The lake is up to 19 km long and 6 km wide, stretching approx. in W-E direction and covering approx. 97 km<sup>2</sup>; it has a maximum depth of 58 m and a mean depth of 30.5 m. (Tafas et al., 1997).

The lake has been studied irregularly since the 1970s with a focus on different limnological or biological aspects (Albrecht et al., 2009; Bottema, 1982; Creer et al., 1981; Koussouris and Diapoulis, 1982; Krüger and Damrath, 2019; Tafas et al., 1997; Zacharias and Ferentinos, 1997; Zotos et al., 2006; and references herein).

According to the Koeppen classification, the lake is located in a Csa climate zone, indicating a temperate climate with hot and dry summers and mild and humid winters (coldest month mean temperature >10°C, warmest month mean temperature >22°C; rainfall during dry period <30 mm) (Köppen, 1936; Tafas et al., 1997). According to Koussouris and Diapoulis (1982) the area is dominated by westerly winds. Precipitation, which mainly falls in winter (figure 2), is controlled by



eastbound cyclones originating from the Atlantic (Finné et al., 2011; Xoplaki et al., 2003a). Inter-annual water level fluctuation in the lake is about 1 m (Tafas et al., 1997).

Lake Trichonida is situated in the Trichonis Graben, a highly tectonised and complex hydrogeological system (Albrecht et al., 2009; Kiratzi et al., 2008). While the mountains surrounding the lake rise up to 2,000 m a.s.l., the lake itself lies in the Agrinion depression at approx. 10 m a.s.l. The Pindos thrust cuts right through the lake and a normal fault, striking E-W and dipping north, bounds the southern flank of the lake (Overbeck et al., 1982).

The size of the lake catchment varies according to the sources between 215 km<sup>2</sup> to 421 km<sup>2</sup> (Dimitriou and Zacharias, 2006; Overbeck et al., 1982; Zacharias et al., 2002) and mainly consists of highly tectonised, karstified calcareous rocks in the NE, where groundwater inflow is of high importance, impermeable flysch formations in the west, and quaternary sediments in the direct vicinity of the lake (Dimitriou and Zacharias, 2006; Overbeck et al., 1982; Tafas et al., 1997). Thirty seasonal streams discharge into the lake (Dimitriou and Zacharias, 2006). Lake Trichonida drains into the smaller, neighbouring Lake Lysimachia through a controlled outflow canal (Avramidis et al., 2013; Dimitriou and Zacharias, 2006) and further into the river Acheloos (Overbeck et al., 1982). The lake's water balance is presented by Overbeck et al. (1982). Lake Trichonida is a warm (mean temperature always >4°C), monomictic lake that is stratified during summer and mixes in winter (Tafas et al., 1997). During summer months the thermocline lies between 14 – 26 m (Overbeck et al., 1982). In respect to its nutrient balance, Tafas et al. (1997) describe it as oligotrophic with mesotrophic tendencies. This is in good agreement with the low amount of chlorophyll-a (2.3 mg/m<sup>3</sup>) reported by Zacharias et al., (2002), which indicates a low algal growth in the water body. Albrecht et al. (2009) found a high number of endemic molluscs in the lake and Tafas and Economou-Amilli (1997) studied seasonal phytoplankton assemblages and also report endemic diatoms.

The catchment area is covered by pine, fir, oak, and Greek maquis shrubland or is used for agriculture (Koussouris and Diapoulis, 1982). For present aquatic vegetation refer to Koussouris and Diapoulis (1982). A pollen study by Bottema (1982) provides some indication on vegetation transformation during the Late Holocene. The continuous presence of anthropogenic indicators (e.g. viticulture) indicates human influence upon the vegetation in the area for the complete investigated period. Nowadays, the area is part of the Natura 2000 Environmental protection network (Dimitriou and Zacharias, 2006).

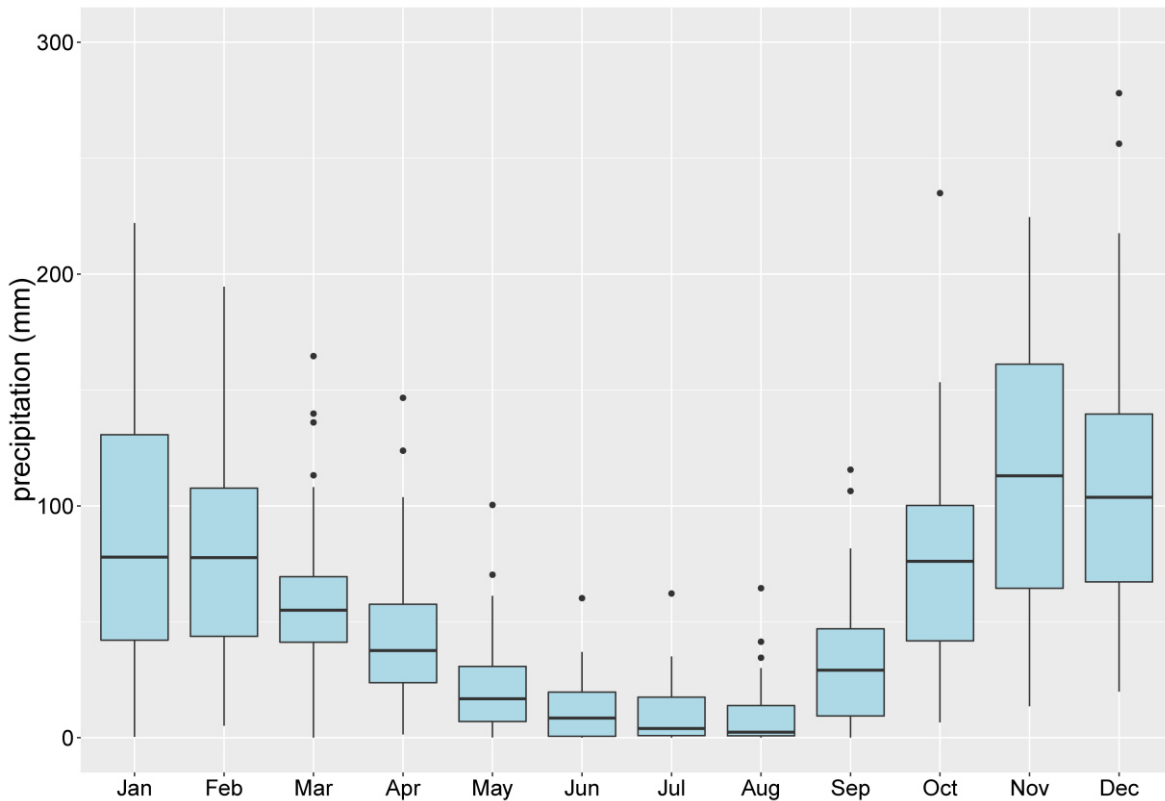


*Figure 2. Mean monthly precipitation for Araxos. The mean monthly precipitation from January to December for the WMO-station Araxos Airport (38.133 °N, 21.416 °E) is shown for the period 1961 – 1990.*

### 3. Materials and Methods

Fieldwork was conducted in spring 2018 using a Useringer piston corer system (Mingram et al., 2007), newly modified with a wire-operated second platform at the lake bottom. The coring site TR11 is located in the deeper central eastern part of the lake (38°33'0.61" N, 21°35'20.76" E). We cored two overlapping parallel cores with 80 mm diameter in the upper part and 55 mm diameter in the lower part and retrieved them in two-meter-sections. Offset between the cores was 50 cm. The sediment cores were removed from the coring equipment, cut into one-meter-sections for better handling, split open longitudinally on site, and transferred into plastic U-channels that were thoroughly labelled and sealed. At Kiel University (Germany), they are stored at +4°C in a cooling container for further processing.

The cores were described, concentrating on lithology, sediment texture and structure as well as on sediment colour according to Munsell soil color charts (Munsell, 2000) and macroscopic remains.

The core sections were visually correlated on distinct marker layers that were used as tie points where possible and fine-tuning was done in a second step based on the RGB values and XRF scans.

The surfaces of the half cores were smoothed and photographed using a digital line-scan camera (resolution: 143 pixels/cm). RGB and L\*a\*b\* colour profiles were created to depict colour variations with depth (figure 3).

The cores were scanned for XRF using an Avaatech core scanner with a Rhodium X-ray source. The scanning settings were a 1 mm resolution at 10 kV (exposure time of 10 s at 250  $\mu$ A) and at 30 kV (exposure time of 10 s at 1000  $\mu$ A using a Pd-thick filter). The XRF scans provide semi-quantitative element intensities in total counts per second (tcps). Twelve elements (10 kV: Al, Si, K, Ca, Ti, Mn, Fe, Co, Cu; 30 kV: Rb, Sr, Zr) show continuous data for 438 cm of TRI1 and are used for further analysis. We analyse relative changes of one element to another by natural logarithmic (log) ratios and interpret these as proxies for palaeoenvironmental variation. Hence, measurement variation caused by sample geometry, physical properties, water content, and the closed-sum effect are minimised (Tjallingii et al., 2007; Weltje and Tjallingii, 2008).

Twenty-four samples, at least one per lithological unit (figure 5), were analysed for their grain size distribution (GSD) using a laser-particle-analyser, Malvern Mastersizer 2000. The 70 measured classes were grouped into the seven common grain-size fractions following the ad-hoc Arbeitsgruppe Boden (2005).

Mineralogical analysis was conducted on 15 representative samples from different lithological units using X-ray diffraction (XRD, Bruker D8 Advance). Determination and qualitative analysis of the results were performed through DIFFRACplus EVA12 software (Bruker-AXS), by calculation of the area method, characterising the method as semi-quantitative. The full width at half maximum (FWHM) of each diagnostic peak was measured for each detected mineral percentage to be calculated. The minimum detection limit is around 2 – 3 % with small variations depending on the state of the studied sample.

Carbon and nitrogen samples were taken at approximately 25 cm resolution. The concentrations of total carbon (TC), total inorganic carbon (TIC), and total nitrogen (TN) was determined on dried, powdered, and homogenised samples, using a Euro EA, Elemental Analyser. Total organic carbon (TOC) was calculated from the difference between TC and TIC. The TOC/TN ratio was calculated to indicate the origin of the sedimentary organic matter. While values for in-lake organic matter, such as algae, are low, generally ranging between 4 and 10, mixed provenance is indicated by a ratio of 10 to 20; values higher than 20 indicate that land-plant organic matter was eroded into the lake (Meyers, 2003).

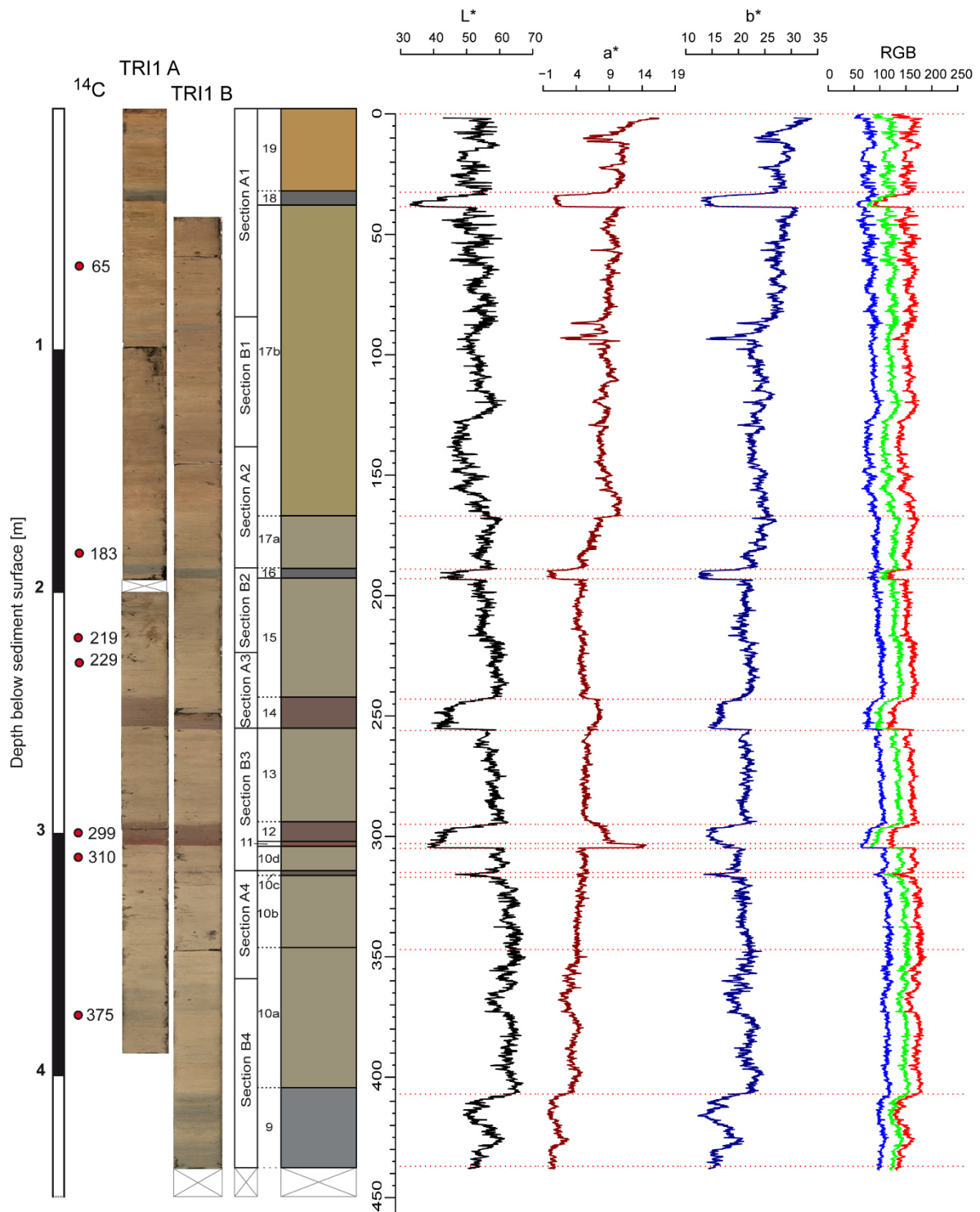


Figure 3: Core pictures of TRI1-A and TRI1-B and lithological profile of the mastercore TRI1 are plotted against depth. The composite sections and the delimited lithological units are indicated. Depths where samples for  $^{14}\text{C}$  dating were taken are marked by red dots. On the right panel, colour sequences in  $L^*a^*b^*$  and RGB colour code are depicted.

All statistical analyses, diagrams and figures were compiled using the software R Version 3.6.1 (R Core Team, 2019). For the RGB and XRF data, cleaning of the datasets, i.e. the removal of explicit outliers due to unevenness or cracks in the sediment core and the re-filling of the missing values by linear interpolation, was done prior to statistical processing.

In this study, the Spearman's correlation coefficient (Spearman, 1904) was employed to examine correlations between two populations, because it is a robust method that is also applicable for non-linear, non-normally distributed variables. We conducted a principal component analysis using the *prcomp* function from the R stats package on a standardised dataset. A hierarchical cluster analysis was performed with *hclust* from the R stats package, using Euclidean distances as distance measure and complete linkage as agglomeration method. All data were standardised before being used for cluster analysis.

#### **4. Core chronology**

The chronology of the Trichonida sediment sequence is based on 13 AMS radiocarbon ( $^{14}\text{C}$ ) dates, processed at the Poznań Radiocarbon Laboratory (table 1). Radiocarbon dating was performed on two groups of samples: organic macro-remains and bulk sediment samples, in case of absence of visible macro-remains. The organic macro-remains consisted of charcoal or plant remains, twigs or leaves (table 1). The age-depth modelling was done using *rbacon* (Blaauw and Christeny, 2011, figure 4). All dates are indicated as calibrated calendar years before present (cal BP), where 'present' is defined as 1950 CE with  $1\sigma$ -uncertainty ranges following Mook and van der Plicht (1999). Mean ages were extracted from the model and used for the representation and interpretation of the proxy data. The model shows a continuous and rather constant sedimentation rate of 1.68 mm/yr over the investigated period.

Where visible, macroscopic plant remains were extracted from the sediment cores, isolated under a reflected light binocular, and rinsed with deionised water. In the lower part of the cores, where no macro-remains could be found, we used bulk sediment samples for  $^{14}\text{C}$  dating.

*Table 1: List of all radiocarbon samples taken from TRII. Indicated  $^{14}\text{C}$  ages are unmodelled ages giving the 68.2 % calendar dating probability. Calibrated ages are cal BP ages using the IntCal13 calibration dataset (Reimer et al., 2013). Dates marked with an asterisk have been excluded from the final age-depth model. 1) Amount of remaining sample material after respective pre-treatment if <1.0 mgC. (following page)*

sample no.	analysis no.	sample material	C content in fraction <sup>1</sup> [mgC]	<sup>14</sup> C age ±1σ [BP]	calibrated <sup>14</sup> C age [cal BP], 1σ-ranges	depth [cm]
TRI-res01	Poz-106295	terrestrial plant for reservoir age	0.5	0 ± 30	236-235 59-42 282-267	0*
TRI-65	Poz-105729	twig		175 ± 30	215-168 153-144 20-0 1171-1161	65
TRI-183	Poz-106296	leave of deciduous tree	0.7	1150 ± 30	1121-1112 1085-1046 1033-984	183
TRI-219	Poz-110650	leave of deciduous tree		1320 ± 30	1292-1257 1202-1188	219
TRI-229	Poz-105452	drupe		2605 ± 35	2758-2730	229*
TRI-299	Poz-110652	bulk sediment		3605 ± 30	3966-3944 3930-3871	299*
TRI-310	Poz-106297	charcoal		1940 ± 30	1926-1865 1840-1835	310
TRI-375	Poz-110651	charred plant remains		2190 ± 30	2304-2237 2182-2148	375
TRI-461	Poz-105390	charred plant remains		2640 ± 35	2774-2745	461
TRI-490	Poz-110653	bulk sediment		9290 ± 50	10567-10416	490*
TRI-532	Poz-110654	bulk sediment	0.8	8210 ± 40	9257- 9117 9104-9093	532*
TRI-559	Poz-106298	bulk sediment	0.8	9080 ± 50	10257-10198	559*
TRI-598	Poz-100656	bulk sediment		8410 ± 50	9493-9404 9340-9332 12522-12471	598*
TRI-627	Poz-106299	bulk sediment	0.8	10440 ± 60	12430-12372 12352-12232 12207-12167	627*

Due to the limestone rich environment, there is a high amount of reworked material and inorganic carbon present in the sediment, which may lead to too old  $^{14}\text{C}$  ages when dating bulk sediment (Grootes et al., 2004; Seguin et al., 2019a). To obtain a higher reliability, the ADM was cut at the lowermost date obtained from organic remains (461 cm) corresponding to an approximate basal age of 2750 cal BP. All bulk sediment samples were finally excluded from the ADM, as they yielded considerably too old ages (cf. supplementary material).

This was best visible comparing the bulk sediment age at 299 cm with the charcoal sample at 310 cm; these two dates are only 11 cm apart, but depict an age difference of 1,700 years. We took a surface sample from aquatic plants (TRI-res01) to analyse for a potential hard water effect or reservoir age, but this sample yielded a recent  $^{14}\text{C}$  age, suggesting that the lake is not affected by reservoir effects at least under current conditions. Dating challenges, due to the low preservation of organic material, hard water and old carbon effects due to the limestone bedrock are known for Greek lakes (Bottema, 1982; Seguin et al., 2019a; Vaezi et al., 2019). However, a critical assessment of the dating results and an extensive modelling approach, if possible, combined with other numeric or relative age information, still yields a solid and reliable ADM.

In TRI1, an independent age indicator, supporting our model, was found in the form of a tephra layer at 315 – 317 cm, lithologically classified as unit 10c (figure 3). In the XRF data, Rb, K, Zr and Sr values have a high peak here. It is the only unit where Rb and Sr correlate, instead of anti-correlating, which suggests that the Sr supply here originates from an allochthonous, minerogenic source, e.g. plagioclase feldspars (Dypvik and Harris, 2001; Kylander et al., 2011). This layer was already found around 310 cm by Bottema (1980) and Creer et al. (1981) and described as a tephra layer. Based on geomagnetic and palynological investigations, Creer et al. (1981) concluded that due to the wind direction this tephra could be associated with the Somma-Vesuvius eruption 79 CE that buried the city of Pompeii. Bottema (1982, 1980) argued based on palynological investigations that the tephra should more likely be associated with the Santorini eruption, which can be rejected based on the recent reconstructions of the pathway of the ash plume (Johnston et al., 2012).

In our age model, this layer dates to 1985 – 1789 cal BP at 316 cm and would thus be in accordance with the Pompeii eruption 79 CE (1875 cal BP). In a recent publication, Insinga et al. (2019) mapped tephra for the period 2000 to 4200 BP in the central Mediterranean. Stratigraphically right below the 79 CE eruption, they report a new horizon, the “FG/Lipari undefined layer”, originating from an unknown eruption dated to  $2187 \pm 37$  – 1970 cal BP. This eruption, which was found at different sites throughout the Ionian Sea (Insinga et al., 2019), also overlaps with the age uncertainty range of our tephra layer and thus would also support our ADM.

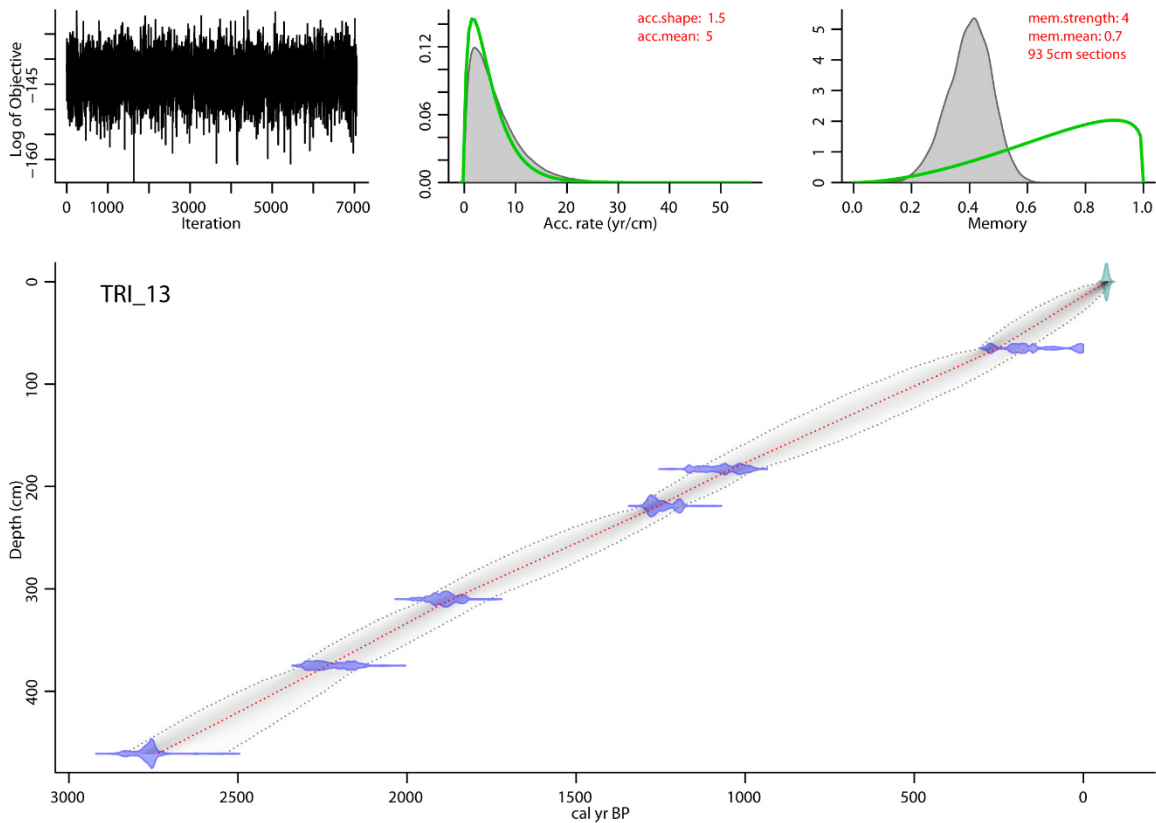


**Figure 4:** Bayesian age-depth model TRI\_13 constructed using the R package rbacon (Blaauw and Christen, 2011). The blue tie bars indicate the  $^{14}\text{C}$  age distribution while the greyscale of the line graph reflects the likelihood; the dotted red line follows the mean ages.

Another independent age marker was found by Bottema (1982) in the form of the presence of maize (*Zea mays*) at 110 cm, which according to him needs to be younger than 250 years but unequivocally posterior to 1492 CE, the discovery of the New World. The main spread of maize in the Mediterranean was observed for the 16<sup>th</sup> and 17<sup>th</sup> century CE (Bintliff, 2012). Our model dates to 554 cal BP (419 – 701 cal BP) at 110 cm in TRI1 and, assuming that the depths were comparable in both cores, it would be slightly too old in the uppermost part.



## 5. Results

### 5.1 Core description

Based on the composition, structure and colour, the investigated core sequence of TRI1 was divided into 15 lithological units and subunits (figure 3, table 2).

The core dominantly consists of homogeneous, non-laminated marls of greyish colour. While few plant macrofossils were found, carbonate macrofossils are completely absent. The sediment sequence does not show any signs of annual lamination or blackish mud, including high organic matter content, although the lake is classified as monomictic, implying a turnover only once a year and a vertical stratification of the water body throughout most of the year. The X-ray diffraction (XRD) analysis indicates that the most prominent mineral phase throughout the core are the clay minerals (25.2 – 53.1 %), followed by chlorite (15.6 – 41.0 %), calcite (4.9 – 41.2 %), and quartz (9.2 – 25.3 %; figure 5); other minerals were absent or below the detection limit.

Changes in lithology are closely related with changes in colour parameters (RGB and L\*, a\*, b\*). Contrary to the RGB values, the a\* parameter, spanning from green to red, and the b\* parameter, spanning from blue to yellow, allow a differentiation of the thin, coloured sedimentary units. Towards the top, the amount of yellow colour particles is steadily increasing (figure 3). This is interrupted by thin layers of very different colouration. Units 11, 12, and 14 have a reddish colour, while units 16 and 18 depict a dark-grey to blueish colour, more intense than unit 9, as visible in the a\* colour proxy (figure 3).

The grain size distribution is very uniform and clearly dominated by silt-sized material; sediment types can be distinguished ranging from clayey to very clayey silt. Clay content varies from 11.95 to 21.74% and the sand fraction is hardly present with only 0 to 4.36 %. A large share of the silt-sized particles is of calcareous origin as can be expected due to the limestone geology of the catchment (figure 5).

The TOC content ranges between 1.21 and 2.33 %, with the TOC/TN ratio being in the range 15.49 – 48.60, indicating an exclusively terrestrial source and allochthonous origin of the organic matter.

**Table 2: Sedimentary units of TRI1 with detailed sedimentological description. The soil type classification follows the German ad-hoc Arbeitsgruppe Boden (2005); (UB = upper boundary, G = gradational, S = sharp).**

Core Depth [cm]	Sediment Unit	Unit Thickness [cm]	Munsell Color	Soil Type	Description
0–32	19	32	2.5Y 4/3 olive brown	Ut4	more yellowish than 17b – terrigenous input, (UB = sediment-water-interface)
32–37	18	5	Gley 1 4/5 GY olive gray	Ut3	silty blue-grayish unit, similar to unit 16 (UB = G)
37–166	17b	129	5Y 6/3 olive gray	Ut3	matrix becomes darker and more yellowish, brown mottles, 0.85 – 1.0 m thin horizontal gray-blueish lines visible, 0.945 thin reddish line, more oxidation (UB = P)
166–189	17a	23	5Y 5/2 olive gray	Ut3	homogeneous gray matrix (UB = G)
189–193	16	27	Gley 1 4/5 GY olive gray	Ut3	thin blue-grayish layer (UB = P)
193–243	15	50	5Y 5/2 olive gray	Ut3- Ut4	homogeneous gray matrix, orange mottled, (UB = P)
243–256	14	13	2.5YR 5/1 reddish gray	Ut3	similar to unit 12, gradual brightening towards top (UB = G)
256–295	13	39	5Y 5/2 olive gray	Ut3	homogeneous gray matrix, occasional black particles (UB = P)
295–303	12	8	2.5YR 4/1– 4/2 dark reddish gray–weak red	Ut3	clayey silt, upper boundary with bubbly intrusions, gradual brightening towards top (UB = G)
303–305	11	2	2.5 YR 4/4 reddish brown	Ut4	compact, homogeneous, clearly defined boundaries (UB = P)
305–315	10d	10	5Y 5/2 – 6/2 (light) olive gray	Ut4	similar to 10b, homogeneous gray matrix (UB = strongly P)
315–317	10c	2	2.5Y 4/1 dark gray	Ut3	tephra layer, more strongly present in B-core, coarser silt, larger pores (UB = P)
317–347	10b	30	5Y 5/2 – 6/2 (light) olive gray	Ut4	homogeneous gray matrix, more compact than 10a, charcoal particles (UB = G)

<b>347–405</b>	10a	58	5Y 5/2 olive gray	Ut3	gray matrix, black streaks, orange mottled, number of degassing holes decreases, gradually more compact (UB = G)
<b>405–437</b>	9	32	5Y 4/1 dark gray	Ut2	no macrofossils in whole core, extremely silty, small holes may indicate degassing (UB = G)

The three independent indicators of calcium carbonate, XRF Ca, TIC, and XRD calcite are generally in good agreement (figure 5). Carbonate content (Ca and Sr) strongly varies along the sequence and is lowest in the coloured sedimentary units (11, 12, 14, 16, and 18) (figure 5). Quartz content shows only minor variation but a distinct maximum in unit 11. Together with several terrigenous elements (Rb, K, Zr), Sr shows an exceptionally high peak in unit 10c, which was addressed as a tephra layer. Strontium substitutes for Ca mainly in carbonate or sulphate minerals and co-precipitate in lakes, but it also occurs in magmatic rocks as part of Ca-rich plagioclase feldspars (Cohen, 2003; Kylander et al., 2011). Both elements show a high correlation ( $r_{\text{Spearman}} = 0.88$ ) and a similar curve progression with depth (figure 5).

The terrigenous elements (Ti, Rb, Fe, Zr, K, Zr, Al, and Si) all show a very similar behaviour along the entire sediment sequence. Highest values occur in the coloured sedimentary units and in the lowermost unit 9.

As Rb, associated with terrigenous sediment input, and Sr, associated mainly with carbonates, show a very different geochemical behaviour, the Rb/Sr ratio is often interpreted as a proxy for chemical weathering (Jin et al., 2006; Xu et al., 2010). While carbonates can be associated either with carbonate weathering in the catchment or with authigenic precipitation of chemical or biogenic carbonates in the lake, notably during dry and warm phases, the clastic elements originate from terrestrial input eroded during wet periods with enhanced precipitation and runoff (Cohen, 2003; Kylander et al., 2011). High Sr values are interpreted to generally indicate higher carbonate precipitation under warm and/or more arid conditions, while higher Rb values hint towards stronger physical weathering of clastic material and enhanced surface runoff related to increased precipitation during colder and wetter conditions (Unkel et al., 2014). The log(Rb/Sr) ratio shows irregular cyclic variation with depth, with higher values in the coloured sedimentary units and below 350 cm (figure 5). Manganese (Mn) values are rather constant along the core with increasing variance only in the uppermost unit 19. In the coloured units 11, 12, 14, and 18, Mn shows enhanced values at the bottom of the unit with a decreasing trend towards the top (figure 5).

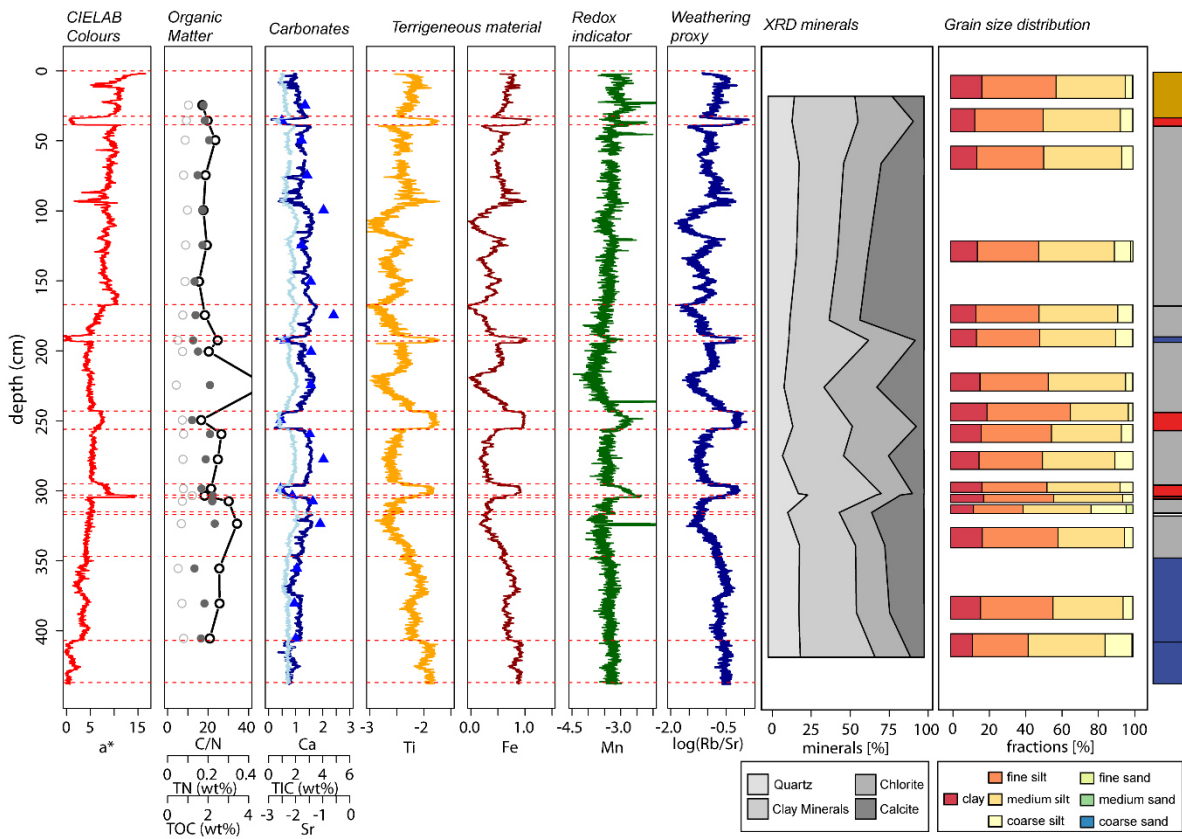


**Figure 5: Overview of selected colour, organic and geochemical proxies for the composite profil TR11 plotted against depth. From left to right: CIELAB colour parameter  $a^*$ , organic matter proxies (TOC (filled points), TN (empty points), and C/N (points on line)), carbonate proxies (Ca (blue line), Sr (bright blue line), TIC (triangles)), terrigenous minerals (Ti, Fe), redox indicator (Mn),  $\log(Rb/Sr)$  as weathering proxy, XRD minerals, and discrete grain size measurements. Bar width for grain size distribution is not at scale. All XRF elements have been normalized against total counts and log-transformed. Horizontal, red dashed lines indicate lithological units. To the right, the lithological units are likewise indicated; colour coding follows the cluster analysis.**

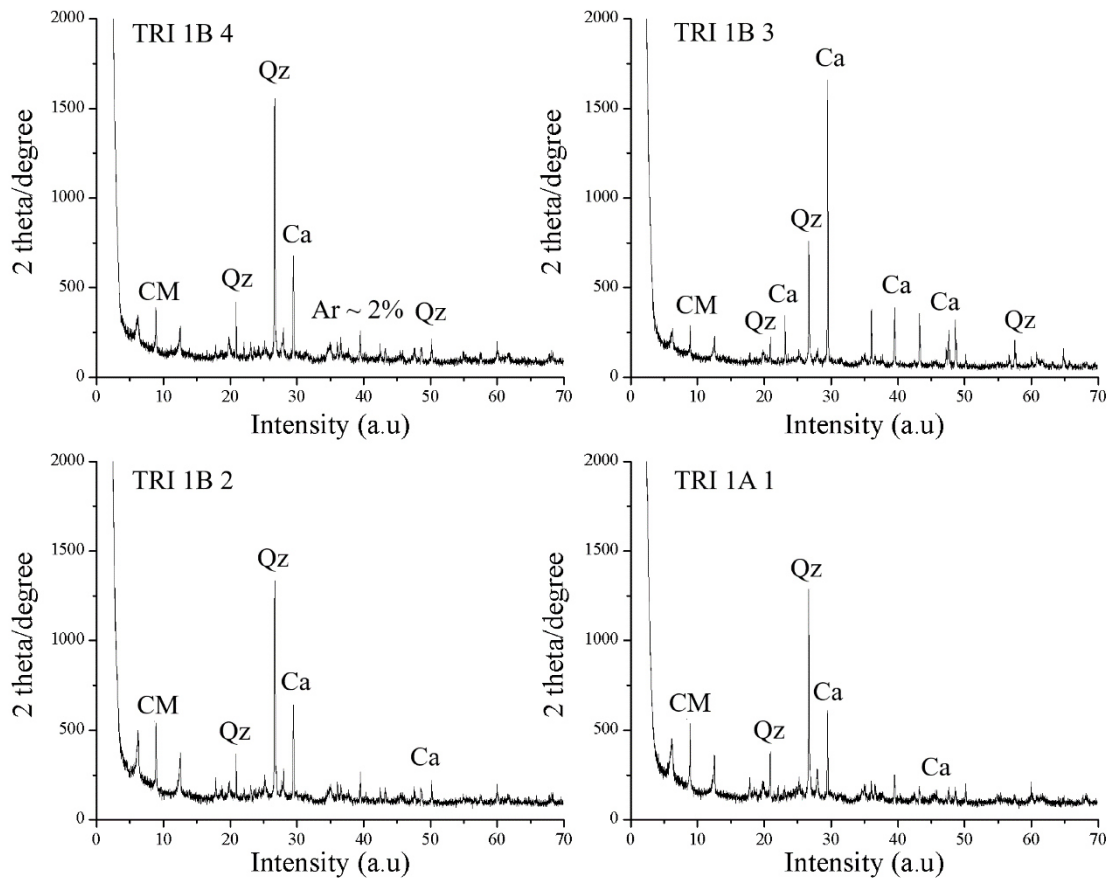


**Figure 6:** Intensity diagrams of representative X-ray diffraction samples from different core sections. They show the presence of the main recognized minerals. CM: Clay minerals, Qz: Quartz, Ca: Calcite, Ar: Aragonite.

## 5.2 Statistical analyses of the geochemical data

### 5.2.1 PCA

A principal component analysis was conducted on 12 geochemical elements (Al, Si, K, Ca, Ti, Mn, Fe, Co, Cu, Rb, Sr, Zr) to reduce the multivariable dataset to a limited amount of uncorrelated components. The first three principal components (PC) cover >80 % of the data information and were thus further analysed in more detail. Figure 7a shows the correlations between the element loadings and the PCs. Elements which show the same variation and whose loadings cluster together are likely influenced by the same environmental processes. The first principal component captures 58.4 % of the variance and spans the axis between carbonate rich (Ca, Sr, Cu) and all the other, mainly mineral rich assemblages (figure 7b). The same distribution has been found in other studies from the area and presumably reflects hydroclimatic variations (Emmanouilidis et al., 2019; Katrantsiotis et al., 2018; Seguin et al., 2019a).

The point cloud reveals that the lowermost part of the core (units 9, 10a; ca. 2,600 – 2,100 cal BP) plots on the positive side of the axis and is strongly dominated by clastic material (figure 7c). The middle part of the core (ca. 2,100 – 100 cal BP) alternates between positive and negative values with a focus in the upper left quadrant, being more strongly influenced by carbonate precipitation. The uppermost approximately 50 cm (the last ca. 150 years) shift towards more positive PC1 scores again, showing an increase in detrital input. Similar fluctuations can be observed in the  $\log(\text{Rb}/\text{Sr})$  proxy plotted over time (figure 7d). Following Seguin et al. (2019), low values of PC1 indicate higher carbonate precipitation under warm and/or more arid conditions, while higher values indicate stronger weathering of clastic material during colder and/or wetter conditions. The same variation is visualised by  $\log(\text{Rb}/\text{Sr})$ . The Spearman correlation between  $\log(\text{Rb}/\text{Sr})$  and PC1 shows an extremely high conformity ( $r_{\text{Spearman}} = 0.91$ ) and thus both proxies are assumed to reflect the most important palaeohydrological changes in the lake catchment.

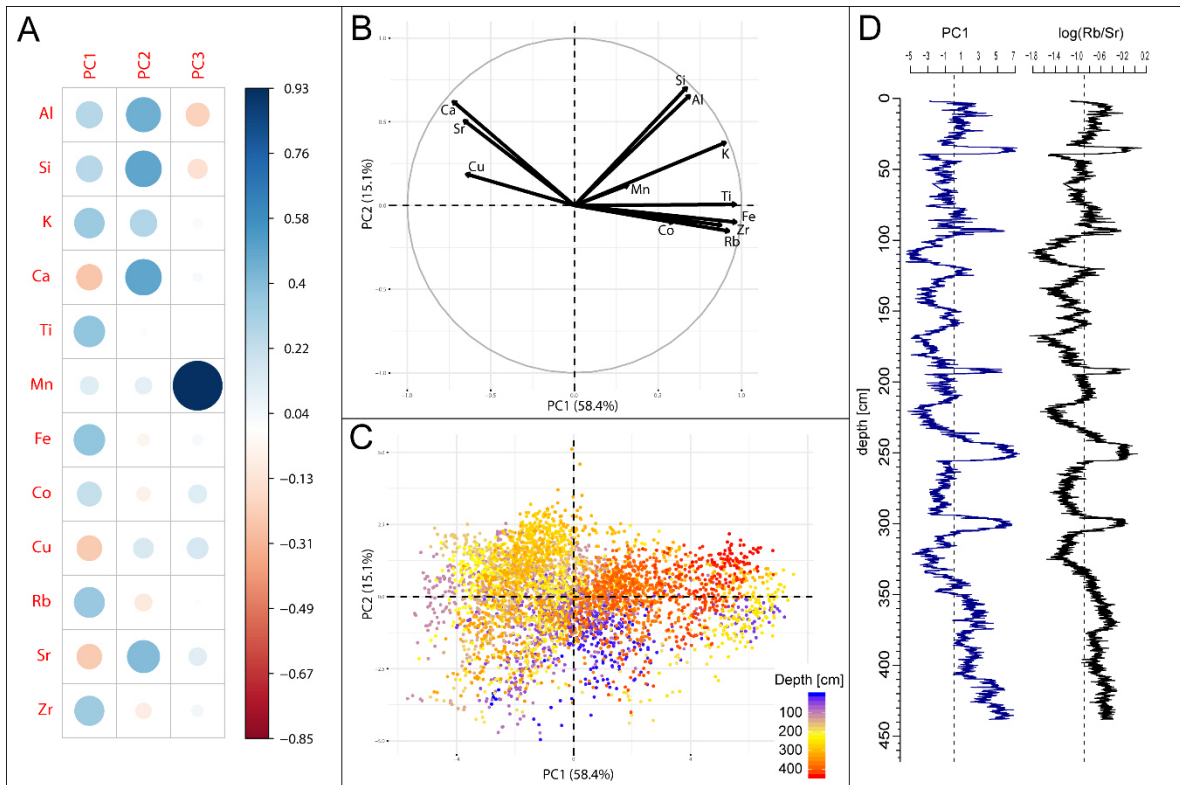


**Figure 7: Principal component analysis (PCA) based on the XRF data. (a) correlation matrix between original elements and principal components (PC) 1 – 3. (b) variable correlation circle displaying the correlation between PC1 and PC2. (c) distribution of the sample points in the PC1 – PC2-scatterplot. The samples are coloured according to their depth in the sediment core from purple (surface) to red (maximum depth). (d) PC1 and  $\log(\text{Rb}/\text{Sr})$  are plotted against depth and show a high conformity.**

PC2 is positively associated with Al, Si, Ca, Sr, K, while the loadings of the other elements are of minor importance (figure 7a). It has a high variance and the interpretation is not straightforward; it could potentially be linked to changes in the grain size distribution or material provenance.

PC3 is clearly dominated by Mn and has only a minor contribution of the loading of all the other elements (Figure 7a). A correlation between PC3 and Mn/Fe ( $r_{\text{Spearman}} = 0.76$ ) yields high conformity and suggests that PC3 may hint towards changes in the redox conditions at the lake bottom.

### 5.2.2 Cluster Analysis

A hierarchical cluster analysis was conducted on the continuous XRF, RGB, L\*a\*b\*, and PC1 – PC3 proxies (23 variables) to classify the 15 determined lithological units and sub-units according to potentially different sedimentary conditions (figure 8).

Recently, Khamnueva-Wendt et al. (2019) successfully applied a hierarchical cluster analysis to core material from a Viking settlement in order to distinguish materials with a natural genesis from anthropogenically reworked material. Lintern et al. (2016) used a similar proceeding on geochemical elements, ratios, and magnetic susceptibility for a zonation of their sediment core from an Australian floodplain.

Our clusters show meaningful correlations with the sedimentological units. The results allow a differentiation into two sound main clusters and five systematically traceable sub-clusters and the results are depicted in a dendrogram (figure 8). Four main lithofacies may be distinguished, leaving aside the tephra, suggesting similar environmental conditions during the deposition of material within the same sub-cluster.

*Cluster 1* comprises the thin units 11 (1830 – 1820 cal BP), 12 (1820 – 1770 cal BP), 14 (1500 – 1420 cal BP), and 18 (110 – 90 cal BP). While the first three are of reddish colour, having high a\* values and low b\*, the latter is of blue-greyish colouration with low a\* and b\* proxy values (figure 3). The geochemical values are similar for all units with very high terrigenous input and local minima in carbonate input (Ca, Sr, and TIC). Unit 11 contains a considerably higher amount of quartz. Log(Rb/Sr) shows maxima in all these units.

*Cluster 2* encompasses the lowermost units 9, 10, and the thin unit 16, which cover the periods 2,600 – 2,080 and 1,100 – 1,080 cal BP. All units are characterised by the lowest a\* and low b\* proxy values, indicating the blue-greyish coloration of the sediment. The amount of terrigenous elements is high, while Ca, Sr, and TIC have minima here. TOC/TN values are slightly elevated. The grain size is slightly coarser here, notably in unit 9, as indicated by the GSD. The log(Rb/Sr) proxy is high in these units (figure 5).

Cluster 3 is the largest cluster comprising all units belonging to the homogeneous greyish marls. The  $a^*$  and  $b^*$  values indicate average values with an increasing trend with time towards more yellowish colouration. The highest amount of carbonates and the lowest  $\log(\text{Rb}/\text{Sr})$  values are found in this cluster.

Cluster 4 represents only the uppermost sedimentary unit 19, which covers the period 90 – 68 cal BP (1860 – 2018 CE). It is characterised by increasing terrigenous elements and decreasing carbonate content, which are more strongly increasing since 1970 CE (uppermost 10 cm). In this phase, highest values for  $a^*$  and  $b^*$  colour proxies are reached, indicating most intensive orange coloration. The Mn profile is very noisy here, generally indicating higher values. The exclusion of this unit as a single cluster suggests that the environmental conditions for this period are significantly different from the preceding times.

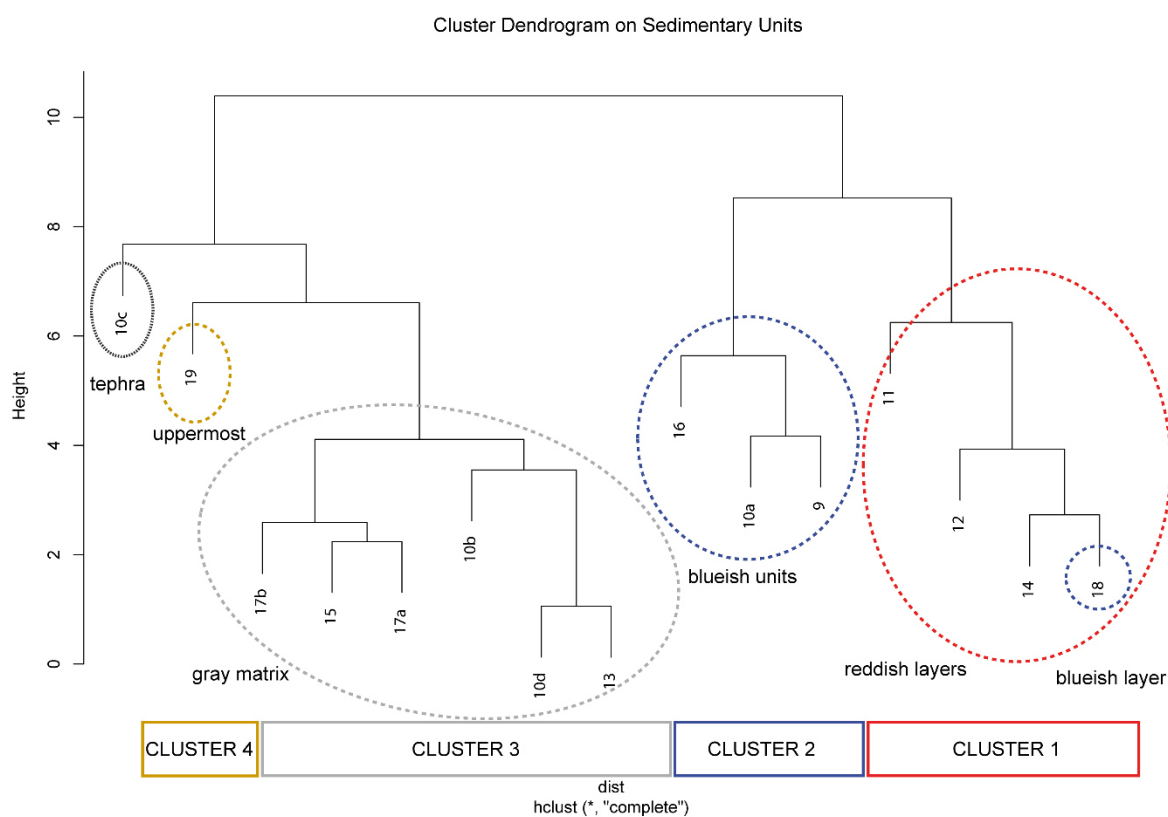


**Figure 8: Dendrogram obtained by the hierarchical cluster analysis. The XRF elements, RGB,  $L^*a^*b^*$  and PC1 – PC3 were used as input variables.**



The clusters show a large coherence with the visually observed differences in the sedimentary units, which may be explained by the use of two sets of colour parameters as input variables. Due to the blueish coloration, unit 18 was rather expected to group into cluster 2, which it did when a different set of variables was selected. It is important to keep in mind that the results strongly depend on the chosen set of input variables (Khamnueva-Wendt et al., 2019). Here, the results using all available continuous variables are shown, but diverse options including different sets of input variables have been calculated. It became obvious that the larger dichotomous pattern, dividing the core into the more calcite rich matrix on one hand, and the reddish and blueish coloured layers on the other, remained unchanged, even if a few sedimentary units were sub-clustered differently.

## **6. Discussion**

### **6.1 Event layers**

Five lithological units of only few centimetres thickness depict a very different colour compared to the remaining sequence (units 11, 12, 14, 16, and 18, figure 3). Their lower sediment boundaries can always be classified as being flat and sharp but not erosive. If these units were the result of an immediate mass movement or turbidite event, one would expect an abrupt increase in coarser material and a sorting with a fining upwards gradient within these units (Sabatier et al., 2017; Wilhelm et al., 2016). The grain size samples show no coarsening compared to the neighbouring units, however the sampling resolution is low. Mn rises steeply at the onset of the units, followed by a gradual decrease within the respective units (figure 5). This pattern suggests bottom water oxygenation (Calvert and Pedersen, 1993) triggered by an abrupt (ventilation) event, which caused Mn enrichment and the changes in colour. Afterwards, the system gradually re-gained its initial status. This would support the hypothesis that the reddish and blueish units were deposited during or following short-term events. We also elaborated the option that the units could have been deposited at once, e.g. by a turbidity current, treating these units as mass movement events during the age modelling process, but the respective age model overlapped completely within the uncertainty range of the model without specific event layers (supplementary material). Hence, we decided to use the model with continuous sedimentation as the final age-depth model.

### **6.2 Sedimentary facies interpretation**

The cluster analysis emphasises similarities between certain sedimentary units of TRI1 based on their colour and geochemical characteristics. As these sediment characteristics are affected by the

palaeoenvironmental conditions during deposition, the dendrogram classification may be used to infer phases with similar palaeoenvironmental conditions. Four different facies were identified during the cluster analysis (figure 8).

Cluster 1 is interpreted as compiling phases with higher terrigenous input and bottom water oxygenation, which was caused by rather abrupt changes in the environmental conditions, e.g. by intensive precipitation. The higher terrigenous input is interpreted as an indicator of catchment erosion during wetter conditions.

Cluster 2 shows likewise a higher amount of detrital material that was transported into the lake. The different colouration of the sediments in both clusters suggests different processes to have influenced their deposition, but it is not possible to unequivocally identify the sedimentary process, as different influential factors would lead to increasing clastic input. Wetter conditions with more intense winter precipitation may have been one trigger. Another possible trigger could have been summer storm events that would break down or disturb the stratification in the water column and increase runoff intensity, which would however most likely also result in turbulent and coarser sediment deposition. Furthermore, one may also expect an increasing amount of micro- and macrofossils, e.g. broken shells or higher organic matter content, which was washed in and deposited before decomposition, which we do not observe here. Human impact, e.g. by deforestation, is also known to increase erosion and detrital material input (Meriam et al., 2017). However, one would expect longer lasting periods, while these facies units lasted maximum 100 years. We interpret cluster 2 also as indicating wetter conditions and attribute the variation in colour compared to cluster 1 to differences in the Mn and Fe oxides (Statham et al., 2017).

The majority of the core is composed of the greyish marls in cluster 3, which have a homogeneous appearance, although the geochemical ratios show intense fluctuations within these units. It is assumed that sediments in this cluster were deposited within a stable, stratified lake ecosystem with anoxic bottom water conditions. Variations in the XRF data may be explained by palaeoclimatic variation. The high Ca content may be linked to intense carbonate precipitation under warm and dry conditions.

The uppermost sedimentary unit forms a cluster by itself and is interpreted as potentially being influenced by anthropogenic activity in the catchment. It seems as if human activity in the area has increased particularly since 1970 CE or that its impacts have increasingly reached the coring spot e.g. through run-off from cultivated, fertilized fields. Mn values in this unit are higher than in unit 3 and have a high variance, potentially indicating instability in the modern monomictic conditions that supply oxygen to the hypolimnion.

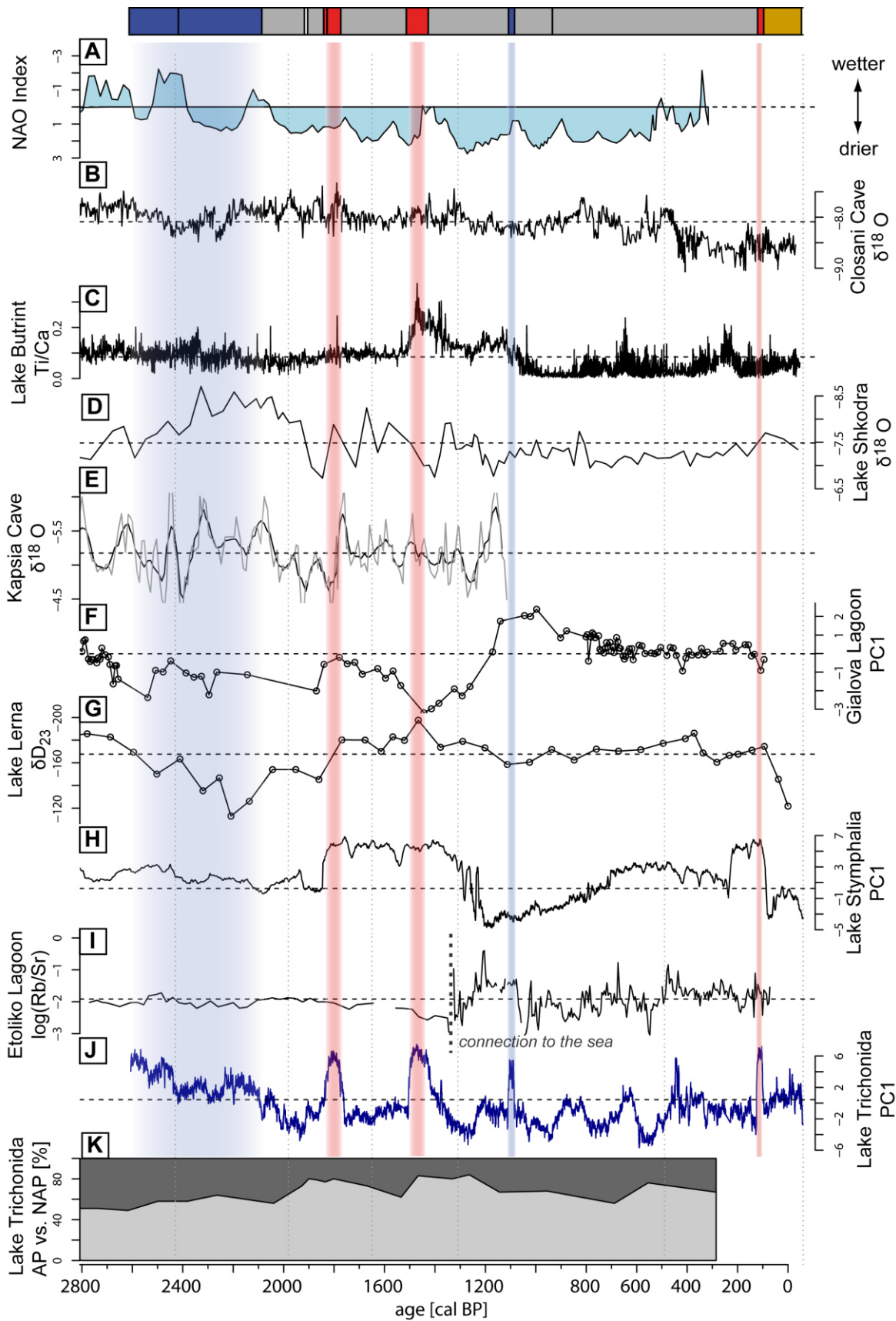


*Figure 9: Comparison of the PCI proxy with other regional hydroclimate records. (a) strength of North Atlantic forcing, indicated by the NAO index reconstructions (axis inverted) from Olsen et al. (2012). (b) Autumn/winter precipitation reconstruction from a speleothem at Closani Cave (SW Romania; Warken et al., 2018). (c) Ti/Ca proxy from Lake Butrint (Albania; Morellón et al., 2016) (d)  $\delta^{18}O$  record from Lake Shkodra (axis inverted; Zanchetta et al., 2012). (e)  $\delta^{18}O$  record from a speleothem in Kapsia Cave (axis inverted; Finné et al., 2014). (f) PCI on XRF data from Gialova Lagoon (Katrantsiotis et al., 2018). (g)  $\delta D_{23}$  proxy from Lake Lerna (axis inverted; Katrantsiotis et al., 2019). (h) PCI on XRF data from Lake Stymphalia (Seguin et al., 2019a). (i)  $\log(Rb/Sr)$  ratio from Etoliko Lagoon (Haenssler et al., 2013). (j) PCI on XRF data from Lake Trichonida (this study). (k) Arboreal (AP) vs. non-arboreal pollen (NAP) from Lake Trichonida (data reconstructed from Bottema (1982) plotted against our ADM). Values plotted to the top generally indicate wetter conditions. Vertical shaded bars indicate relatively more humid phases at Lake Trichonida (see text for more detail). (previous page)*

### **6.3 Palaeoenvironmental reconstruction for the last 2,600 years in comparison to other regional archives**

Lake Trichonida has been studied irregularly since the 1980s (for example: Albrecht et al., 2009; Bottema, 1982, 1980; Dimitriou and Zacharias, 2006; Koussouris and Diapoulis, 1982; Tafas et al., 1997b). However, radiocarbon dating on the sediments has been challenging back then and methodological approaches were less advanced. Due to the high sedimentation rate of approximately 1.7 mm/yr, the core sequence in principle provides palaeoenvironmental information in annual resolution. However, even though the age-depth model is based on terrestrial macro remains, it only provides an average probability range of 278 years. Hence, we do not discuss our data on an annual but rather on a decadal to centennial scale. Nevertheless, within the constraints of the age-depth model, we can be more precise about the duration of periods and events than about absolute timing. The presented TRI1 core sequence continuously covers the last 2,600 cal BP over more than 4 metres of sediments, which is – though not laminated – a much higher temporal resolution than any other geoarchive from the area provides so far.

In an earlier pollen study, Bottema (1982) identified 71 pollen types from the sociological relevé-list at Lake Trichonida. The AP/NAP ratio of arboreal vs. non-arboreal pollen types was reproduced and is shown in figure 9k. As Bottema (1982) abstained from creating an age-depth model, we used our ADM to plot the data on a time scale, assuming that the depth scales of the two cores were comparable. Overall, the number of pollen types correlated positively with the AP/NAP ratio and negatively with the degree of forestation (Bottema, 1982), which means that land opening increased the pollen diversity and lower AP/NAP values hint towards natural or anthropogenic deforestation. Lowest degrees of forestation are depicted for the period 2600 – 2000 cal BP, which suggests that

deforestation may have already taken place previously and forest slowly recovered. Highest arboreal pollen amounts can be observed during the wet phases of the reddish units. Apart from that, the resolution is too coarse to reasonably compare it to the XRF proxies.

For the last 2,600 years, Lake Trichonida shows different phases of palaeohydrological fluctuation. It has witnessed several phases of wetter or drier climatic conditions, as observed in the log(Rb/Sr) and PC1 proxies. We assume that the lake level has fluctuated over a few metres – modern inter-annual variation is about 1 m (Tafas et al., 1997) – but due to its depth and the sedimentary characteristics, we exclude the option of complete desiccation, as it was shown for shallow lakes in southern Greece (Seguin et al., 2019b).

From around 2600 to 2000 cal BP, PC1 generally shows a decreasing trend towards drier conditions in the study area with a minimum occurring around 2000 – 1800 cal BP. The NAO index for this interval shows an increasing trend that is likewise connected with drier climatic conditions (Olsen et al., 2012, figure 9a). Centring around 2500 and 2200 cal BP, two short periods with slightly wetter conditions can be identified in the general trend of the PC1 record and are largely in agreement with the negative NAO indices. Katrantsiotis et al. (2019) suggest that the North Atlantic Oscillation controls the climate in Greece notably during winter. When the NAO index is positive, the westerlies are stronger than usual and the humid air masses run further north, leading to drier and colder winters in Greece, while negative NAO indices relate to wetter and warmer conditions (Katrantsiotis et al., 2019; Nieto-Moreno et al., 2011). Drying climate conditions before 2000 cal BP are also reported from Lake Lerna (Katrantsiotis et al., 2019), the Asea valley (Unkel et al., 2014), and Skala Marion Cave (Psomiadis et al., 2018). Unlike these archives, Lake Malik (Fouache and Pavlopoulos, 2010) and Lake Shkordra (Zanchetta et al., 2012, figure 9d) to the north, as well as the Agios Floros fen (Norström et al., 2018) to the south, reveal a trend towards wetter conditions during the same period from 2600 to 2000 cal BP. The resolution of the  $\delta D_{23}$  record from Agios Floros (Norström et al., 2018), however, is too low to reasonably compare the proxy to Lake Trichonida. This inconsistent observation is in general agreement with Finné et al. (2011) who summarize the hydrological situation during this time period as an incoherent picture without “discernable spatial patterns” and report generally warmer temperatures, which would be in agreement with the increase in carbonates in the sediment sequence at Trichonida. This drier/warmer phase ends abruptly around 1750 cal BP with a rapid increase of terrigenous material input into Lake Trichonida, most likely due to increased precipitation and surface run-off in the catchment. Lithologically, this period corresponds to the very distinct reddish units 11 and 12 (figure 3). Lake Lerna (Katrantsiotis et al., 2019, figure 9g), Kapsia Cave (Finné et al., 2014, figure 9e), Closani Cave (Warken et al., 2018) and Skala Marion Cave

(Psomiadis et al., 2018) all provide evidence for higher humidity for the period around 1800 cal BP. Lake Shkodra and Gialova Lagoon also give evidence for a short wetter period, but from a medium term perspective the proxies rather follow a drying trend lasting until 1400 cal BP (Katrantsiotis et al., 2018; Zanchetta et al., 2012). Interestingly, this wet century at Lake Trichonida coincides with the aqueduct construction at Lake Stymphalia, that was interpreted as triggering the abrupt shift in the proxy (Seguin et al., 2019, figure 9h). The AP/NAP ratio depicts an increase in arboreal pollen for 2050 – 1800 cal BP (Bottema, 1982, figure 9k), which on one hand supports the wetter conditions favourable for tree growth. On the other hand, an increasing input of terrigenous material may generally induce more pollen from the catchment and a transformation in the pollen transport process may influence the spectrum composition. A similar coincidence occurs in 1500 cal BP; an abrupt increase in terrigenous material coincides with an increase in the AP/NAP ratio.

The following interval, ca. 1700 – 1500 cal BP (250 – 450 CE), can be interpreted as a phase of stable, drier conditions at Lake Trichonida. Kapsia Cave (Finné et al., 2014) and Closani Cave (Warken et al., 2018) also show relatively stable conditions and the NAO index is solely positive (Olsen et al., 2012, figure 9a). For Anatolia and the Levant, Izdebski et al. (2016) speak of a late Roman drought lasting from ca. 350 to 470 CE, which was then followed by a dramatic shift to much wetter climatic conditions. An abrupt shift to wetter conditions can also be observed at Lake Trichonida in ca. 1500 cal BP and lasts about 100 years. It almost coincides with an abrupt shift towards a slightly negative, neutral NAO index and the wettest period at Lake Lerna (Katrantsiotis et al., 2019). Highest values of the Ti/Ca proxy, indicating increasing runoff under wetter conditions, at Lake Butrint also fall exactly in this phase (Morellón et al., 2016). Wetter conditions are reported from various sites in the Eastern Mediterranean region for approximately 1600 – 1200 cal BP (350 – 750 CE; Finné et al., 2011; Haliuc et al., 2017; Seguin et al., 2019). In central and northern Europe this period is known as Late Antique Little Ice Age or Migration Period and experienced colder and more arid climatic conditions (Büntgen et al., 2016; Helama et al., 2017; McCormick et al., 2012).

During the following millennium, PC1 at Lake Trichonida alternates between drier phases (1350 – 1200 cal BP, 1050 – 900 cal BP, 800 – 650 cal BP, 600 – 450 cal BP), intermediate phases, and shorter wet spells (around 1100 cal BP, 450 – 300 cal BP, around 120 cal BP). With a slight offset, most likely due to dating uncertainties, the wet spells broadly correlate with more negative NAO indices. Probably due to its coarse resolution, the AP/NAP ratio is unaffected by these fluctuations and shows a constant decrease between 1250 and 700 cal BP (700 – 1250 CE) which may hint towards human deforestation activity, but does not indicate any abrupt landscape changes. The period lasting approximately from 1000 to 700 BP (950 – 1250 CE) is often referred to as Medieval Climate

Anomaly and is generally considered a period with warmer temperatures on the northern hemisphere (Luterbacher et al., 2012; Mann et al., 2009; Roberts et al., 2012). According to Finné et al. (2011), its beginning can be characterised by generally wetter conditions in the Eastern Mediterranean. The Lake Trichonida proxy indicates drier or warmer conditions for the period 1050 – 900 cal BP.

The period of the Little Ice Age, approximately 700 – 200 cal BP (1250 – 1750 CE), is generally characterised by colder conditions and glacier advances in the Alps (Magny et al., 2012; Mann et al., 2009) and by wetter conditions in the Mediterranean (Roberts et al., 2012) and on the Peloponnese (Katrantsiotis et al., 2019). The NAO index is more variable at this time (Olsen et al., 2012).

At Lake Trichonida, PC1 shows intermediate values with a higher variability/stronger oscillations, which could suggest more unstable hydroclimatic conditions. Lake Buntrit depicts increased clastic input during wetter conditions for the LIA (Morellón et al., 2016). Lake Lerna shows wetter conditions for 700 – 350 cal BP, followed by a progressive drying (ca 250–100 cal BP; Katrantsiotis et al., 2019). While the Gialova  $\delta D_{31}$  profile distinctly shows a period of wetter conditions (700 – 300 cal BP; Katrantsiotis et al., 2018), PC1 from Trichonida shows very little variation for this period. The youngest and shortest wet period (sedimentary unit 18) around 100 cal BP (1850 CE) is not visible in any other archive.

For the last 100 years, we observe an increasing trend in PC1 that would indicate wetter conditions. More intense anthropogenic impact causing soil erosion, however, would cause a similar signal and it thus seems possible that human activity blurs the climatic signal (Seguin et al., 2019a; Zanchetta et al., 2012).

## **7. Conclusion**

According to their sedimentology, four main facies clusters were identified and described for the Lake Trichonida. High-resolution imagery and the analysis of colour variation along the core is a fast and cheap method that contains unused potential to detect palaeoenvironmental changes. For the future, it would be desirable to further develop it and consider it a standard methodology during sediment core analysis.

The multi-proxy data from Lake Trichonida shows palaeoenvironmental, notably palaeohydrological changes for the last 2,600 years for a region, where high-resolution climate records are sparse, but which would be essential to understand variation in the hydrological pattern in the past in this transitional zone between two very different climatic zones. Evidence of anthropogenic impact on the landscape was only clearly observed for the last 100 years. The majority of the observed fluctuations

in Lake Trichonida were contemporaneous with phases of a more negative NAO index, as reconstructed by Olsen et al. (2012), and thus our record suggests a connectivity between local hydrological variation and the North Atlantic Oscillation on centennial timescales. Our study suggests that during the last 2,600 years, Lake Trichonida and the Eastern Mediterranean/Carpathian region (namely Lake Butrint, Lake Shkodra) are linked by the same moisture source and a positive NAO index regionally translates to drier conditions in the study area. Due to the spatial heterogeneity of the area and the location at a transitional climatic zone, the record also exhibits some local peculiarities such as the coloured sedimentary units that were triggered by short-term events. It thus seems coherent that the signal cannot fully be traced back to climatic oscillations, but additional forcing mechanisms influenced the system and further research is necessary to identify these factors.

### **Acknowledgements**

This research was performed and financed in the framework of the Collaborative Research Centre 1266 ‘Scales of Transformation – Human-environmental interaction in prehistoric and archaic societies’ of the German Research Foundation (DFG, project number 2901391021). In alphabetical order, we kindly thank our following colleagues and students for their invaluable support in the field: Mathias Bahns, Ioannis Prevedouros, Evaggelos Tsiotsis, and Jan Weber. Yasmin Dannath, Sophia Dazert, McKenzie Elliott, and Clemens von Scheffer are acknowledged for support and assistance during laboratory work. The project was carried out with the relevant permits from the Greek authorities, the Institute of Geology and Mineral Exploration of Greece (IGME) and the Water Management Body of Decentralization Prefecture of Peloponnese-Western Greece and Ionian Islands.

### **Author Contributions**

JS conducted the lab work and statistical analyses and wrote the manuscript with contributions of IU, AE and PA. AE conducted the measurement and evaluation of the XRD data and with PA supported the fieldwork and sampling campaign. JS and IU interpreted the data. IU designed the project and headed the fieldwork. WD provided the coring equipment and directed the coring proceeding during fieldwork.



## ORCHID IDs

Pavlos Avramidis: <https://orcid.org/0000-0002-8204-970X>

Joana Seguin: <https://orcid.org/0000-0002-4364-512X>

Ingmar Unkel: <https://orcid.org/0000-0002-8940-1657>

## References

- ad-hoc Arbeitsgruppe Boden: Bodenkundliche Kartieranleitung, E. Schweizerbart'sche Verlagbuchhandlung, Hannover., 2005.
- Albrecht, C., Hauffe, T., Schreiber, K., Trajanovski, S. and Wilke, T.: Mollusc Biodiversity and Endemism in the Potential Ancient Lake Trichonis, Greece, *Malacologia*, 51(2), 357–375, doi:10.4002/040.051.0209, 2009.
- Avramidis, P., Samiotis, A., Kalimani, E., Papoulis, D., Lampropoulou, P. and Bekiari, V.: Sediment characteristics and water physicochemical parameters of the Lysimachia Lake, Western Greece, *Environ. Earth Sci.*, 70(1), 383–392, doi:10.1007/s12665-012-2134-9, 2013.
- Barnston, A. G. and Livezey, R. E.: Classification, Seasonality and Persistence of Low-Frequency Atmospheric Circulation Patterns, *Mon. Weather Rev.*, 115(6), 1083–1126, doi:10.1175/1520-0493(1987)115<1083:CSAPOL>2.0.CO;2, 1987.
- Bintliff, J. L.: *The Complete Archaeology of Greece, from Hunter-Gatherers to the Twentieth Century AD*, Blackwell-Wiley, Oxford, New York., 2012.
- Blaauw, M. and Christeny, J. A.: Flexible paleoclimate age-depth models using an autoregressive gamma process, *Bayesian Anal.*, 6(3), 457–474, doi:10.1214/11-BA618, 2011.
- Bottema, S.: ON THE HISTORY OF THE WALNUT (*JUGLANS REGIA L.*) IN SOUTHEASTERN EUROPE, *Acta Bot. Neerl.*, 29(5–6), 343–349, doi:10.1111/j.1438-8677.1980.tb01240.x, 1980.
- Bottema, S.: Palynological Investigations in Greece with Special Reference to Pollen as an Indicator of Human Activity, *Palaeohistoria*, 24, 257–288, 1982.
- Büntgen, U., Myglan, V. S., Ljungqvist, F. C., McCormick, M., Cosmo, N. Di, Sigl, M., Jungclaus, J., Wagner, S., Krusic, P. J., Esper, J., Kaplan, J. O., Vaan, M. A. C. De, Luterbacher, J., Wacker, L., Tegel, W. and Kirilyanov, A. V.: Cooling and societal change during the Late Antique Little Ice Age from 536 to around 660 AD, *Nat. Geosci.*, 9(March), 231–237,

- doi:10.1038/NGEO2652, 2016.
- Calvert, S. E. and Pedersen, T. F.: Geochemistry of Recent oxic and anoxic marine sediments: Implications for the geological record, *Mar. Geol.*, 113(1–2), 67–88, doi:10.1016/0025-3227(93)90150-T, 1993.
- Christiansen, B. and Ljungqvist, F. C.: Challenges and perspectives for large-scale temperature reconstructions of the past two millennia, *Rev. Geophys.*, 55(1), 40–96, doi:10.1002/2016RG000521, 2017.
- Cohen, A. S.: *Paleolimnology: the history and evolution of lake systems*, 1st ed., Oxford University Press, Oxford., 2003.
- Creer, K. M., Readman, P. W. and Papamarinopoulos, S.: Geomagnetic secular variations in Greece through the last 6000 years obtained from lake sediment studies, *Geophys. J. R. astr. Soc.*, 66, 193–219, 1981.
- Dimitriou, E. and Zacharias, I.: Quantifying the rainfall-water level fluctuation process in a geologically complex Lake catchment, *Environ. Monit. Assess.*, 119(1–3), 491–506, doi:10.1007/s10661-005-9039-y, 2006.
- Dypvik, H. and Harris, N. B.: Geochemical facies analysis of fine-grained siliciclastics using Th/U, Zr/Rb and (Zr + Rb)/Sr ratios, *Chem. Geol.*, 181(1–4), 131–146, doi:10.1016/S0009-2541(01)00278-9, 2001.
- Emmanouilidis, A., Katrantsiotis, C., Norström, E., Risberg, J., Kylander, M., Sheik, T. A., Iliopoulos, G. and Avramidis, P.: Middle to late Holocene palaeoenvironmental study of Gialova Lagoon, SW Peloponnese, Greece, *Quat. Int.*, 476(March), 46–62, doi:10.1016/j.quaint.2018.03.005, 2018.
- Emmanouilidis, A., Unkel, I., Triantaphyllou, M. and Avramidis, P.: Late-Holocene coastal depositional environments and climate changes in the Gulf of Corinth, Greece, *The Holocene*, 095968361987579, doi:10.1177/0959683619875793, 2019.
- Finné, M., Holmgren, K., Sundqvist, H. S., Weiberg, E. and Lindblom, M.: Climate in the eastern Mediterranean, and adjacent regions, during the past 6000 years - A review, *J. Archaeol. Sci.*, 38(12), 3153–3173, doi:10.1016/j.jas.2011.05.007, 2011.
- Finné, M., Bar-Matthews, M., Holmgren, K., Sundqvist, H. S., Liakopoulos, I. and Zhang, Q.: Speleothem evidence for late Holocene climate variability and floods in Southern Greece,

- Quat. Res. (United States), 81(2), 213–227, doi:10.1016/j.yqres.2013.12.009, 2014.
- Finné, M., Woodbridge, J., Labuhn, I. and Roberts, C. N.: Holocene hydro-climatic variability in the Mediterranean: A synthetic multi-proxy reconstruction, *The Holocene*, 29(5), 847–863, doi:10.1177/0959683619826634, 2019.
- Fouache, E. and Pavlopoulos, K.: The Interplay between Environment and People from Neolithic to Classical Times in Greece and Albania, in *Landscapes and Societies: Selected Cases*, edited by I. P. Martini and W. Chesworth, pp. 155–166, Springer Science & Business Media., 2010.
- Grootes, P. M., Nadeau, M.-J. and Rieck, A.: 14C-AMS at the Leibniz-Labor: radiometric dating and isotope research, *Nucl. Instruments Methods Phys. Res. Sect. B Beam Interact. with Mater. Atoms*, 223–224(SPEC. ISS.), 55–61, doi:10.1016/j.nimb.2004.04.015, 2004.
- Haenssler, E., Nadeau, M. J., Vött, A. and Unkel, I.: Natural and human induced environmental changes preserved in a Holocene sediment sequence from the Etoliko Lagoon, Greece: New evidence from geochemical proxies, *Quat. Int.*, 308–309, 89–104, doi:10.1016/j.quaint.2012.06.031, 2013.
- Haliuc, A., Veres, D., Brauer, A., Hubay, K., Hutchinson, S., Begy, R. and Braun, M.: Palaeohydrological changes during the mid and late Holocene in the Carpathian area, central-eastern Europe, *Glob. Planet. Change*, 152, 99–114, doi:10.1016/j.gloplacha.2017.02.010, 2017.
- Helama, S., Jones, P. D. and Briffa, K. R.: Dark Ages Cold Period: A literature review and directions for future research, *The Holocene*, 16(Eteläranta 55), 095968361769389, doi:10.1177/0959683617693898, 2017.
- Insinga, D. D., Petrosino, P., Alberico, I., Lange, G. J., Lubritto, C., Molisso, F., Sacchi, M., Sulpizio, R., Wu, J. and Lirer, F.: The Late Holocene tephra record of the central Mediterranean Sea: Mapping occurrences and new potential isochrons for the 4.4–2.0 ka time interval, *J. Quat. Sci.*, jqs.3154, doi:10.1002/jqs.3154, 2019.
- Izdebski, A., Pickett, J., Roberts, N. and Waliszewski, T.: The environmental, archaeological and historical evidence for regional climatic changes and their societal impacts in the Eastern Mediterranean in Late Antiquity, *Quat. Sci. Rev.*, 136, 189–208, doi:10.1016/j.quascirev.2015.07.022, 2016.
- Jin, Z., Cao, J., Wu, J. and Wang, S.: A Rb/Sr record of catchment weathering response to Holocene

- climate change in Inner Mongolia, *Earth Surf. Process. Landforms*, 31(3), 285–291, doi:10.1002/esp.1243, 2006.
- Johnston, E. N., Phillips, J. C., Bonadonna, C. and Watson, I. M.: Reconstructing the tephra dispersal pattern from the Bronze Age eruption of Santorini using an advection-diffusion model, *Bull. Volcanol.*, 74(6), 1485–1507, doi:10.1007/s00445-012-0609-x, 2012.
- Katrantsiotis, C., Kylander, M. E., Smittenberg, R. H., Yamoah, K. K. A., Hättestrand, M., Avramidis, P., Strandberg, N. A. and Norström, E.: Eastern Mediterranean hydroclimate reconstruction over the last 3600 years based on sedimentary n-alkanes, their carbon and hydrogen isotope composition and XRF data from the Gialova Lagoon, SW Greece, *Quat. Sci. Rev.*, 194, 77–93, doi:10.1016/j.quascirev.2018.07.008, 2018.
- Katrantsiotis, C., Norström, E., Smittenberg, R. H. and Finne, M.: Climate changes in the Eastern Mediterranean over the last 5000 years and their links to the high-latitude atmospheric patterns and Asian monsoons, *Glob. Planet. Change*, 175(January), 36–51, doi:10.1016/j.gloplacha.2019.02.001, 2019.
- Keigwin, L. D.: The Little Ice Age and Medieval Warm Period in the Sargasso Sea, *Science* (80-. ), 274(5292), 1504–1508, doi:10.1126/science.274.5292.1504, 1996.
- Kelly, M. and Ó Grada, C.: The Waning of the Little Ice Age: Climate Change in Early Modern Europe, *J. Interdiscip. Hist.*, XLIV(3), 369–377, doi:10.1162/JINH, 2014.
- Khamnueva-Wendt, S., Mitusov, A. V., Wendt, J. and Bork, H.-R.: Classification of buried soils, cultural, and colluvial deposits in the Viking town Hedeby, *Geoarchaeology*, in press(January), gea.21777, doi:10.1002/gea.21777, 2019.
- Kiratzi, A., Sokos, E., Ganas, A., Tselentis, A., Benetatos, C., Roumelioti, Z., Serpetsidaki, A., Andriopoulos, G., Galanis, O. and Petrou, P.: The April 2007 earthquake swarm near Lake Trichonis and implications for active tectonics in western Greece, in *Tectonophysics*, vol. 452, pp. 51–65., 2008.
- Köppen, W.: *Das geographische System der Klimate*, Gebrüder B., Berlin., 1936.
- Koussouris, T. S. and Diapoulis, A. C.: The aquatic vegetation of a large deep and oligotrophic lake (Lake Trichonis, western Greece), *Thalassographica*, 5(2), 33–40, 1982.
- Krüger, S. and Damrath, M.: In search of the Bølling-Oscillation: a new high resolution pollen record from the locus classicus Lake Bølling, Denmark, *Veg. Hist. Archaeobot.*, (Overbeck 1975),

doi:10.1007/s00334-019-00736-3, 2019.

- Kylander, M. E., Ampel, L., Wohlfarth, B. and Veres, D.: High-resolution X-ray fluorescence core scanning analysis of Les Echets (France) sedimentary sequence: new insights from chemical proxies, *J. Quat. Sci.*, 26(1), 109–117, doi:10.1002/jqs.1438, 2011.
- Lintern, A., Leahy, P. J., Zawadzki, A., Gadd, P., Heijnis, H., Jacobsen, G., Connor, S., Deletic, A. and McCarthy, D. T.: Sediment cores as archives of historical changes in floodplain lake hydrology, *Sci. Total Environ.*, 544, 1008–1019, doi:10.1016/j.scitotenv.2015.11.153, 2016.
- Luterbacher, J., García-Herrera, R., Akcer-On, S., Allan, R., Alvarez-Castro, M.-C., Benito, G., Booth, J., Büntgen, U., Cagatay, N., Colombaroli, D., Davis, B., Esper, J., Felis, T., Fleitmann, D., Frank, D., Gallego, D., Garcia-Bustamante, E., Glaser, R., Gonzalez-Rouco, F. J., Goosse, H., Kiefer, T., Macklin, M. G., Manning, S. W., Montagna, P., Newman, L., Power, M. J., Rath, V., Ribera, P., Riemann, D., Roberts, N., Sicre, M.-A., Silenzi, S., Tinner, W., Tzedakis, P. C., Valero-Garcés, B., van der Schrier, G., Vannièrè, B., Vogt, S., Wanner, H., Werner, J. P., Willett, G., Williams, M. H., Xoplaki, E., Zerefos, C. S. and Zorita, E.: A Review of 2000 Years of Paleoclimatic Evidence in the Mediterranean, in *The Climate of the Mediterranean Region*, edited by P. Lionello, pp. 87–185, Elsevier., 2012.
- Luterbacher, J., Werner, J. P., Smerdon, J. E. E., Fernández-Donado, L., González-Rouco, F. J. J., Barriopedro, D., Ljungqvist, F. C., Büntgen, U., Zorita, E., Wagner, S., Esper, J., McCarroll, D., Toreti, A., Frank, D., Jungclaus, J. H. H., Barriendos, M., Bertolin, C., Bothe, O., Brázdil, R., Camuffo, D., Dobrovolný, P., Gagen, M., García-Bustamante, E., Ge, Q., Gómez-Navarro, J. J. J., Guiot, J., Hao, Z., Hegerl, G. C. C., Holmgren, K., Klimenko, V. V. V., Martín-Chivelet, J., Pfister, C., Roberts, N., Schindler, A., Schurer, A., Solomina, O., Von Gunten, L., Wahl, E., Wanner, H., Wetter, O., Xoplaki, E., Yuan, N., Zanchettin, D., Zhang, H. and Zerefos, C.: European summer temperatures since Roman times, *Environ. Res. Lett.*, 11(2), 024001, doi:10.1088/1748-9326/11/2/024001, 2016.
- Magny, M., Joannin, S., Galop, D., Vannièrè, B., Haas, J. N., Bassetti, M., Bellintani, P., Scandolari, R. and Desmet, M.: Holocene palaeohydrological changes in the northern Mediterranean borderlands as reflected by the lake-level record of Lake Ledro, northeastern Italy, *Quat. Res.*, 77(3), 382–396, doi:10.1016/j.yqres.2012.01.005, 2012.
- Mangini, A., Spötl, C. and Verdes, P.: Reconstruction of temperature in the Central Alps during the past 2000 yr from a  $\delta^{18}\text{O}$  stalagmite record, *Earth Planet. Sci. Lett.*, 235(3–4), 741–751,

- doi:10.1016/j.epsl.2005.05.010, 2005.
- Mann, M. E., Zhang, Z., Rutherford, S., Bradley, R. S., Hughes, M. K., Shindell, D., Ammann, C., Faluvegi, G. and Ni, F.: Global Signatures and Dynamical Origins of the Little Ice Age and Medieval Climate Anomaly, *Science* (80-. ), 326(5957), 1256–1260, doi:10.1126/science.1177303, 2009.
- McCormick, M., Büntgen, U., Cane, M. A., Cook, E. R., Harper, K., Huybers, P., Litt, T., Manning, S. W., Mayewski, P. A., More, A. F. M., Nicolussi, K. and Tegel, W.: Climate Change during and after the Roman Empire: Reconstructing the Past from Scientific and Historical Evidence, *J. Interdiscip. Hist.*, 43(2), 169–220, doi:10.1162/JINH\_a\_00379, 2012.
- Mercuri, A. M. and Sadori, L.: Mediterranean Culture and Climatic Change: Past Patterns and Future Trends., in *The Mediterranean Sea: Its History and Present Challenges*, edited by S. Goffredo and Z. Dubinsky, pp. 507–526, Springer, Heidelberg, New York, London., 2014.
- Meriam, E. O., Aurélia, H., Héléne, L., Volkan, K., Jacqueline, V. A., Gilles, L., Olivier, D. and Sabine, S.: Soil erosion in relation to land-use changes in the sediments of Amik Lake near Antioch antique city during the last 4 kyr, *The Holocene*, 1–15, doi:10.1177/0959683617715702, 2017.
- Meyers, P. A.: Applications of organic geochemistry to paleolimnological reconstructions: A summary of examples from the Laurentian Great Lakes, *Org. Geochem.*, 34(2), 261–289, doi:10.1016/S0146-6380(02)00168-7, 2003.
- Mingram, J., Negendank, J. F. W., Brauer, A., Berger, D., Hendrich, A., Köhler, M. and Usinger, H.: Long cores from small lakes - Recovering up to 100 m-long lake sediment sequences with a high-precision rod-operated piston corer (Usinger-corer), *J. Paleolimnol.*, 37(4), 517–528, doi:10.1007/s10933-006-9035-4, 2007.
- Mook, W. G. and van der Plicht, J.: Reporting  $^{14}\text{C}$  activities and concentrations, *Radiocarbon*, 41(3), 227–239, doi:10.1017/S0033822200057106, 1999.
- Morellón, M., Anselmetti, F. S., Ariztegui, D., Brushulli, B., Sinopoli, G., Wagner, B., Sadori, L., Gilli, A. and Pambuku, A.: Human-climate interactions in the central Mediterranean region during the last millennia: The laminated record of Lake Butrint (Albania), *Quat. Sci. Rev.*, 136, 134–152, doi:10.1016/j.quascirev.2015.10.043, 2016.
- Munsell, A. H.: *Munsell Soil Color Charts, Munsell Color, Grand Rapids.*, 2000.

- Neukom, R., Steiger, N., Gómez-Navarro, J. J., Wang, J. and Werner, J. P.: No evidence for globally coherent warm and cold periods over the preindustrial Common Era, *Nature*, 571(7766), 550–554, doi:10.1038/s41586-019-1401-2, 2019.
- Nieto-Moreno, V., Martínez-Ruiz, F., Giral, S., Jiménez-Espejo, F., Gallego-Torres, D., Rodrigo-Gámiz, M., García-Orellana, J., Ortega-Huertas, M. and De Lange, G. J.: Tracking climate variability in the western Mediterranean during the Late Holocene: A multiproxy approach, *Clim. Past*, 7(4), 1395–1414, doi:10.5194/cp-7-1395-2011, 2011.
- Norström, E., Katrantsiotis, C., Finné, M., Risberg, J., Smittenberg, R. H. and Bjursäter, S.: Biomarker hydrogen isotope composition ( $\delta D$ ) as proxy for Holocene hydroclimatic change and seismic activity in SW Peloponnese, Greece, *J. Quat. Sci.*, 33(5), 563–574, doi:10.1002/jqs.3036, 2018.
- Olsen, J., Anderson, N. J. and Knudsen, M. F.: Variability of the North Atlantic Oscillation over the past 5,200 years, *Nat. Geosci.*, 5(11), 808–812, doi:10.1038/ngeo1589, 2012.
- Overbeck, J., Anagnostidis, K. and Economou-Amilli, A.: A limnological survey of three Greek lakes: Trichonis, Lyssimachia and Amvrakia, *Arch Hydrobiol*, 95(January 1982), 365–394, 1982.
- Psomiadis, D., Dotsika, E., Albanakis, K., Ghaleb, B. and Hillaire-Marcel, C.: Speleothem record of climatic changes in the northern Aegean region (Greece) from the Bronze Age to the collapse of the Roman Empire, *Palaeogeogr. Palaeoclimatol. Palaeoecol.*, 489(January), 272–283, doi:10.1016/j.palaeo.2017.10.021, 2018.
- R Core Team: R: A language and environment for statistical computing, R Foundation for Statistical Computing, Vienna, Austria, Austria. [online] Available from: <https://www.r-project.org/>, 2019.
- Roberts, N., Eastwood, W. J., Kuzucuoğlu, C., Fiorentino, G. and Caracuta, V.: Climatic, vegetation and cultural change in the eastern Mediterranean during the mid-Holocene environmental transition, *The Holocene*, 21(1), 147–162, doi:10.1177/0959683610386819, 2011.
- Roberts, N., Moreno, A., Valero-Garcés, B. L., Corella, J. P., Jones, M., Allcock, S., Woodbridge, J., Morellón, M., Luterbacher, J., Xoplaki, E. and Türkeş, M.: Palaeolimnological evidence for an east-west climate see-saw in the Mediterranean since AD 900, *Glob. Planet. Change*, 84–85, 23–34, doi:10.1016/j.gloplacha.2011.11.002, 2012.

- Sabatier, P., Wilhelm, B., Ficetola, G. F., Moiroux, F., Poulenard, J., Develle, A.-L., Bichet, A., Chen, W., Pignol, C., Reyss, J.-L., Gielly, L., Bajard, M., Perrette, Y., Malet, E., Taberlet, P. and Arnaud, F.: 6-kyr record of flood frequency and intensity in the western Mediterranean Alps – Interplay of solar and temperature forcing, *Quat. Sci. Rev.*, 170, 121–135, doi:10.1016/j.quascirev.2017.06.019, 2017.
- Seguin, J., Bintliff, J. L., Grootes, P. M., Bauersachs, T., Dörfler, W., Heymann, C., Manning, S. W., Müller, S., Nadeau, M.-J., Nelle, O., Steier, P., Weber, J., Wild, E.-M., Zagana, E. and Unkel, I.: 2500 years of anthropogenic and climatic landscape transformation in the Stymphalia polje, Greece, *Quat. Sci. Rev.*, 213, 133–154, doi:10.1016/j.quascirev.2019.04.028, 2019a.
- Seguin, J., Avramidis, P., Haug, A., Kessler, T., Schimmelmann, A. and Unkel, I.: Inter-comparison of palaeoenvironmental records from four lacustrine archives on the Peloponnese (Greece) over the last 5,000 years. Manuscript submitted for publication, 2019b.
- Spearman, C.: The Proof and Measurement of Association between Two Things, *Am. J. Psychol.*, 15(1), 72, doi:10.2307/1412159, 1904.
- Statham, P. J., Homoky, W. B., Parker, E. R., Klar, J. K., Silburn, B., Poulton, S. W., Kröger, S., Pearce, R. B. and Harris, E. L.: Extending the applications of sediment profile imaging to geochemical interpretations using colour, *Cont. Shelf Res.*, 185(November 2017), 16–22, doi:10.1016/j.csr.2017.12.001, 2017.
- Tafas, T. and Economou-Amilli, A.: Limnological survey of the warm monomictic lake Trichonis (central western greece). II. Seasonal phytoplankton periodicity – a community approach, *Hydrobiologia*, 344(February 1986), 141–153, doi:https://doi.org/10.1023/A:1002962513146, 1997.
- Tafas, T., Danielidis, D., Overbeck, J. and Economou-Amilli, A.: Limnological survey of the warm monomictic lake Trichonis (central western greece). I. The physical and chemical environment, *Hydrobiologia*, 344(February 1986), 129–139, doi:https://doi.org/10.1023/A:1002914629984, 1997.
- Tjallingii, R., Röhl, U., Kölling, M. and Bickert, T.: Influence of the water content on X-ray fluorescence coresampling measurements in soft marine sediments, *Geochemistry, Geophysics. Geosystems*, 8(2), 1–12, doi:10.1029/2006GC001393, 2007.
- Unkel, I., Schimmelmann, A., Shriner, C., Forsén, J., Heymann, C. and Brückner, H.: The environmental history of the last 6500 years in the Asea Valley (Peloponnese, Greece) and



- its linkage to the local archaeological record, *Zeitschrift für Geomorphol. Suppl. Issues*, 58(2), 89–107, doi:10.1127/0372-8854/2014/S-00160, 2014.
- Vaezi, A., Ghazban, F., Tavakoli, V., Routh, J., Beni, A. N., Bianchi, T. S., Curtis, J. H. and Kylin, H.: A Late Pleistocene-Holocene multi-proxy record of climate variability in the Jazmurian playa, southeastern Iran, *Palaeogeogr. Palaeoclimatol. Palaeoecol.*, 514(January), 754–767, doi:10.1016/j.palaeo.2018.09.026, 2019.
- Warken, S. F., Fohlmeister, J., Schröder-Ritzrau, A., Constantin, S., Spötl, C., Gerdes, A., Esper, J., Frank, N., Arps, J., Terente, M., Riechelmann, D. F. C., Mangini, A. and Scholz, D.: Reconstruction of late Holocene autumn/winter precipitation variability in SW Romania from a high-resolution speleothem trace element record, *Earth Planet. Sci. Lett.*, 499, 122–133, doi:10.1016/j.epsl.2018.07.027, 2018.
- Weiberg, E., Unkel, I., Kouli, K., Holmgren, K., Avramidis, P., Bonnier, A., Dibble, F., Finné, M., Izdebski, A., Katrantsiotis, C., Stocker, S. R., Andwinge, M., Baika, K., Boyd, M. and Heymann, C.: The socio-environmental history of the Peloponnese during the Holocene: Towards an integrated understanding of the past, *Quat. Sci. Rev.*, 136, 40–65, doi:10.1016/j.quascirev.2015.10.042, 2016.
- Weltje, G. J. and Tjallingii, R.: Calibration of XRF core scanners for quantitative geochemical logging of sediment cores: Theory and application, *Earth Planet. Sci. Lett.*, 274(3–4), 423–438, doi:10.1016/j.epsl.2008.07.054, 2008.
- Wilhelm, B., Nomade, J., Crouzet, C., Litty, C., Sabatier, P., Belle, S., Rolland, Y., Revel, M., Courboulex, F., Arnaud, F. and Anselmetti, F. S.: Quantified sensitivity of small lake sediments to record historic earthquakes: Implications for paleoseismology, *J. Geophys. Res. Earth Surf.*, 121(1), 2–16, doi:10.1002/2015JF003644, 2016.
- Wilson, R., Anchukaitis, K., Briffa, K. R., Büntgen, U., Cook, E., Arrigo, R. D., Davi, N., Esper, J., Frank, D., Hegerl, G., Helama, S., Klesse, S., Krusic, P. J., Linderholm, H. W., Myglan, V., Osborn, T. J., Zhang, P., Zorita, E., Schurer, A., Wiles, G., Gunnarson, B., Frank, D., Hegerl, G., Helama, S., Klesse, S., Krusic, P. J., Linderholm, H. W., Myglan, V., Osborn, T. J., Rydval, M. M., Schneider, L., Schurer, A., Wiles, G., Zhang, P., Zorita, E., Schurer, A., Wiles, G., Gunnarson, B., Frank, D., Hegerl, G., Helama, S., Klesse, S., Krusic, P. J., Linderholm, H. W., Myglan, V., Osborn, T. J., Rydval, M. M., Schneider, L., Schurer, A., Wiles, G., Zhang, P., Zorita, E., Schurer, A., Wiles, G., D'Arrigo, R., Davi, N., Esper, J.,

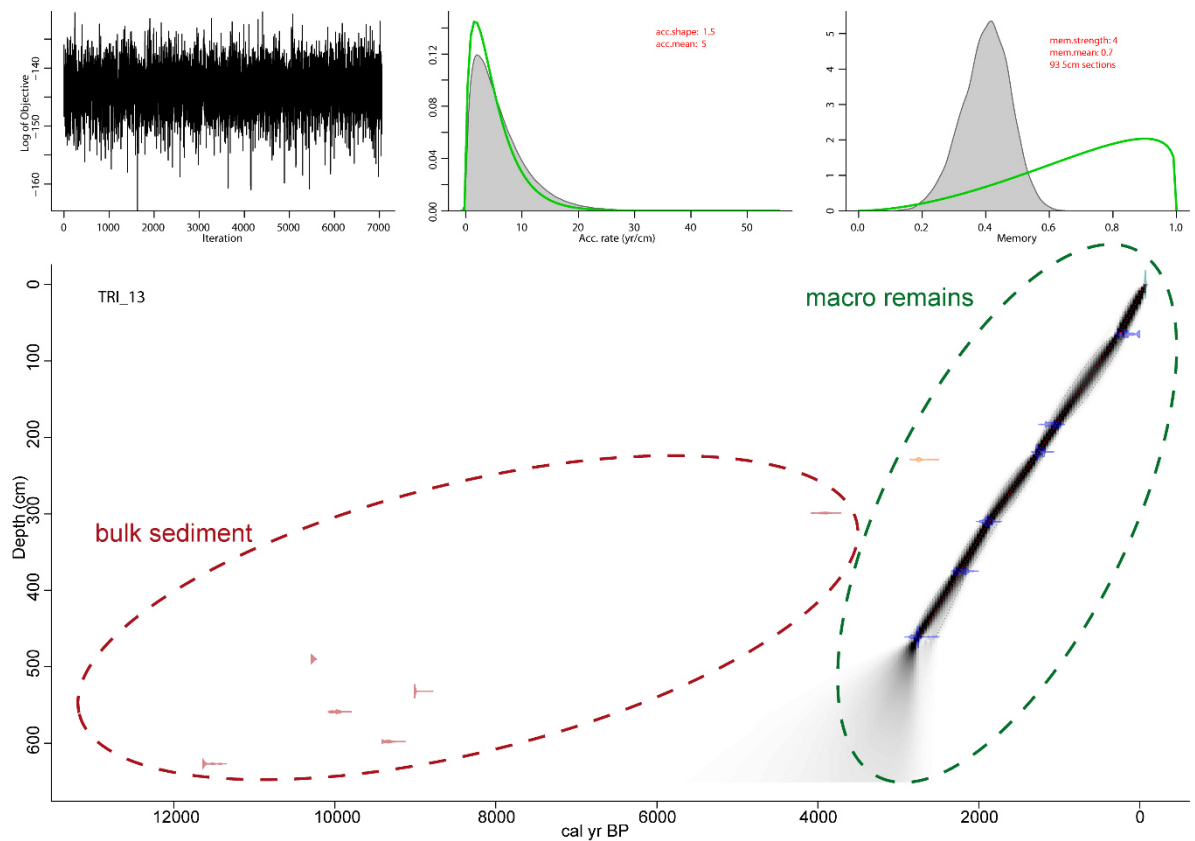
- Frank, D., Gunnarson, B., Hegerl, G., Helama, S., Klesse, S., Krusic, P. J., Linderholm, H. W., Myglan, V., Osborn, T. J., Rydval, M. M., Schneider, L., Schurer, A., Wiles, G., Zhang, P. and Zorita, E.: Last millennium northern hemisphere summer temperatures from tree rings: Part I: The long term context, *Quat. Sci. Rev.*, 134, 1–18, doi:10.1016/j.quascirev.2015.12.005, 2016.
- Xoplaki, E., González-Rouco, J. F., Gyalistras, D., Luterbacher, J., Rickli, R. and Wanner, H.: Interannual summer air temperature variability over Greece and its connection to the large-scale atmospheric circulation and Mediterranean SSTs 1950-1999, *Clim. Dyn.*, 20(5), 537–554, doi:10.1007/s00382-002-0291-3, 2003a.
- Xoplaki, E., González-Rouco, J. F., Luterbacher, J. and Wanner, H.: Mediterranean summer air temperature variability and its connection to the large-scale atmospheric circulation and SSTs, *Clim. Dyn.*, 20(7–8), 723–739, doi:10.1007/s00382-003-0304-x, 2003b.
- Xu, H., Liu, B., Wu, F., Dasch, E., Liu, C., Zhang, J., Li, C., Chen, J., An, Z., Head, J., Chen, J., An, Z., Liu, L., Ji, J., Yang, J., Chen, Y., Jin, Z., Cao, J., Wu, J., Wang, S., Xu, H., Liu, X., An, Z., Hou, Z., Dong, J., Xu, H., Ai, L., Tan, L., An, Z., Xu, H., Hou, Z., An, Z., Liu, X., Dong, J., Pang, J., Huang, C., Zhang, Z., Li, F., Xie, C., Pan, G., Xu, H., Hou, Z., Ai, L. and Tan, L.: Spatial and temporal variations of Rb/Sr ratios of the bulk surface sediments in Lake Qinghai, *Geochem. Trans.*, 11(1), 3, doi:10.1186/1467-4866-11-3, 2010.
- Zacharias, I. and Ferentinos, G.: A numerical model for the winter circulation in Lake Trichonis, Greece, *Environ. Model. Softw.*, 12(4), 311–321, doi:10.1016/S1364-8152(97)00021-2, 1997.
- Zacharias, I., Bertachas, I., Skoulikidis, N. and Koussouris, T.: Greek Lakes: Limnological overview, *Lakes Reserv. Res. Manag.*, 7(1), 55–62, doi:10.1046/j.1440-1770.2002.00171.x, 2002.
- Zanchetta, G., Van Welden, A., Baneschi, I., Drysdale, R., Sadori, L., Roberts, N., Giardini, M., Beck, C., Pascucci, V. and Sulpizio, R.: Multiproxy record for the last 4500 years from Lake Shkodra (Albania/Montenegro), *J. Quat. Sci.*, 27(8), 780–789, doi:10.1002/jqs.2563, 2012.
- Zotos, A., Raus, T. and Dimopoulos, P.: New floristic reports from the lakes Trichonis and Lisimachia (W Greece), *Willdenowia*, 36(2), 731–739, doi:10.3372/wi.36.36208, 2006.

## Supplementary Material

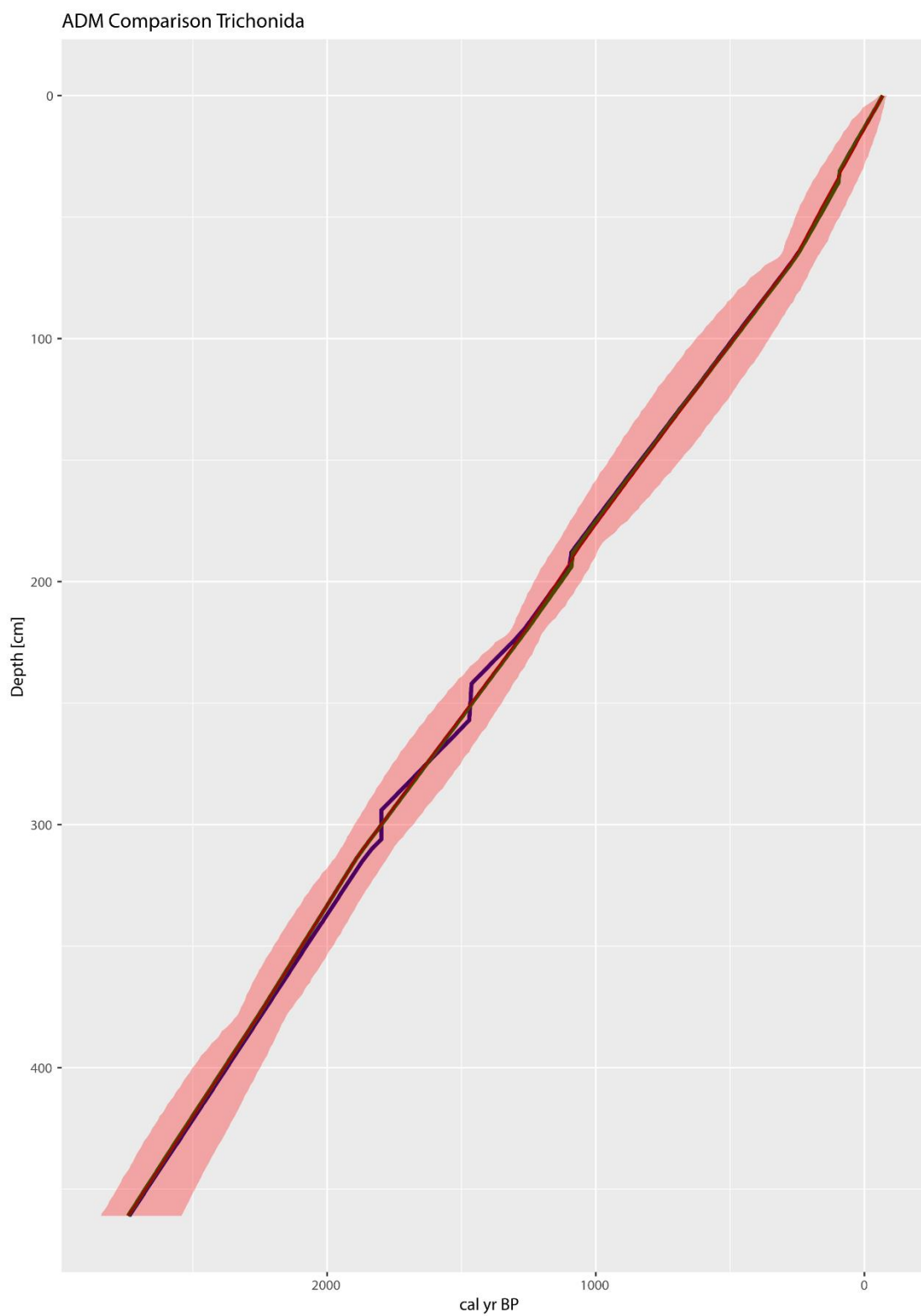
**Supplementary Material 1: Masterscale TRI1 indicating the respective sections used for the composite core composition.**

Core	Segment	Masterscale top [cm]	Masterscale bottom [cm]	Section length [cm]	explanation for anchor point
TRI1 A	1	0	86	86	thin dark gray layer in unit 17 in both cores
TRI1 B	1	86	140	54	defined
TRI1 A	2	140	189	49	upper boundary of dark unit 16
TRI1 B	2	189	225	36	defined
TRI1 A	3	225	256	31	lower boundary of reddish unit 14
TRI1 B	3	256	315	59	lower boundary of reddish unit 11
TRI1 A	4	315	360	45	defined
TRI1 B	4	360	438.5	78.5	end of core segment

**Supplementary Material 2: Age-depth graph indicating all measured radiocarbon ages. Samples taken from bulk sediment (in red) consequently yield too old ages.**



**Supplementary Material 3: Comparison graph with different age-depth models showing continuous sedimentation model (red) vs. event layer models (green, purple).**



# Appendix IV



# **Mastering a master sediment core compilation from parallel drill cores using RGB values**

Joana Seguin<sup>1\*</sup>, Ingmar Unkel<sup>1</sup>

<sup>1</sup>Institute for Ecosystem Research, Christian-Albrechts-University, Olshausenstraße 75, 24118 Kiel, Germany

\*Corresponding author: jseguin@ecology.uni-kiel.de

## **Keywords**

*R; reproducible research; environmental modelling, Palaeolimnology; Sedimentology; RGB values*

## **Abstract**

Sediment cores from marine or lacustrine environments, serving as geo-archives, are often not drilled en bloc but section by section. Frequently, parallel drillings are performed with an offset to ensure that the transitional parts are also covered. Proxy measurements from both cores are subsequently merged computationally to obtain one continuous master core sequence that serves for palaeoenvironmental reconstruction.

This report provides a transparent and reproducible approach, using the open-source programming language R, on how to compile a master sediment core based on several core sections from parallel drill cores. We use continuous RGB values as recorded by line-scan camera imagery. This approach is transparent, reproducible, quick, clean, and cheap.

## **Kurzfassung**

Sedimentkerne aus marinen oder lakustrinen Untersuchungsgebieten dienen als Geoarchive und werden in der Regel nicht vollständig sondern abschnittsweise erbohrt. Häufig erfolgen versetzte Parallelbohrungen, um Überlappungsbereiche abzudecken. Am Computer wird das Material anschließend zu einem durchgängigen Masterkern zusammengesetzt, der dann als Basis der Paläoumweltrekonstruktionen dient. Dieser Report stellt einen methodischen Ansatz vor, wie die Zusammensetzung eines Masterkerns mittels der open-source Software R transparent nachvollziehbar, reproduzierbar, schnell, sauber und kostengünstig erfolgen kann. Hierzu werden kontinuierliche RGB-Werte einer Line-Scan Kamera verwendet.

## **1. Introduction**

Sediment cores are widely used geo-archives to study palaeoenvironmental history or landscape evolution. When extracted from a marine or lacustrine environment, sediment cores are not recovered as a whole, but are generally retrieved section-wise. The length of the sections thereby depends on the drilling equipment and usually ranges from one-meter- to several-meter-sections. There is a large number of studies published on sediment sequences, where the various sediment core sections from one bore hole have simply been stuck one below the other and were then used as master core. This proceeding may lead to gaps (of unknown thickness) or inconsistencies at the transitions, because the material at the edges may often be altered or partly gets lost during the recovery. Other studies indicate that they have compiled a master core sequence, master record, or composite core from two or more parallel sediment cores without further specification how this was done exactly (for example Vannièrè et al., 2013; Francke et al., 2013), although there are different possible approaches how to achieve this goal.

In palaeoenvironmental research, especially in an interdisciplinary context with the aim to combine palaeoenvironmental reconstructions from the geo-archive with archaeological evidence for human activity from the surrounding landscape, continuous, accurate, high-resolution proxies indicating even slight changes are highly important. The basis for a credible interpretation is a solid and, at best, trackable and reproducible data preparation.

We here present one methodological approach on how to compile a continuous, high-resolution sediment master core sequence based on several sections from two parallel cores. The emphasis of this report is on the methodological approach. The compilation process is transparent, reproducible, more accurate than a simple visual correlation on the material, and can be modified at any time. Furthermore, we outline some sensitive choices that need to be made at the beginning of the workflow and that have a considerable impact on the data quality and interpretation. We use the open-source computing environment R (R Core Team, 2017), because it is independent, cost and time saving and it is one of the most widely used scientific programming languages in academia, notably in environmental sciences and archaeology (Lai et al., 2019; Marwick, 2018). Our paper aims at presenting a workflow that allows a large community of palaeoenvironmental scientists to reproduce, replicate, apply, adopt and further develop our approach.



## **2. Challenges in sediment core compilation**

In order to obtain a continuous sediment sequence, there is the need for drilling parallel sediment cores with an ideally small horizontal and a constant vertical offset. Traditionally, the matching of parallel cores is done visually on the material. Then, the compilation of proxy datasets from both cores is done manually at defined tie points or anchor points.

This proceeding has some challenges:

- (1) It can only be applied decently, when there are facies changes or sedimentary units that can be clearly visually identified. However, sometimes one would find several meters of homogeneous, unicoloured sediment.
- (2) It frequently occurs that sedimentary units in the parallel cores are of different thickness, due to the potential horizontal heterogeneity of the sediment units and the offset between the boreholes.
- (3) If geochemical element curves are used to combine the core sections, the risk of circular reasoning is high when interpreting the coexistence of elemental peaks as a non-ambiguous environmental event that were purposely superimposed during the compilation step.

In the RGB values in a high resolution core photo, ideally derived from a line-camera scan, variations in the sediment can be seen more clearly compared to simple visual inspection and hence tie points can be identified more easily and precisely. When using the computational approach, differences in the thickness of sedimentary units can be taken care of by applying an interpolation method that stretches or compresses the respective unit to make it fit into the gap in the parallel core. This way, the total depth remains unchanged, which may be of advantage depending on the research aim. When using the RGB values for data compilation instead of e.g. geochemical elements derived from XRF-scans, one obtains the color information as an additional proxy. Especially when financial resources are very limited, the master core compilation based on line scan camera images (or similar high-resolution core photos) and RGB values is a quick and cost-efficient method.

## **3. Methodology**

The methodological proceeding is exemplified here using the uppermost sediment core sections from karstic Lake Stymphalia, Southern Greece. Palaeoenvironmental studies on this site and sediment sequence can be found in (Heymann et al., 2013; Seguin et al., 2019; Unkel et al., 2011).

### **3.1 Material acquisition**

Sediment coring in Lake Stymphalia was conducted in 2010 and 2011 using a Usinger drilling equipment. Core segments with 2 m length were drilled and cut into 1 m sections on the site to facilitate handling and transport. It was decided to use sediment core STY-1A as the main core and retrieve a parallel core STY-1B, with a vertical offset of approximately 50 cm, to fill the gaps between the sections in STY-1A in order to obtain a continuous sequence. The core sections were split longitudinally and in a first step, the parallel cores were sedimentologically described, subdivided into sedimentary units and visually correlated. The surfaces of the archive half cores were smoothed, scraped clean and digitally photographed using a line-scan camera with a resolution of 143 pixels\*cm-1 in longitudinal direction and analysed geochemically via non-destructive X-ray fluorescence (XRF) scans using an Avaatech XRF Core Scanner.

### **3.2 Data acquisition**

The line scan image and the RGB-values were saved automatically and one could directly work with the txt-file containing the pixels and the RGBs. However, an additional step was included, because the automated RGB values were interpolated over the whole image width, which not only covered the sediment core, as the camera slit is wider than the core. ImageJ, a Java-based open-source image processing program, was used to extract the RGB values only for the sediment core and store them as a .csv file. The pixel-resolution was converted into mm-resolution (143 pixel = 1 mm) to get the same unit of measure for all further proxies (*local\_depth*). Data cleaning was done in R according to approved standards (cf. e.g. Jonge and Loo, 2013; Marwick, 2017) for detecting and removing incorrect, inconsistent values, which were replaced by spline interpolation to obtain a complete sequence.

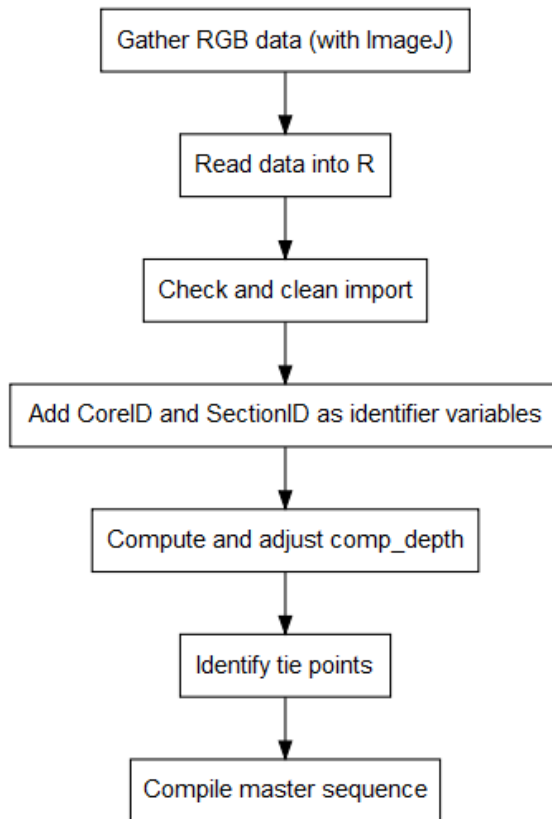


*Figure 1: Workflow for data processing.*

### **3.3 Data preparation**

Combining the different datasets into one continuous sequence as well as data quality assurance was all done using R Version 3.4.2 (R Core Team, 2017). The respective code is included in the supplementary material. For the master core compilation, the continuous, high-resolution profile of only one color is needed. However, the additional information of the remaining two colors are valuable for cross-checking. We here use the red color values from the RGB color spectrum. In a second step, other scanning proxy parameters could be added in the same way to validate the color-based core correlation. Initially, the line-camera scanning produces one data file for each core section. To facilitate and accelerate the workflow, the data frame structure for all sections has to be identical and follow the guidelines for clean data structure (Marwick, 2017).

### 3.4 Data processing

The data for each core section were loaded into R as different data frames. Identifier factor variables (*CoreID* and *SectionID*), indicating the sediment core (1A or 1B) and the section (labelling was done in coring order from top to bottom), were added to each data frame to facilitate retracing the data source after merging the data frames to the final master sequence.

A composite depth variable (*comp\_depth*) was created for all sections in STY-1A based on the *local\_depth*, which set the uppermost limit of the core sections to the full meters based on the applied coring strategy. In the current example, the sections of the parallel STY-1B core were adapted one-by-one to the pre-defined STY-1A frame to cover the gaps between the A-core sections. Firstly, the STY-1B segments were shifted up and down along the *comp\_depth*-scale, until the greatest concordance in the RGB-profiles between the overlapping parts of 1A and 1B was reached. The sedimentary units in segments STY-1B2 and STY-1B4 were slightly thicker than the corresponding units in the STY-1A sequence. Hence, the respective 1B-segments were rescaled using a linear interpolation (*approxm* function from the FreqProf package in R) to make the variables fit to the mm-resolution again. In the last step, anchor points were identified, where the B-core was cut and integrated into the master core sequence. We attempted to take into account the following pre-conditions:

- (1) the sequences taken from the parallel STY-1B core were rather short, but provided a continuous sequence;
- (2) the anchor points were set at full centimetre or half-cm depths as most discrete samples followed this resolution;
- (3) the proxy values (R color, but also checked for geochemical elements Ca, Ti, Fe) at the tie points were approximately the same in both cores, to avoid artificial jumps in the dataset.

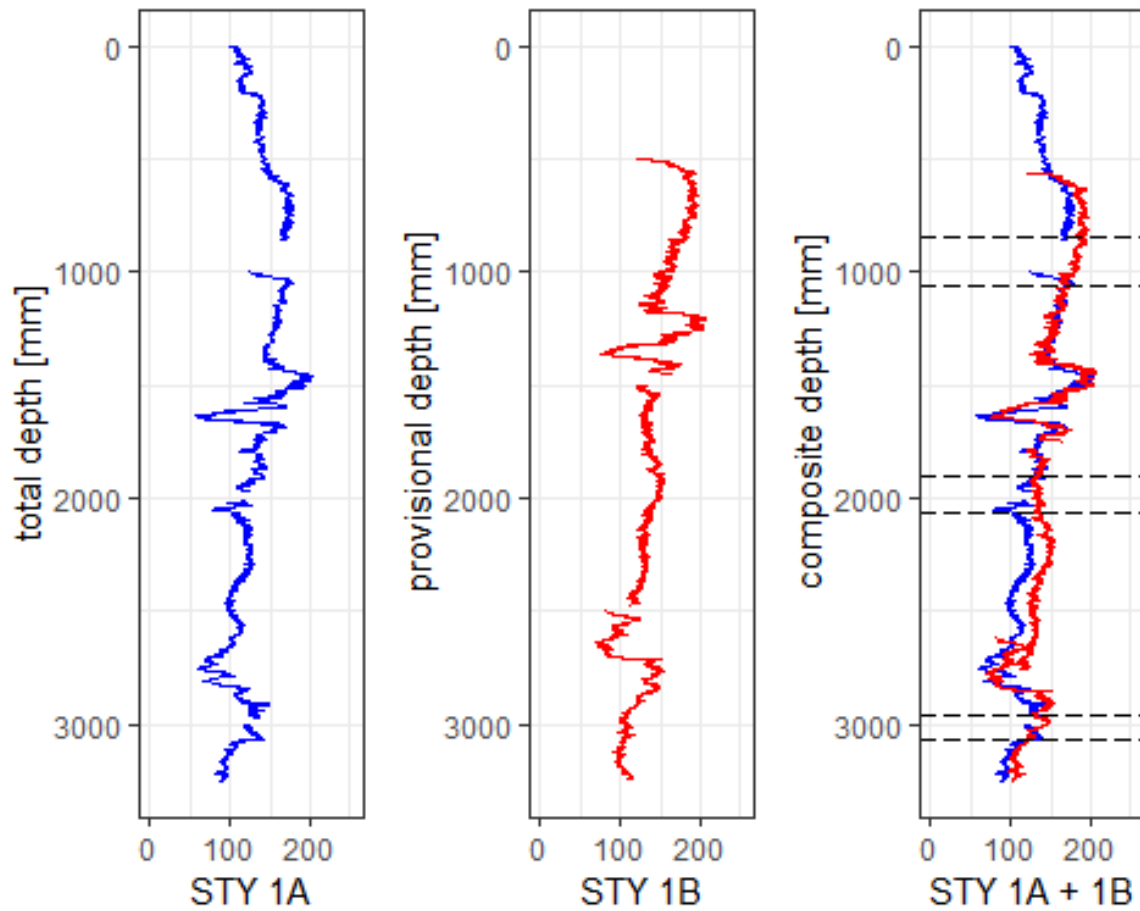


*Figure 2: Composite Core Compilation based on R color. [Left] R color for core sections in STY 1A. [Centre] R color for core sections in STY 1B. The sections provisional start at 500, 1500, and 2500 mm respectively. [Right] R color for STY 1A (blue) and STY 1B (red) combined. STY 1B was shifted and interpolated if necessary to fit to STY 1A.*

## 4. Discussion

### 4.1 The advantage of reproducible research

Facing the increasing amount of data, computation and programming have become essential components of palaeoenvironmental studies (Lai et al., 2019). As R is an open-source programming environment, there is a large (online) community that constantly refines and shares codes, gives support, and helps with problem solving (Marwick, 2018). This makes R a suitable, convenient and neat tool for data analysis and visualization.

Writing a script that executes the code has several advantages. First, it makes the analysis process transparent and readers do not only see the final results, but can systematically follow the analysis and the record of all the decisions made within the process (Marwick, 2017; Peng, 2011). Second, the scientist himself can trace back the individual analysis steps and modify them if necessary.

Furthermore, we can repeat the exact same methodological procedure for different cores and sites in the future, which improves the intercomparability of the data.

#### **4.2 The compiling strategy**

Right from the start of the analysis, there are numerous questions and the scientists need to make certain decisions that are essential for the following analysis process but that are often not visible or justified in the later publication. Is it better to use one drill core as the main core and fill up the gaps with the second one? In addition, does it make sense to set the tie points only at sedimentary unit boundaries? Alternatively, should you rather take complete sedimentary units from both cores and stick them one below the other? Thus, the master core may become longer than the individual parallel cores, but you can be sure that each unit in itself is undisturbed. May there be another, alternate, more suitable option to compile the sediment for the ongoing research? Do we see hiatus, turbidites, slumped or disturbed units in one or in both cores and how do we deal with them?

The approach presented here, including the use of an R script, makes the decisions taken during the core compilation process traceable. We decided to make STY-1A the master core and only fill up small gaps with STY-1B. Here, we did not set the pre-condition to switch from core to the parallel one only at sedimentary unit boundaries, because we did not see the advantage of this approach here. One of our main research aims with the core presented as example here was to detect phases of transformation (Seguin et al., 2019), which potentially come along with visible changes in the sediment. If we had defined the tie points in these most relevant periods at the unit boundaries, it would have been more difficult to explain, whether an observed change in the proxies at this point was an authentic environmental change, we were analyzing, or an artificial shift caused by switching the core, which we may ignore. An example for the latter may be seen in the RGB values at the 84.4 cm transition (cf. Figure 3).

To be consistent in our strategic approach, sampling of organic material for radiocarbon dating and discrete sampling e.g. for grain size analysis or total organic carbon content were all performed on the master core sections of STY-1A and only to a minor extent on STY-1B. This way, it was more straightforward to link the sediment sequence to the later created age-depth-model.

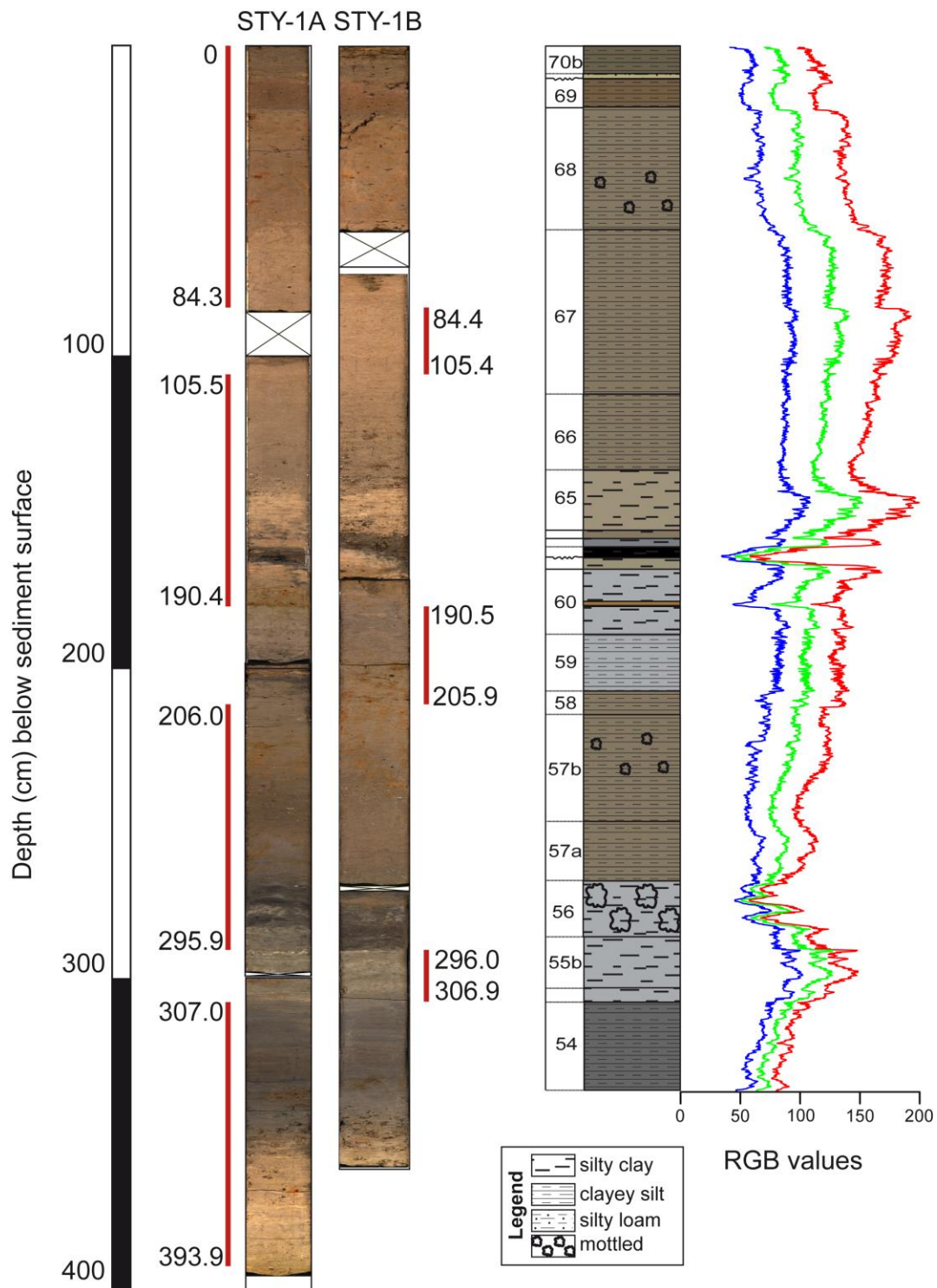


Figure 3: Overview. (Left) Line scan photographs of the upper 4 m of the Lake Stymphalia STY-1A and -1B cores with the master core sequence indicated by the vertical red line. (Right) Schematic representation of the sedimentological units and the distribution of the RGB values against the composite depth in 1 mm resolution.

## 5. Prospect

The use of the open-source software R for the master core compilation as well as for the whole data analysis proceeding brings us a significant step forward in terms of transparency and reproducibility of our research. Furthermore, the reuse and adaptation of scripted code to following study sites with sediment core drillings is not only efficient and timesaving, but ensures the application of the same methodological and statistical approach and facilitates the inter-comparability of different study sites. It should become common practice to publish the code, which an analysis was based on, in the supplementary of the presented study.

Furthermore, we show that continuous RGB colors are a suitable variable to carry out master core compilation with a higher precision than the visual approach. RGB colors additionally hold the potential to serve as palaeoenvironmental proxies, as for example a strong correlation between the red color and calcium content was observed in the cores from Stymphalia. This may open up new future possibilities of using the color vector representative for Ca in palaeoenvironmental studies. For certain elements like Ca or Fe, this could potentially (1) allow for a higher resolution than the XRF scanning, because RGB values are obtained pixel by pixel or (2) save time and money, because the resolution of the XRF scanning may be reduced and the element counts be extrapolated based on the RGB values or the latter could be used as a substitute for the geochemical elements. Including RGB values in palaeoenvironmental reconstruction is thus an asset to the study.

**Author contribution.** IU designed the study. JS performed the analysis and wrote the code. JS prepared the manuscript with contributions of IU. The authors declare that they have no conflict of interest.

**Acknowledgments.** This research was performed in the framework of the CRC 1266 “Scales of transformation” (project number: 2901391021) funded by the DFG (German Research Foundation). We kindly thank our colleague Georg Hörmann for his invaluable support, his coding suggestions and debugging. Further thanks to Ben Marwick and ISAAKiel who introduced JS to the use of open-source code scripting and the topic of reproducibility.



## References

- Francke, A., Wagner, B., Leng, M. J. and Rethemeyer, J.: A Late Glacial to Holocene record of environmental change from Lake Dojran (Macedonia, Greece), *Climate of the Past*, 9(1), 481–498, doi:10.5194/cp-9-481-2013, 2013.
- Heymann, C., Nelle, O., Dörfler, W., Zagana, H., Nowaczyk, N., Xue, J. and Unkel, I.: Late Glacial to mid-Holocene palaeoclimate development of southern Greece inferred from the sediment sequence of Lake Stymphalia (NE-Peloponnese), *Quaternary International*, 302, 42–60, doi:10.1016/j.quaint.2013.02.014, 2013.
- Jonge, E. de and Loo, M. van der: An introduction to data cleaning with R, 53, doi:60083 201313-X-10-13, 2013.
- Lai, J., Lortie, C. J., Muenchen, R. A., Yang, J. and Ma, K.: Evaluating the popularity of R in ecology, *Ecosphere*, 10(1), 1–7, doi:10.1002/ecs2.2567, 2019.
- Marwick, B.: Computational Reproducibility in Archaeological Research: Basic Principles and a Case Study of Their Implementation, *Journal of Archaeological Method and Theory*, 24(2), 424–450, doi:10.1007/s10816-015-9272-9, 2017.
- Marwick, B.: R Coding and Modeling, in *The encyclopedia of archaeological sciences*, pp. 1–5, John Wiley & Sons, Inc., Hoboken, NJ, USA., 2018.
- Peng, R. D.: Reproducible Research in Computational Science, *Science*, 334(6060), 1226–1227, doi:10.1126/science.1213847, 2011.
- R Core Team: R: A language and environment for statistical computing, R Foundation for Statistical Computing, Vienna, Austria. [online] Available from: <https://www.r-project.org/>, 2017.
- Seguin, J., Bintliff, J. L., Grootes, P. M., Bauersachs, T., Dörfler, W., Heymann, C., Manning, S. W., Müller, S., Nadeau, M. J., Nelle, O., Steier, P., Weber, J., Wild, E. M., Zagana, E. and Unkel, I.: 2500 years of anthropogenic and climatic landscape transformation in the Stymphalia polje, Greece, *Quaternary Science Reviews*, 213, 133–154, doi:10.1016/j.quascirev.2019.04.028, 2019.
- Unkel, I., Heymann, C., Nelle, O. and Zagana, E.: Climatic influence on Lake Stymphalia during the last 15 000 years, in *Advances in the research of aquatic environment*, edited by N. Lambrakis, G. Stournaras, and K. Katsanou, pp. 75–82, Springer Berlin Heidelberg, Berlin, Heidelberg., 2011.

Vanni re, B., Magny, M., Joannin, S., Simonneau, A., Wirth, S. B., Hamann, Y., Chapron, E., Gilli, A., Desmet, M. and Anselmetti, F. S.: Orbital changes, variation in solar activity and increased anthropogenic activities: Controls on the Holocene flood frequency in the Lake Ledro area, Northern Italy, *Climate of the Past*, 9(3), 1193–1209, doi:10.5194/cp-9-1193-2013, 2013.

# Appendix V





## LETTER

## Land use patterns and climate change—a modeled scenario of the Late Bronze Age in Southern Greece

## OPEN ACCESS

RECEIVED  
31 July 2019REVISED  
10 October 2019ACCEPTED FOR PUBLICATION  
25 October 2019PUBLISHED  
27 November 2019

Original content from this work may be used under the terms of the [Creative Commons Attribution 3.0 licence](#).

Any further distribution of this work must maintain attribution to the author(s) and the title of the work, journal citation and DOI.

Daniel Knitter<sup>1</sup> , Gerrit Günther<sup>1</sup> , Wolfgang Berengar Hamer<sup>1</sup> , Torben Keßler<sup>3</sup>, Joana Seguin<sup>2</sup> , Ingmar Unkel<sup>2</sup> , Erika Weiberg<sup>4</sup> , Rainer Duttmann<sup>1</sup> and Oliver Nakoinz<sup>5</sup> <sup>1</sup> Christian-Albrechts-Universität zu Kiel, Physical Geography, Ludwig-Meyn-Str. 14, 24118 Kiel, Germany<sup>2</sup> Christian-Albrechts-Universität zu Kiel, Physical Geography, Institute of Ecosystem Research, Olshausenstr. 75, 24118 Kiel, Germany<sup>3</sup> Christian-Albrechts-Universität zu Kiel, Classical Archaeology, Johanna-Mestorf-Str. 5, 24118 Kiel, Germany<sup>4</sup> Department of Archaeology and Ancient History, Uppsala University, Sweden<sup>5</sup> Christian-Albrechts-Universität zu Kiel, Pre- and Protohistoric Archaeology, Johanna-Mestorf-Str. 3, 24118 Kiel, GermanyE-mail: [knitter@geographie.uni-kiel.de](mailto:knitter@geographie.uni-kiel.de)**Keywords:** land-use, subsistence, fuzzy, landscape archaeology, vulnerabilitySupplementary material for this article is available [online](#)**Abstract**

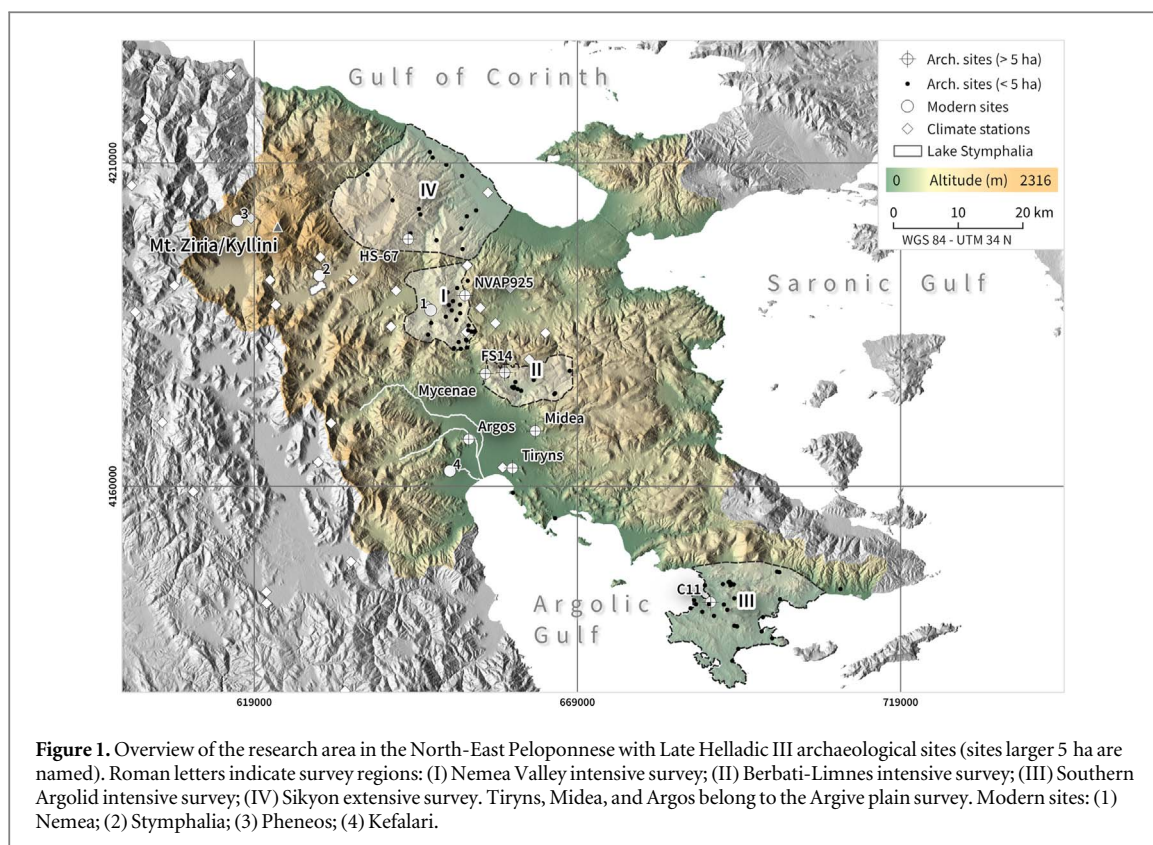
In this study, we present a modeling approach that investigates how much cultivable land was required to supply a society and whether societies were in need when environmental conditions deteriorated. The approach is implemented for the North-Eastern Peloponnese and is based upon the location of Late Helladic IIIB (1300–1200 BCE) archaeological sites, an assessment of their sizes, and a proposed diet of the people. Based on these information, the areal requirement of each site is calculated and mapped. The results show that large sites do not have sufficient space in their surroundings in order to supply themselves with the required food resources and thus they depended on supplies from the hinterland. Dry climatic conditions aggravate the situation. This indicates that potential societal crisis are less a factor of changing environmental conditions or a shortage of arable land but primarily caused by socio-economic factors.

**1. Introduction**

To which degree are societies impacted by climate change? An age-old question that gained new relevance in the so called Anthropocene and the ongoing global environmental change (see Lewis and Maslin 2015, Haraway 2015, Ruddiman 2017). Archaeological examples derive from all parts of the globe, such as Mesoamerica, Greenland, the Indus valley and Cambodia (see Weiss 2017, Middleton 2017b). By investigating past societal dynamics, in the present case that of the Peloponnese peninsula in Southern Greece during the 2nd millennium BCE, we can derive narratives and heuristics that might enrich the current debates on (a) resilience, vulnerability, and collapse, as well as (b) the causes of the breakdown of Mycenaean palace economy (see Middleton 2012, 2017a, and references therein).

The Peloponnese peninsula has been the home of farming communities since the beginning of the 7th

millennium BCE (see Bintliff 2012). Most well-known during prehistory is the Mycenaean palatial period (ca. 1400–1200 BCE), during which Mycenaean ways of life became dominant in the Aegean area until the Mycenaean palace economies came, rather abruptly, to an end. The reasons for this breakdown have been massively debated (see Middleton 2010, Cline 2014, Finné *et al* 2017, and references therein). The possible impact of climate change on these sequences of events has long been an issue (for a historical overview see Knapp and Manning 2016) but one that has come increasingly to the fore in the advent of local paleoclimate records (Drake 2012, Knapp and Manning 2016, Finné *et al* 2017). The end of the palatial period coincides with a period of arid climate (the so called 3.2ka event) and can be chronologically connected to societal transformations throughout the Eastern Mediterranean region (Roberts *et al* 2011, Langgut *et al* 2013, Wiener 2014, Kaniewski *et al* 2015). The question is how much influence should be ascribed to



climate, and how the balance between climate and internal socio-economic or other factors should be understood (Middleton 2017a, Weiberg and Finné 2018).

One conceptual framework to address this issue and related questions of human-environmental interaction revolves around the concept of resilience, the adaptive cycle, and socio-ecological systems thinking (see Folke 2006, Smit and Wandel 2006, Bollig 2014, Bratdmöller *et al* 2017). Such frameworks allow grand narratives of societies and their dynamics to be drawn (e.g. Weiberg and Finné 2018, for the region of this study). Here, we offer a complementary view that focus specifically on issues of vulnerability. We follow Adger (2006, 268) who understands vulnerability as loose antonym of resilience and defines it as ‘(...) the state of susceptibility to harm from exposure to stresses associated with environmental and social change and from the absence of capacity to adapt’ (see also Adger 2000). This exposure can be objective and subjective (see Christmann and Ibert 2012) and is often related to the way a society is internally structured, when exposed to external stresses (see De Keyzer 2016).

Such considerations, linking external drivers and internal societal structure, are intrinsic to recent frameworks for vulnerability assessments (e.g. Kok *et al* 2016, Nelson *et al* 2016). The social conditions commonly relate to aspects of human well-being, connectedness and mobility, as well as to population dynamics. Here, we primarily aim for what Nelson *et al* (2016) define as ‘population-resource conditions’,

and specifically the availability of food, where the pressure of resources can be calculated by setting estimates of population density against the spatial needs for sustenance. The motivation is that the balance between resources and population numbers reduces the risk of shortfalls and thereby increases food security.

In this study, we present an approach that investigates (a) to which degree locally available resources were exploited in order to meet the needs for a society’s annual sustenance and (b) whether these were deficient when environmental conditions changed. The approach is tested on the north-eastern Peloponnese peninsula during the Late Helladic IIIB period (ca. 1300–1200 BCE). Based on the location and size of the archaeological sites, as well as the proposed diet of the people, the areal requirement of each settlement with its annual sustenance demands is calculated and mapped.

## 2. Study area

### 2.1. Geographical setting

Geomorphologically, the Peloponnese peninsula (21 550 km<sup>2</sup>) in Southern Greece is characterized by a mountainous relief and including strong altitudinal gradients on relatively short distances. The highest mountains reach altitudes of more than 2400 m above sea level, only few kilometers away from the coast—e.g. the highest peak of the study area, Mt. Ziria/Kyllini (2374 m), is situated only 20 km away from the coast of the Gulf of Corinth (figure 1).

Limestones and carbonate rich conglomerates dominate the geology of the study area (Morfis and Zojer 1986). Most of the limestones are strongly karstified, which becomes apparent i.a. in typical geomorphological, hydrological features such as large flat plains (poljes). The largest poljes in the study area, Pheneos, Stymphalia and Phlious/Nemea, which surround the limestone massif of Mt. Ziria have an area extent between 30 and 50 km<sup>2</sup>. Depending on the prevailing climate conditions and the human impact on the drainage system at different periods, these plains were covered by large lakes. Substantial water management practices in the study area are known at least since the Late Bronze Age, like the Late Helladic IIIB dam near Tiryns from around 1300 BCE (Zangger 1994). At the turn of the 19th to 20th century CE, most of the poljes were artificially drained to obtain more flat areas for agricultural use, with Lake Stymphalia remaining the only lake that survived until present. Many slopes in the area show signs of agricultural terracing, in some places even in altitudes above 1500 m. However, neither the age of the terraces nor what was cultivated on them is known (an exception are the terraces of Kalamianos, see Kvapil 2012).

The karst waters draining from the mountains and poljes in the west of the study area supply huge springs (e.g. Lerna, Kiveri, Kefalari) in the Argive Plain, which today covers approx. 150 km<sup>2</sup> at the north-eastern coast of the Peloponnese. The river Erasinos, issuing from the spring at Kefalari, formed Lake Lerna at the coast south of Argos, which existed at least during a period from approx. 4800 BCE until 800 CE (Jahns 1993, Zangger 1993, Katrantsiotis *et al* 2019).

The area is characterized by a warm temperate climate with hot and dry summers (Csa after Köppen and Geiger; Kottek *et al* 2006). Data from meteorological stations on the peninsula shows that the annual rainfall exceeds the critical 250 mm isohyet—that is essential for rain-fed agriculture (see Bruins *et al* 1986)—everywhere with a decreasing trend towards the east. Following Finné *et al* (2017) and Weiberg and Finné (2018) the climate during the period in question shows a dry episode of some 20 years at 1250 BCE ( $\pm 30$  yrs), but otherwise generally ‘wet’ conditions, although probably more volatile than during the previous century. Only after 1200/1170 BCE does a trend towards severely arid conditions set in, with increasingly dry conditions until around 1050 BCE.

## 2.2. Archaeological setting

Around 1200 BCE, after two centuries of Mycenaean dominance in the Aegean world, the palaces at Mycenae, Tiryns, Midea, Thebes, and other former centers were destroyed and not re-built (Dickinson 2006, Maran 2006, Deger-Jalkotzy 2008). For about a century, certain citadels (e.g. Tiryns in the Argolid, Teichos Dymaion in Achaëa) witnessed continued activities; these were taking place, however,

on a much smaller scale than before and supposedly not under the lead of a palatial authority (maybe with a short-term exception at Tiryns, see Maran 2006).

During the palatial period, the NE Peloponnese was densely populated with a hierarchy of settlements spread throughout the landscape, on the plains, and in the uplands. It is proposed that Mycenae exercised some control over large parts of NE Peloponnese, and hence dominated other palatial centers in the region (Bennet 2013). The Mycenaean polities (see Drake 2012) were dependent on a secure supply from their agricultural economic system, the basis of which were field crop cultivation (barley, einkorn, and emmer, but diversified during Mycenaean times to include also free-threshing wheat, millet, and spelt) and animal husbandry (goat/sheep, pigs, and cattle; Weiberg *et al* 2019, with references).

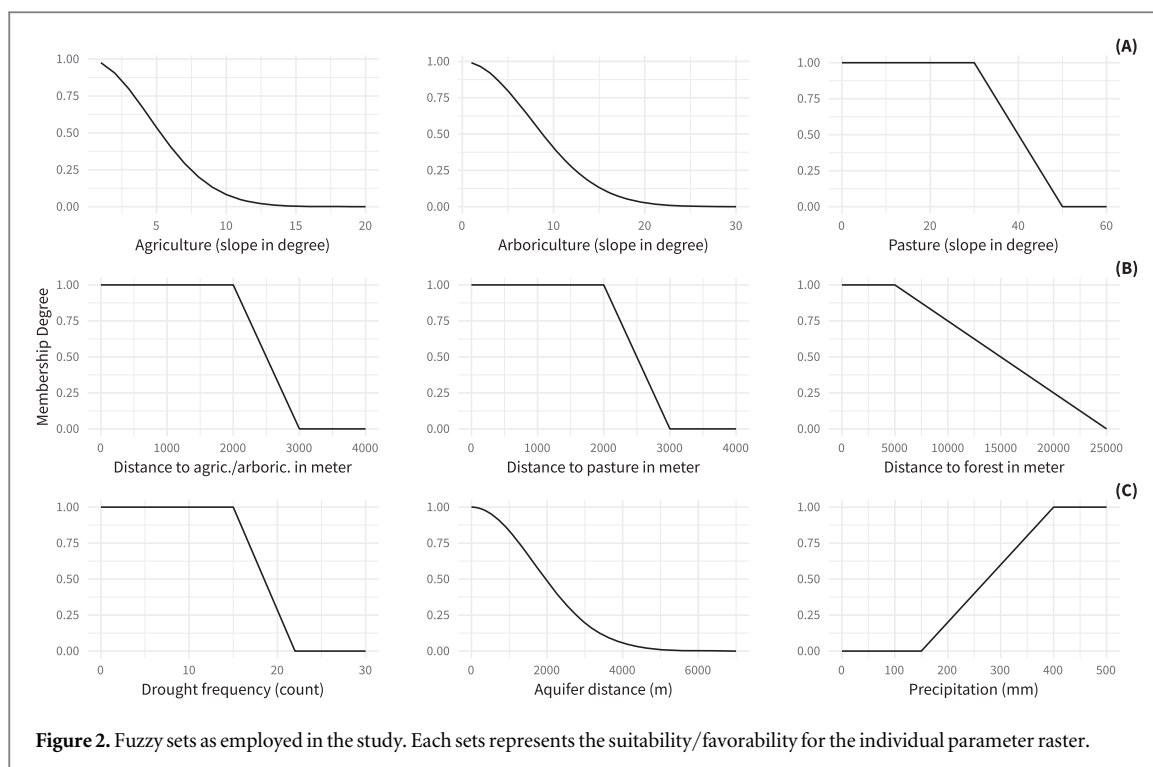
## 3. Methods

Our methodological approach is to calculate the areal requirements for selected archaeological sites. Environmental suitability mapping is combined with a population and diet based nutrient requirement calculation to arrive at a measure of spatial needs for different land use practices per settlement. This allows to assess for which sites the available space was sufficient. We expand the approach by adjusting the suitability mapping to reflect drier climatic conditions.

### 3.1. Archaeological information

In the present study, only dietary needs are modeled, and the results therefore indicate the minimum needs of the settlements. The prescribed diet is based on estimations by Weiberg *et al* (2019) and is cereal based, complemented primarily by legumes, fruits and nuts, dairy, and only a limited amount of meat (see supplemental material 1 available online at [stacks.iop.org/ERL/14/125003/mmedia](https://stacks.iop.org/ERL/14/125003/mmedia)). Our modeling approach uses settlement data for the second half of the palatial period (Late Helladic IIIB period: ca. 1300–1200 BCE), derived from three regions covered by differently intensive archaeological surveys (Wright *et al* 1990, Jameson *et al* 1994, Wells and Runnels 1996, Lolos 2011, Cloke 2016, see supplemental material 2). No such data exists for the Argive Plain and for this region we have thus used population estimates for the main settlements only. The population of the Argive Plain has been estimated to around 20 000 inhabitants, of which Mycenae, the largest settlement in the region, held around 6400 inhabitants (Bennet 2013, Bintliff 2016). It should be noted, however, that all population estimates are inherently uncertain (see Osborne 2004). They are generally generated from estimations of settlements sizes, more readily identified in excavated areas than from surface reconnaissance. Hectare values for excavated sites are hence





more secure, but even excavations do very rarely cover the full extent of the original settlement in one specific phase. To allow for these uncertainties, we have incorporated three population scenarios, calculating 100, 150, and 200 inhabitants per hectare.

### 3.2. Land use suitability

The assessment of the environmental suitability for land use activities (i.e. agriculture, arboriculture, pasture, and wood) is based on the integration of expert-knowledge on land use practices with empirical data on environmental characteristics. Both are combined in a fuzzy rule-based system. Fuzzy logic allows to exemplify our assumptions by stating them as linguistic variables (Zadeh 1965). Furthermore, using fuzzy in place of crisp sets helps to classify data where clear borders are hard to establish. Fuzzy methodology is used in different contexts in (landscape) archaeology; examples range from site location analysis (Jasiewicz 2009, Popa and Knitter 2015), over viewshed methods (Loots *et al* 1999), to chronology (Nakoinz 2012). We employ the R package Fuzzy-Landscapes (Hamer and Knitter 2018), inspired by Jasiewicz (2011), to analyze a raster based fuzzy rule-based system.

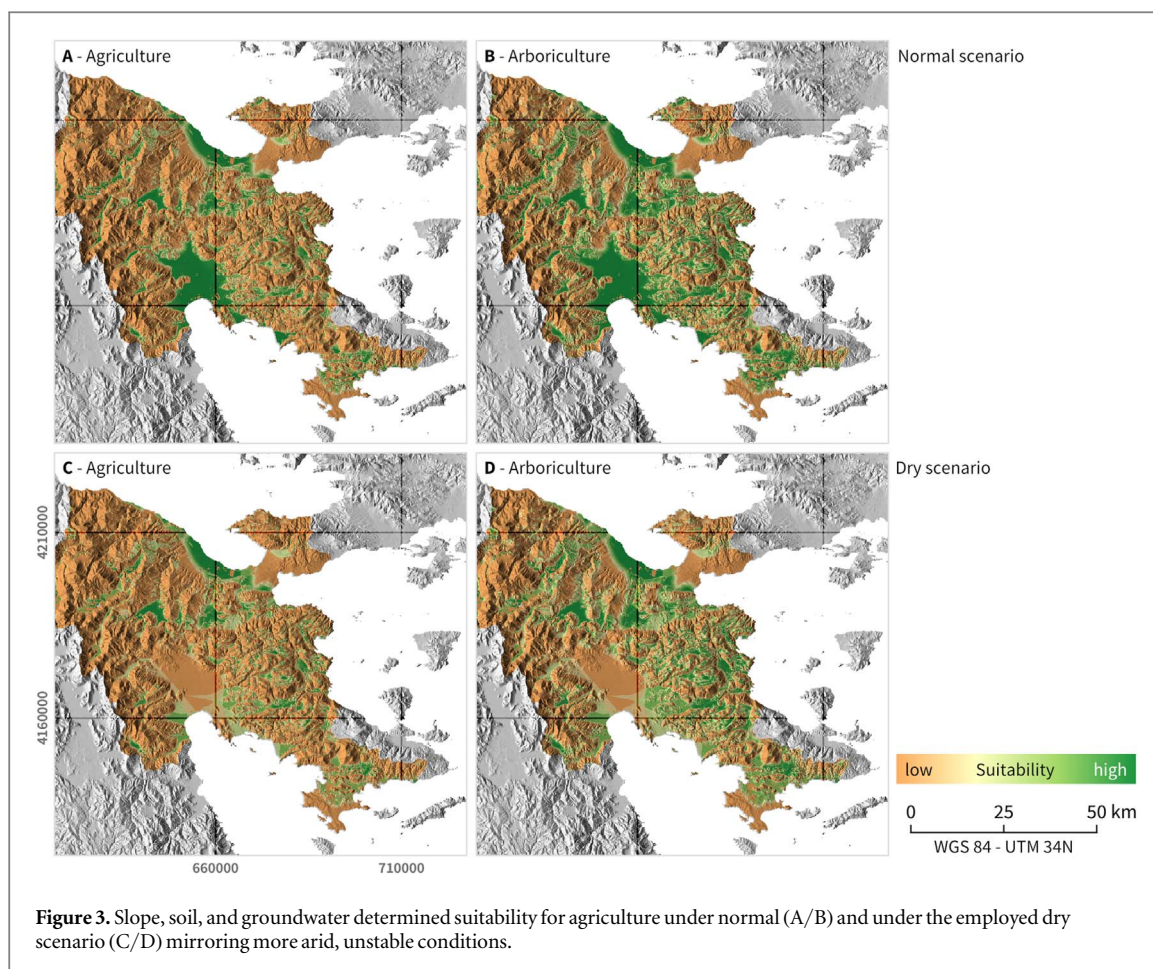
Different raw data were employed: information on slope in degrees is derived from the European Digital Elevation Model (EU Copernicus programme 2016, version 1.1), via GRASS GIS (GRASS Development Team 2017). Information on precipitation are provided by the Greek Special Secretariat for Water and is derived from 68 climate stations located on the Peloponnese. These data are interpolated using multiple linear regression and the independent parameter

latitude, longitude, and elevation. Calculations are conducted using R (Core Team 2019) and the packages dplyr (Wickham *et al* 2019) and raster (Hijmans 2019). The construction of wells requires suitable geological conditions, in particular highly productive porous or fissured aquifers. These information are derived from International Hydrogeological Map of Europe 1:1500 000 (BGR *et al* 2008). Soils of very high to medium productivity on the Peloponnese—i.e. Fluvisols, Cambisols, Calcisols, and Luvisols (according to Yassoglou *et al* 2017)—were accessed from SoilGrids250m, a Global 3D Soil Information System, provided by ISRIC World Soil Information (further information on SoilGrids and the corresponding methodology to create the grids is given by Hengl *et al* 2017). To reduce computation time, all calculations are conducted with a spatial resolution of 75 by 75 m.

Following Hughes *et al* (2018), we distinguish between four different categories of land use, for which suitability maps are created based on the following assumptions:

- *Agriculture*, i.e. cereals and legumes, are considered to grow (a) on areas with little to no slope induced erosion (figure 2(A)), (b) in areas with sufficient rainfall for rainfed agriculture (figure 2(C)), (c) on fertile soils (according to Yassoglou *et al* 2017, 24f.), and (d) in areas with easy access to groundwater resources (figure 2(C)). Terrace farming is not considered here, since it would introduce another level of eco-social complexity. Not considering terraces leads to an underestimation of available land. However, an appropriate representation of





terraces also necessitates extended assumptions on nutrient requirements for which we are lacking empirical data. The same holds true for water-management techniques utilized for irrigating the fields. These are likewise not considered.

- *Arboriculture*, i.e. the cultivation of fruit trees, nuts, olives, as well as vine, has the same requirements as crops, however, the slope is less restrictive (figure 2(A)).
- *Pasture*: Pastoral activities are only restricted by very steep slopes, following the assumption that these areas are too steep to have vegetation (figure 2(A)).
- *Wood*: Forest could potentially grow everywhere (see Beuermann 1956).

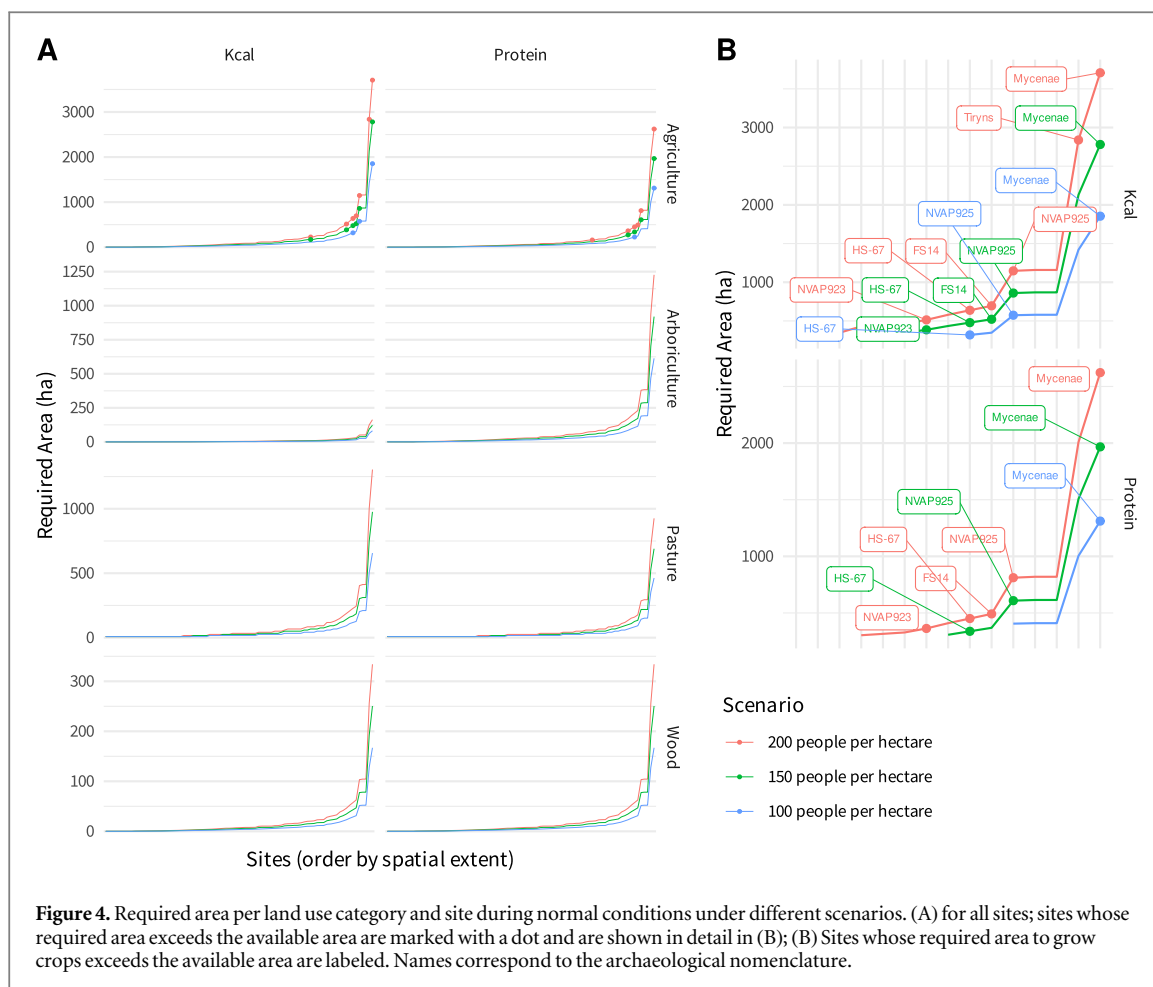
Agriculture and arboriculture are labor intensive. Accordingly, the suitability maps are combined with shortest walking distances to archaeological sites (calculated using GRASS GIS; GRASS Development Team 2017): suitable areas that are more than 2 km distant from a site decrease in suitability until the areas are treated as unsuitable at distances larger than 3 km (2.5 km commonly used for agricultural societies; Flannery 1976, Bintliff 2012, Farinetti 2016, Bonnier *et al* 2019). Pasturage is less labor intensive hence the determining distance for pastoral activities is 5 and

6 km. Wood resources are increasingly difficult to acquire after 5 km distance from a site (figure 2(B)).

### 3.3. Area requirement assessment

The calculation of the areal requirements per site is an extended version of the approach presented by Hughes *et al* (2018), implemented in the R package Land-UseQuantifier (Knitter *et al* 2019). It is based on assumptions about the general nutrient, i.e. kilocalorie (kcal) as well as protein requirements of an individual with an active lifestyle and information on population size (for further details and exact empirical values see Knitter *et al* 2019). These values are combined with the data on diet characteristics (see supplemental material 1) and information on the nutrient density of plants and animals (for exact empirical data see Knitter *et al* 2019) in order to assess the minimum area that is required to fulfill the calorie and protein needs of the population.

The calculated areal demands are mapped in relation to the modeled suitability of the area: each grid cell has a certain suitability for agriculture, arboriculture, pasture, and wood (see section 3.2). The algorithm for the distribution of these area requirements is based on a combination of the shortest walking distance to archaeological sites and the Euclidean Norm—the square root of the sum of squares of the distances in each dimension—of suitability for the



different land uses. The assignment of land use to the individual pixels is done in an iterative process. The initial value for the iteration equals the Euclidean Norm of the maximal suitability value of a land use category that has minimal distance to an archaeological site. The iteration runs through all cells, ordered consecutively from smallest to largest distance. In each step, the land use category with the largest quotient, i.e.  $LU_k$ , is assigned to the cell base upon:

$$LU_k = \max \left( \frac{E_{k,0..i}}{E_{k,0..i-1}} \right),$$

where  $E$  is the Euclidean Norm,  $k$  is the land use category (i.e. agriculture, arboriculture, pasture, or wood),  $0..i$  are all as  $k$  categorized cells including the current cell, and  $0..i - 1$  are all hitherto as  $k$  categorized cells.

### 3.4. Changing environmental conditions

In order to test the effects of dry climatic conditions during the Late Helladic IIIB period (see Finné *et al* 2017, Weiberg and Finné 2018), we employ modern climate station information and relate them to the standardized precipitation-evapotranspiration index (SPEI, McKee *et al* 1993). The idea is based on the study of Beckers and Schütt (2013) and assumes that general atmospheric dynamics are similar between today and the period under study. The R package SPEI

(Beguería and Vicente-Serrano 2017) is employed to calculate SPEI values. Since the index is related to the general precipitation record, negative values indicate times where less precipitation occurs than expected. Accordingly, it can be translated to be a measure of the strength of rainfall variability. Droughts impact the ability to conduct rain fed agriculture. Thus, areas with generally lower precipitation values are more vulnerable to variable rainfall than other areas.

The SPEI is calculated for each year between 1970 and 2000 for a data set of 68 climate stations on the Peloponnese. Subsequently, the SPEI values of the individual stations are interpolated using multiple linear regression with the independent variables latitude, longitude, and elevation. Based on this an areal representation of SPEI for the Peloponnese for each year is achieved. Afterwards the drought maps were summed up to arrive at a drought frequency map for the area. If there were more than 15 droughts, i.e. in more than 50% of the cases in the recorded period, we regarded this area as increasingly unsuitable for rain-fed agricultural purposes (figure 2). Note that the findings have to be treated with caution, since the utilized time series is rather short and its dynamics might not be similar to earlier periods.

Based on this analysis, it gets obvious that drought conditions are heterogeneously distributed

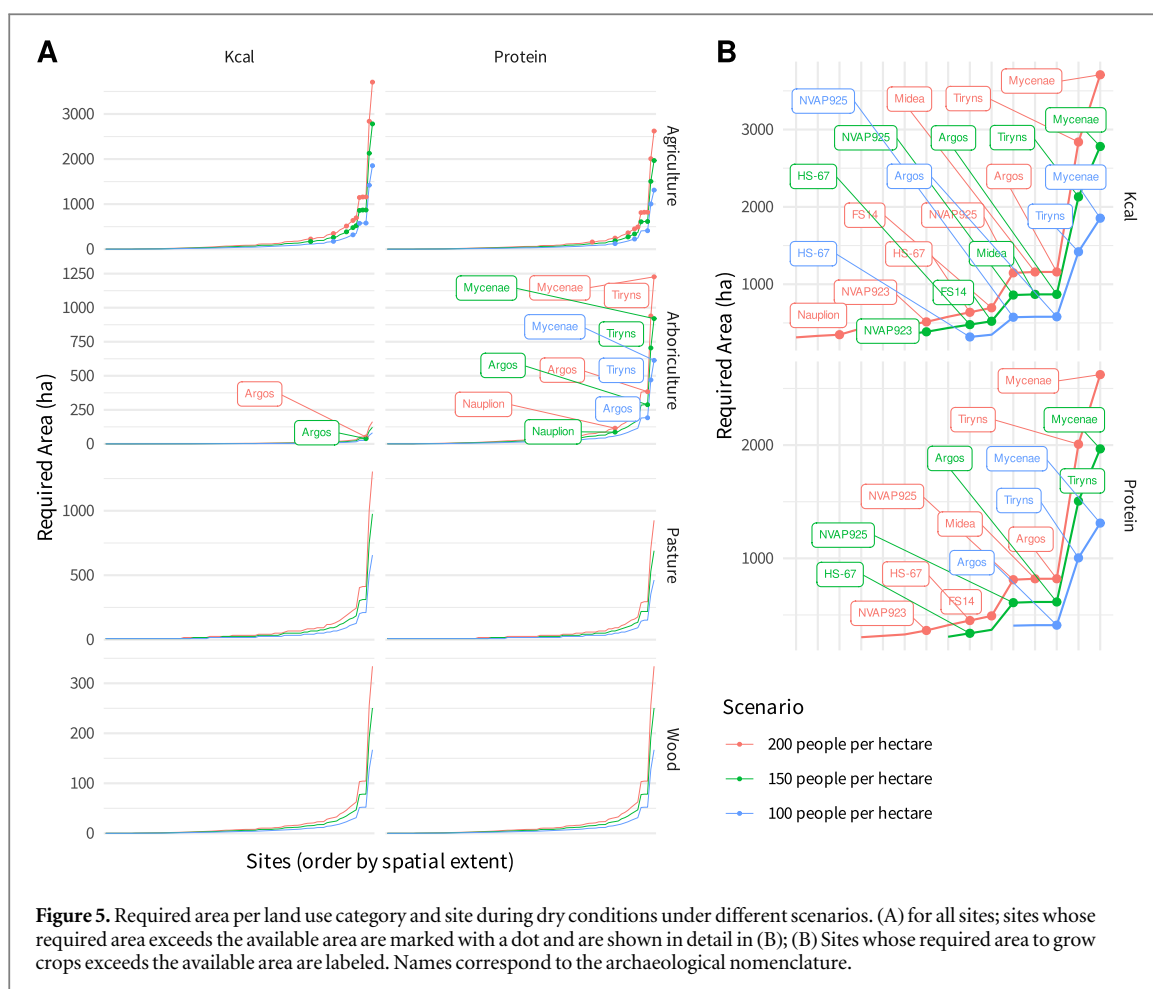


**Figure 5.** Required area per land use category and site during dry conditions under different scenarios. (A) for all sites; sites whose required area exceeds the available area are marked with a dot and are shown in detail in (B); (B) Sites whose required area to grow crops exceeds the available area are labeled. Names correspond to the archaeological nomenclature.

throughout the study region, threatening sustainable rainfed agriculture (see figure 3). This threat to experience a drought is implemented as scenario by integrating it as fuzzy variable to the suitability for agriculture, arboriculture, and pasture: the higher the risk of droughts, the lower the suitability of an area for these land use practices (figure 2(C)).

#### 4. Results

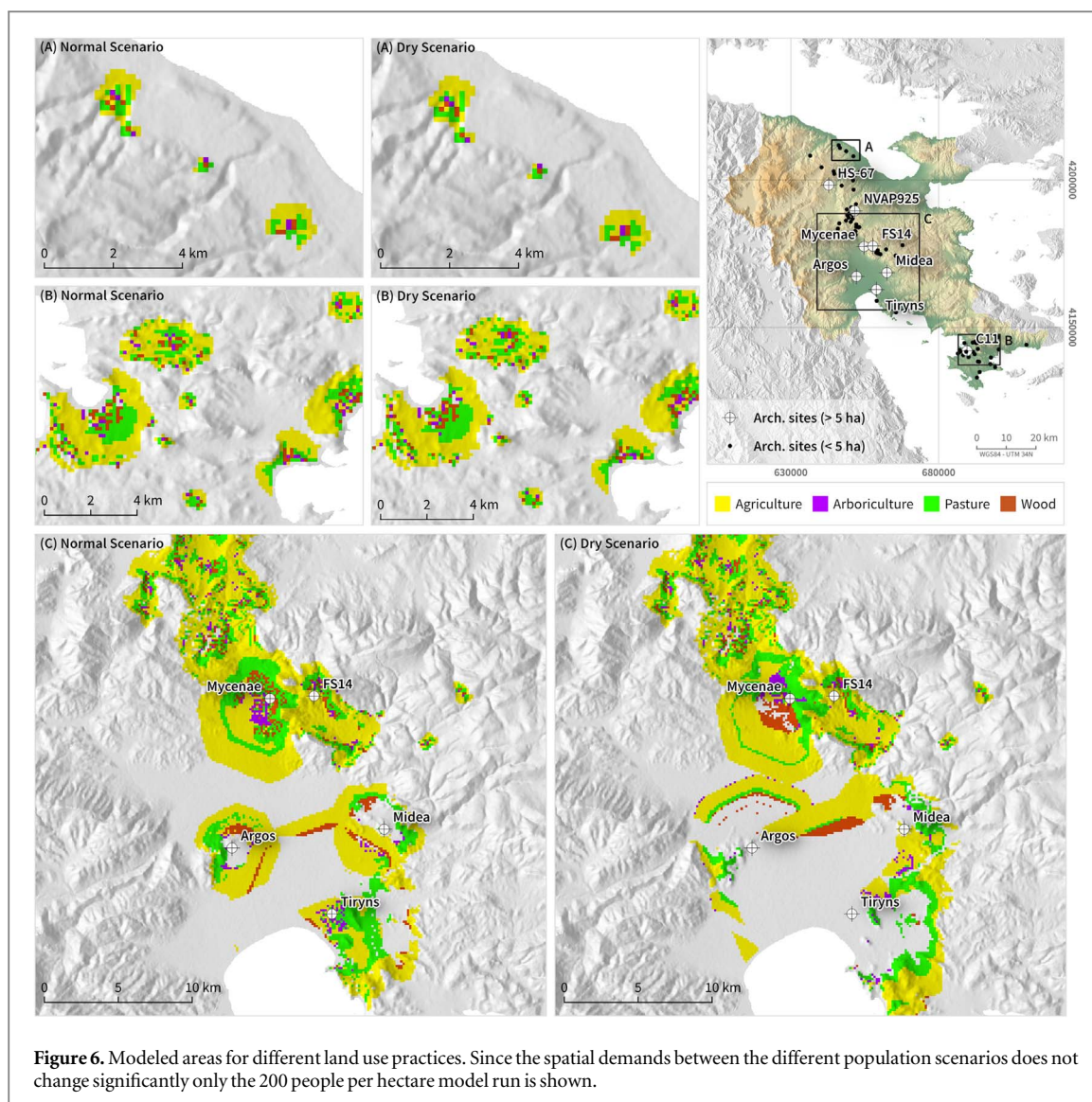
Small to medium sites (approx. < 3 ha) have sufficient space to fulfill their caloric or protein requirements (figure 4(A)). This is also the case under dry climatic conditions (figure 5(A)). Only regarding crops, the largest sites (approx. > 3 ha) do not have sufficient space for agricultural purposes (figure 4(B)). This pattern aggravates during the dry scenario, during which also the space to produce arboriculture products is insufficient (figure 5(B)). The deficit of sufficient space, as recorded for larger sites, is independent of the assumed population scenario. Arboriculture and pasture show an opposing trend with marked difference in required area between protein and kcal (compare figures 4(A) and 5(A)). Especially the variation in areal requirements for arboriculture between the kcal-based and the protein-based scenario is considerable.

The mapping of land use areas shows a similar pattern for small sites (figures 6(A) and (B)) while in the Argive plain that is characterized notably by large sites, differences between the two scenarios are discernible (figure 6(C)). Besides, the effect of input data—especially the interpolated droughts, as well as the integrated settlement-distance—becomes obvious as artificial looking rings or stripes in the plain. The unused areas in the northern part of the Argive plain are related to the distance constraint, i.e. those areas are too far apart from one of the prescribed settlements to be used for agricultural practices.

#### 5. Discussion

The results show some artifacts that are related to selected methods and input data. For instance, the drought scenario, due to low data density, leads to unrealistically sharp-edged boundaries. More data or a different interpolation method could improve the results. However, since the scenario-approach itself follows simplifying assumptions, further data-tweaking might cause an overconfidence in the result that is not backed by input data or proxy information. Furthermore, decisions during the creation of the model (e.g. constraining distances for land use practices or the assumption that people will conduct





activities as close as possible to their homes) and definitions of fuzzy sets have a strong influence on the modeled results. Accordingly, less conservative values, e.g. regarding slope or size of the agricultural hinterland, might lead to different interpretations. However, since the chosen values are based on empirical studies the results can be regarded as reasonable estimates.

The differences in areal requirements when considering calories or protein as nutrient base are apparent. This highlights the importance of the utilized land use technique and the assumed diet. It has to be analyzed in more detail in future studies on nutrient requirements, diet structure, and cooking habits of different parts of society, as outlined, e.g. by ancient authors like Galen (see Grant 2000). Furthermore, in the current version of the model yields are reflected only by one productivity measure. Manuring, soil conditions, harvest time, or weather conditions are all aspects that determine the eventual yield of a crop. Due to the lack of empirical information and our decision to have a simple model with as little as possible complicating extra assumptions, the mentioned yield

influencing elements are not integrated. This again highlights the fact that not the resulting values itself but the general pattern should be considered when drawing conclusions.

Besides these limitations, the results show that large sites do not have sufficient space in their surroundings in order to supply themselves with the required food resources. This confirms the suggestion that the large sites were always dependent on external food supplies (e.g. Halstead 1999, Bintliff 2016). This holds true for the normal scenario as well as for a scenario of dry climatic conditions indicating thus, that a potential societal crisis is less a factor of changing environmental conditions or a shortage of arable land but rather caused by socio-economic factors.

Climate, however, may have been an aggravating factor, adding to a socially produced vulnerability. The content of direct control from the palaces on the surrounding regions and lower-order settlements is still debated but is generally assumed to include primarily resources needed for palace-controlled production, for local use and for exchange (Foxhall 1995).

Incoming grain listed by palace administrators appear primarily not as provisions for the daily diet of palace inhabitants, but as rations for workers, for sacrifice, and for feasting (Bennet 2013). Large scale feasting events were one strategy for the palatial elites to build cohesion and loyalty and to uphold authority. Extended possibilities for grain storage within palace boundaries during the Late Helladic IIIB (ca. 1300–1200 BCE) at Mycenae—also known from Pylos in Messenia—may have been a way to secure such activities (Whitelaw 2001, Maran 2009). Another way for palatial elites to make themselves essential beyond their peers may have been to provide food-security in case of shortfalls, due to droughts or other factors (Foxhall 1995, Finné *et al* 2017). Some movement of grain from external entities to the palaces was thus already part of the Mycenaean palatial system, through taxation, exchange and/or agricultural partnerships (e.g. Halstead 1999). If, however, the palaces and other major settlements experienced additional food deficiencies, as modelled in the dry scenario, this may have compromised their authority and the overall cohesion in the region. If smaller settlements could produce what they needed, they were in a position to provide relief food. Whether such relief was provided by free will or by coercion, such a relationship could have affected the power balance in the region. An imbalance would have added to the overall vulnerability of the Mycenaean polities, a vulnerability that was likely already high due to a stretched economy, including largescale building projects and perhaps generally turbulent times within the Eastern Mediterranean trade- and contact networks important to the Mycenaean elites (Bennet 2013, Weiberg and Finné 2018).

## 6. Conclusions

The fuzzy suitability modeling helps to create contextualized and spatially constrained information on the general subsistence patterns of an area. This updated modeling method showed that area requirements are a function of scale: small sites are not affected by a need for space even under worse climatic conditions; on the contrary, large sites are always affected. Accordingly, a functioning socio-economic and socio-ecological system, organizing production and exchange, was a prerequisite to sustain the largest Mycenaean settlements. In the Late Helladic IIIB context, such a reliance of the palaces on external agricultural produce would have added to the vulnerability of the overall system even in the normal scenario, through a built-in imbalance of supply and demand. External stresses, as mirrored in a dry scenario, are very likely to have aggravated this situation, threatening the food-security of the large sites and the overall power balance. Any societal transformations that followed, however, should rather

be seen as symptoms of a pre-existing vulnerability than as direct effects of climate change.

## Acknowledgments

We are very grateful for the comments and remarks of two anonymous reviewers who have helped to improve the paper.

The data and R code that support the findings of this study are (a) given in the supplemental material as well as (b) openly available at DOI [10.5281/zenodo.3478243](https://doi.org/10.5281/zenodo.3478243). Archaeological site data are available from the corresponding author upon reasonable request. Climate information are available upon request from ‘Greek Special Secretariat for Water’ (<http://ypeka.gr/Default.aspx?tabid=430&locale=en-US&language=el-GR>).

The research was conducted and financed in context of the Collaborative Research Center 1266 ‘Scales of Transformation—Human-environmental interaction in prehistoric and archaic societies’ of the German Research foundation (DFG, German Research Foundation—project number 2901391021—CRC 1266). EW acknowledges funding for the Domesticated Landscapes of the Peloponnese project (The Swedish Research Council, grant number 421-2014-1181), within which the digitalization of the archaeological data and the initial calculation of the Late Helladic areal requirements were conducted.

## ORCID iDs

Daniel Knitter  <https://orcid.org/0000-0003-3014-4497>

Gerrit Günther  <https://orcid.org/0000-0002-9930-2708>

Wolfgang Berengar Hamer  <https://orcid.org/0000-0002-5943-5020>

Joana Seguin  <https://orcid.org/0000-0002-4364-512X>

Ingmar Unkel  <https://orcid.org/0000-0002-8940-1657>

Erika Weiberg  <https://orcid.org/0000-0001-6583-387X>

Rainer Duttman  <https://orcid.org/0000-0001-5606-2938>

Oliver Nakoinz  <https://orcid.org/0000-0003-2113-0157>

## References

- Adger W N 2000 Social and ecological resilience: are they related? *Prog. Hum. Geogr.* **24** 347–64
- Adger W N 2006 Vulnerability *Glob. Environ. Change* **16** 268–81
- Beckers B and Schütt B 2013 The elaborate floodwater harvesting system of ancient Resafa in Syria—construction and reliability *J. Arid Environ.* **96** 31–47
- Beguéría S and Vicente-Serrano S M 2017 SPEI: Calculation of the Standardised Precipitation-Evapotranspiration Index. R

- package version 1.7 ([https://cran.r-project.org/src/contrib/SPEL\\_1.7.tar.gz](https://cran.r-project.org/src/contrib/SPEL_1.7.tar.gz))
- Bennet J 2013 Bronze Age Greece *The Oxford Handbook of the State in the Ancient Near East and Mediterranean* ed P Fibiger Bang and W Scheidel (Oxford: Oxford University Press) pp 235–58
- Beuermann A 1956 Die Waldverhältnisse im Peloponnes unter besonderer Berücksichtigung der Entwaldung und Aufforstung *Erdkunde* **10** 122–36
- BGR, EGS and UNESCO 2008 IHME1500—International Hydrogeological Map of Europe 1:1500000 (Hannover: BGR) (<https://fishy.bgr.de/ihme1500/>)
- Bintliff J 2016 The Argos Plain through its ages and my ages *J. Greek Archaeol.* **1** 33–44
- Bintliff J L 2012 *The Complete Archaeology of Greece: From Hunter-Gatherers to the 20th Century AD* (New York: Wiley)
- Bollig M 2014 Resilience—analytical tool, bridging concept of development goal? anthropological perspectives on the use of a border object *Z. Ethnol.* **139** 253–79
- Bonnier A, Finné M and Weiberg E 2019 Examining land-use through GIS-Based kernel density estimation: a Re-Evaluation of legacy data from the berbati-limnes survey *J. Field Archaeol.* **44** 70–83
- Bradt Möller M, Grimm S and Riel-Salvatore J 2017 Resilience theory in archaeological practice—an annotated review *Quat. Int.* **446** 3–16
- Bruins H J, Evenari M and Nessler U 1986 Rainwater-harvesting agriculture for food production in arid zones: the challenge of the African famine *Appl. Geogr.* **6** 13–32
- Christmann P D G B and Ibert P D O 2012 Vulnerability and resilience in a socio-spatial perspective *Raumforsch. Raumordnung* **70** 259–72
- Cline E H 2014 *1177 B.C.: The Year Civilization Collapsed (Turning Points in Ancient History)* (Princeton: Princeton University Press)
- Cloke J F 2016 The Landscape of the Lion: Economies of Religion and Politics in the Nemean Countryside (800 B.C. to A.D. 700) *PhD Thesis* (Cincinnati, OH: University of Cincinnati)
- De Keyzer M 2016 All we are is dust in the wind: the social causes of a ‘subculture of coping’ in the late medieval coversand belt *J. Hist. Environ. Soc.* **1** 1–35
- Deger-Jalkotzy S 2008 Decline, destruction, and aftermath *The Cambridge Companion to the Aegean Bronze Age* ed C Shelmerdine (New York: Cambridge University Press) pp 387–415
- Dickinson O 2006 *The Aegean from Bronze Age to Iron Age: Continuity and Change Between the Twelfth and Eighth Centuries BC* (New York: Routledge)
- Drake B L 2012 The influence of climatic change on the Late Bronze Age Collapse and the Greek Dark Ages *J. Archaeol. Sci.* **39** 1862–70
- EU Copernicus programme 2016 *European Digital Elevation Model (EU-DEM), Version 1.1* (Copenhagen: European Environment Agency)
- Farinetti E 2016 *Boeotian Landscapes: A GIS-Based Study for the Reconstruction and Interpretation of the Archaeological Datasets of Ancient Boeotia* (Oxford: BAR Publishing)
- Finné M, Holmgren K, Shen C-C, Hu H-M, Boyd M and Stocker S 2017 Late Bronze Age climate change and the destruction of the Mycenaean Palace of Nestor at Pylos *PLoS One* **12** e0189447
- Flannery K V (ed) 1976 *The Early Mesoamerican Village* 1st edn (New York: Academic)
- Folke C 2006 Resilience: the emergence of a perspective for social-ecological systems analyses *Glob. Environ. Change* **16** 253–67
- Foxhall L 1995 Bronze to iron: agricultural systems and political structures in Late Bronze Age and early iron age greece *Ann. Br. Sch. Athens* **90** 239–50
- Grant M 2000 *Galen on Food and Diet* (London: Routledge)
- GRASS Development Team 2017 Geographic Resources Analysis Support System (GRASS GIS) Software, Version 7.2, Open Source Geospatial Foundation
- Halstead P 1999 Surplus and share-croppers: the grain productions strategies of Mycenaean palaces *Meletemata: Studies in Aegean Archaeology Presented to Malcolm H. Wiener as He Enters His 65th Year* ed P P Betancourt and M H Wiener (Liège: Université de Liège) pp 319–26
- Hamer W and Knitter D 2018 FuzzyLandscapes – Fuzzy analyses with a focus on raster data *Zenodo* (<https://doi.org/10.5281/zenodo.1747005>)
- Haraway D 2015 Anthropocene, Capitalocene, Plantationocene, Chthulucene: Making Kin *Environ. Humanit.* **6** 159–65
- Hengl T *et al* 2017 SoilGrids250m: Global gridded soil information based on machine learning *PLoS One* **12** e0169748
- Hijmans R J 2019 raster: Geographic Data Analysis and Modeling. R package version 2.8-19 ([https://cran.r-project.org/src/contrib/Archive/raster/raster\\_2.8-19.tar.gz](https://cran.r-project.org/src/contrib/Archive/raster/raster_2.8-19.tar.gz))
- Hughes R E, Weiberg E, Bonnier A, Finné M and Kaplan J O 2018 Quantifying land use in past societies from cultural practice and archaeological data *Land* **7** 9
- Jahns S 1993 On the Holocene vegetation history of the Argive Plain (Peloponnese, southern Greece) *Vegetation Hist. Archaeobot.* **2** 187–203
- Jameson M H, Runnels C N and Van Andel T H 1994 *A Greek Countryside: The Southern Argolid from Prehistory to the Present Day* (Stanford: Stanford University Press)
- Jasiewicz J 2011 A new GRASS GIS fuzzy inference system for massive data analysis *Comput. Geosci.* **37** 1525–31
- Jasiewicz J and Hildebrandt-Radke I 2009 Using multivariate statistics and fuzzy logic system to analyse settlement preferences in lowland areas of the temperate zone: an example from the Polish Lowlands *J. Archaeol. Sci.* **36** 2096–107
- Kaniewski D, Guiot J and Campo E V 2015 Drought and societal collapse 3200 years ago in the eastern mediterranean: a review *Wiley Interdiscip. Rev. Clim. Change* **6** 369–82
- Katrantsiotis C, Norström E, Smittenberg R H, Finne M, Weiberg E, Hättstrand M, Avramidis P and Wastegård S 2019 Climate changes in the Eastern Mediterranean over the last 5000 years and their links to the high-latitude atmospheric patterns and Asian monsoons *Glob. Planet. Change* **175** 36–51
- Knapp A B and Manning S W 2016 Crisis in context: the end of the Late Bronze Age in the eastern mediterranean *Am. J. Archaeol.* **120** 99–149
- Knitter D, Hamer W, Günther G and Vorspel-Rüter C 2019 LandUseQuantifier, Version 1.1. *Zenodo* (<https://doi.org/10.5281/zenodo.3476674>)
- Kok M, Lüdeke M, Lucas P, Sterzel T, Walther C, Janssen P, Sietz D and de Soysa I 2016 A new method for analysing socio-ecological patterns of vulnerability *Reg. Environ. Change* **16** 229–43
- Kottek M, Grieser J, Beck C, Rudolf B and Rubel F 2006 World Map of the Köppen-Geiger climate classification updated *Meteorol. Z.* **15** 259–63
- Kvapil L A 2012 The Agricultural Terraces of Korphos-Kalamianos: A Case Study of the Dynamic Relationship Between Land Use and Socio-Political Organization in Prehistoric Greece *PhD Thesis* University of Cincinnati
- Langgut D, Finkelstein I and Litt T 2013 Climate and the late bronze collapse: new evidence from the southern levant *Tel Aviv* **40** 149–75
- Lewis S L and Maslin M A 2015 Defining the anthropocene *Nature* **519** 171–80
- Lolos Y A 2011 *Land of Sikyon: Archaeology and History of a Greek City-State* (Princeton: American School of Classical Studies at Athens)
- Loots L, Nackaerts K and Waelkens M 1999 Fuzzy viewshed analysis of the Hellenistic city defence system at Sagalassos, Turkey. Archaeology in the Age of the Internet. CAA97. Computer Applications and Quantitative Methods in Archaeology *Proc. 25th Anniversary Conf.* vol 750 (*BAR International Series*) (April 1997) (Birmingham: University of Birmingham) pp 82–82
- Maran J 2006 Coming to terms with the past: ideology and power in late helladic III C *Ancient Greece: From the Mycenaean Palaces*



- to the Age of Homer ed S Deger-Jalkotzy and I Lemos (Edinburgh: Edinburgh University Press) pp 123–50
- Maran J 2009 The crisis years? Reflections on signs of instability in the last decades of the Mycenaean palaces *Studi di antichità* **15** 241–62
- McKee T B, Doesken N J and Kleist J 1993 The relationship of drought frequency and duration to time scales *Eighth Conf. on Applied Climatology* 17–22 January 1993 (Anaheim, California) **6**
- Middleton G 2012 Nothing lasts forever: environmental discourses on the collapse of past societies *J. Archaeol. Res.* **20** 257–307
- Middleton G D 2010 *The Collapse of Palatial Society in LBA Greece and the Postpalatial Period* (Oxford: Archaeopress)
- Middleton G D 2017a The show must go on: collapse, resilience, and transformation in 21st-century archaeology *Rev. Anthropol.* **46** 78–105
- Middleton G D 2017b *Understanding Collapse: Ancient History and Modern Myths* (Cambridge: Cambridge University Press)
- Morfis A and Zojer H (ed) 1986 *Karst-Hydrogeology of the Central and Eastern Peloponnesus (Greece), number 37/38 in Steirische Beiträge Zur Hydrogeologie* (Graz: Leykam)
- Nakoinz O 2012 Datierungskodierung und chronologische Inferenz – Techniken zum Umgang mit unscharfen chronologischen Informationen *Prähistorische Z.* **87** 1
- Nelson M C *et al* 2016 Climate challenges, vulnerabilities, and food security *Proc. Natl Acad. Sci.* **113** 298–303
- Osborne R 2004 Demography and survey *Side-by-Side Survey (Comparative Regional Studies in the Mediterranean World)* ed S E Alcock and J F Cherry (Oxford: Oxbow Books) pp 163–72
- Popa C N and Knitter D 2015 From environment to landscape. Reconstructing environment perception using numerical data *J. Archaeol. Method Theory* **23** 1285–306
- R Core Team 2019 *R: A Language and Environment for Statistical Computing* (Vienna, Austria: R Foundation for Statistical Computing)
- Roberts N, Eastwood W J, Kuzucuoğlu C, Fiorentino G and Caracuta V 2011 Climatic, vegetation and cultural change in the eastern Mediterranean during the mid-Holocene environmental transition *Holocene* **21** 147–62
- Ruddiman W 2017 Geographic evidence of the early anthropogenic hypothesis *Anthropocene* **20** 4–14
- Smit B and Wandel J 2006 Adaptation, adaptive capacity and vulnerability *Glob. Environ. Change* **16** 282–92
- Weiberg E and Finné M 2018 Resilience and persistence of ancient societies in the face of climate change: a case study from Late Bronze Age Peloponnese *World Archaeol.* **0** 1–19
- Weiberg E, Hughes R E, Finné M, Bonnier A and Kaplan J O 2019 Mediterranean land use systems from prehistory to antiquity: a case study from Peloponnese (Greece) *J. Land Use Sci.* **14** 1–20
- Weiss H (ed) 2017 *Megadrought and Collapse: From Early Agriculture to Angkor* (New York: Oxford University Press)
- Wells B and Runnels C N 1996 *The Berbati-Limnes Archaeological Survey, 1988–1990*, Skrifter Utgivna Av Svenska Institutet i Athen, 44, Svenska Institutet i Athen, Stockholm
- Whitelaw T 2001 Reading between the tablets: Assessing Mycenaean palatial involvement in ceramic production and consumption *Economy and Politics in the Mycenaean Palace States* ed S Voutsaki and J Killen (Cambridge: Cambridge Philological Society) pp 51–79
- Wickham H, François R, Henry L and Müller K 2019 dplyr: A Grammar of Data Manipulation. R package version 0.8.0.1. ([https://cran.r-project.org/src/contrib/Archive/dplyr/dplyr\\_0.8.1.tar.gz](https://cran.r-project.org/src/contrib/Archive/dplyr/dplyr_0.8.1.tar.gz))
- Wiener M H 2014 The interaction of climate change and agency in the collapse of civilizations ca. 2300–2000 BC *Radiocarbon* **56** S1–16
- Wright J C, Cherry J F, Davis J L, Mantzourani E, Sutton S B Jr. and Sutton R F Jr. 1990 The Nemea Valley Archaeological Project a preliminary report *Hesperia. J. Am. Sch. Class. Stud. Athens* **59** 579
- Yassoglou N, Tsadilas C and Kosmas C 2017 *The Soils of Greece (World Soils Book Series)* (Berlin: Springer)
- Zadeh L A 1965 Fuzzy sets *Inf. Control* **8** 338–53
- Zangger E 1993 *The Geoarchaeology of the Argolid* (Berlin: Gebr. Mann Verlag)
- Zangger E 1994 Landscape changes around Tiryns during the bronze age *Am. J. Archaeol.* **98** 189–212






# Appendix VI



# SCIENTIFIC REPORTS



OPEN

## High-resolution record reveals climate-driven environmental and sedimentary changes in an active rift

Lisa C. McNeill<sup>1</sup>, Donna J. Shillington<sup>2</sup>, Gareth D. O. Carter<sup>3</sup>, Jeremy D. Everest<sup>3</sup>, Robert L. Gawthorpe<sup>4</sup>, Clint Miller<sup>5</sup>, Marcie P. Phillips<sup>6</sup>, Richard E. L. Collier<sup>7</sup>, Aleksandra Cvetkoska<sup>8</sup>, Gino De Gelder<sup>9</sup>, Paula Diz<sup>10</sup>, Mai-Linh Doan<sup>11</sup>, Mary Ford<sup>12</sup>, Maria Geraga<sup>13</sup>, Jack Gillespie<sup>14</sup>, Romain Hemelsdaël<sup>15</sup>, Emilio Herrero-Bervera<sup>16</sup>, Mohammad Ismaiel<sup>17</sup>, Liliane Janikian<sup>18</sup>, Katerina Kouli<sup>19</sup>, Erwan Le Ber<sup>20</sup>, Shunli Li<sup>21</sup>, Marco Maffione<sup>22</sup>, Carol Mahoney<sup>7</sup>, Malka L. Machlus<sup>2,23</sup>, Georgios Michas<sup>24</sup>, Casey W. Nixon<sup>4</sup>, Sabire Asli Oflaz<sup>25</sup>, Abah P. Omale<sup>26</sup>, Kostas Panagiotopoulos<sup>27</sup>, Sofia Pechlivanidou<sup>4</sup>, Simone Sauer<sup>28</sup>, Joana Seguin<sup>29</sup>, Spyros Sergiou<sup>13</sup>, Natalia V. Zakharova<sup>30</sup> & Sophie Green<sup>3</sup>

Young rifts are shaped by combined tectonic and surface processes and climate, yet few records exist to evaluate the interplay of these processes over an extended period of early rift-basin development. Here, we present the longest and highest resolution record of sediment flux and paleoenvironmental changes when a young rift connects to the global oceans. New results from International Ocean Discovery Program (IODP) Expedition 381 in the Corinth Rift show 10s–100s of kyr cyclic variations in basin paleoenvironment as eustatic sea level fluctuated with respect to sills bounding this semi-isolated basin, and reveal substantial corresponding changes in the volume and character of sediment delivered into the rift. During interglacials, when the basin was marine, sedimentation rates were lower

<sup>1</sup>School of Ocean and Earth Science, University of Southampton, Southampton, S014 3ZH, United Kingdom.

<sup>2</sup>Lamont-Doherty Earth Observatory of Columbia University, 61 Route 9W, Palisades, NY, 10964, USA. <sup>3</sup>British Geological Survey, The Lyell Centre, Edinburgh, United Kingdom. <sup>4</sup>Department of Earth Science, University of Bergen, Bergen, Norway. <sup>5</sup>Department of Earth, Environmental and Planetary Sciences, Rice University, Houston, USA. <sup>6</sup>Institute for Geophysics, University of Texas at Austin, Austin, USA. <sup>7</sup>School of Earth and Environment, The University of Leeds, Leeds, United Kingdom. <sup>8</sup>Department of Animal Ecology and Systematics, Justus Liebig University, Giessen, Germany. <sup>9</sup>Institut de Physique du Globe de Paris, Sorbonne Paris Cité, Université Paris Diderot, Paris, France. <sup>10</sup>Departamento Geociencias Marinas y Ordenación del Territorio, Facultad de Ciencias del Mar, Universidad de Vigo, Vigo, Spain. <sup>11</sup>Université Grenoble Alpes, Université Savoie Mont Blanc, CNRS, IRD, IFTTAR, and ISTerre, Le Bourget-du-Lac, France. <sup>12</sup>CRPG, UMR 7358, France. Also at: Université de Lorraine, ENSG, INP, Nancy, France. <sup>13</sup>Department of Geology, University of Patras, Patras, Greece. <sup>14</sup>Center for Tectonics, Resources, and Exploration (TRaX), Department of Earth Sciences, School of Physical Sciences, University of Adelaide, Adelaide, Australia. <sup>15</sup>Géosciences Montpellier, Université de Montpellier, Montpellier, France. <sup>16</sup>University of Hawai'i at Manoa, Hawai'i Institute of Geophysics and Planetology, Honolulu, USA. <sup>17</sup>University Centre for Earth and Space Sciences, University of Hyderabad, Hyderabad, India. <sup>18</sup>Universidade Federal de São Paulo, Departamento de Ciências do Mar, Sao Paulo, Brazil. <sup>19</sup>Department of Geology and Geoenvironment, National and Kapodistrian University of Athens, Athens, Greece. <sup>20</sup>School of Geography, Geology and the Environment, University of Leicester, Leicester, United Kingdom. <sup>21</sup>School of Energy Resources, China University of Geosciences, Beijing, China. <sup>22</sup>School of Geography Earth and Environmental Sciences, University of Birmingham, Birmingham, United Kingdom. <sup>23</sup>Department of Physical Sciences, Kingsborough Community College, City University of New York, New York, USA. <sup>24</sup>Laboratory of Geophysics and Seismology, Technological Educational Institute of Crete, Irakleio, Greece. <sup>25</sup>Graduate School "Human Development in Landscapes", Christian-Albrechts-Universität zu Kiel, Kiel, Germany. <sup>26</sup>Department of Geology and Geophysics, Louisiana State University, Baton Rouge, USA. <sup>27</sup>Institute of Geology and Minerology, University of Cologne, Cologne, Germany. <sup>28</sup>Ifremer, Department of Marine Geosciences, Centre Bretagne, Plouzané, France. <sup>29</sup>Institute for Ecosystem Research, Christian-Albrechts-Universität zu Kiel, Kiel, Germany. <sup>30</sup>Department of Earth and Atmospheric Sciences, Central Michigan University, Mount Pleasant, USA. Correspondence and requests for materials should be addressed to L.C.M. (email: [lcmm@noc.soton.ac.uk](mailto:lcmm@noc.soton.ac.uk))

(excepting the Holocene), and bioturbation and organic carbon concentration higher. During glacials, the basin was isolated from the ocean, and sedimentation rates were higher (~2–7 times those in interglacials). We infer that reduced vegetation cover during glacials drove higher sediment flux from the rift flanks. These orbital-timescale changes in rate and type of basin infill will likely influence early rift sedimentary and faulting processes, potentially including syn-rift stratigraphy, sediment burial rates, and organic carbon flux and preservation on deep continental margins worldwide.

Active continental rift zones generate rapidly subsiding basins with significant accumulations of sediments. These settings are thought to be highly sensitive to the interplay of extensional tectonics, sedimentary processes, climate and sea level change<sup>1,2</sup>. Rift basins and other basins in active environments close to sea level are known to experience dramatic changes in environment due to glacio-eustatic fluctuations<sup>3,4</sup>. Both pronounced environmental change and active faulting are thought to control sediment delivery and accumulation in active basins<sup>1–3</sup>. This includes changes in temperature, precipitation and amount and type of vegetation cover affecting erosion and sediment flux, and tectonics driving changes in catchment relief and area, erosion of different lithologies and shifting loci of sedimentation within a basin. However, the paucity of high-resolution constraints makes it difficult to isolate each of these contributions. Erosion and deposition of sediments also appear to have profound effects on rift localisation, fault longevity, crustal creation, and thermal structure<sup>5–9</sup>. However, the record of these processes is deeply buried and inaccessible in most ancient and mature rifts; high resolution data on age and rates of process are not available for deep and old sediments, the spatial resolution of seismic data is low, and sections are deeply buried and often overprinted by later deformational phases so do not preserve information on early fault history and its link to sedimentary processes. Basins in active environments tend to only have very short (mostly <15–25 ka) records from piston cores. Rare longer temporal records exist (Black Sea, Lake Malawi<sup>2,10</sup>) but in environments of lower tectonic activity or without ocean connection. Therefore, our ability to constrain in sufficient resolution temporal and spatial variations in basin paleoenvironment, sedimentation patterns or rift development, or the role of climate and sea level in moderating these factors is severely restricted. As a result, many hypotheses tend to be model derived and remain untested.

The Corinth Rift (Fig. 1) is a region of rapid, localised extension and high seismic activity. Current extension rates reach 10–15 mm/yr<sup>11–13</sup>, some of the highest in the world. Corinth's high rates of tectonic activity, high sediment fluxes, closed drainage system and preservation of the syn-rift record make it a unique laboratory for the study of extension, sedimentation and paleoenvironment in a young rift.

Rifting began ~5 Ma with 3 main phases identified by integration of onshore depositional records and offshore seismic stratigraphy<sup>1,14–21</sup>. Following an early continental and lacustrine phase (phase 1), depocentre deepening occurred ~2 Ma (phase 2) resulting in increased subsidence and sediment supply at the location of the modern Gulf of Corinth. At ~0.5–0.8 Ma, fault activity generally stepped northward, establishing the dominant N-dipping rift fault system along the southern boundary (Fig. 1) and development of fan deltas along the western part of the southern Gulf margin (phase 3). The transition from Phase 2 to 3 may mark the onset of repeated connection to the open ocean, although earlier marine incursions are recognised onshore<sup>21</sup>.

From onshore deposits and seismic imaging of offshore stratigraphy, the rift basin environment during phase 3 has been interpreted to alternate between marine conditions during interglacial/highstand periods and isolated from the open ocean during glacial/lowstand periods, as eustatic sea level fluctuated relative to the boundaries of the basin in the Late Quaternary<sup>17–19,21–25</sup>. Sills at the western mouth of the Corinth Basin (Rion sill: ~60 m; Acheloos-Cape Pappas sill: ~50–55 m) currently control the connection with the Ionian Sea (Fig. 1) and are interpreted to control connection for at least the last 200 kyr<sup>22,26,27</sup>. Prior to this, the cyclical connection to the ocean was either controlled by these sills in the west or by one or more sills in the east, primarily the Corinth Isthmus (Fig. 1), currently above sea level but submerged in the past<sup>28</sup>. Prior to IODP Expedition 381, the only data available to constrain paleoenvironment evolution, and thus to examine alternating conditions, were shallow piston cores recovering sediments no deeper than 30 metres below seafloor (mbsf) and no older than 50 ka<sup>29,30</sup>. These data showed a change in sediment facies and micropaleontological assemblages at ~12 ka, marking the timing of transgression above the basin sill following the last glacial maximum. To date, these short records and similar records from other active basins do not provide a sufficiently long-duration record to evaluate sea-level driven changes in environment and their implications for sedimentation and rift processes.

IODP Expedition 381 drilled and cored the most recent ~1–2 Myr of syn-rift sediments to a depth of 705 mbsf, in October–December, 2017 (Fig. 1)<sup>31</sup>. This is the longest and highest resolution record of its kind in a young extensional basin at the point of connection to the global oceans, and it provides the first constraints on the age of the full rift sequence, syn-rift stratigraphy, rates and timings of rift tectonic processes, sediment fluxes and basin environmental conditions. Here we use this new record to test the hypothesis that glacial-interglacial timescale (10's–100 kyr) climatic and environmental change strongly influences the nature and volume of accumulating sediment within the Corinth basin. If such change occurs, we explore how sediment delivery and accumulation are affected, including effects on sediment fluxes, grain size and lithostratigraphy. Alternatively, the basin is insensitive to regional and local short-term environmental and climatic change being, instead, dominated by longer term tectonic-driven changes. Finally, we hypothesise that regional climatic change at 10–100 kyr timescales results in major basin environmental change with a corresponding change in aquatic biota.

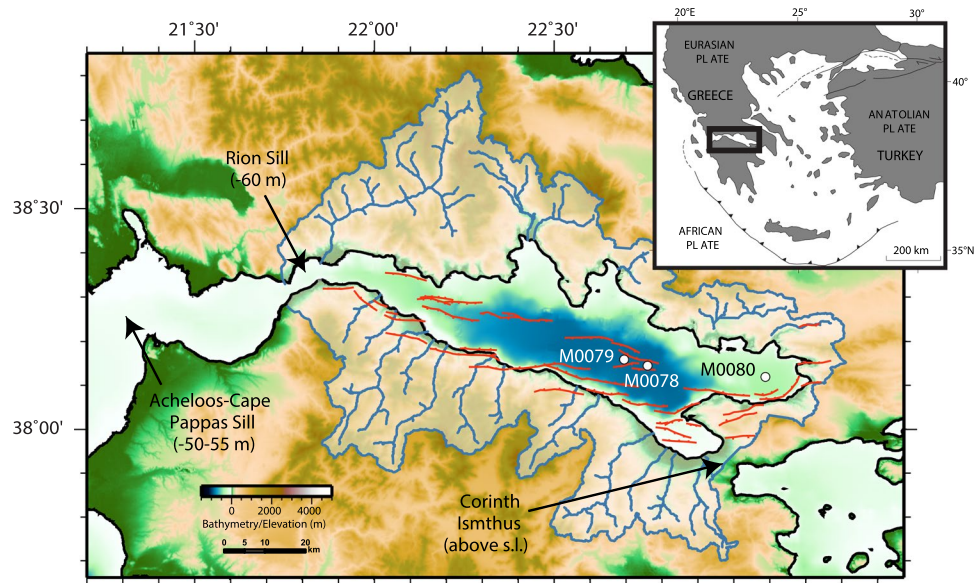


**Figure 1.** Map of the Gulf of Corinth and Corinth Rift system. Includes primary active rift faults (after ref.<sup>17</sup>), positions of bounding sills to the Gulf, IODP drillsites, and primary catchment areas and rivers feeding the offshore basin (from ref.<sup>42</sup>). Inset shows regional setting.

## Results

Three sites were drilled during Expedition 381 (Fig. 1). Site M0079, the focus of observations in this paper, is in the central Corinth basin, the primary depocentre of the Gulf of Corinth (Fig. S4). The nature of the site, within a primary locus of sedimentation, is based on analysis of syn-rift sediment thicknesses from integration of seismic profiles around the rift<sup>17</sup>. This site samples an expanded section of the most recent rift phase (phase 3), and thus provides a high-resolution record of extension, sedimentation and sea level change over the last ~750 ka. The site contains a thick, continuous succession of fine-grained distal facies and no faults. Thus, the depositional history including sediment accumulation rates (both absolute and variations through time) from this borehole are representative of the Corinth primary depocentre. The upper lithostratigraphic Unit 1, the focus of this paper, is subdivided into 16 subunits and has its base at 677 mbsf (Fig. 2), with a thin Unit 2 section beneath.

**Evidence for cyclical rift basin paleoenvironment.** Microfossil assemblages in Unit 1 alternate primarily between “marine” assemblages composed exclusively of marine microfossils, and assemblages with significant amounts of both non-marine and marine microfossils that reflect a range of complex conditions that are neither fully marine nor freshwater, with different degrees of marine influence (hereafter, “isolated”). During marine intervals, both marine and terrestrial microfossils are abundant, including calcareous nannofossils, marine diatoms, planktic and benthic foraminifera, dinoflagellate cysts, foraminifera test linings, pollen and spores (Figs 2 and 3, Table S1). During isolated intervals, non-marine diatoms are typically present in moderate to high abundances (Figs 2 and 3, Table S1), and observed in combination with moderate to high abundances of green algae coenobia and spores, marine or brackish dinoflagellate cysts, pollen and spores and low abundances of marine microfossils. The variability of microfossil and palynomorph assemblages within and between marine and isolated intervals directly indicates changes in aquatic basin paleoenvironment (e.g., salinity) and in terrestrial environment around the rift basin, paleoclimate and depositional setting. Based on these assemblages, the 16 subunits of Unit 1 were identified as marine or isolated intervals as a function of connection to or isolation from the open ocean. A combination of lithology, microfossil assemblages and core physical properties data provided the basis for pinpointing the subunit boundaries<sup>31</sup>.

**Mid-Late Quaternary Chronostratigraphy.** Biostratigraphy and magnetostratigraphy provide age control that allows us to link changing paleoenvironment to the eustatic sea level curve (Fig. 2). Calcareous nannofossils in the marine intervals confirm that Unit 1 is Middle Pleistocene through Recent based on (1) the Last Occurrence (LO) of *Pseudoemiliania lacunosa* (0.43 Ma) at 496 mbsf; (2) the First Occurrence (FO) of *Emiliania huxleyi* (0.29 Ma) at 405 mbsf; and (3) the crossover in dominance between *E. huxleyi* and *Gephyrocapsa* “small” (<3 μm) within subunit 1–2 (Fig. 2), documented at ~70 ka in the Mediterranean<sup>32</sup>. Due to the fluctuating environment within the basin, the syn-rift stratigraphy does not contain a continuous marine section, thus the LO of *P. lacunosa* and FO of *E. huxleyi* may not mark the true respective LO and FO (see Methods). However, the observed specimens are well preserved and moderately to highly abundant, and support other age markers. Magnetostratigraphy indicates the Brunhes-Matuyama chron boundary (0.773 Ma) occurs at ~665 mbsf at the base of Unit 1 (Fig. 2).

The overall pattern of downhole cyclicity of the Unit 1 subunits (marine vs isolated) strongly supports the paleoenvironment being predominantly controlled by eustatic sea level fluctuation; tectonic control of this cyclical

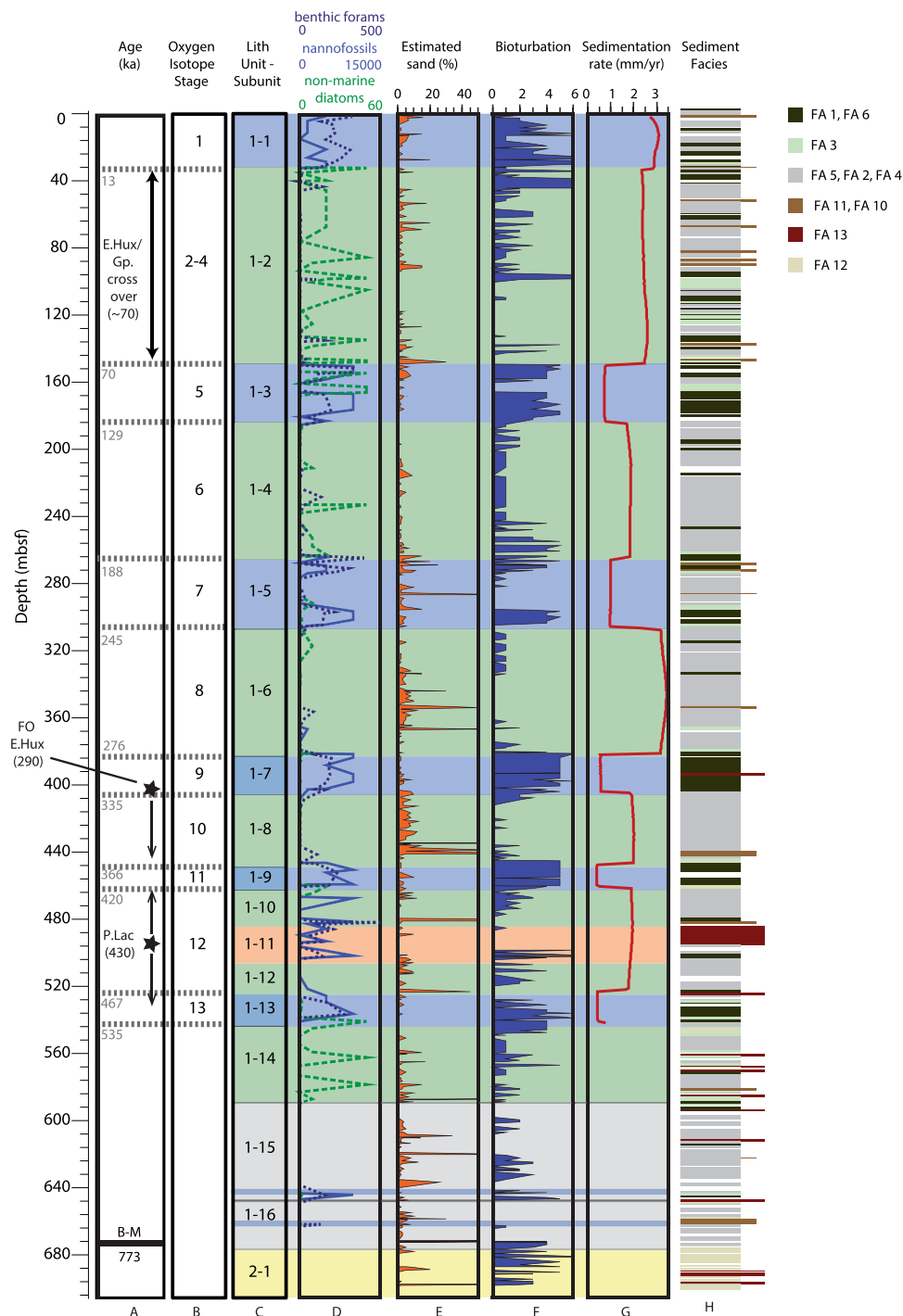


**Figure 2.** Results from Site M0079. (A) Age constraints from calcareous nannofossils and magnetostratigraphy (black text) and interpreted ages from correlation of basin environment with eustatic sea level curve (grey dotted lines and text, see Methods). (B–M) Brunhes–Matuyama chron boundary; E. Hux.: first occurrence (FO) of *E. huxleyi*; P.Lac: last occurrence (LO) of *P. lacunosa*; E.Hux/Gp. crossover: crossover in dominance between *E. huxleyi* and *Gephyrocapsa*. Arrows indicate potential uncertainty of true depth position of age marker (see text and Methods), and age is given in parentheses; (B) Oxygen isotope stages (OIS); (C) Lithostratigraphic units and subunits, coloured by basin environment interpretation (blue: marine; green: isolated/semi-isolated; grey: undetermined), subunit 1–11 is slumped interval (orange), yellow denotes Unit 2; (D) Abundance/counts of calcareous nannofossils (light blue), benthic foraminifer (dark blue, dotted) and non-marine diatoms (green, dashed); (E) Estimated sand percent; (F) Bioturbation intensity; (G) Decompacted sedimentation rate (see Methods); and (H) Sediment lithology coloured according to facies association, longer bars representing coarser intervals (Table S3; ref.<sup>31</sup>).



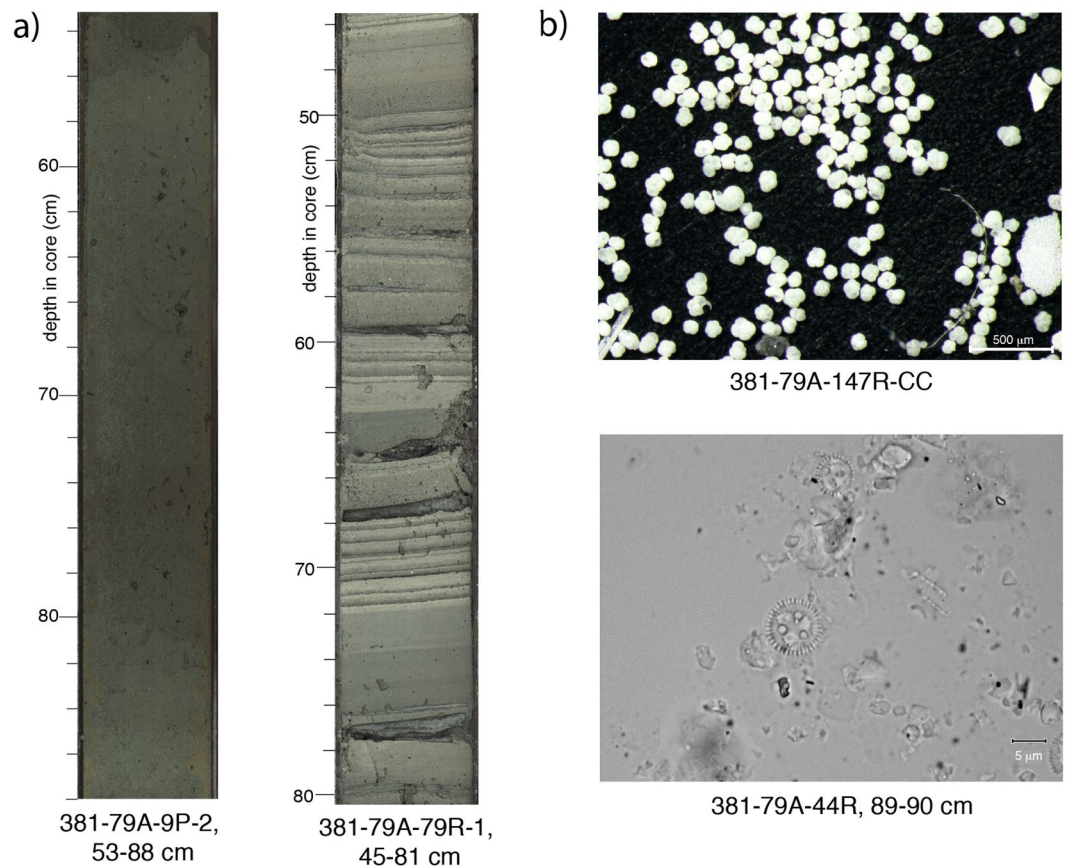


**Figure 3.** Core images. (a) Core section examples (from Site M0079) of typical sedimentary facies in marine (left; Facies Association 1, homogeneous mud) and isolated (right; Facies Association 4, laminated greenish grey to grey mud with mud beds) intervals; (b) Typical microfossil assemblages from marine (above) and isolated (below) intervals (from Site M0079). Marine assemblage image shows planktic forams from  $>125\ \mu\text{m}$  fraction; isolated assemblage (at 1000x magnification) shows non-marine planktonic diatom taxon *Pantocsekiella ocellata*.

nature can be ruled out. In addition, the marine phases include short-lived isolated intervals, and vice versa, as expected from details of the eustatic fluctuations (e.g., within subunit 1–2, Fig. 2). We correlated the transitions between marine and isolated intervals to the eustatic sea level curve of Spratt and Lisecki<sup>33</sup> assuming a bounding sill depth of  $-60\ \text{m}$  (present day Rion sill depth<sup>27</sup>) and that flooding of this sill marks the transition between isolated and marine conditions (Fig. 2). This correlation and a sill depth of  $-60\ \text{m}$  agree with age constraints from bio- and magnetostratigraphy and work exceptionally well to  $\sim 545\ \text{mbsf}$  and the base of subunit 1–13, which is correlated with oxygen isotope stage (OIS) 13 at  $\sim 535\ \text{ka}$  (Fig. 2). Below this depth, marine fauna occur in thin stratigraphic intervals within subunits 1–15 and 1–16 (Fig. 2). This may be explained by the basin-controlling sill being at a shallower level at this earlier stage, resulting in a limited record of earlier highstands in the basin.

Currently the primary age uncertainty derives from the presumption of a constant sill depth. As above, the nature of the marine record in the deeper part of Unit 1 suggests the sill was potentially shallower at this time. However, the persistence of the marine intervals and their relatively consistent thickness until we reach the deeper part of Unit 1 gives strong support to the controlling sill remaining close to this depth, supported by previous studies<sup>27</sup>. A significant shift of the sill to shallower depths (e.g.,  $0\text{--}20\ \text{m}$ ) would severely restrict marine incursions, and this is not observed (unless we invoke very significant differences in sedimentation rate between marine intervals with time). Shallowing the sill level by up to  $30\ \text{m}$  does not significantly change the inferred age model, and the relative differences in sedimentation rates between isolated and marine intervals persist (see Methods, Fig. S3). In the absence of additional constraints, a constant sill depth is the most conservative assumption. As further research is undertaken on these drill cores, we will be able to add further absolute age constraints, including from tephra that are starting to be identified. This will reduce uncertainties of the age model and in turn provide constraints on sill height.

**Syn-rift sedimentary stratigraphy and processes.** Fine-grained (mud dominated), carbonate-rich turbiditic and hemipelagic sediments dominate the syn-rift succession of the Corinth Rift basin. However, we observe significant differences in lithology and depositional processes between the marine and isolated intervals of lithostratigraphic Unit 1. Marine subunits of Site M0079 are moderately to highly bioturbated and dominated by homogeneous to poorly-bedded greenish grey muds (Figs 2 and 3a). Biogenic material is common and

comprises calcareous nannofossils, foraminifera and marine diatoms, and fragments of gastropods and bivalves. Marine subunits are also characterised by increased total organic carbon (TOC) concentration with respect to the isolated subunits<sup>34</sup>. Isolated subunits are characterised by laminated to thinly bedded and homogeneous grey and greenish grey muds (Fig. 3a), some with black, organic-rich laminations and beds, and are generally lacking or having sparse bioturbation (Fig. 2). Overall, isolated intervals contain a higher proportion of relatively coarser grained lithologies (silts and sands). This is particularly well expressed in the deeper subunits of Unit 1, for example compare sand content of marine subunits 1–5, 1–7 and 1–9 with isolated subunits 1–6 and 1–8 (Fig. 2).

We calculated sedimentation rates for each marine and isolated subunit using decompacted thicknesses of total sediment (hemipelagic plus gravity flow deposit) derived using borehole porosity data (see Methods)<sup>31</sup>. The primary uncertainties in these calculations include the sill depth, which controls the precise estimated timing of the transition between marine and isolated intervals and their duration, potential differences in seafloor porosity in the past, and the applicability of the decompaction curve used, particularly for the marine versus isolated intervals, which may compact differently (see Methods). Unit 1 has an average sedimentation rate of 1.1 mm/yr, but a striking result is the clear difference in sedimentation rate between the marine and isolated intervals/subunits within Unit 1 (Fig. 2). Sedimentation rates in isolated intervals/subunits (range of averages per interval: 1.7–3.3 mm/yr) are generally higher than those of the marine intervals/subunits (range of averages per interval: 0.3–0.7 mm/yr). For each pair of successive marine-isolated intervals (e.g., between subunits 1–3 and 1–2), excluding the Holocene subunit 1–1, the rates are 1.9–6.7 times greater in the isolated than the marine intervals. This result is supported by indicators<sup>35</sup> of enhanced fluvial input into the basin during glacial periods. Sedimentation rates for the 0–12 ka (Holocene) marine interval (subunit 1-1) are unusually high (average 2.9 mm/yr) compared to older marine intervals and are more similar to those of the isolated intervals. This suggests that the Holocene section recovered by piston cores in the Gulf of Corinth cannot be used to generalise conditions farther back in time. Overall there is also a slight pattern of increased rates from the past to present for both isolated and marine intervals. Deviating from this pattern, the sedimentation rate is particularly high in subunit 1–6 (MIS 8) at 3.3 mm/yr, and this is considerably higher than the prior and subsequent isolated subunits (Fig. 2).

Translating results from Site M0079 to the thickest Unit 1 section of the whole rift basin (1.5 km versus 0.68 km at Site M0079) using seismic stratigraphic unit thickness<sup>17</sup> generates a maximum average sedimentation rate for Unit 1 in the basin of ~2 mm/yr and rates up to 3–4 mm/yr over individual ~100 kyr time periods. Overall these results indicate high sediment accumulation rates overall and large differences in sediment accumulation between marine/interglacial and isolated/glacial intervals.

## Discussion

**Changing environment in the Late Quaternary rift basin.** The changing environmental conditions reflected by the microfossil assemblages are interpreted to arise from fluctuating eustatic sea level with respect to the bounding sills of the Gulf of Corinth. Many previous studies have hypothesised that alternating marine and isolated conditions in the Gulf are driven by sea level change<sup>15,18,25</sup>, but previous observations on this and other semi-isolated basins (e.g., Sea of Marmara, Black Sea) primarily came from piston cores and thus only sampled part of the most recent glacial cycle and the Holocene<sup>3,4,29,30</sup>. The cores recovered during IODP Expedition 381 provide the first direct evidence of sea-level driven changes in paleoenvironment in an active rift basin over hundreds of thousands of years (0–750 ka).

Observations from Site M0079 demonstrate profound climate and sea-level driven changes in the basin paleoenvironment, sediment accumulation and geochemistry<sup>31,34</sup> of this young rift over the last ~750 kyr. The microfossil assemblages are highly complex and variable – this is particularly true within the isolated intervals and within the marine-isolated transitions. We also note variations between the successive marine and isolated intervals. This variability suggests a much wider range of basin environments than simple marine versus freshwater end members for the marine and isolated intervals, respectively. The primary controls on the distribution of microfossil assemblages present are salinity, nutrient availability, pH, light, turbidity, temperature, and transport. Salinity, apparently the primary driver, is likely to be controlled by the combined effects of connection to the open ocean, freshwater influx/dilution, precipitation, evaporation, sill overflow from the Mediterranean Sea, and water body stratification and overturning that together result in a variety of conditions as eustatic sea level and climate fluctuated. Further research will investigate the specific environmental conditions indicated by the full suite of microfossils and how these vary through time.

Distinct differences in sedimentary processes and sedimentation rate are also observed between the marine and isolated intervals. The marine intervals are characterised by more homogeneous mud sequences, reduced coarse-grained sediment, and increased TOC concentration<sup>34</sup>. The changes in accumulation of organic carbon between marine and isolated intervals result from the interplay between basin productivity, terrestrial carbon input, preservation and sediment flux, all driven by cycling climate and basin environment<sup>34</sup>. Finally, the correspondence of increased bioturbation and homogeneity of sediments in the marine intervals indicates increased benthic organism activity. In summary, the clear increase in sedimentation rate during glacial periods when sea level is low and the basin is isolated (Fig. 2) implies that sediment fluxes (rates, volumes and grain size) into the basin from the subaerial rift flanks are increased during glacial times, probably leading to reduced benthic faunal activity within the basin.

**Influences on sediment flux into the basin.** Compared to other basins at similar evolutionary stages and over comparable time periods, sedimentation rates in Corinth (up to ~3–4 mm/yr) are high (e.g., Sea of Marmara, Lake Baikal, Malawi, Northern Gulf of California<sup>2,3,36,37</sup>). The Northern Gulf of California and Sea of Marmara have comparable sedimentation rates (up to 2–4 mm/yr<sup>3,37</sup>). In Corinth, sediment flux is primarily controlled by combinations of high uplift rates of the rift flanks (Late Quaternary rates of 1–5 mm/yr<sup>15,38–41</sup>) and erosion of weakly consolidated/lithified materials into accommodation space created through rapid extension



and subsidence. The ability of the fluvial systems to transport sediment is also an important control on delivery of sediments to the basin. However, in the Corinth system, fluvial systems do not appear to be limited by their ability to transport sediment<sup>38</sup>, and thus the increased sediment fluxes during glacial periods reflect increased sediment production and supply.

Many of the most significant catchments are located on the southern rift margin, i.e., the N. Peloponnese (with the exception of the Mornos on the NW rift margin), coincident with highest uplift rates in the footwall of the southern rift boundary N-dipping fault system<sup>1</sup> (Fig. 1). In spite of the exceptionally high sedimentation rates shown here, the Corinth basin is presently underfilled, and it is likely that it has been underfilled for many 100's of kyr and potentially at least 1.5 Myr based on the height of delta foresets on the Gulf margins and those exposed onshore<sup>21</sup>. This highlights that rift basin subsidence rates exceed sediment accumulation rates, even during glacial/lowstand periods when sediment flux into the basin is enhanced by a factor of 2–7. This may be amplified by catchment averaged erosion rates being insufficient to keep pace with uplifting topography.

Although tectonic subsidence and uplift clearly control the larger-scale development of the basin, they would not be expected to fluctuate cyclically on timescales of 10's kyr, as sedimentation rates fluctuate here. Therefore, we propose that basin sediment accumulation, including variations between glacial and interglacial periods, is a function of one or more of the following: (a) climate (temperature, precipitation) controlling erosion rates and sediment flux<sup>29,42</sup>; (b) vegetation type and cover changing runoff and sediment retention/erosion rates; (c) changing basin salinity driving more efficient hyperpycnal flows during isolated/glacial intervals<sup>1</sup>. Because the shelf is narrow in much of the Gulf of Corinth, enhanced slope failure due to direct sediment supply to the shelf edge is unlikely to contribute and catchments are unlikely to significantly increase in area, during sea level lowstands. However, the fluvial and deltaic material exposed on the shelf during lowstands may be more easily erodable, and the partially exposed, relatively unstable margin slopes may be more susceptible to failure<sup>27</sup>. A previous study proposed that a combination of cool, wet winters in the last glacial and reduction in tree cover led to increased sediment availability and flux during glacials estimated over the last ~100 kyr in the eastern Corinth rift<sup>29</sup>. However, pollen-based precipitation reconstructions from the region<sup>43–45</sup> indicate a decrease in precipitation during glacials, not an increase. Long pollen records across the Balkan Peninsula suggest interglacial forested landscapes alternating with open vegetation during glacials<sup>44–46</sup>, and our new drill cores in the Corinth basin show the same results. Our new cores also have lower pollen and higher corroded pollen grain concentrations in isolated intervals, the latter indicating increased reworking attributed to increased soil erosion, often linked to open vegetation<sup>47</sup>. These pollen and sedimentation rate results from the new IODP borehole record and previous studies lead us to conclude that both reduction and change in type of vegetation cover resulted in increased soil erosion and higher sediment flux into the basin during the isolated/glacial intervals. Analysis of bedrock fault scarp weathering shows evidence for enhanced physical weathering during glacial periods in the Mediterranean region<sup>48</sup>, which may add to the observed Corinth sediment flux increase. Contrasts in seasonality and storminess between glacials and interglacials may have also contributed to erosion rates, but this parameter has not yet been resolved from our new sedimentary record, or previous studies in the region. Sedimentation rates from piston cores and drilling have also revealed variations in sedimentation rates over glacial/interglacial cycles in the Sea of Marmara and Black Sea<sup>3,10</sup>.

The Holocene (last marine/interglacial interval) appears to have significantly higher sedimentation rates than earlier marine/interglacial intervals and is comparable to isolated/glacial intervals (Fig. 2). Forest clearance and agriculture are visible in pollen records from Greece since the mid-Holocene (~6 ka)<sup>49</sup>, therefore it is likely that human activity in the study region is responsible for the high sediment fluxes observed in Holocene subunit 1–1<sup>50</sup>.

**Implications for the early history of rifts.** The Corinth Rift basin provides a unique window into an active rift basin environment at the point in time where the rift basin connects to the global ocean system due to rifting and resulting subsidence. It therefore is intermediate between terrestrial rift basins that have yet to achieve a connection to the open oceans (e.g., Lake Baikal, the majority of the East African Rift system) and rifts that have fully connected and no longer oscillate between open and isolated basin environment (e.g., Gulf of California, passive rifted margins). The new Corinth boreholes provide an extended record with unprecedented resolution over multiple glacio-eustatic cycles and will add insight to how the environment of other semi-isolated basins will have developed over time, such as the Sea of Marmara and Black Sea. Our new results illustrate the significant impact of regional climate at orbital timescales (10 s–100 s kyr) on sediment accumulation, and how this in turn affects patterns of organic matter accumulation, preservation and burial history (see also ref.<sup>34</sup>). We would expect to see similar cyclical patterns of organic carbon to those observed here in other rift basins regularly connecting to the oceans. Observed sedimentation patterns, controlled by sea level and climate, could have implications for the distribution of potential source and reservoir rocks within the early phase of sediment build-up on rifted margins, in particular where icehouse conditions prevailed. This is because sediment build up impacts the burial history, preservation and thermal evolution of deep rifted margin sediments and organic matter. Cyclical fluctuations in sediment accumulation combined with feedbacks on fault activity will have important implications for how tectonics and climate interact to control the stratigraphy of mature rifts and rifted margins worldwide<sup>51</sup>.

The observation of high average rates of sedimentation that vary substantially over ~10–100 kyr timescales could have important consequences for tectonic processes in Corinth and early rifting in general. Surface processes can impact lithospheric extensional processes, in particular, the redistribution of mass from the uplifted footwalls into the basin promotes greater extension on rift faults before they are abandoned in favour of new faults<sup>9</sup>. Thicker sediments could also reduce differences in buoyancy forces resulting from thinning, and thus promote narrow rifting<sup>5</sup>. Many of these inferences are based on modelling or larger scale structure but with limited temporal constraints. For the relatively high slip rates on faults bounding the Corinth Rift (2–10 mm/yr)<sup>15</sup>, the temporal changes in erosion onshore and deposition offshore observed here could modulate fault evolution.

Further application of the new drilling results in the Corinth rift to analysis of the fault activity will allow us to test whether sedimentation changes, even on relatively short timescales, can impact rift faulting.

## Conclusions

A new scientific drill core record from the syrift sequence of the active Corinth rift provides the first direct observations that basin environment fluctuated between marine conditions during eustatic highstands and isolated conditions during eustatic lowstands when the basin is cut off by bounding sills over the last ~700 ky. Sedimentation rates in the basin show significant variations on 10's-100 kyr timescales and are markedly increased during glacial/isolated periods. In contrast, bioturbation and organic carbon concentrations are reduced during glacial/isolated periods. The new borehole data, supported by other studies, suggest sedimentation rate changes are a function of a decrease and change in type of vegetation cover in glacial periods, resulting in increased erosion and basin sediment flux. The aquatic basin environment is clearly influenced by 10–100 kyr sea level fluctuation and climate, with the microfossil assemblages sampled indicating much greater complexity than simple alternations between fully marine to freshwater conditions. These results thus reveal the dominant role of climate and sealevel change in generating ~100-ky variations in sedimentation rate and basin environment in this active rift basin.

## Methods

**Micropaleontology and Basin Environment.** Microfossils (calcareous nannofossils, marine and non-marine diatoms, planktic and benthic foraminifer, dinoflagellate cysts, foraminifer test linings, freshwater algae coenobia and spores, and aquatic pollen and spores) were used to distinguish basin paleoenvironment, principally differentiating “marine” or “isolated”. Supplementary Table S1 gives abundances of key microfossil groups: calcareous nannofossils and benthic foraminifer (marine indicators) and non-marine diatoms (isolated indicators) with depth in Hole M0079A. Qualitative counts of calcareous nannofossils and non-marine diatoms are based on the Cascading Count Method<sup>52</sup>. The numerical approximations associated with abundance in Fig. 2 (abundance: Barren (B), Very Rare (VR), Rare (R), Few (F), Common (C) and Abundant (A)) for calcareous nannofossils and non-marine diatoms are outlined below:

Calcareous Nannofossils: B = 0; VR = 1–5; R = 6–100; F = 101–1500; C = 1501–5000; A = 5001–10,000+

Non-marine Diatoms: B = 0; VR = 1; R = 2; F = 3–10; C = 11–20; A = 21–50+

The abundance of benthic foraminifer is represented by the number of individuals found in ~10 cc of wet sediment. Benthic foraminifer were counted in the >125 µm fraction. In the isolated intervals, where abundance in the >125 µm is generally lower than 10 individuals, the 63–125 µm fraction was also screened.

**Age Model.** Age constraints were from shipboard biostratigraphic (calcareous nannofossils) and magnetostratigraphic analyses. Biozonation of calcareous nannofossils was applied using existing studies<sup>53,54</sup>. The website [www.mikrotax.org](http://www.mikrotax.org) aided identification of calcareous nannofossils. Calcareous nannofossils provide three age markers (shown on Fig. 2). Due to the fluctuating environment within the basin, the syn-rift stratigraphy does not contain a continuous marine section, thus the LO of *P. lacunosa* and FO of *E. huxleyi* may not mark the true respective LO and FO. We note that *P. lacunosa* was identified in a coherent interval within a large-scale slump that defines subunit 1–11 (Fig. 2)<sup>31</sup> surrounded by intervals interpreted as isolated. The stratigraphic interval containing this marine calcareous nannofossil assemblage is intact with no evidence for reworking. Therefore, this coherent interval of slumped sediments containing *P. lacunosa* is interpreted to represent a part of an older marine interval, most likely the time equivalent of the underlying marine subunit 1–13. Preliminary magnetostratigraphy analysis provides one age marker in Hole M0079A, the Brunhes-Matuyama chron boundary at 0.773 Ma at a depth of 665 mbsf (Fig. 2). A total of 532 discrete sediment cubic samples were collected from working halves at intervals of ~1.5 m throughout the borehole. All samples were demagnetised using alternating field (AF) treatment in 14 progressive field steps from 5 to 40 mT (with 5-mT increments) and from 40 to 100 mT (with 10-mT increments). Remanent magnetisation direction and intensity were measured before and after each demagnetization step using the horizontal pass-through super-conducting cryogenic rock magnetometer (SRM 755–4000, 2G Enterprises) at the University of Bremen. The inclination of the remanence after AF demagnetisation at 40 mT was used to determine the polarity of each sample (i.e., normal or reversed) and build a magnetostratigraphy downhole. Magnetozones identified from the data were correlated to the Geomagnetic Polarity Time Scale – GPTS<sup>54,55</sup>.

In addition to the above age markers, the age model was developed by tying the Unit 1 subunit boundaries between the marine and isolated intervals to eustatic sea level (Supplementary Fig. S1 and Table S2<sup>33</sup>). A sill depth of –60 m (the current depth of the Rion sill at the western end of the Gulf of Corinth<sup>27</sup>) was used to determine the transition timing between marine and isolated. See Supplementary Information for further discussion of sill depth and impact of its depth change on sedimentation rates. All ages between these transitions were extrapolated linearly. Below a depth of ~545 mbsf, marine intervals were thin or absent (Fig. 2). Therefore, the age model developed from microfossil-based sea level correlation could not be applied from here to the base of the hole; however, the Brunhes-Matuyama chron boundary at 665 mbsf provides absolute age constraint near the base of the hole. Ages and depths in Hole M0079A are shown in Supplementary Table S2.

**Facies Associations and Bioturbation.** The lithostratigraphy of the syn-rift sediments drilled during Expedition 381 were categorised into facies associations (FA<sup>31</sup>) defined by physical and biogenic features of the sediment, including bedding and lamination style, grain size, colour, body and trace fossils. The facies associations used in this paper are defined in Supplementary Table S3 and a simplified version is depicted in Fig. 2. The degree of bioturbation applied to the cores is a semi-quantitative assessment ranging from 0 (no bioturbation) to 6 (completely bioturbated)<sup>56</sup>.

**Sedimentation Rate.** Sedimentation rates were calculated using ages described above and decompacted sediment thicknesses. Decompaction was based on porosities measured using the “moisture and density” technique on discrete 6 cm<sup>3</sup> samples spaced at ~1.5 m on cores from Hole M0079A. The wet and dry masses of these samples were measured before and after being dried in a convection oven at 60° ± 5 °C for 24 hrs, respectively. The volume of dried sample was measured with a helium-displacement pycnometer. These measurements were then used to calculate the volume and mass of water originally in the samples, and the porosity of the samples (Supplementary Table S4<sup>31</sup>).

Next, we determined a smooth porosity function to use for decompaction. We first removed outliers by fitting a 2<sup>nd</sup> order polynomial to the measured porosities and discarding values with residuals greater than 1.5, and then fit a 35<sup>th</sup> order polynomial to the remaining points. A high-order polynomial was required to capture the observed variations in porosity between marine and isolated subunits (Supplementary Fig. S2 and Table S5).

The decompacted thickness of sediments from a given depth interval,  $T_i^*$ , was determined (Supplementary Table S5) assuming that there is not alteration of the grains:

$$T_i^* = \frac{T_i(1 - \phi_i)}{(1 - \phi_i^*)}$$

where  $T_i$  and  $\phi_i$  are the compacted thickness and porosity of a given interval, respectively, where the porosity is taken from the smoothed function.  $\phi_i^*$  is the initial porosity, and is assumed to be 56%, the porosity at the modern seafloor in Hole M0079A (Supplementary Table S4<sup>31</sup>).

## Data Availability

All data and material pertinent to this study is contained within the manuscript and Supplementary Information, and/or the IODP Expedition 381 Preliminary Report (Shillington *et al.*, 2019; ref.<sup>31</sup>). The full Expedition Report and dataset from IODP Expedition 381 will become openly available on March 1, 2019 (McNeill *et al.*, 2019; ref.<sup>34</sup>) via the IODP website (<https://www.iodp.org/resources/access-data-and-samples>), including access to core materials and logging data.

## References

- Gawthorpe, R. L. *et al.* Tectono-sedimentary evolution of the Plio-Pleistocene Corinth rift, Greece. *Basin Research*, <https://doi.org/10.1111/bre.12260> (2017).
- Lyons, R. *et al.* Continuous 1.3-million-year record of East African hydroclimate, and implications for patterns of evolution and biodiversity. *PNAS* **51**, 15568–15573 (2015).
- McHugh, C. M.G. *et al.* The last reconnection of the Marmara Sea (Turkey) to the World Ocean: A paleoceanographic and paleoclimatic perspective. *Marine Geol.*, <https://doi.org/10.1016/j.margeo.2008.1007.1005> (2008).
- Mudie, P., Rochon, A., Aksu, A. & Gillespie, H. Dinoflagellate cysts, freshwater algae and fungal spores as salinity indicators in Late Quaternary cores from Marmara and Black seas. *Marine Geol.* **190**, 203–231 (2002).
- Bialas, R. W. & Buck, W. R. How sediment promotes narrow rifting: Application to the Gulf of California. *Tectonics* **28**, <https://doi.org/10.1029/2008TC002394> (2009).
- Dorsey, R. & Umhoefer, P. J. In *Tectonics of Sedimentary Basins: Recent Advances*. (eds Busby, C. & Azor, A.) 209–225 (2012).
- Han, L. *et al.* Seismic imaging of the metamorphism of young sediment into new crystalline crust in the actively rifting Imperial Valley, California. *Geochem. Geophys. Geosys.* **17**, 4566–4584 (2016).
- Lizarralde, D. *et al.* Variation in styles of rifting in the Gulf of California. *Nature* **448**, 466–469 (2007).
- Olive, J.-A., Behn, M. D. & Malatesta, L. C. Modes of extensional faulting controlled by surface processes. *Geophys. Res. Lett.* **41**, 6725–6733 (2014).
- Hsü, K. J. *et al.* In *Deep Sea Drilling Project Initial Reports*, **42**, 509–524 (1978).
- Bernard, P. *et al.* Seismicity, deformation and seismic hazard in the western rift of Corinth: New insights from the Corinth Rift Laboratory (CRL). *Tectonophysics* **426**, 7–30 (2006).
- Briole, P. *et al.* Active deformation of the Corinth rift, Greece: Results from repeated Global Positioning System surveys between 1990 and 1995. *J. Geophys. Res.* **105**, 25605–25625 (2000).
- Clarke, P. *et al.* Crustal strain in central Greece from repeated GPS measurements in the interval 1989–1997. *J. Geophys. Res.* **135**, 195–214 (1998).
- Armijo, R., Meyer, B., King, G., Rigo, A. & Papanastassiou, D. Quaternary evolution of the Corinth Rift and its implications for the Late Cenozoic evolution of the Aegean. *Geophys. J. Intl.* **126**, 11–53 (1996).
- Bell, R. E. *et al.* Fault architecture, basin structure and evolution of the Gulf of Corinth, central Greece. *Basin Research*, <https://doi.org/10.1111/j.1365-2117.2009.00401.x> (2009).
- Higgs, B. Syn-sedimentary structural controls on basin deformation in the Gulf of Corinth, Greece. *Basin Research* **1**, 155–165 (1988).
- Nixon, C. *et al.* Rapid spatiotemporal variations in rift structure during development of the Corinth Rift, central Greece. *Tectonics* **35**, 1225–1248, <https://doi.org/10.1002/2015TC004026> (2016).
- Sachpazi, M., Clement, C., Laigle, M., Hirn, A. & Roussos, N. Rift structure, evolution, and earthquakes in the Gulf of Corinth, from reflection seismic images. *Earth Planet Sci. Lett.* **2003**, 243–257 (2003).
- Taylor, B. *et al.* The structures, stratigraphy and evolution of the Gulf of Corinth rift, Greece. *Geophys. J. Intl.* **185**, 1189–1219 (2011).
- Ford, M., Hemelsdael, R., Mancini, M. & Palyvos, N. Rift migration and lateral propagation: evolution of normal faults and sediment-routing systems of the western Corinth rift (Greece). In: *The Geometry of Normal Faults* (Ed. by Childs, C., Holdsworth, R. E., Jackson, C.A.-L., Manzocchi, T., Walsh, J. J., Yielding, G.) Geol. Soc. London, Spec. Publ., (439) London (2016).
- Ford, M. *et al.* Tectono-sedimentary evolution of the western Corinth Rift (Central Greece). *Basin Res.* **25**, 3–25 (2013).
- Bell, R. E., McNeill, L. C., Bull, J. M. & Henstock, T. J. Evolution of the offshore western Gulf of Corinth. *GSA Bulletin* **120**, 156–178 (2008).
- Leeder, M. *et al.* Tectono-sedimentary processes along an active marine/lacustrine half-graben margin: Alkyonides Gulf, E. Gulf of Corinth, Greece. *Basin Research* **14**, 25–41 (2002).
- Lykousis, V., Sakellariou, D., Moretti, I. & Kaberi, H. Late Quaternary basin evolution of the Gulf of Corinth: Sequence stratigraphy, sedimentation, fault-slip and subsidence rates. *Tectonophysics* **440**, 29–51 (2007).
- Heezen, B. C., Ewing, M. & Johnson, G. L. The Gulf of Corinth floor. *Deep Sea Research* **13**, 381–411 (1966).
- Beckers, A. *et al.* Influence of bottom currents on the sedimentary processes at the western tip of the Gulf of Corinth, Greece. *Marine Geol.* **378**, 312–332 (2016).

27. Perissoratis, C., Piper, D. J. W. & Lykousis, V. Alternating marine and lacustrine sedimentation during late Quaternary in the Gulf of Corinth rift basin, central Greece. *Marine Geol.* **167**, 391–411 (2000).
28. Collier, R. E. L. & Thompson, J. Transverse and linear dunes in an upper pleistocene marine sequence, Corinth basin, Greece. *Sedimentology* **38**, 1021–1040 (1991).
29. Collier, R. *et al.* High sediment yields and cool, wet winters: Test of last glacial paleoclimates in the northern Mediterranean. *Geology* **28**, 999–1002 (2000).
30. Moretti, I. *et al.* Sedimentation and subsidence rate in the Gulf of Corinth: what we learn from the Marion Dufresne's long-piston coring. *Tectonics* **336**, 291–299 (2004).
31. Shillington, D. J., McNeill, L. C. & Carter, G. D. O. & the Expedition 381 Participants. Expedition 381 Preliminary Report: Corinth Active Rift Development. *College Station, TX, International Ocean Discovery Program.*, <https://doi.org/10.14379/iodp.pr.381.2018> (2019).
32. Anthonissen, D. E. & Ogg, J. *The Geologic TimeScale* **2012**, 1083–1127 (2012).
33. Spratt, R. M. & Lisecki, L. E. A Late Pleistocene sea level stack. *Climate of the Past* **12**, 1079–1092 (2016).
34. McNeill, L. C., Shillington, D. J., Carter, G. D. O. & Expedition 381 Participants. Corinth Active Rift Development. *Proceedings of the International Ocean Discovery Program*, **381**, College Station, TX, International Ocean Discovery Program., <https://doi.org/10.14379/iodp.proc.381.2019> (2019).
35. Toucanne, S. *et al.* Tracking rainfall in the northern Mediterranean borderlands during sapropel deposition. *Quat. Sci. Rev.* **129**, 178–195 (2015).
36. Edginton, D. N. *et al.* Sedimentation rates, residence times and radionuclide inventories in Lake Baikal from <sup>137</sup>Cs and <sup>210</sup>Pb in sediment cores. *Nature* **350**, 601–604 (1991).
37. Dorsey, R. Sedimentation and crustal recycling along an active oblique-rift margin: Salton Trough and northern Gulf of California. *Geology* **38**, 443–446 (2010).
38. Demoulin, A., Beckers, A. & Hubert-Ferrari, A. Patterns of Quaternary uplift of the Corinth rift southern border (N Peloponnese, Greece) revealed by fluvial landscape morphometry. *Geomorph.* **246**, 188–204 (2015).
39. Michas, G., Vallianatos, F. & Sammonds, P. Statistical mechanics and scaling of fault populations with increasing strain in the Corinth Rift. *Earth Planet Sci. Lett.* **431**, 150–163 (2015).
40. Palyvos, N., Pantosti, D. & Zabczi, C. Paleoseismological evidence of recent earthquakes on the 1967 Mudurnu Valley earthquake segment of the North Anatolian fault. *Bull. Seis. Soc. Am.* **97**, 1646–1661 (2007).
41. Pirazzoli, P. A., Stiros, S. C., Fontugne, M. & Arnold, M. Holocene and Quaternary uplift in the central part of the southern coast of the Corinth Gulf (Greece). *Marine Geol.* **212**, 35–44 (2004).
42. Watkins, S. E. *et al.* Are landscapes buffered in high frequency climate change? A comparison of sediment fluxes and depositional volumes in the Corinth Rift, central Greece, over the past 130 kyrs. *Geol. Soc. Am. Bull.*, <https://doi.org/10.1130/B31953.1> (2018).
43. Dormoy, I. *et al.* Terrestrial climate variability and seasonality changes in the Mediterranean region between 15 000 and 4000 years BP deduced from marine pollen records. *Climate of the Past* **5**, 615–632 (2009).
44. Sadori, L. *et al.* Climate, environment and society in southern Italy during the last 2000 years. A review of the environmental, historical and archaeological evidence. *Quat. Sci. Rev.* **136**, 173–188 (2016).
45. Tzedakis, P., Hooghiemstra, H. & Palike, H. The last 1.35 million years at Tenaghi Philippon: revised chronostratigraphy and long-term vegetation trends. *Quat. Sci. Rev.* **25**, 3416–3430 (2006).
46. Tzedakis, P. *et al.* Ecological thresholds and patterns of millennial-scale climate variability: The response of vegetation in Greece during the last glacial period. *geology* **32**, 109–112 (2004).
47. Wilmshurst, J. M. & McGlone, M. S. Corroded pollen and spores as indicators of changing lake sediment sources and catchment disturbance. *J. Paleolimnol.* **34**, 503–517 (2005).
48. Tucker, G. E. *et al.* 2011, Geomorphic significance of postglacial bedrock scarps on normal-fault footwalls. *J. Geophys. Res.* **116**, F01022 (2011).
49. Weiberg, E. *et al.* The socio-environmental history of the Peloponnese during the Holocene: Towards an integrated understanding of the past. *Quat. Sci. Rev.* **136**, 40–65 (2016).
50. Butzer, K. Environmental history in the Mediterranean world: cross-disciplinary investigation of cause-and-effect for degradation and soil erosion. *J. Archaeological Sci.* **32**, 1773–1800 (2005).
51. Balázs, A., Granjeon, D., Matenco, L., Sztanó, O. & Cloetingh, S. Tectonic and Climatic Controls on Asymmetric Half-Graben Sedimentation: Inferences From 3-D Numerical Modeling. *Tectonics* **36**, 2123–2141, <https://doi.org/10.1002/2017TC004647> (2017).
52. Styzen, M. J. Cascading Counts of Nannofossil Abundance. *J. Nannoplankton Res.*, **19** (1) (1997).
53. Backman, J., Raffi, I., Rio, D., Fornaciari, E. & Pälike, H. Biozonation and biochronology of Miocene through Pleistocene calcareous nannofossils from low and middle latitudes. *Newsletters on Stratigraphy* **45**(3), 221–244 (2012).
54. Ogg, J., Ogg, G. & Gradstein, F. *A Concise Geologic Time Scale 2016*. Elsevier B.V., ISBN 978-0-444-63771-0 (2016).
55. Cande, S. C. & Kent, D. V. Revised calibration of the geomagnetic polarity timescale for the Late Cretaceous and Cenozoic. *J. Geophys. Res.* **100**(B4), 6093–6095, <https://doi.org/10.1029/94JB03098> (1995).
56. Taylor, A. M. & Goldring, R. Description and analysis of bioturbation and ichnofabric. *J. Geol. Soc. London* **150**, 141–148, <https://doi.org/10.1144/gsjgs.150.1.0141> (1993).

## Acknowledgements

We sincerely thank all involved with the successful completion of IODP Expedition 381, including ECORD Science Operator staff, ship and drilling crew of the D/V *Fugro Synergy*, and staff at MARUM, University of Bremen. We thank Bill Ryan for useful comments on an earlier version of the manuscript. We thank two anonymous reviewers for their very helpful reviews and comments that improved the paper.

## Author Contributions

McNeill, Shillington, Gawthorpe, Miller and Phillips synthesised results and prepared the publication. Phillips, Cvetkoska, Diz Ferreriro, Geraga, Kouli, Oflaz, Panagiotopoulos characterised paleoenvironment based on microfossil assemblages. Gawthorpe, Collier, De Gelder, Ford, Gillespie, Hemelsdaël, Janikian, Li, Nixon, Pechlivanidou and Sergiou characterised sediment lithology and assigned facies associations. Phillips undertook biostratigraphy with calcareous nannofossils, and Herrero-Bervera and Maffione undertook magnetostratigraphy. Le Ber, Doan, Ismaïel, Machlus, Michas, Omale and Zakharova acquired and analysed physical properties data, including density and porosity. Miller, Mahoney, Sauer and Seguin acquired and analysed geochemical data, including TOC. Miller and McNeill established ties to the sea level curve, and Miller and Shillington calculated decompaction and sediment rates. McNeill, Shillington, Carter, Everest and Green organised the expedition that produced these results. All authors generated and analysed core and log data during Expedition 381 and contributed to the preparation of this paper.

## Additional Information

**Supplementary information** accompanies this paper at <https://doi.org/10.1038/s41598-019-40022-w>.

**Competing Interests:** The authors declare no competing interests.

**Publisher's note:** Springer Nature remains neutral with regard to jurisdictional claims in published maps and institutional affiliations.



**Open Access** This article is licensed under a Creative Commons Attribution 4.0 International License, which permits use, sharing, adaptation, distribution and reproduction in any medium or format, as long as you give appropriate credit to the original author(s) and the source, provide a link to the Creative Commons license, and indicate if changes were made. The images or other third party material in this article are included in the article's Creative Commons license, unless indicated otherwise in a credit line to the material. If material is not included in the article's Creative Commons license and your intended use is not permitted by statutory regulation or exceeds the permitted use, you will need to obtain permission directly from the copyright holder. To view a copy of this license, visit <http://creativecommons.org/licenses/by/4.0/>.

© The Author(s) 2019



# Declaration





## **Eidesstattliche Erklärung**

Hiermit erkläre ich, dass ich die von mir vorgelegte Dissertation selbständig verfasst und dass ich – abgesehen von der Beratung durch meine Betreuer – keine anderen als die angegebenen Quellen und Hilfsmittel benutzt habe. Die allgemein gültigen Zitierregeln für wissenschaftliches Arbeiten habe ich befolgt. Die Dissertation wurde an keiner anderen Fakultät oder Universität im Rahmen eines Prüfungsverfahrens vorgelegt. Mit Ausnahme der angegebenen Teilpublikationen ist sie nicht veröffentlicht worden und ich versichere eine solche Veröffentlichung vor Abschluss des Promotionsverfahrens nicht vorzunehmen. Die Arbeit wurde unter Einhaltung der Regeln guter wissenschaftlicher Praxis der Deutschen Forschungsgemeinschaft angefertigt. Kein akademischer Grad wurde je entzogen.

*I declare that I prepared this thesis independently only using the indicated tools and sources and the personal consultation by my supervisors. Where the work of others has been quoted or reproduced, the source is always given. The thesis has been submitted neither partially nor wholly as part of a doctoral examination procedure to another examining body and has not been published or submitted for publication – except for the articles explicitly stated. The thesis has been prepared subject to the rules of good scientific practice of the German Research Foundation. No academic degree has ever been withdrawn.*

Kiel, 13.01.2020, \_\_\_\_\_

Joana Seguin